

Electronic Thesis and Dissertation Repository

12-2-2011 12:00 AM

Fault Location and Incipient Fault Detection in Distribution Cables

Zhihan Xu, *The University of Western Ontario*

Supervisor: Tarlochan Sidhu, *The University of Western Ontario*

A thesis submitted in partial fulfillment of the requirements for the Doctor of Philosophy degree
in Electrical and Computer Engineering

© Zhihan Xu 2011

Follow this and additional works at: <https://ir.lib.uwo.ca/etd>



Part of the [Power and Energy Commons](#)

Recommended Citation

Xu, Zhihan, "Fault Location and Incipient Fault Detection in Distribution Cables" (2011). *Electronic Thesis and Dissertation Repository*. 319.

<https://ir.lib.uwo.ca/etd/319>

This Dissertation/Thesis is brought to you for free and open access by Scholarship@Western. It has been accepted for inclusion in Electronic Thesis and Dissertation Repository by an authorized administrator of Scholarship@Western. For more information, please contact wlsadmin@uwo.ca.

FAULT LOCATION AND INCIPIENT FAULT DETECTION IN DISTRIBUTION
CABLES

(Spine title: Fault Location and Incipient Fault Detection in Distribution Cables)

(Thesis format: Monograph)

by

Zhihan Xu

Graduate Program in Engineering Science
Department of Electrical and Computer Engineering

A thesis submitted in partial fulfillment
of the requirements for the degree of
Doctor of Philosophy

The School of Graduate and Postdoctoral Studies
The University of Western Ontario
London, Ontario, Canada

© Zhihan Xu, 2011

THE UNIVERSITY OF WESTERN ONTARIO
School of Graduate and Postdoctoral Studies

CERTIFICATE OF EXAMINATION

Supervisor

Examiners

Dr. Tarlochan Sidhu

Dr. Yuan Liao

Dr. Kazimierz Adamiak

Dr. Anestis Dounavis

Dr. Jin Zhang

The thesis by

Zhihan Xu

entitled:

Fault Location and Incipient Fault Detection in Distribution Cables

is accepted in partial fulfillment of the
requirements for the degree of
Doctor of Philosophy

Date

Chair of the Thesis Examination Board

Abstract

A set of fault location algorithms for underground medium voltage cables, two incipient fault detection schemes for distribution cables and a state estimation method for underground distribution networks are developed in this thesis.

Two schemes are designed to detect and classify incipient faults in underground distribution cables. Based on the methodology of wavelet analysis, one scheme is to detect the fault-induced transients, and therefore identify the incipient faults. Based on the analysis of the superimposed fault current and negative sequence current in time domain, the other scheme is particularly suitable to detect the single-line-to-ground incipient faults, which are mostly occurring in underground cables. To verify the effectiveness and functionalities of the proposed detection algorithms, different fault conditions, various system configurations, real field cases and normal operating transients are examined. The simulation results have demonstrated a technical feasibility for practical implementations of both schemes.

Based on the methodology of the direct circuit analysis, a set of location algorithms are proposed to locate the single phase related faults in the typical underground medium voltage cables. A large number of complex equations are effectively solved to find the fault distance and fault resistance. The algorithms only utilize the fundamental phasors of three-phase voltages and currents recorded at single end, normally at substation. The various system and fault conditions are taken into account in the development of algorithms, such as effects of shunt capacitance, mutual effects of metallic sheaths, common sheath bonding methods and different fault scenarios. The extensive simulations have validated the accuracy and effectiveness of the proposed algorithms.

In order to extend the proposed fault location algorithms to underground distribution networks, a state estimation algorithm is developed to provide the necessary information for the location algorithms. Taking account of the complexity and particularity of cable circuits, the problem of the state estimation is formulated as a nonlinear optimization problem that is solved by the sequential quadratic programming technique. The simulation studies have indicated that the proposed fault location scheme incorporating with the state estimation algorithm can achieve good performance under different load and fault conditions.

Keywords

Fault Location, Distribution State Estimation, Incipient Fault Detection, Underground Medium Voltage Cables.

Acknowledgments

I would like to express my deepest gratitude to my advisor Dr. Tarlochan S. Sidhu for his advice, encouragement and guidance throughout my studies at the University of Western Ontario. Without his support and patience, this research would have never been possible.

I am grateful to the advisory committee members, Dr. Liao, Dr. Adamiak, Dr. Dounavis and Dr. Zhang, for their careful reading of the thesis and insightful technical suggestions.

Sincere thanks are owed to all the fine people, especially at the power group in the Department of Electrical and Computer Engineering, who have made my time here enjoyable.

Thanks are due to my mentor and friend, Mr. Xiaochuan Liu. Thank you for allowing me the opportunity to learn from you, listening to me patiently, answering me accordingly and helping me generously.

Finally, I would like to extend my heartfelt gratitude to my parents, my wife Wei and my son Ray, for their love, support, encouragement, understanding and patience. They are the foundation for who I am, and anything I have been able to accomplish is a tribute to them.

Table of Contents

CERTIFICATE OF EXAMINATION	ii
Abstract	iii
Acknowledgments	v
Table of Contents	vi
List of Tables	xi
List of Figures	xiii
List of Appendices	xx
List of Symbols	xxi
Nomenclature	xxiv
Chapter 1	1
1 Introduction	1
1.1 Incipient Fault Detection Methods	1
1.2 Fault Location Methods for Cables	3
1.2.1 Offline Methods	3
1.2.2 Online Methods	5
1.3 Fault Location Methods for Distribution Networks	9
1.3.1 Technical Cruces in Selected Location Methods	14
1.3.2 Summary of Line Model	18
1.3.3 Summary of Load Model	21
1.3.4 Existing Limitations and Problems	22
1.4 Distribution State Estimation Methods	24
1.5 Objectives of the Thesis	25
1.6 Contributions of the Thesis	26
1.7 Scope of the Thesis	27

Chapter 2.....	29
2 Incipient Fault Detection Schemes for Distribution Cables.....	29
2.1 Background.....	29
2.1.1 Incipient Faults in Cables.....	29
2.1.2 Model of Arc.....	32
2.2 Wavelet-based Detection Scheme.....	34
2.2.1 Principles.....	34
2.2.2 System Description.....	35
2.2.3 Detection and Classification Rules.....	40
2.2.4 Thresholds.....	42
2.3 Superimposed Components-based Detection Scheme.....	43
2.3.1 Detection of Transient Inception.....	43
2.3.2 Selection of Faulty Phase.....	49
2.3.3 Classification.....	53
2.3.4 Thresholds.....	53
2.4 Simulations.....	54
2.4.1 Configuration of Simulation System.....	54
2.4.2 Test Systems.....	55
2.4.3 Cases Studied.....	57
2.4.4 Simulation Results.....	58
2.4.5 Results Using Field Recorded Data.....	62
Chapter 3.....	69
3 Fault Location Algorithms for Medium Voltage Cables.....	69
3.1 Background.....	70
3.1.1 Structure of a Typical XLPE Cable.....	70
3.1.2 Sheath Bonding Methods.....	71

3.1.3	Complexities in Fault Location for Cables	72
3.1.4	Fault Scenarios.....	73
3.2	Model of Cable	74
3.3	Location Algorithm for Cables with SPBS.....	78
3.3.1	Problem Formulation	78
3.3.2	Locating Core-Sheath-Ground Fault.....	82
3.3.3	Locating Core-Ground Fault.....	91
3.3.4	Locating Core-Sheath Fault	92
3.3.5	General Location Scheme	93
3.4	Location Algorithm for Cables with SPBR	94
3.4.1	Differences from SPBS.....	94
3.4.2	Similarities with SPBS.....	96
3.5	Location Algorithm for Cables with SPBM	97
3.5.1	Fault in the First Half Section.....	97
3.5.2	Fault in the Second Half Section	104
3.5.3	Location Scheme for Entire Cable.....	105
3.6	Location Algorithm for Cables with SBBE.....	106
3.6.1	Differences from SPBS.....	106
3.6.2	Similarities with SPBS.....	108
3.7	Location Algorithm for Cables with XB	109
3.7.1	Fault in the First Section.....	109
3.7.2	Fault in the Middle Section.....	116
3.7.3	Fault in the Last Section	119
3.7.4	Other Issues.....	121
3.7.5	Location Scheme for Entire Cable.....	121
3.8	Summary of Location Algorithms	122

3.9	Load Impedance Estimation	125
3.9.1	Constant Impedance Load Model	125
3.9.2	Static Response Load Model	128
3.10	Simulations	129
3.10.1	Test Cases	129
3.10.2	Simulation Results	129
3.10.3	Summary of Effects	150
Chapter 4.....		152
4	Extension of the Proposed Fault Location Algorithms to Medium Voltage Cables in Distribution Networks.....	152
4.1	Background.....	153
4.1.1	Complexities in Fault Location in Distribution Networks.....	153
4.1.2	Complexities in State Estimation for Distribution Networks	153
4.1.3	Emerging Issues Caused by Extension to Distribution Networks	154
4.1.4	Introduction to Sequential Quadratic Programming	155
4.2	Development of State Estimation Algorithm.....	156
4.2.1	Problem Formulation	156
4.2.2	State Estimation Algorithm.....	156
4.3	General Location Procedure Combined with State Estimation	161
4.3.1	Prefault Load Estimation by DSE.....	163
4.3.2	Estimation of Quantities during Fault.....	165
4.3.3	Determination of Faulty Section.....	177
4.3.4	Fault Location	188
4.3.5	Summary of Location Procedure	188
4.4	Application of Static Response Load Model	189
4.5	Simulations	190

4.5.1	Test System and Cases.....	190
4.5.2	Performance Indices.....	193
4.5.3	State Estimation Results	194
4.5.4	Fault Location Results	196
Chapter 5	219
5	Conclusions and Future Works	219
5.1	Conclusions.....	219
5.2	Future Works	223
References	225
Appendices	234

List of Tables

Table 1.1: Summary of Fault Location Methods for Distribution Networks – I	10
Table 1.2: Summary of Fault Location Methods for Distribution Networks - II	12
Table 2.1: Detection and Classification Results (Wavelet-based Scheme)	59
Table 2.2: Detection and Classification Results (Superimposed Components-based Scheme)	62
Table 3.1: Decision of Fault Scenarios in Theory	74
Table 3.2: List of Unknown Variables – SPBS & CSGF	81
Table 3.3: List of Equations – SPBS & CSGF	81
Table 3.4: List of Unknown Variables – SPBS & CGF	92
Table 3.5: List of Equations – SPBS & CGF	92
Table 3.6: List of Unknown Variables – SPBS & CSF	93
Table 3.7: List of Equations – SPBS & CSF	93
Table 3.8: Decision of Fault Scenarios in Practice	94
Table 3.9: List of Unknown Variables – SPBM-1 & CSGF.....	100
Table 3.10: List of Equations – SPBM-1 & CSGF.....	101
Table 3.11: List of Unknown Variables – XB & CSGF	113
Table 3.12: List of Equations – XB & CSGF	113
Table 3.13: Summary of Algorithms for Single Point Bonding.....	123
Table 3.14: Summary of Algorithms for Solid and Cross Bonding	124
Table 3.15: Average of Absolute Values of Location Errors	130

Table 3.16: Distribution of Absolute Values of Location Errors.....	147
Table 3.17: Effects of Bonding Methods and Fault Types on Location Accuracy.....	151
Table 4.1: Category of Sub-Algorithms.....	166
Table 4.2: Estimation of Nodal Voltages and Branch Currents.....	174
Table 4.3: Details of Test System.....	191
Table 4.4: Performance Indices for Initial Loads	194
Table 4.5: Performance Indices for Estimated Loads.....	195
Table 4.6: Percent Reduction in Error - Load Estimation	196
Table 4.7: Average of Absolute Values of Location Errors – Individual Load Pattern	197
Table 4.8: Distribution of Absolute Values of Relative Errors – Individual Load Pattern ..	198
Table 4.9: Distribution of Absolute Values of Absolute Errors – Individual Load Pattern .	199
Table 4.10: Average of Absolute Values of Location Errors – Combination of Load Patterns	216
Table 4.11: Percent Reduction in Error – Combination of Load Patterns	217
Table 4.12: Distribution of Absolute Values of Relative Errors – Combination of Load Patterns.....	217
Table 4.13: Distribution of Absolute Values of Absolute Errors – Combination of Load Patterns.....	218

List of Figures

Figure 1.1: Lumped π line model.....	19
Figure 2.1: Illustrations of water tree (WT) and electrical tree (ET) [76].	30
Figure 2.2: Sub-cycle incipient fault.....	32
Figure 2.3: Multi-cycle incipient fault.	32
Figure 2.4: Detail and approximation coefficients after wavelet decomposition and reconstruction.....	35
Figure 2.5: Flowchart of detection and classification procedures.	36
Figure 2.6: Time sequence diagram.....	38
Figure 2.7: Feeder current for the event of multi-cycle incipient fault.....	39
Figure 2.8: Current for the event of capacitor switching.....	39
Figure 2.9: Waveforms from Rule S1 – Phase-A-ground sub-cycle incipient fault.	44
Figure 2.10: Waveforms from Rule S1 – Phase-A-ground multi-cycle incipient fault.	45
Figure 2.11: Waveforms from Rule S1 – Phase-A-ground permanent fault.	45
Figure 2.12: Waveforms from Rule S1 – Phase-B-C permanent fault.	45
Figure 2.13: Waveforms from Rule S1 – Phase-A-B-ground permanent fault.	46
Figure 2.14: Waveforms from Rule S1 – Three-phase-ground permanent fault.	46
Figure 2.15: Waveforms from Rule S1 – Capacitor switching.....	46
Figure 2.16: Waveforms from Rule S2 – Phase-A-ground sub-cycle incipient fault.	47
Figure 2.17: Waveforms from Rule S2 – Phase-A-ground multi-cycle incipient fault.	47

Figure 2.18: Waveforms from Rule S2 – Phase-A-ground permanent fault.	47
Figure 2.19: Waveforms from Rule S2 – Phase-B-C permanent fault.	48
Figure 2.20: Waveforms from Rule S2 – Phase-A-B-ground permanent fault.	48
Figure 2.21: Waveforms from Rule S2 – Three-phase-ground permanent fault.	48
Figure 2.22: Waveforms from Rule S2 – Capacitor switching.....	49
Figure 2.23: Waveforms of $I_{\Delta mg}$ (Phase-A-ground multi-cycle fault, primary side, Δ/Y_0). ...	50
Figure 2.24: Waveforms of $I_{\Delta mg}$ (Phase-A-ground multi-cycle fault, primary side, Y/Y_0). ...	51
Figure 2.25: Amplitude of currents (3LG, primary side, Y/Y_0).	52
Figure 2.26: Amplitude of currents (SLG, primary side, Y/Y_0).	52
Figure 2.27: Configuration of simulation system.	55
Figure 2.28: Test system 1.	56
Figure 2.29: Test system 2.	57
Figure 2.30: Undetected sub-cycle fault (30 ohm).	59
Figure 2.31: Undetected multi-cycle fault (50 ohm).	60
Figure 2.32: Events with similar changing.	61
Figure 2.33: Analysis process of a sub-cycle incipient fault (Wavelet-based).....	64
Figure 2.34: Analysis process of a sub-cycle incipient fault (Superimposed components-based).....	65
Figure 2.35: Analysis process of a multi-cycle incipient fault (Wavelet-based).....	66
Figure 2.36: Analysis process of a multi-cycle incipient fault (Superimposed components-based).....	67

Figure 3.1: Structure of a typical single-conductor XLPE cable and laid formations of three-phase cables.	70
Figure 3.2: Sheath bonding methods.	71
Figure 3.3: Fault scenarios.	74
Figure 3.4: Model of three single-conductor XLPE cables. There exist the mutual impedances among all six conductors (Only the mutual impedances related to the core conductor of phase A are shown in the dash-dot lines above).	75
Figure 3.5: A CSGF in cable with SPBS.	79
Figure 3.6: Conical surface to estimate current of the healthy sheath.	85
Figure 3.7: Three-dimensional illustration to estimate current of the faulty sheath.	86
Figure 3.8: Contour of Figure 3.7 at zero planes.	87
Figure 3.9: A set of estimated currents of sheath A marked as round dots.	88
Figure 3.10: Example to show results of pinpoint criteria.	89
Figure 3.11: Location procedure for CSGF & SPBS.	90
Figure 3.12: General location scheme - SPBS.	94
Figure 3.13: A CSGF in cable with SPBM-1.	98
Figure 3.14: Location scheme for entire cable - SPBM.	106
Figure 3.15: A CSGF in cable with XB-1.	110
Figure 3.16: Location scheme for entire cable - XB.	122
Figure 3.17: Effect of fault type - SPBS.	131
Figure 3.18: Effect of fault type - SPBR.	132
Figure 3.19: Effect of fault type - SPBM.	133

Figure 3.20: Effect of fault type - SBBE.	134
Figure 3.21: Effect of fault type - XB.....	135
Figure 3.22: Effect of bonding method - CSGF.	136
Figure 3.23: Effect of bonding method - CSF.	138
Figure 3.24: Effect of bonding method - CGF.....	139
Figure 3.25: Effect of fault distance – SBBE&CSGF.	140
Figure 3.26: Effect of fault distance – XB&CGF.....	141
Figure 3.27: Effect of fault distance – SPBM&CSF.....	142
Figure 3.28: Effect of fault resistance – SPBS&CSGF.	144
Figure 3.29: Effect of fault resistance – SBBE&CGF.....	145
Figure 3.30: Effect of fault resistance – XB&CSF.....	146
Figure 3.31: Calculation of fault resistance – SPBR.	148
Figure 3.32: Calculation of fault resistance – SPBM.	149
Figure 3.33: Calculation of fault resistance – SPBS.....	150
Figure 4.1: Example to calculate injected power.....	159
Figure 4.2: A radial unbalanced underground distribution network.....	162
Figure 4.3: General circuit section to categorize sub-algorithms.	165
Figure 4.4: Flowchart of SA4.	169
Figure 4.5: Node with no lateral and tapped load.....	171
Figure 4.6: Node with tapped load and with no lateral.....	172

Figure 4.7: Node with lateral and with no tapped load.....	172
Figure 4.8: Node with lateral and tapped load.....	172
Figure 4.9: Calculation of seen impedance.....	173
Figure 4.10: Calculation processed on branch 1 (CSGF at branch 1).	178
Figure 4.11: Calculation processed on branch 2 (CSGF at branch 1).	178
Figure 4.12: Calculation processed on branch 14 (CSGF at branch 14).	179
Figure 4.13: Calculation processed on branch 13 (CSGF at branch 14).	180
Figure 4.14: Calculation processed on branch 15 (CSGF at branch 14).	180
Figure 4.15: Calculation processed on branch 18 (CSGF at branch 14).	181
Figure 4.16: Calculation processed on branch 21 (CSGF at branch 21).	182
Figure 4.17: Calculation processed on branch 19 (CSGF at branch 21).	182
Figure 4.18: Calculation processed on branch 20 (CSGF at branch 21).	183
Figure 4.19: Calculation processed on branch 1 (CGF at branch 1).....	184
Figure 4.20: Calculation processed on branch 2 (CGF at branch 1).....	184
Figure 4.21: Calculation processed on branch 14 (CGF at branch 14).....	185
Figure 4.22: Calculation processed on branch 13 (CGF at branch 14).....	185
Figure 4.23: Calculation processed on branch 15 (CGF at branch 14).....	186
Figure 4.24: Calculation processed on branch 18 (CGF at branch 14).....	186
Figure 4.25: Calculation processed on branch 21 (CGF at branch 21).....	187
Figure 4.26: Calculation processed on branch 19 (CGF at branch 21).....	187

Figure 4.27: Calculation processed on branch 20 (CGF at branch 21).....	188
Figure 4.28: Effect of cable length (CSGF @25%).....	200
Figure 4.29: Effect of cable length (CSF @50%).....	201
Figure 4.30: Effect of cable length (CGF @75%).....	202
Figure 4.31: Effect of faulty section (CSGF @25%).....	203
Figure 4.32: Effect of faulty section (CSF @50%).	204
Figure 4.33: Effect of faulty section (CGF @75%).....	205
Figure 4.34: Effect of load profile (CSGF@50%, Generic profile).	206
Figure 4.35: Effect of load profile (CSGF@50%, Uniform profile).	207
Figure 4.36: Effect of load profile (CGF@50%, Generic profile).....	208
Figure 4.37: Effect of load profile (CGF@50%, Uniform profile).	209
Figure 4.38: Effect of fault distance (CSGF, LP1).	210
Figure 4.39: Effect of fault distance (CSF, LP1).	211
Figure 4.40: Effect of fault distance (CGF, LP1).	212
Figure 4.41: Effect of fault type (25%, LP2).	213
Figure 4.42: Effect of fault type (50%, LP4).	214
Figure 4.43: Effect of fault type (75%, LP6).	215
Figure A.1: Fault currents.	234
Figure A.2: Wavefronts of traveling waves.	235
Figure A.3: Illustration of propagation of traveling waves in spatiotemporal domain.....	236

Figure A.4: Two dimension illustration of propagation of traveling wave.	236
Figure A.5: Bewley lattice diagram.	237
Figure A.6: Arc voltage.	238
Figure A.7: Arc current.	238
Figure A.8: Arc resistance.	238

List of Appendices

Appendix A: Illustration of Traveling Wave	234
Appendix B: Example of Kizilcay's Arc Model.....	237

List of Symbols

Unless otherwise specified, the following symbols are applied to the context.

V_x : Voltage phasor vector (6×1) at the location x , containing three-phase core voltage phasors and three-phase sheath voltage phasors. The lowercase x could be s, r, f, m, p or t .

V_{xu} : Three-phase voltage phasor vector (3×1) of the conductor u at the location x . The lowercase x could be s, r, f, m, p or t . The lowercase u could be c or n .

V_{xu}^W : Voltage phasor scalar of the conductor u of the phase W at the location x . The lowercase x could be s, r, f, m, p or t . The lowercase u could be c or n . The capital W could be A, B or C .

I_x : Current phasor vector (6×1) at location x , containing three-phase core current phasors and three-phase sheath current phasors. The lowercase x could be s, r, f, m, p or t .

I_{xu} : Three-phase current phasor vector (3×1) of the conductor u at the location x . The lowercase x could be s, r, f, m, p and t . The lowercase u could be c or n .

I_{xu}^W : Current phasor scalar of the conductor u of the phase W at the location x . The lowercase x could be s, r, f, m, p or t . The lowercase u could be c or n . The capital W could be A, B or C .

Z : 6×6 series impedance matrix of cable circuit.

Z_{xu} : 3×3 series impedance matrix between conductors x and u . The lowercase x and u could be c or n .

z_{xx}^{EE} : Self-impedance scalar of the conductor x of the phase E . The lowercase x could be c or n . The capital E could be A, B or C .

z_{xu}^{EF} : Series mutual impedance scalar between the conductor x of the phase E and the conductor u of the phase F . The lowercase x and u could be c or n . The capital E and F could be A, B or C .

Z_{load} : 3×3 or 6×6 load impedance matrix. The dimension would be specified in the context.

z_{load}^E : Load impedance scalar of the Phase E .

z_{xu} : Series impedance scalar between the conductor x and u . The lowercase x and u could be c or n . The phase is not specified.

Y : 6×6 shunt admittance matrix of cable circuit.

Y_{xu} : 3×3 shunt admittance matrix between conductors x and u . The lowercase x and u could be c or n .

y_{xx}^{EE} : Shunt admittance impedance scalar of the conductor x of the phase E . The lowercase x could be c or n . The capital E could be A, B or C .

y_{cn} : Shunt impedance scalar between the core conductor c and sheath n . The phase is not specified.

y_{ng} : Shunt impedance scalar between the sheath n and ground g . The phase is not specified.

L : Length of a cable section (or subsection).

D : Fault distance from the sending terminal of the faulty section to the fault point.

core X: Core conductor of the phase X . The capital X could be A, B or C .

sheath X: Sheath conductor of the phase X . The capital X could be A, B or C .

j : $\sqrt{-1}$

c at subscript: quantities of core conductor

n at subscript: quantities of sheath conductor

s at subscript: quantities at sending terminal

r at subscript: quantities at receiving terminal

f at subscript: quantities at fault point

m at subscript: quantities at middle point of cables with SPBM

p at subscript: quantities at the first joint of cables with XB

t at subscript: quantities at the second joint of cables with XB

A at superscript: Phase A

B at superscript: Phase B

C at superscript: Phase C

Nomenclature

3L	Three-phase fault
3LG	Three-phase-ground fault
BFSA	Backward/Forward Sweep Algorithm
CGF	Core-Ground Fault
CSF	Core-Sheath Fault
CSGF	Core-Sheath-Ground Fault
CT	Current Transformer
DAE	Distribution of Absolute Error
DFT	Discrete Fourier Transform
DMS	Distribution Management System
DRE	Distribution of Relative Error
DSE	Distribution State Estimation
EMTP	Electromagnetic Transients Program
ET	Electrical Tree
IU	Identity matrix
KVL	Kirchhoff's Voltage Law
LL	Phase-to-Phase fault
LP	Load Pattern
MV	Medium Voltage

PE	Polyethylene
PRE	Percent Reduction in Error
QP	Quadratic Programming
SA	Sub-Algorithm
SBBE	Solid Bonding at Both Ends
SE	State Estimation
SLG	Single-Line-Ground fault
SNR	Signal Noise Ratio
SPBM	Single Point Bonding at Middle Point
SPBM-1	First Half Section with Single Point Bonding at Middle Point
SPBM-2	Second Half Section with Single Point Bonding at Middle Point
SPBR	Single Point Bonding at Receiving Terminal
SPBS	Single Point Bonding at Sending Terminal
SQP	Sequential Quadratic Programming
TDR	Time Domain Reflectrometer
WLS	Weighted Least Squares
WT	Water Tree
XB	Cross Bonding
XB-1	First Section with Cross Bonding
XB-2	Middle Section with Cross Bonding

XB-3 Last Section with Cross Bonding

XLPE Cross-Linked Polyethylene

Chapter 1

1 Introduction

Underground cables have been widely applied in power distribution networks due to the benefits of underground connection, involving more secure than overhead lines in bad weather, less liable to damage by storms or lightning, no susceptible to trees, less expensive for shorter distance, environment-friendly and low maintenance. However, the disadvantages of underground cables should also be mentioned, including 8 to 15 times more expensive than equivalent overhead lines, less power transfer capability, more liable to permanent damage following a flash-over, and difficult to locate fault.

Faults in underground cables can be normally classified as two categories: incipient faults and permanent faults. Usually, incipient faults in power cables are gradually resulted from the aging process, where the localized deterioration in insulations exists. Electrical overstress in conjunction with mechanical deficiency, unfavorable environmental condition and chemical pollution, can cause the irreparable and irreversible damages in insulations. Eventually, incipient faults would fail into permanent faults sooner or later.

The detection of incipient faults can provide an early warning for the breakdown of the defective cable, even trip the suspected feeder to limit the repetitive voltage transients. The location of permanent faults in cables is essential for electric power distribution networks to improve network reliability, ensure customer power quality, speed up restoration process, minimize outage time, reduce repairing cost, dispatch crews more efficiently and maintain network reliability. The state estimation (SE) is an auxiliary tool to provide the necessary information for the proposed location algorithms. The related methods published in journals and proceedings are reviewed, summarized and compared in the next subsections.

1.1 Incipient Fault Detection Methods

Comparing with the detection methods for arcing faults in overhead lines, there are relatively fewer literatures and reports discussing the detection of incipient faults in

underground cables. The existing detection methods are generally based on the analysis of waveforms rather than phasors. Basically, the process of detection is to examine the characteristics of voltages and currents in time domain, frequency domain and time-frequency domain.

The advantages and disadvantages of four existing techniques developed for field applications were reviewed and evaluated from the point of a power engineer in [1]. These techniques include detection of partial discharges, time and frequency domain reflectometry, measurements of dielectric ohmic and polarization, and acoustic and pressure wave techniques.

Charytoniuk et al. studied the feasibility of detecting arcing faults in underground cables [2]. An experiment was carried out in one secondary distribution network by personnel from the Consolidated Edison Company of New York. Through analyzing the collected data, three feasible methods are considered, i.e. analysis of voltages and currents in time domain, in frequency domain and in time-frequency domain with the aid of the wavelet analysis. Furthermore, it is pointed out that the potential approaches can process the instantaneous values of currents, and combine the arc fault features in time, frequency and time-frequency domains.

Kojovic et al. proposed an incipient cable splice failure detection scheme, which is integrated into a universal relay platform as an additional function to enhance the distribution feeder protection [3], [4]. The basic principle is to monitor instantaneous overcurrent, counter the number of fault occurrences, record the frequency of fault occurrences, and provide alarming or tripping capability.

Kasztenny et al. proposed a simple, fast and robust method for detecting incipient faults in cables and implemented it in a commercial relay [5]. The method employs the superimposed current components and neutral current to monitor the consistency of currents before and after the event, find the phase where the event occurs, check the event duration, and set the alarming or tripping signal.

Both the magnitude of neutral current and the magnitude of rate of change of neutral current were used to detect self-clearing cable transient faults and distinguish them from normal system switching as well as other system faults, such as fast fuse operations [6]. The faulty phase is selected by a phase current rate of change based detector.

The wavelet analysis and neural network were combined to detect on-line incipient transients in underground distribution cable laterals and predict the remaining life of the cable lateral [7]. The wavelet packet analysis technique is applied to decompose the current into separate frequency bands and to extract features. Then, a type of artificial neural network, self-organizing map, is used for pattern identification. Therefore, the data sets are clustered and incipient behavior is identified and categorized.

The pattern analysis techniques were applied to classify load change transients and incipient abnormalities in an underground distribution cable lateral [8]. A set of features are extracted by the wavelet packet analysis and output to k-nearest-neighbor classifiers. The methods of dimensionality reduction are used to reduce the dimensionality for the pattern recognition and preserve the good classification accuracy as well.

1.2 Fault Location Methods for Cables

Basically, the location methods for cables are divided into the offline and online methods. The offline methods employ the special instruments to test the out of service cable in field. On the other hand, the online methods utilize and process the sampled voltages and currents to determine the fault point.

1.2.1 Offline Methods

There are two offline location approaches, i.e. terminal approaches and tracer approaches. Terminal methods rely on measurements made from either one or both terminals of the cable to prelocate fault points approximately, but not accurately enough to allow dig. Tracer methods rely on measurements taken along the cable to pinpoint the fault location very accurately. Both methods are on-site technique and performed with low efficiency.

Eighteen terminal methods are introduced in [9] and listed below.

- Halfway Approach Method
- Charging Current Method
- Murray Loop Method
- Murray Loop Two-End Method
- Varley Loop Method
- Open-and-closed Loop Method
- Impulse Current Method
- Standing Wave Differential
- Time Domain Reflectometer (TDR)/Cable Radar Method
- TDR/Cable Radar and Thumper Method
- Voltage Drop Ratio Method
- Insulation Resistance Ratio Method
- Capacitance Ratio Method
- Murray-Fisher Loop Method
- Hilborn Loop Method
- Werren Overlap Method
- Pulse Decay Method
- DC Charging Current Method

Following the prelocation by the terminal methods, a tracer method is generally applied to pinpoint the fault point and this method usually requests the repair crews to walk along the cable route. Nine tracer methods introduced in [9] are listed below.

- Magnetic Pickup Method
- Earth gradient Method
- Thumper/Acoustic Method
- Sheath Coil Method
- DC Sheath Potential Difference Method
- Tracing current Method
- Hill-of-Potential Method
- Thumper/Electromagnetic Wave Method
- Pick Method

Some extension works were proposed as an aid for the offline methods. An expert system was developed for the Electric Power Research Institute (EPRI) [10]. The system creates a reference manual [9] to provide the guidance for field crews to diagnose a cable failure, recommend applicable fault location techniques, and trouble-shoot resulting difficulties which occur during the process of locating underground cable faults.

For the sake of clarifying the results obtained from the terminal methods, an expert system approach was proposed to locate fault on high voltage underground cable systems [11]. The experience and expertise of many different engineers is accumulated to build a truly expert system. With the data acquired from diagnostic tests, the system can infer the fault type, advise the further location techniques, and conclude the probable fault location. The operator is then advised to carry out the tracer methods to locate the fault precisely.

1.2.2 Online Methods

The online location methods for underground cables are comparatively fewer than the ones applied for overhead lines. Two principal techniques have been proposed for the online location, i.e. signal analysis and knowledge-based [12]. The former one is further classified into the approaches based on fundamental frequency phasor quantities and high frequency traveling waves.

1.2.2.1 Fundamental Phasor-based Methods

The fundamental phasor-based methods utilize the voltage and current phasors at the fundamental frequency. Basically, the impedance is calculated and used to decide the fault distance, so it is also called the impedance-based methods [13], [14].

Filomena et al. extended the traditional impedance-based location algorithms to calculate the apparent impedance of cables in cases of single phase to ground fault (SLG) and three-phase fault (3L) [15]. The single-end voltages and currents are used. An iterative algorithm is proposed to compensate the capacitive characteristic in typical underground cables. The fault location scheme can be applied in balanced or unbalanced distribution systems with laterals and tapped loads.

Based on the estimation of the fault-loop impedance, Saha et al. presented four location algorithms to consider the following scenarios [16]: SLG fault with measurements available in the faulty feeder (voltages and currents), SLG fault with measurements available at the substation level (total currents are measured at the supplying transformer), phase to phase (LL) or 3L fault with measurements available in the faulty feeder, LL or 3L fault with measurements available at the substation. Only positive sequence impedance calculation is needed for LL or 3L fault, while the zero-sequence impedance calculation is required for SLG fault. The algorithms can be applied in radial medium voltage (MV) systems, which include many intermediate load taps. The non-homogeneity of the feeder sections is also taken into account.

The apparent seen impedance was calculated using local measuring quantities available at substation [17]. Upon the different fault type, the different apparent impedance

parameters, voltage and current quantities are utilized. Then, a fault distance is estimated using the conventional apparent impedance computation. Finally, an iterative compensation mechanism is executed to eliminate the estimation errors caused by the charging currents in cables. The basic procedure is similar to the work in [15] except that the symmetrical components are used.

The location algorithm in [18] extended the traditional Takagi's method [19] into distribution cable networks. The sequence phase impedance model is used to model laterals and circuit sections. The line shunt capacitance is taken into account to optimize the result so that the major source of error in conventional impedance based methods, particularly for cable networks, is minimized.

Differentiating from the above extended impedance-based methods, an iterative algorithm was proposed for locating faults in cables [20]. The circuit is modeled by the distributed parameter approach and the voltage and current equations are formulated based on the sequence networks. The Newton–Raphson method is applied to calculate the fault distance. The algorithm is also extended to the radial multi-section cables with tapped loads.

A double-end based location algorithm was presented, particularly for aged power cables [21]. The aging process in cables would cause the change of the relative permittivity and in turn result in the changes in the positive, negative, and zero sequence capacitance. The fault location scheme is based on phasor measurements from both ends of the cable, incorporating with the distributed line model, Clarke transformation theory and discrete Fourier transform (DFT).

One algorithm implemented in the Con Edison of New York was presented in [22]. The voltages and currents are recorded by the power quality monitors and processed for calculations in the control center. The reactance to fault is calculated based on the fault measurements and prior knowledge of known fault information. The calculation results combined with up-to-date distribution feeder models and geographic information system data are used to generate the estimated fault location tables and viewing maps. The estimation would typically take ten minutes after the inception of a fault. The location

accuracy is within 10% of the total number of feeder structures, for about 80% of the single phase faults.

One more implementation in the Dutch grid operator Alliander was presented in [23], [24]. The fault locators only use the calculated reactance since the reactance of fault impedance is zero and the cable reactance is well known and not current dependent. Then, the scenarios of short circuits on all nodes in the faulted feeder are simulated on an actual network model. The calculated impedance is compared with the simulated impedances to find the exact location. The location algorithm is known to find the distance within 5 minutes after the occurrence of a fault. The system is able to locate LL and 3L faults within 100 meters and SLG faults within 500 meters.

1.2.2.2 Traveling wave-based Methods

Traveling waves are generated by the change of stored energy in capacitance and inductance in lines or cables after the occurrence of a fault. Both voltage and current traveling waves propagate along the circuit at the speed as high as the light speed until meeting any impedance discontinuities, and then the fault-induced high frequency waves would reflect back to the origin and transmit through towards other side.

Almost all traveling waves-based methods are based on the principle of the Bewley lattice diagram [25], and the fault distance is calculated by the multiplication of the propagation velocity and the interval, which is the time difference between the arrival instant of the initial wavefront and the arrival instant of the reflected wavefront. The basic location principle and common locator types are introduced in [26].

Appendix A visually illustrates and explains an example of the traveling wave, which is generated by an SLG fault in a transmission line and can be used for the purpose of the line protection and fault location.

Bo et al. designed a special transient capturing unit to extract the fault-generated high frequency voltage transient signals in cables [27]. The principle of the fault location method is to identify the successive arrivals of the traveling high frequency voltage signals arriving at the busbar where the locator is installed. Particularly the first and the

subsequent arriving wavefronts with reference to the first wavefront are used to locate the fault position. The above work is enhanced by applying new technique, wavelet transform, to effectively extract a band of high frequency transient voltage signals [28].

A cable fault location scheme was proposed based on the principle of the traditional traveling wave principle, synchronized sampling technique and wavelet analysis [29]. The current signals at the two terminals are synchronized with the help of GPS and the arrival time of fault-induced traveling waves is precisely detected by the wavelet analysis. Then, the location is obtained from the multiplication of the propagation velocity and the time interval.

Similarly, based on the principle of the traditional Bewley lattice, a double-end traveling wave fault location scheme was proposed for locating faults in aged cables [30]. The wavelet analysis is applied to analyze the synchronized voltage signals at the two terminals to capture the singularity in high frequency transients. The calculations are processed with the modal quantities rather than the phase quantities. The effect of changes in the propagation velocity of traveling wave is eliminated.

The fault section and location was determined by the analysis of traveling waves in current signals [31]. First, the fault section is identified by the comparison between the distance of each peak in the high frequency current signals and the known reflection points in distribution feeders. Then, the simulation is processed with the possible location in a transient power system simulator, which is modeled from the actual network. The simulated currents are cross correlated with the measured currents to find the match degree in high frequency transients of both current signals. The cross-correlation coefficients would be a high positive value if the estimated fault location is correct.

1.2.2.3 Knowledge-based Methods

Knowledge-based techniques, such neural network, fuzzy logic and expert system, are applied to fault location for cables. The usage of artificial intelligence techniques usually requires the specific learning process for each analyzed feeder. Additionally, the signal

processing techniques can also be used to preprocess the signals and extract the features fed into the analysis of artificial intelligence.

Sadeh et al. proposed a fault location algorithm for combined overhead transmission line with underground power cable [32]. First, one adaptive network-based fuzzy inference system (ANFIS) is used to classify the fault type. Then, another ANFIS is applied to detect the faulty section, whether the fault is on the overhead line or on the underground cable. Other eight ANFIS networks are utilized to pinpoint the fault, in which two networks are used for one fault type. The neuro-fuzzy inference systems are trained by the data obtained from simulations.

Moshtagh and Aggarwal proposed a location algorithm combined the neural network and wavelet analysis [33]. The power distribution system transient signals are generated by the EMTP software, analyzed using the wavelet analysis to extract the useful fault features, and applied to the artificial neural networks (ANNs) for locating ungrounded shunt faults. A three-layer feed-forward ANN with Levenberg-Marquardt learning algorithm is used for the fault classification and fault location. One network is designed to classify the fault type and several ANNs related to each fault type are designed to locate the actual ungrounded fault position.

1.3 Fault Location Methods for Distribution Networks

The fault location techniques have been well developed and applied in transmission systems. However, relatively less research work has been conducted in the development of fault location approaches for distribution networks. An effective and accurate fault location algorithm is essential for electric power distribution networks to locate the fault point, improve the service reliability, ensure the customer power quality, and speed up the restoration process. Particularly, it appears more important for locating faults in underground distribution cables due to the complexities in electrical characteristics of cables, underground placement environment and wide applications in high density commercial districts.

Similarly, two principal techniques have been proposed for such methods, i.e., signal analysis and knowledge-based [12]. The former one is further classified into the approaches based on fundamental frequency phasor quantities and high frequency traveling waves. The knowledge-based and traveling wave-based techniques have been briefly discussed in Section 1.2.2.

The utility companies and researchers have been turning more and more attention to the location methods only using voltages and currents recorded at substation [34]. The fundamental phasor-based methods utilize and process the recorded voltages and currents to determine the fault point. Since the proposed algorithm is to use the fundamental phasors, the existing fundamental phasor-based methods would be discussed in this subsection.

The basic location methods, such as the reactance method and Takagi method, have been reviewed in [13], [14] and [35]. Ten most cited impedance-based fault location methods are compared, analyzed and tested, and thereafter the main problems existing in these methods are concluded [36]. The practical experience and the fault location systems used in utilities are introduced in [37] and [38]. Most of the previously proposed location techniques concern the location problem in overhead distribution lines, and a few of literatures discuss the algorithms for underground distribution cables. Twenty algorithms are selected, compared and summarized in Table 1.1 and Table 1.2. The specifications of the proposed algorithm are listed as well.

Table 1.1: Summary of Fault Location Methods for Distribution Networks – I

Fault Location Methods	Voltage and Current				Distribution Networks				
					Line / Cable				
	PrF	DF	PsF	Phasor or Sequence	Line Cable	Model	CAP	UTL	HOL
Srinivasan et al. [39]	√	√		Sequence	Line	Distributed	√		
Girgis et al. [40]	√	√		Sequence	Line	Lumped			√
Zhu et al. [41]	√	√	√	Phasor	Line	Lumped		√	√

**Table 1.1: Summary of Fault Location Methods for Distribution Networks – I
(Continued)**

Fault Location Methods	Voltage and Current				Distribution Networks				
	PrF	DF	PsF	Phasor or Sequence	Line / Cable				
					Line Cable	Model	CAP	UTL	HOL
Aggarwal et al. [42][43]	√	√		Superimposed Phasor	Line	Lumped			√
Das et al. [44][45]	√	√		Sequence	Line	Distributed	√		√
Novosel et al. [46]	√	√		Sequence	Line	Lumped			
Santoso et al. [47]	√	√		Sequence	Line	Lumped			√
Saha et al. [16][48][49]	√	√		Sequence	Line Cable	Lumped		√	√
Lee et al. [50]	√	√		Phasor	Line	Lumped		√	√
Jamali et al. [18]	√	√		Superimposed Sequence	Line	Distributed	√		√
Senger et al. [51]	√	√		Phasor	Line	Lumped		√	√
Yang et al. [20]	√	√		Sequence	Cable	Lumped	√		√
Salim et al. [52]	√	√		Phasor	Line	Lumped		√	√
Pereira et al. [53]	√	√		Phasor	Line	Lumped		√	√
Filomena et al. [15]	√	√		Phasor	Cable	Lumped	√	√	√
Morales-Espana et al. [54]		√		Phasor	Line	Lumped		√	√
Alamuti et al. [55]	√	√		Sequence	Line	Distributed	√		√
Mirzai et al. [56]	√	√		Superimposed Phasor	Line Cable	Lumped	√	√	√
Kawady et al. [17]		√		Sequence	Cable	Lumped	√		√
Liao [57]	√	√		Phasor	Line	Lumped		√	√

**Table 1.1: Summary of Fault Location Methods for Distribution Networks – I
(Continued)**

Fault Location Methods	Voltage and Current				Distribution Networks				
	PrF	DF	PsF	Phasor or Sequence	Line / Cable				
					Line Cable	Model	CAP	UTL	HOL
Proposed method in this work	√	√		Phasor	Cable	Two-layer π model by approx. distributed model	√	√	√

PrF: Prefault; DF: During Fault; PsF: Postfault; CAP: Capacitance; UTL: Untransposed Line; HOL: Heterogeneity of Lines.

Table 1.2: Summary of Fault Location Methods for Distribution Networks - II

Fault Location Methods	Distribution Networks					Additional Information
	Load			Other Techniques		
	Lateral Load Tap	Load Model	UBL	Load Estimation	Multiple Estimation	
Srinivasan et al. [39]	Tap	Static response				Iterative
Girgis et al. [40]	Both	Constant impedance	√			Iterative SLG
Zhu et al. [41]	Both	Current injection	√	Radial power flow ¹	Fault Diagnosis	Iterative PM
Aggarwal et al. [42][43]	Both	Voltage related	√			Iterative
Das et al. [44][45]	Both	Static response	√	Scaling	Fault indicator	Iterative
Novosel et al. [46]	Tap	Constant impedance				Iterative
Santoso et al. [47]	Both	Constant impedance	√			Extension of [40]

¹ Concept is mentioned with no reference and detail.

**Table 1.2: Summary of Fault Location Methods for Distribution Networks – II
(Continued)**

Fault Location Methods	Distribution Networks					Additional Information
	Load			Other Techniques		
	Lateral Load Tap	Load Model	UBL	Load Estimation	Multiple Estimation	
Saha et al. [16][48][49]	Both	Constant impedance	√		Eliminated	A set of algorithms
Lee et al. [50]	Both	Constant impedance	√		Current Pattern	Iterative
Jamali et al. [18]	Both	Constant impedance	√			Takagi's algorithm
Senger et al. [51]	Both	Constant impedance	√	Nominal TF rating	Ranked by possibility	
Yang et al. [20]	Tap	Constant impedance				Iterative SLG
Salim et al. [52]	Both	Constant impedance	√	Power flow [58]		Iterative
Pereira et al. [53]	Both	Constant impedance	√	Load flow analysis[59]		Iterative
Filomena et al. [15]	Both	Constant impedance	√	Power flow [58]		Extension of [52]
Morales-Espana et al. [54]	Both	Constant impedance	√		Eliminated	Iterative
Alamuti et al. [55]	Both	Constant impedance	√			Iterative
Mirzai et al. [56]	Both	Constant impedance	√	Load flow file	Current Pattern	Iterative
Kawady et al. [17]	Tap	Constant impedance	√			Iterative
Liao [57]	Both	Constant impedance	√			Analytical
Proposed method in this work	Both	Static response	√	State estimation by SQP	Eliminated	A set of iterative algorithms

UBL: Unbalanced Load; TF: Transformer; SLG: Single-Line-Ground; PM: Probabilistic Modeling.

The voltages and/or currents measured at substation are used in all selected methods. Most of them utilize the prefault and during-fault quantities.

The phasors, symmetrical components, and/or superimposed components of voltages and currents are employed. However, the usage of symmetrical components restricts its application to ideally balanced and transposed feeders, which is not true in a typical distribution network.

The location methods for cables should take the capacitance into account since the capacitance has significant effect on the voltage and current along cables and cannot be ignored.

The untransposed lines and cables are very normal in a distribution system, which makes the system unbalanced and restricts the application of symmetrical components.

Heterogeneity of feeders is characterized by the presence of multiple sections of different size and length of overhead lines and underground cables.

The distribution network is unbalance due to the presence of single-phase, double-phase and three-phase loads.

The laterals and tapped loads along the main feeder are presented in a typical distribution network.

The representative technical cruces, load models and line models in selected methods are concluded in the following subsections.

1.3.1 Technical Cruces in Selected Location Methods

The general logic principle in most of the selected algorithms, including the proposed one, is first to determine the fault point in a single plain line or cable with no laterals and tapped loads. Subsequently, the location algorithm is extended to distribution networks taking account of the presence of laterals, tapped loads, unbalanced loads, and heterogeneity of lines, etc.

Some very general fundamentals in the selected methods are somehow similar and behave like a technical crux in the development of the location algorithms. However, the principle and procedure of a specific method may appear considerable diversity, which depends on many factors, such as locating strategy and logic, assumptions, unknown variables, utilized quantities, applied line and load models, and particular application environment. Three mostly used cruces in the selected location methods are explained below. It should be mentioned that only the very basic fundamentals are introduced and the application details may have considerable diversity and can be referred to the related literatures.

1.3.1.1 Apparent Impedance-based

It is well known that the apparent impedance can be calculated by the voltages and currents of the faulty phase and/or zero sequence current. For example, the apparent impedance for an SLG fault in phase A can be expressed as,

$$Z_{app} = \frac{V_{select}}{I_{select}} = \frac{V_a}{I_a + kI_0} \quad (1.1)$$

and,

$$k = \frac{Z_0 - Z_1}{Z_1}$$

where Z_{app} is the apparent impedance, V_a is the phase A voltage, I_a is the phase A current, k is the compensating factor, I_0 is the zero sequence current, Z_0 and Z_1 are the zero and positive impedances of the line.

The KVL equation for V_a can be given as,

$$V_a = (I_a + kI_0)Z_1 + I_{comp}R_f \quad (1.2)$$

where R_f is the fault resistance, I_{comp} is the compensating current flowing through the fault resistance, which can be described as below for an SLG fault,

$$I_{comp} = 3I_0 \quad (1.3)$$

Therefore,

$$\frac{V_a}{I_a + kI_0} = Dz_1 + \frac{3I_0 R_f}{I_a + kI_0} \quad (1.4)$$

where D is the fault distance, z_l is the positive impedance per unit length.

There are two unknown real variables in Equation (1.4), i.e. D and R_f , and other variables can be measured at the substation or obtained from the database. The equation can be rewritten in terms of real and imaginary components so that the unknown variables can be solved.

The apparent impedance for other faults can be calculated accordingly. Basically, the apparent impedance-based technique is used in [40], [46], [47] and [17].

The impedance measurement principle is also used in [16], [48] and [49], and the real value nature of the fault resistance is employed to find the fault distance.

1.3.1.2 Direct Circuit KVL Equations-based

Taking an SLG in phase A as an example, the KVL equation describing the circuit between the sending terminal and the fault point can be given as,

$$\begin{bmatrix} V_a \\ V_b \\ V_c \end{bmatrix} = D \begin{bmatrix} z_{aa} & z_{ab} & z_{ac} \\ z_{ba} & z_{bb} & z_{bc} \\ z_{ca} & z_{cb} & z_{cc} \end{bmatrix} \begin{bmatrix} I_a \\ I_b \\ I_c \end{bmatrix} + \begin{bmatrix} I_f R_f \\ 0 \\ 0 \end{bmatrix} \quad (1.5)$$

where $V_{a,b,c}$ is the three-phase voltages, $I_{a,b,c}$ is the three-phase currents, I_f is the fault current, R_f is the fault resistance, D is the fault distance, z_{aa} is the self-impedance of phase A, z_{ab} is the mutual impedance between phase A and B, and so on.

The KVL equation for phase A can be expressed as,

$$V_a = D(z_{aa}I_a + z_{ab}I_b + z_{ac}I_c) + I_f R_f \quad (1.6)$$

where V_a is the phase A voltage, I_a , I_b , and I_c are the currents of phases A, B, and C.

In [41], [50], [51], [52], [15] and [56], the fault current or load current is first assumed or estimated, thus the fault distance D and the fault resistance R_f can be solved by two real equations, which are generated by separating Equation (1.6) into the real part and the imaginary part. Then, an iterative process is carried out to update the fault current or load current until a small tolerance is satisfied.

In [42] and [43], starting with a set of assumed fault distances and using the superimposed components, the KVL equations describing the circuit between the fault point and the receiving terminal are also formulated to determine the fault distance on the condition that there exists a minimal value of the difference between healthy phase currents around the exact fault point.

The equations are simplified on the assumption that the fault current is equal to the phase current [54].

1.3.1.3 Fault Resistance-based

The fault resistance is a non-negative real number, which can be used as a criterion to find the fault distance. Taking an SLG in phase A as an example, the imaginary part of fault resistance is given as,

$$\text{Imag}(R_f) = \text{Imag}\left(\frac{V_f}{I_f}\right) = \text{Imag}\left(\frac{V_{fp} + V_{fn} + V_{fz}}{I_{fp} + I_{fn} + I_{fz}}\right) = 0 \quad (1.7)$$

where R_f is the fault resistance, V_f is the fault voltage, I_f is the fault current, V_{fp} , V_{fn} , and V_{fz} are the positive, negative and zero sequence voltages at the fault point, I_{fp} , I_{fn} , and I_{fz} are the positive, negative and zero sequence fault currents.

Basically, an initial variable, for example, the fault distance, is first guessed or estimated, V_f and I_f can be estimated by the application of some skills, an iterative procedure is used

to calculate the mismatch between the new estimated variable and the old one, then the assumed variable is adjusted until a small tolerance is satisfied [39], [44], [45] and [55].

1.3.2 Summary of Line Model

An appropriate line model is required to obtain a more accurate location result. However, a distribution system consists of multiple sections of lines and cables with different types, sizes and lengths, which may result in the different model for each section. It seems inefficient to combine multiple line models into one fault location scheme. Therefore, the strategy and logic of a fault location method can determine the specific line model to be applied. The commonly used distribution feeder line models are reviewed in [60]. Two line models are normally used in the selected methods.

- Distributed parameter model is normally used to model long lines, considering the capacitive and inductive effects [61]. This model is used in [18], [39], [44], [45], and [55].

$$\begin{bmatrix} V_R \\ I_R \end{bmatrix} = \begin{bmatrix} \cosh(\lambda x) & -Z_c \sinh(\lambda x) \\ \frac{\sinh(\lambda x)}{Z_c} & -\cosh(\lambda x) \end{bmatrix} \begin{bmatrix} V_S \\ I_S \end{bmatrix} \quad (1.8)$$

and,

$$\lambda = \sqrt{(r + j\omega l)(g + j\omega c)}$$

$$Z_c = \sqrt{\frac{r + j\omega l}{g + j\omega c}}$$

where V_R and V_S are voltages at the receiving and sending terminals, I_R and I_S are currents at the receiving and sending terminals, x is the length of line section, λ is the propagation constant, Z_c is the surge impedance, r is the line resistance per unit length, l is the line inductance per unit length, g is the line conductance per unit length, and c is the line capacitance per unit length.

- Lumped parameters model is normally used to model short lines. A general model is also called π model as illustrated in Figure 1.1.

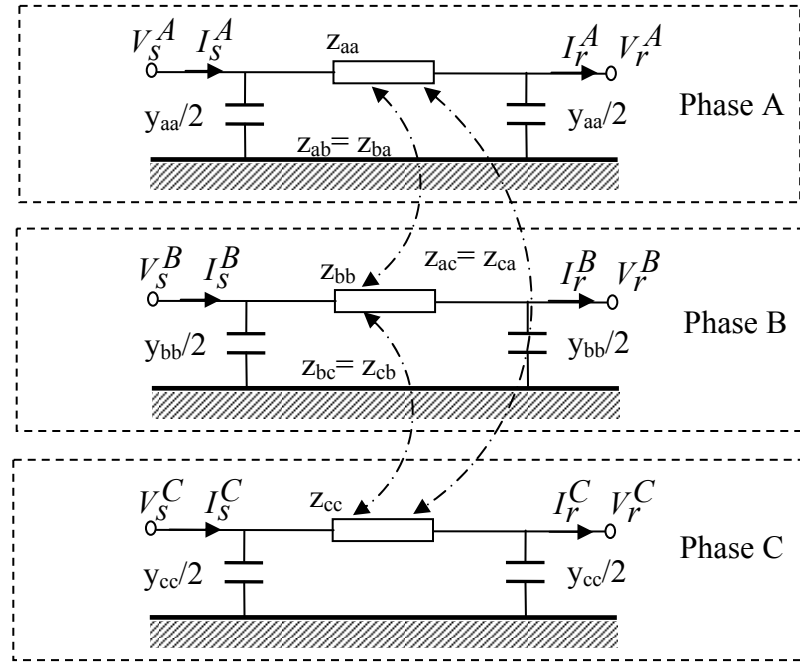


Figure 1.1: Lumped π line model.

The voltages and currents of a three-phase circuit can be described as,

$$\begin{bmatrix} V_r^A \\ V_r^B \\ V_r^C \end{bmatrix} = \begin{bmatrix} V_s^A \\ V_s^B \\ V_s^C \end{bmatrix} - \begin{bmatrix} z_{aa} & z_{ab} & z_{ac} \\ z_{ba} & z_{bb} & z_{bc} \\ z_{ca} & z_{cb} & z_{cc} \end{bmatrix} \begin{bmatrix} I_s^A \\ I_s^B \\ I_s^C \end{bmatrix} - \frac{1}{2} \begin{bmatrix} y_{aa} & 0 & 0 \\ 0 & y_{bb} & 0 \\ 0 & 0 & y_{cc} \end{bmatrix} \begin{bmatrix} V_s^A \\ V_s^B \\ V_s^C \end{bmatrix} \quad (1.9)$$

$$\begin{bmatrix} I_r^A \\ I_r^B \\ I_r^C \end{bmatrix} = \begin{bmatrix} I_s^A \\ I_s^B \\ I_s^C \end{bmatrix} - \frac{1}{2} \begin{bmatrix} y_{aa} & 0 & 0 \\ 0 & y_{bb} & 0 \\ 0 & 0 & y_{cc} \end{bmatrix} \left(\begin{bmatrix} V_r^A \\ V_r^B \\ V_r^C \end{bmatrix} + \begin{bmatrix} V_s^A \\ V_s^B \\ V_s^C \end{bmatrix} \right) \quad (1.10)$$

where $V_r^{A,B,C}$ and $I_r^{A,B,C}$ are voltages and currents at the receiving terminal, $V_s^{A,B,C}$ and $I_s^{A,B,C}$ are voltages and currents at the sending terminal, $z_{ab}, z_{ac}, z_{ba}, z_{bc}, z_{ca}$ and z_{cb} are the mutual impedances between three phases, z_{aa}, z_{bb} and z_{cc} are the self-impedances of three phases, y_{aa}, y_{bb} and y_{cc} are the shunt admittances of three phases.

If the capacitance is not considered, the above model can be simplified as,

$$\begin{bmatrix} V_r^A \\ V_r^B \\ V_r^C \end{bmatrix} = \begin{bmatrix} V_s^A \\ V_s^B \\ V_s^C \end{bmatrix} - \begin{bmatrix} z_{aa} & z_{ab} & z_{ac} \\ z_{ba} & z_{bb} & z_{bc} \\ z_{ca} & z_{cb} & z_{cc} \end{bmatrix} \begin{bmatrix} I_s^A \\ I_s^B \\ I_s^C \end{bmatrix} \quad (1.11)$$

$$\begin{bmatrix} I_r^A \\ I_r^B \\ I_r^C \end{bmatrix} = \begin{bmatrix} I_s^A \\ I_s^B \\ I_s^C \end{bmatrix} \quad (1.12)$$

The above model is used in [41], [50], [51], [52], [53], [15], [54], [56] and [57]. If all mutual impedances have the same value, the lumped model can be simplified as,

$$\begin{bmatrix} V_r^A \\ V_r^B \\ V_r^C \end{bmatrix} = \begin{bmatrix} V_s^A \\ V_s^B \\ V_s^C \end{bmatrix} - \begin{bmatrix} z_s & z_m & z_m \\ z_m & z_s & z_m \\ z_m & z_m & z_s \end{bmatrix} \begin{bmatrix} I_s^A \\ I_s^B \\ I_s^C \end{bmatrix} \quad (1.13)$$

where z_m is the mutual impedance and z_s is the self-impedance.

This model can be further transformed to the symmetrical components due to the balance nature of the impedance matrix. This model is used in [40], [42], [43], [46], [47], [16], [48], [49], [20] and [17].

1.3.3 Summary of Load Model

An appropriate load model is helpful for improving the location accuracy; however, it is not easy to get an accurate load model on account of the time-variant loads. Most methods use the constant impedance load model, which is independent of voltages and currents at load terminals. Besides, other three load models are also applied in some of the selected methods.

- The static response type models in Equation (1.14) have been found to satisfactorily explain the behavior of large composite loads at most points [39].

$$Y = G_r \left| \frac{V}{V_0} \right|^{n_p - 2} + jB_r \left| \frac{V}{V_0} \right|^{n_q - 2} \quad (1.14)$$

where Y is the load admittance, V is the voltage at the load point, V_0 is the nominal voltage, n_p and n_q are the response parameters for the active and reactive components of the load, G_r and B_r are the constants proportional to the load conductance and load susceptance.

The response parameters of n_p and n_q reflect the dynamic response of a particular type of customer load. The values can be selected to describe three types of loads as follows.

- $n_p = n_q = 0$ for constant power load.
- $n_p = n_q = 1$ for constant current load.
- $n_p = n_q = 2$ for constant impedance load.

It has been mentioned in [39] that the composite effect of many loads leads to n_p values in the range of 1.0 to 1.7 and n_q in the range of 1.8 to 4.5. The response parameters can be determined from the prefault data and hence can be assumed to be known [62]. The practical values of n_p and n_q for a particular type of load are suggested in [63].

With the known n_p and n_q , the values of G_r and B_r can be estimated by the following equation.

$$Y_r = \frac{I_r}{V_r} = G_r \left| \frac{V_r}{V_0} \right|^{n_p - 2} + jB_r \left| \frac{V_r}{V_0} \right|^{n_q - 2} \quad (1.15)$$

where I_r and V_r are the current and voltage at the load terminal.

The static response load model is used in [39], [44] and [45].

- A current injection load model is similar to the static response load model.

$$I = I_r \left| \frac{V}{V_0} \right|^{n_p - 2} + jI_i \left| \frac{V}{V_0} \right|^{n_q - 2} \quad (1.16)$$

where V_0 is the nominal voltage, I_r and I_i are the active and reactive current components which can be estimated by integrating energy consumption information stored in the customer database with the daily load patterns of customers [41].

- A voltage related load model is used in [42], [43].

$$Z_L = \frac{|V_L|^2}{M} \angle \cos^{-1} p_f \quad (1.17)$$

where V_L is the voltage at the load point, M is the nominal transformer rating, and p_f is the load power factor which varies typically from about 0.8 to 0.95.

1.3.4 Existing Limitations and Problems

The methods discussed in the referred papers may have one or more limitations and problems in the following aspects.

- Application of transformations. Due to the unbalanced circuit parameters, the whole circuit cannot be completely decoupled by the commonly used transformations.

- Presence of tap loads and laterals. The tap loads and/or laterals are not considered in some fault location algorithms.
- Heterogeneity of line sections. The heterogeneity of line sections is not considered in some fault location algorithms.
- Untransposed line. Most line and cable sections in a typical distribution network are not ideally transposed so that the usage of symmetrical components is not proper.
- Applications for underground cables. Most methods are applied for overhead lines in distribution systems. However, only very few papers discuss the applications for underground cables in distribution systems. The possibility and functionality is not discussed if the algorithms developed for overhead lines are applied in the cases of underground cables.
- Effect of capacitance. The capacitance in cables is relatively larger than that in lines, which would affect the voltage and current along the cable circuit.
- Effect of sheaths in cables. There exist the voltage and current in the metallic sheaths surrounding the core conductors.
- Effect of bonding methods. Five bonding methods are widely used, namely, single point bonding at sending terminal (SPBS), single point bonding at receiving terminal (SPBR), single point bonding at middle point (SPBM), solid bonding at both ends (SBBE), and cross bonding (XB). None of the published location algorithms considered all bonding situations.
- Problem of the multiple estimations. The present algorithms may find multiple fault points, which specially exist in the impedance-based location algorithms. In some papers, the multiple estimated points are ranked by possibilities [51], limited by fault indicators [44] and [45], or eliminated by the fault diagnosis techniques [41], [54] and [56].
- Estimation of loads. In order to ensure the accuracy and performance of the location algorithms in distribution networks, the techniques of load estimation, power flow

analysis or state estimation have to be applied. The load information can be acquired either by the power flow analysis or load estimation based on the real time measurements and historical load profile [15], [41], [52] and [53] where the existing analysis methods [58] and [59] are used, or by the scaling methods based on the real time measurements, load flow files and/or nominal transformer ratings [44], [51] and [56].

1.4 Distribution State Estimation Methods

The state estimation for distribution networks is an important application in the distribution management system (DMS) to provide the essential information for operation, management, control and planning in distribution networks. It also assists in the fault location algorithms by providing the necessary information of load flows and bus states (voltage magnitudes and phases).

The present distribution state estimation (DSE) methods are reviewed below since a DSE algorithm is proposed for underground distribution networks in this work.

Usually, the weighted least squares (WLS) technique is employed. Wan et al. proposed two WLS approaches to estimate loads in unbalanced power distribution networks [64], [65]. One is the WLS load parameter method to solve the constrained optimization problem where loads are treated as variables. The constrained optimization problem is transformed into an unconstrained problem by the exterior penalty method. The loads and voltages are estimated simultaneously. Incorporating the operating and loading constraints, the other one is a constrained WLS distribution state estimation-based method to estimate voltages by a constrained WLS DSE, then to estimate loads sequentially based on the estimated voltages.

Baran et al. proposed a three-phase state estimation method based on the WLS method in [66]. A two-stage algorithm is developed to overcome the observability problems associated with the branch current magnitude measurements. Rather than using nodal voltages as estimation variables, the branch currents are used as state variables in the state estimation to solve the WLS problem [67], where the Jacobian matrix is well

conditioned and can be decoupled on a phase basis. This method was substantially revised in [68] where a new algorithm with the constant gain matrix and a decoupled form was developed.

The problem of load estimation was formulated as a weighted least absolute values estimation problem and solved by WLS [69]. The Newton-Raphson approach is applied to eliminate the nonlinear effect of power losses.

In addition to WLS methods, the modified conventional algorithms were also proposed. Extending the work in [59], the custom-tailored Gauss-Seidel load flow analysis was proposed in [70]. A computationally efficient solution scheme based on the Newton-Raphson method was proposed in [71]. An algorithm was developed to build a constant Jacobian matrix [72] and the Newton-Raphson algorithm was also used to solve the load flow problem.

The load flow problem of a radial distribution system was formulated as a convex optimization problem, particularly a conic quadratic program [73]. The solution of the distribution load flow problem can be obtained in polynomial time using interior-point methods.

1.5 Objectives of the Thesis

The following objectives are proposed to be achieved during the course of this thesis:

- Design of the incipient fault detection scheme for distribution cables;
- Development of the fault location scheme for a medium voltage cable with no laterals;
- Design of the state estimation algorithm for underground distribution networks;
- Extension of the proposed location algorithm to underground distribution networks with the aid of the proposed state estimation algorithm.

1.6 Contributions of the Thesis

The contributions of the thesis are summarized as follows:

- A wavelet analysis-based method is developed to detect incipient faults in cables in time and frequency domains, additionally, identify transient and fault types, remove effect of noise and supervise almost entire cable circuit.
- A simple and practical algorithm based on the analysis of superimposed components and negative sequence is particularly designed to detect single-line-to-ground incipient faults in cables. The fewer thresholds and less computation are required.
- A two-layer π circuit is formulated and examined to approximate the behavior and characteristic of a typical medium voltage cable.
- A set of fault location algorithms are proposed for underground cables. The characteristics of underground cables in real systems are comprehensively considered and analyzed in the development of algorithms, such as the shunt capacitance, metallic sheath, heterogeneity and untransposition. The cable configurations and fault scenarios are taken into account as well, such as five bonding methods and three fault pathways. Besides, a large number of fault equations are solved effectively and efficiently and the fault resistance can be calculated.
- The state estimation for underground distribution networks is formulated as a nonlinear optimization problem and solved by the sequential quadratic programming technique. The characteristics and configurations of underground cables and distribution networks are considered in the development of the algorithm, such as the shunt capacitance, metallic sheath, bonding method, unbalance loads and presence of laterals and tapped loads.
- A section-by-section estimation algorithm combined with the backward/forward sweep algorithm is presented to estimate the nodal voltage and branch current for each circuit section in a distribution network with laterals and tapped loads.

- The combination of the fault location and state estimation algorithms is proposed to solve the fault location problem in distribution cables.
- The faulty section in distribution networks can be determined and the problem of multiple estimations is eliminated.
- Only the fundamental voltage and current phasors recorded at the single-end are utilized in the proposed fault location and state estimation methods.
- The performance and functionalities of the all proposed algorithms are examined and verified with the extensive simulations, considering various fault conditions and system configurations.

1.7 Scope of the Thesis

The thesis is organized in five chapters and two appendices. The first chapter outlines and compares the present methods in the fields of incipient fault detection for cables, fault location for cables, fault location for distribution networks and state estimation for distribution networks. The objectives, contributions and scope of the thesis are introduced and summarized as well.

Chapter 2 describes the development of the incipient fault detection algorithms for distribution cables. The basic concept of incipient faults in cables is first introduced and the model of arc is formulated. Then two algorithms are proposed, one is based on the wavelet analysis and the other is based on the analysis of the superimposed fault current and negative sequence current in time domain. Two test distribution systems, extensive simulation cases and field cases are investigated.

Chapter 3 focuses on proposing a set of fault location algorithms for underground medium voltage cables with no laterals. First, a series of the basic background knowledge is introduced. Then the principle and procedure of the location algorithms are specially explicated for a cable with sheaths grounded at the sending terminal. The differences and similarities of the algorithms for other bonding methods are compared and summarized as well. The estimation of constant load impedance is explained and the application of the

static response load model is also discussed. The extensive simulations are carried out and explained to demonstrate the accuracy and effectiveness of the proposed algorithms.

Chapter 4 is to extend the proposed fault location algorithms to underground distribution networks. Since the distribution state estimation is capable of providing the additional information for the fault location algorithms, this chapter includes two parts: development of a state estimation algorithm for underground distribution networks and extension of the proposed location algorithms to underground distribution networks with the aid of the proposed state estimation algorithm. The basic background knowledge is first introduced and the details of the proposed state estimation algorithm are discussed. Then a general location procedure combined with the state estimation is described as well. The algorithms are examined on a radial underground distribution network with different load and fault conditions.

Chapter 5 presents the conclusions and the suggested future works, followed by the list of references.

Appendices describe the supplement document and additional work performed during the course of this research. An example of traveling waves is illustrated in a spatiotemporal domain to demonstrate a clear process of the propagation and reflection of traveling waves in a transmission line. The voltage, current and resistance of an arc are also illustrated.

Chapter 2

2 Incipient Fault Detection Schemes for Distribution Cables

The incipient faults in underground cables are largely caused by voids in cable insulations or defects in splices or other accessories. This type of fault would repeatedly occur and subsequently develop to a permanent fault sooner or later after its first occurrence. Two algorithms are presented to detect and classify the incipient faults in underground cables at the distribution voltage levels. Based on the methodology of wavelet analysis, one algorithm is to detect the fault-induced transients, and therefore identify the incipient faults. Based on the analysis of the superimposed fault current and negative sequence current in the time domain, the other algorithm is particularly suitable to detect the single-line-to-ground incipient faults, which are mostly occurring in underground cables. Both methods are designed to be applied in real systems. Hence, to verify the effectiveness and functionalities of the proposed schemes, different fault conditions, various system configurations and real field cases are examined, and other normal operating transients caused by permanent fault, capacitor switching, load changing, etc., are studied as well.

The basic concept of incipient faults in cables is first introduced and the model of arc is formulated. Then the wavelet-based scheme is explained and the system structure, time sequence diagram, detection rules and classification rules are also discussed.

Subsequently, the details of the superimposed components-based scheme are presented. Two test distribution systems, extensive simulation cases, field cases, and simulation results are examined, where, more specially, the detailed detection process is explicated by analyzing four incipient faults recorded from real systems.

2.1 Background

2.1.1 Incipient Faults in Cables

Underground cables may first experience incipient faults for an unpredicted duration before they fail into permanent faults. Usually, incipient faults in power cables are

gradually resulted from the aging process, where the localized deterioration in insulations exists. The local defect or void initiates a process such that the insulation damage spot can propagate through a section of the insulation, branch into channels, and evolve to a tree-shape damage area. Two trees are mostly observed, i.e. water tree (WT) and electrical tree (ET).

The water tree in insulation can initiate from a water-filled microcavity and would be growing under the influence of moisture and electric field [74]. The voltage drop on a water tree is quite small compared to the voltage across the dry insulation surrounding it since the insulation at the water tree area has a higher conductivity. The progress of water trees is permanent and there is no detectable partial discharge existing in water trees.

The electrical tree can initiate from a point of high stress due to a local defect and/or water tree in dry dielectrics and propagate relatively quickly through the insulation due to the repetitive partial discharges [75]. The formation of electrical trees would lead to final cable failure sooner or later within a relatively short time.

The example of water tree and electrical tree are shown in Figure 2.1, which are cited from [76].

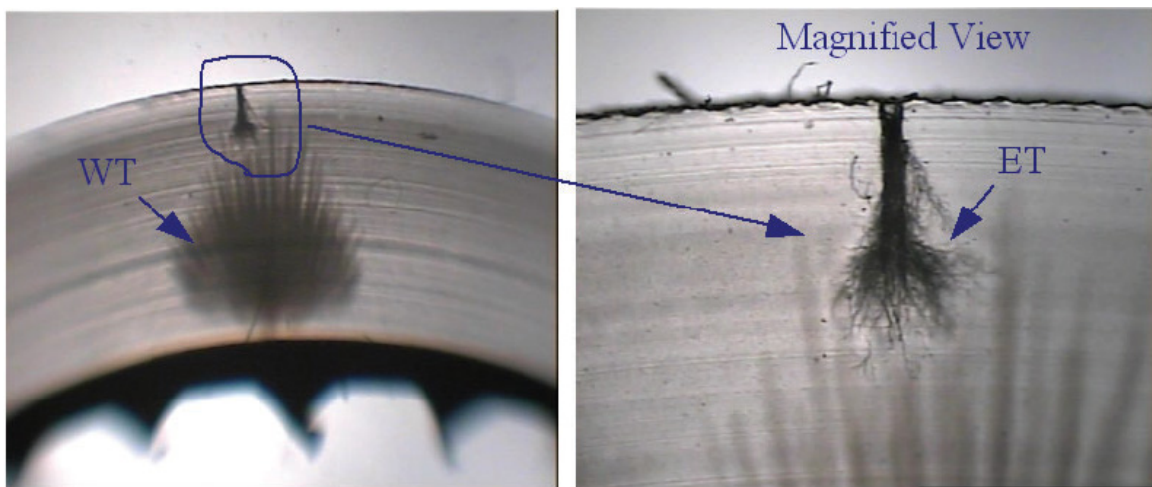


Figure 2.1: Illustrations of water tree (WT) and electrical tree (ET) [76].

Overall, electrical overstress in conjunction with mechanical deficiency, unfavorable environmental condition, and chemical pollution, can cause the irreparable and irreversible damages in insulations. The details of the inception of aging and propagation mechanisms are explained in [77].

The formation of electrical trees would generate partial discharges, which can be considered as the early stage of incipient faults before the condition of insulation gets worse. The partial discharge is characterized by a series of short discharge current pulses with the width of about one nanosecond and with the time interval of several tens of nanoseconds between successive discharges. Therefore, the detection of early cable defects or failures can be classified into two categories: detection of partial discharges and detection of incipient faults. Both of them are concerned by the utility companies, and the power protection engineers would pay more attention on the latter one. The proposed method is also directly associated with the latter one.

Incipient faults are normally characterized as the faulty phenomena with the relatively low fault currents and the relatively short duration ranging from one-quarter cycle to multi-cycle. These short lasting current variations cannot be detected by the traditional distribution protection schemes because of their short duration and low increment in magnitude. However, such faults must be detected at the early stage to avoid the consequent catastrophe induced by the degradation themselves. The field experience and laboratory experiments of incipient faults are investigated in [78], [79].

In underground cables, the incipient fault is one type of transients in power systems, which is prone to an intermittent arc fault. The typical incipient faults are composed of two types: sub-cycle incipient fault and multi-cycle incipient fault. The sub-cycle incipient fault always occurs near a voltage peak where arc is ignited, lasts around one-quarter cycle, and self-clears when the current crosses zero. Figure 2.2 shows the three-phase feeder currents when a sub-cycle incipient fault occurs between phase A and ground at the 2 km location of a 9 km cable in the first test system in Section 2.4.2. The multi-cycle incipient fault also likely occurs near a voltage peak, lasts 1-4 cycles, and

self-clears when arc is quenched. The waveforms of the currents for such a fault are shown in Figure 2.3.

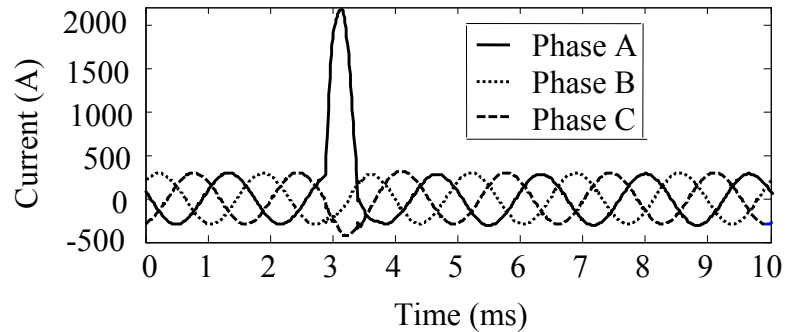


Figure 2.2: Sub-cycle incipient fault.

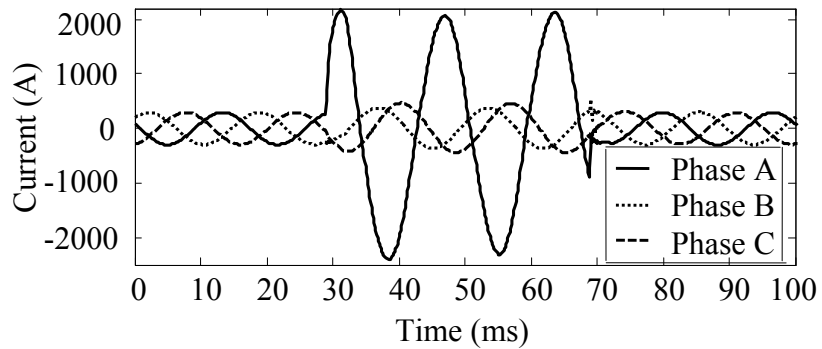


Figure 2.3: Multi-cycle incipient fault.

2.1.2 Model of Arc

The incipient fault is prone to the intermittent arc fault in underground cables. The model of arc is essential to effectively process the arcing fault analysis. A series of arc models is introduced in [80]-[85]. It has been commonly recognized in the theory and experiments that the nature of arc manifests itself in the nonlinear and time-varying variation that would produce high frequency components. In turn, the waveform of arc voltage is distorted into a near square wave.

Due to the simple implementation and good representation of the arc properties, the Kizilcay's model [85] is the mostly used model in arcing faults analysis [86], where the arc can be represented by a time-varying nonlinear resistance. Accordingly, this model is selected in this work and presented as below.

The arc conductance is given as,

$$\frac{dg}{dt} = \frac{1}{\tau} (G - g) \quad (2.1)$$

where τ is the arc time constant, g is the instantaneous arc conductance, and G is the stationary arc conductance.

The stationary arc conductance is defined as,

$$G = \frac{i_{arc}}{u_{st}} \quad (2.2)$$

$$u_{st} = u_0 + r_0 |i_{arc}| \quad (2.3)$$

where i_{arc} is the current flowing through arc.

The arc time constant is defined as,

$$\tau = \tau_0 \left(\frac{l_{arc}}{l_0} \right)^\alpha \quad (2.4)$$

where τ_0 is the initial time constant, l_0 is the initial arc length, and α is the coefficient of negative value.

The elongation speed of the arc is given as,

$$\frac{dl_{arc}}{dt} = \frac{7l_0}{\frac{0.2}{v_{max}} v_{th}^{+0.2}} \quad (2.5)$$

where v_{ih} is the instantaneous value of voltage at the inception instant, and v_{max} is the maximum magnitude of voltage at the normal condition.

An example of Kizilcay's arc model is shown in Appendix B.

2.2 Wavelet-based Detection Scheme

2.2.1 Principles

It is well known that the wavelet analysis has an attractive function of analyzing electromagnetic transients in power systems [87]. The wavelet analysis can analyze the physical situations where signals contain discontinuities, abrupt changes and sharp spikes, and then separate different frequency components into different frequency bands. More specifically, the wavelet analysis can decompose the measured signal into the low frequency approximation coefficients to represent the fundamental frequency component and the high frequency detail coefficients to express the transient state. The detailed process of the decomposition and implementation of the wavelet analysis are explained in [87]. Since the mother wavelet of 'Daubechies 4' has good performance in capturing the fast transient in power systems [88], the signals in this paper are decomposed and analyzed by this mother wavelet [89]. The fault current in Figure 2.3 is decomposed into three levels by the mother wavelet of 'Daubechies 4', as shown in Figure 2.4.

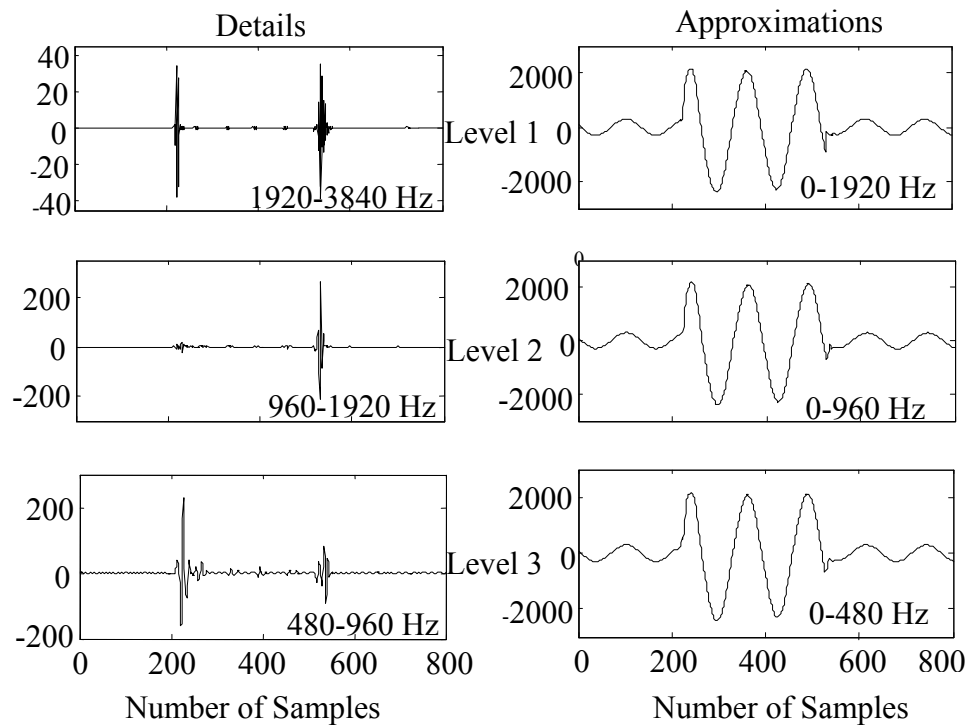


Figure 2.4: Detail and approximation coefficients after wavelet decomposition and reconstruction.

It is apparent that there exist the remarkable changes in the detail coefficients at the moments of the inception and termination of the transient. This phenomenon can be utilized to detect the presence of the transient. The small spikes, locating among the two large changes in the detail coefficients in the level one, represent the process of arc reignition and extinction.

2.2.2 System Description

The proposed system is to detect the transient first, classify the transient type, and thus identify the incipient fault in real time. The emphasis is to detect the incipient fault, which does not trigger the conventional relays since the fault current is relatively low and the duration is relatively short. The designed system is desired to be embedded in the existing numerical relay, therefore, only the sampled currents are utilized and the sampling rate is 64 samples/cycle.

The system is comprised of two modules, detection module and classification module. The wavelet analysis is applied in the detection module to detect the inception of any transients. The classification module is to identify the transient type and find the incipient fault as required. The detailed detection and classification procedure is introduced in Figure 2.5, and the principles of the detection and classification will be explained in the next subsections.

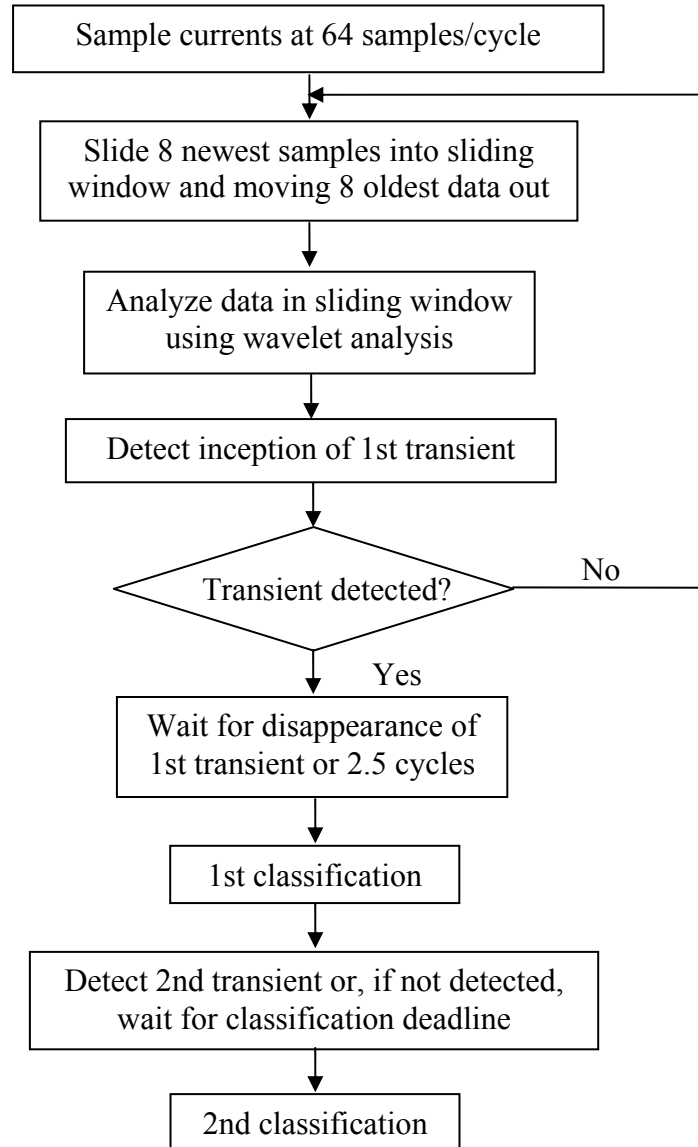


Figure 2.5: Flowchart of detection and classification procedures.

The detection module includes two detection steps. The first step is to detect the inception of transient, and the second is to recognize the possible subsequent transient, such as the breaker operation, end of incipient fault, and arc quench, etc.

The classification module also includes two steps. The first step is to pre-classify the transient type at the moment of the disappearance of the first transient or 2.5 cycles later than the inception of the first transient. This pre-classified result is not definitely correct because some events may have the similar initial transient phenomena after the occurrence of the first transient. Hence, the second classification is applied to revise the previous result at the moment of the disappearance of the second detected transient or at the moment of the preset deadline time. Usually, the deadline time can be set up as 4 or 5 cycles after the first transient is detected.

The time sequence diagram of the detection and classification procedures is shown in Figure 2.6. Two examples are illustrated in Figure 2.7 and Figure 2.8 to give a more visualized demonstration.

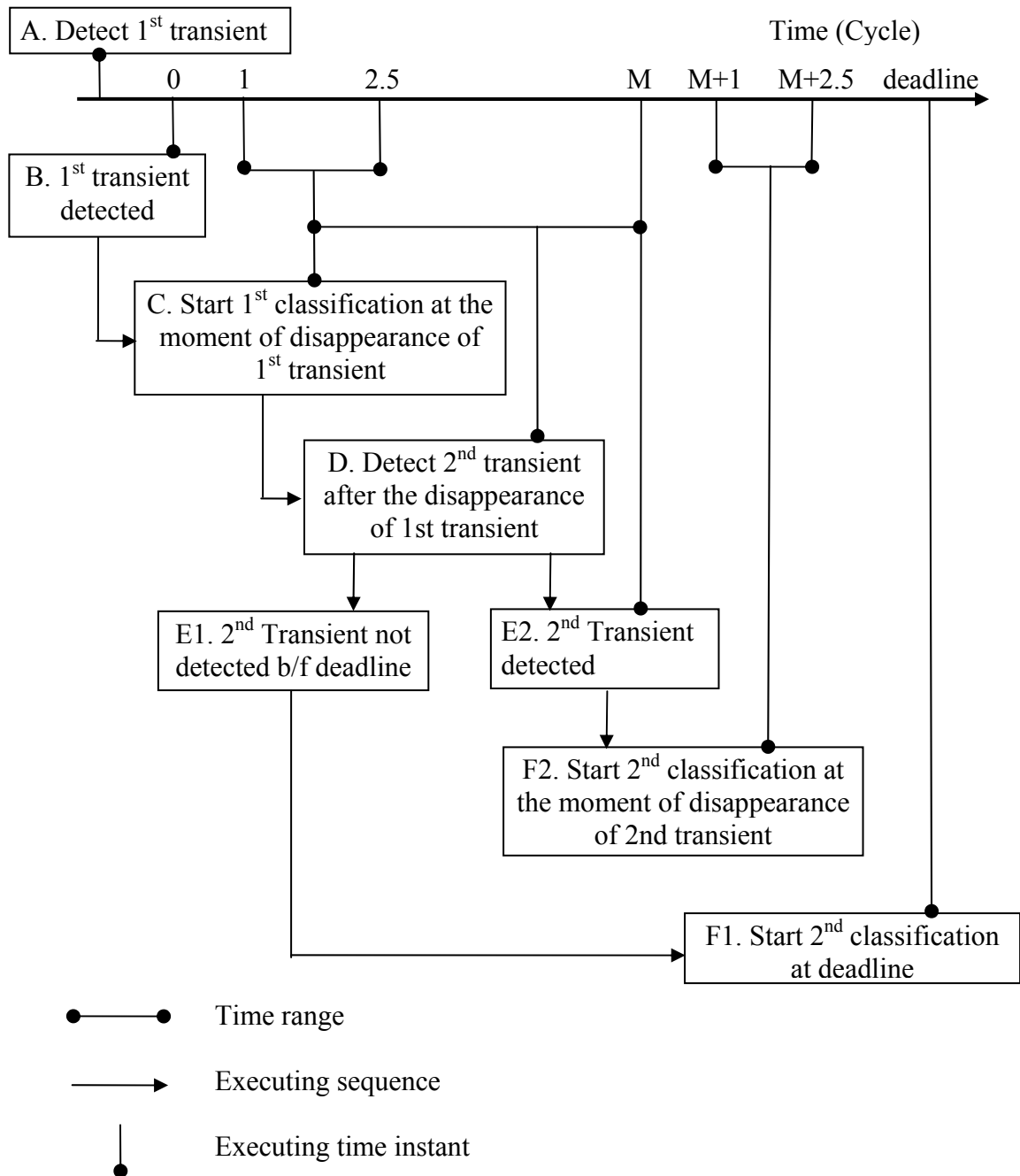
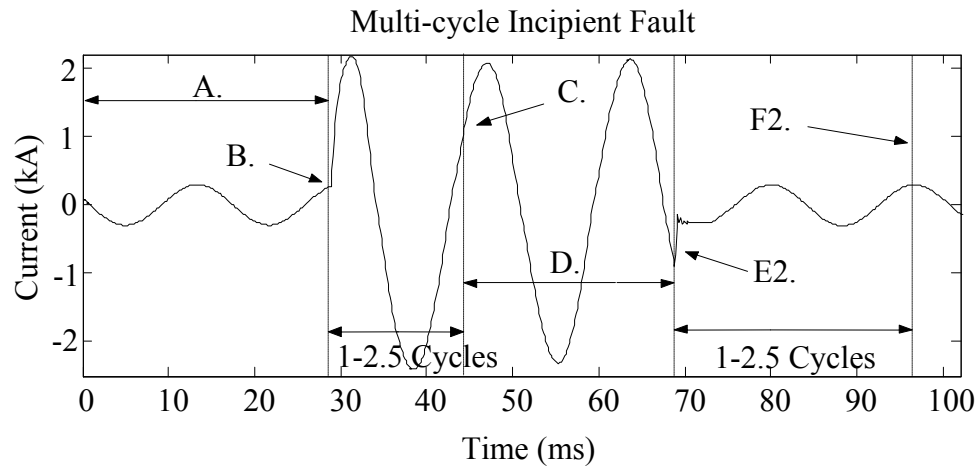
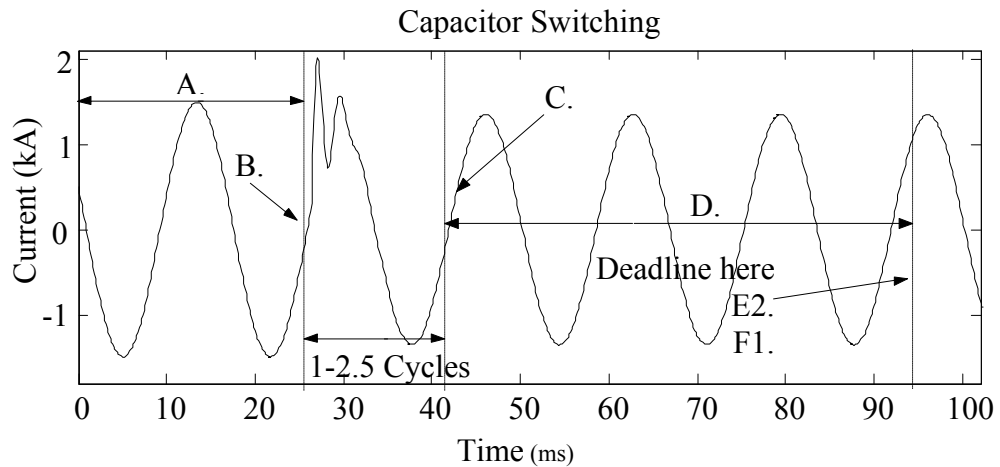


Figure 2.6: Time sequence diagram.



- | | |
|--|---------------------------------------|
| A. Detect 1 st Transient | B. 1 st Transient Detected |
| C. 1 st Classification | D. Detect 2 nd Transient |
| E2. 2 nd Transient Detected | F2. 2 nd Classification |

Figure 2.7: Feeder current for the event of multi-cycle incipient fault.



- | | |
|--------------------------------|---------------------------|
| A. Detect 1st Transient | B. 1st Transient Detected |
| C. 1st Classification | D. Detect 2nd Transient |
| E2. 2nd Transient Not Detected | F1. 2nd Classification |

Figure 2.8: Current for the event of capacitor switching.

2.2.3 Detection and Classification Rules

After the decomposition by the wavelet analysis, the measured currents are divided into the different frequency bands. The detail coefficients in the high frequency band and approximation coefficients in the low frequency band are used for the detection and classification respectively.

2.2.3.1 Detection Rules for 1st Detection

Two rules are involved in the first detection. The transient would be detected if either one is triggered.

Rule W1: This detection rule processes the detail coefficients in the frequency band of 240-960Hz and is less related to the fundamental frequency. If Equation (2.6) is satisfied, then a transient is detected.

$$ENGR = \frac{Energy_{latest} - MEAN(Energy_{past})}{STD(Energy_{past})} > threshold \quad (2.6)$$

where $Energy_{latest}$ is the energy of the latest detail coefficients, $Energy_{past}$ is an array of the energy of the past detail coefficients, $MEAN$ is the average function, and STD is the standard deviation function.

In the low noise environment, most transients can be detected by this rule. It can capture the abrupt changes, singularities, and short duration spikes, which contain the large energy in the high frequency domain. It is insensitive to the slow change of fundamental frequency because it does not consider the low frequency component. Although noise may also have the energy to a certain extent, this rule has partially eliminated this negative effect to avoid the false detection. However, the heavy noise may still cause the missing detection.

Rule W2: This detection rule processes the approximation coefficients in the frequency band of 0-240Hz and is less related to the high frequency components. If Equation (2.7) is satisfied, then a transient is detected.

$$RMSCR = \left| \frac{RMS_{latest\ half\ cycle} - RMS_{one\ cycle\ before}}{RMS_{one\ cycle\ before}} \right| > threshold \quad (2.7)$$

where RMS is the root mean square value.

In the high noise environment, most transients can be detected by this rule. It can capture the abrupt and slow continuous changes in amplitude. It is not related to the high frequency components, so it is insensitive to the heavy noise. This rule would result in a short detection delay.

2.2.3.2 Classification Rules for 1st Classification

Rule WA: RMS ratio of the approximation coefficients between the prior-transient stage and post-transient stage.

$$RMSR = \frac{RMS_{post-transient}}{RMS_{prior-transient}} \quad (2.8)$$

Rule WB: Balance of RMSR in three phases.

$$BRMSR = \frac{MAX(RMSR)}{MIN(RMSR)} \quad (2.9)$$

Rule WC: Ratio of maximum amplitude.

$$MAR = \frac{MAX(AMPLITUDE_{post-transient})}{MAX(AMPLITUDE_{prior-transient})} \quad (2.10)$$

where RMS is the root mean square value, MAX is the maximum value, and MIN is the minimum value.

When the values of $RMSR$, $BRMSR$, and MAR fall into some particular zones, the combination of three rules can approximately determine the transient type. However, some transients, for instant, the multi-cycle incipient fault and permanent fault, have very

similar phenomena during a short interval after the inception, therefore, the exact transient type will be confirmed by the second classification.

2.2.3.3 Detection and Classification Rules for 2nd Step

Rule W1 in the second stage is exactly same as the one in the first stage, even the thresholds can be kept the same. Rule W2 is similar to the one in the first stage, only differing in less than a predetermined threshold.

Rule WA and Rule WB in this stage are the same as the ones in the stage of the first classification. Rule WC is very similar to Rule WA, while the latter one is less than a threshold and the former is greater than a value.

After being classified by this stage, the transient type can be identified determinedly.

2.2.4 Thresholds

To set the thresholds, the meaning and behavior of the relative detection or classification rule is analyzed. Then, based on the qualitative analysis, an appropriate value is selected while considering two opposite aspects, i.e., robustness and sensitivity. To decrease the false alarm and misclassification, it is desired that the approach is robust to noise, disturbance, or variations in parameters, structures, and system conditions. To decrease the missing detection, the sensitivity to changes in signals is required. Since the proposed algorithm is designed to be applied in real systems, the effect of variations, which inherently exist in different systems, has the higher priority to be taken into account. Therefore, the principal consideration in the threshold setting is to reduce the false alarm and misclassification while sustaining the satisfactory detection accuracy.

The simulations assist in the setting process. Moreover, large numbers of simulations are performed to verify the validity of the established thresholds. It should be mentioned that the same thresholds are used for all simulation cases and field cases. Therefore, it is safe to say that the values in this work can be used as a group of the reference values and slightly adjusted according to the particular application environment and the requirement of utility companies. The meanings of the thresholds or behaviors of the rules are explained below.

The threshold in Rule W1 shows the changing tendency of the energy in the high frequency domain.

The threshold in Rule W2 indicates the changing percentage of the current RMS value in the low frequency domain.

Rule WA assigns two zones representing the changing ratio of the current RMS value.

Rule WB also defines two zones expressing the balance degree among the changing ratios of three-phase currents.

Rule WC establishes two zones describing the ratio of the peak value between the post-transient current and prior-transient current. Since noise has been eliminated from the approximation coefficients after the wavelet analysis, this rule can identify abrupt changes, especially for short duration spikes.

2.3 Superimposed Components-based Detection Scheme

Utilizing the superimposed fault current and negative sequence current in time domain, an algorithm is developed to be embedded into the existing relays by easily upgrading the firmware so that the new functionality is supported.

Most faults are of SLG type in distribution cables. Therefore, this scheme is particularly designed to detect an SLG incipient fault. Only three steps are included in this scheme, namely, detection of transient inception, selection of faulty phase and classification.

2.3.1 Detection of Transient Inception

Two rules are used together to detect the transients. Rule S1 is related to the negative sequence current and superimposed fault current. Rule S2 is to find the magnitude of the superimposed fault current at the power frequency. The detection algorithm is independent to the transformer winding connections, CT locations, and balance of three-phase load currents.

$$\begin{aligned}
i_{\Delta,j}(k) &= i_j(k) - i_j(k-2N) \\
i_{NEG,A}(k) &= i_A(k) + i_B(k-N/3) - i_C(k-N/6) \\
i_{NEG,B}(k) &= i_B(k) + i_C(k-N/3) - i_A(k-N/6) \\
i_{NEG,C}(k) &= i_C(k) + i_A(k-N/3) - i_B(k-N/6) \\
E_j(k) &= \sqrt{\frac{1}{N/2} \sum_{k=1}^{N/2} (i_{NEG,j}(k) - i_{\Delta,j}(k))^2} \quad (2.11) \\
I_{\Delta mg,j} &= \text{MAG}(\text{FFT}(i_{\Delta,j}(k-N+1:k))) \\
E_j(k)/I_{\Delta mg,j}(k) &< K_{11} \quad \text{-- Rule S1} \\
I_{\Delta mg,j}(k) &> K_{12} \quad \text{-- Rule S2} \\
j &= A, B, C
\end{aligned}$$

where N is the number of samples in one cycle, MAG is the magnitude value, i_{Δ} is the superimposed fault current, i_{NEG} is the negative sequence current, K_{11} and K_{12} are the thresholds, and $I_{\Delta mg}$ is the magnitude of the superimposed fault current at the power frequency, which is extracted by the Discrete Fourier Transform (DFT) [90].

The unbalanced fault or unbalanced load will cause the occurrence of the negative sequence current, which is calculated in time domain in Equation (2.11) and it can also be calculated in frequency domain by using phasors extracted by DFT. The neutral current is not used due to its availability in some transformer winding connections.

The examples of waveforms of different events obtained by Rule S1 and Rule S2 are illustrated in Figure 2.9 to Figure 2.22, where the currents are sampled from the feeder.

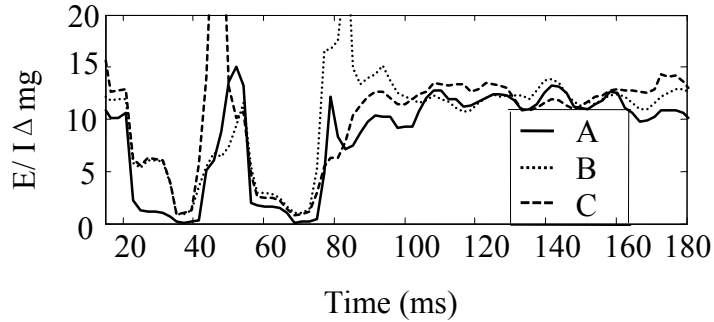


Figure 2.9: Waveforms from Rule S1 – Phase-A-ground sub-cycle incipient fault.

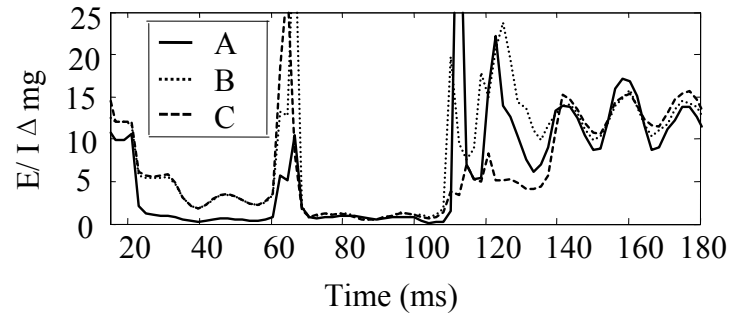


Figure 2.10: Waveforms from Rule S1 – Phase-A-ground multi-cycle incipient fault.

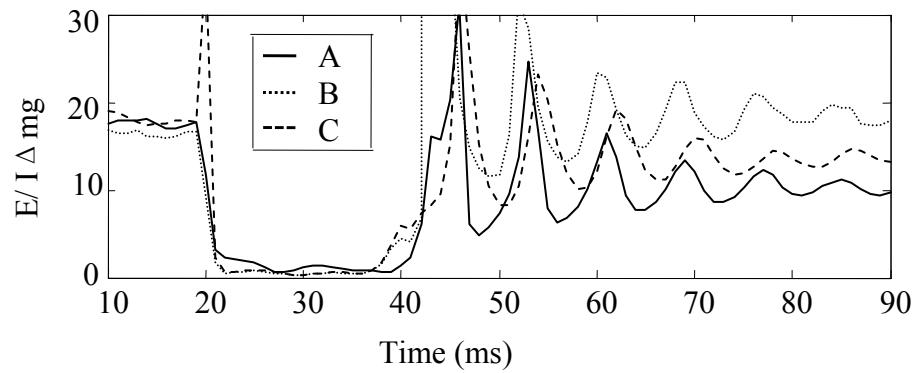


Figure 2.11: Waveforms from Rule S1 – Phase-A-ground permanent fault.

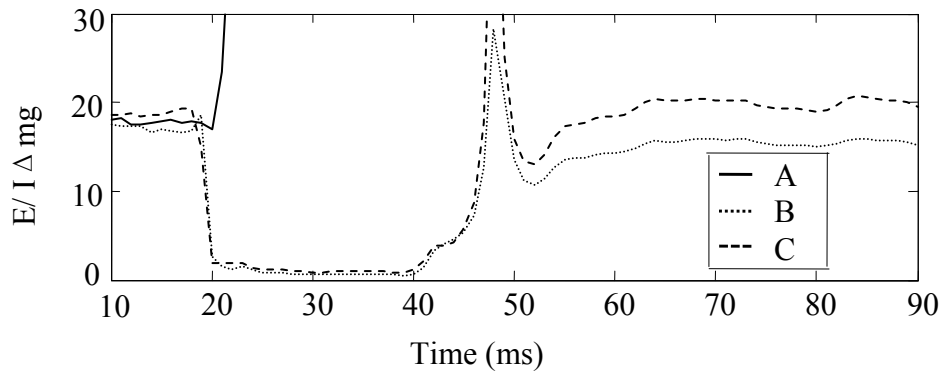


Figure 2.12: Waveforms from Rule S1 – Phase-B-C permanent fault.

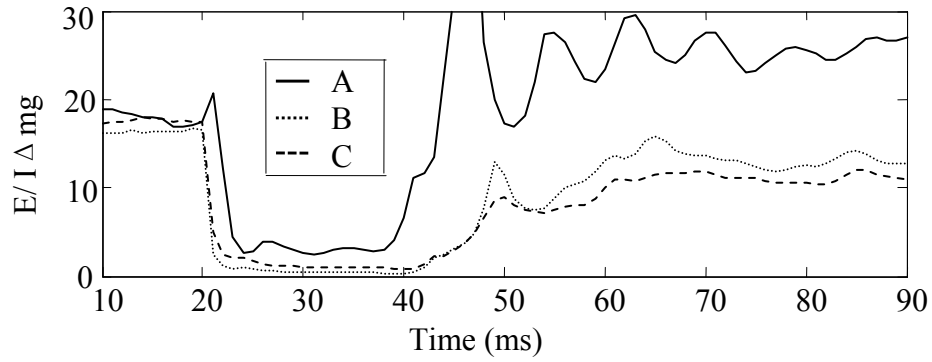


Figure 2.13: Waveforms from Rule S1 – Phase-A-B-ground permanent fault.

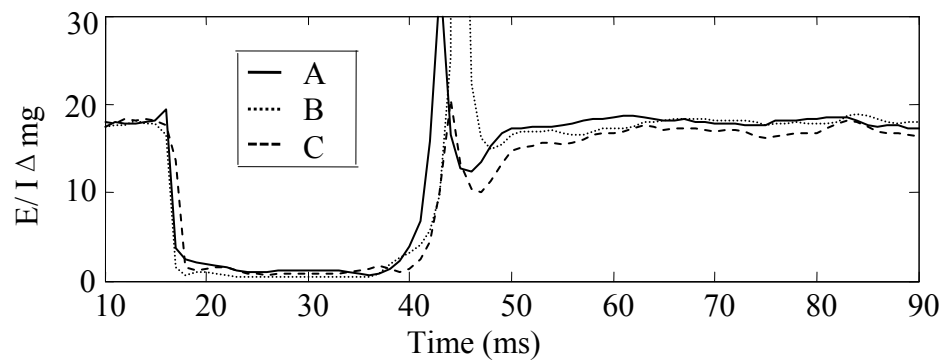


Figure 2.14: Waveforms from Rule S1 – Three-phase-ground permanent fault.

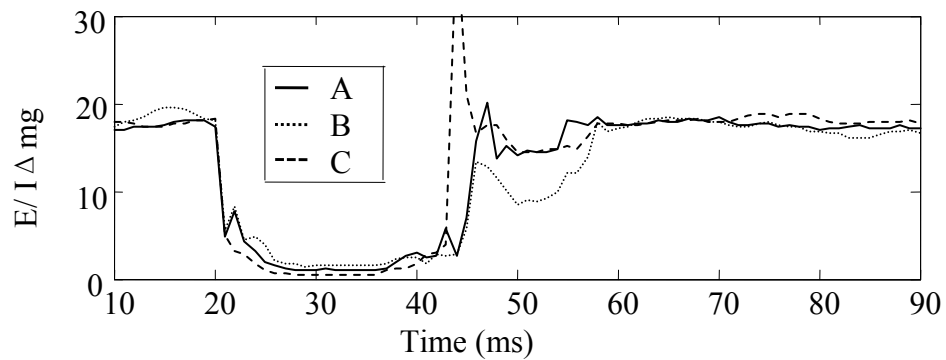


Figure 2.15: Waveforms from Rule S1 – Capacitor switching.

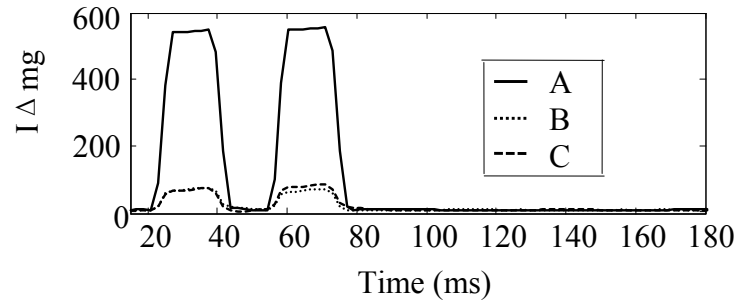


Figure 2.16: Waveforms from Rule S2 – Phase-A-ground sub-cycle incipient fault.

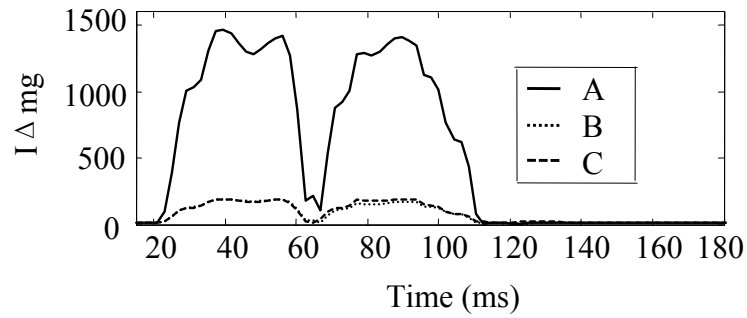


Figure 2.17: Waveforms from Rule S2 – Phase-A-ground multi-cycle incipient fault.

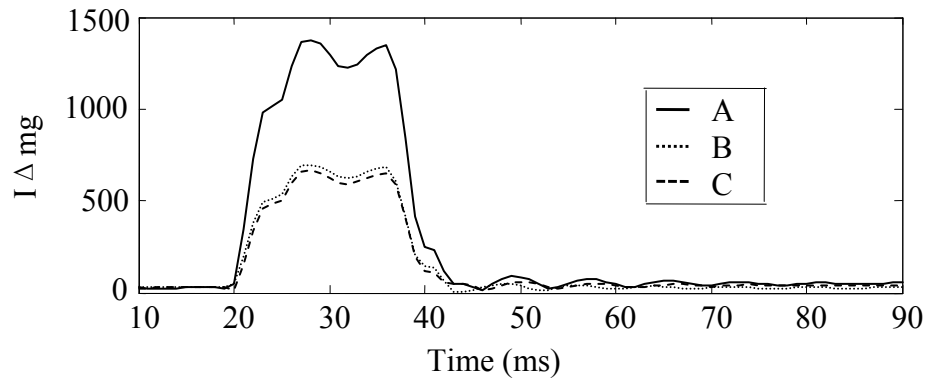


Figure 2.18: Waveforms from Rule S2 – Phase-A-ground permanent fault.

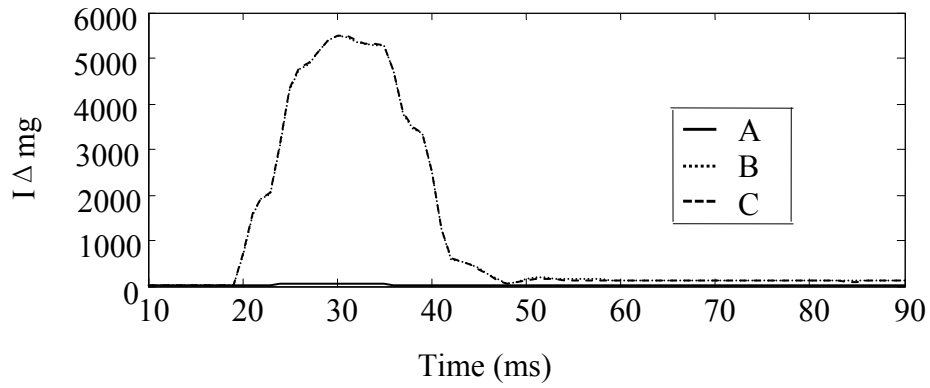


Figure 2.19: Waveforms from Rule S2 – Phase-B-C permanent fault.

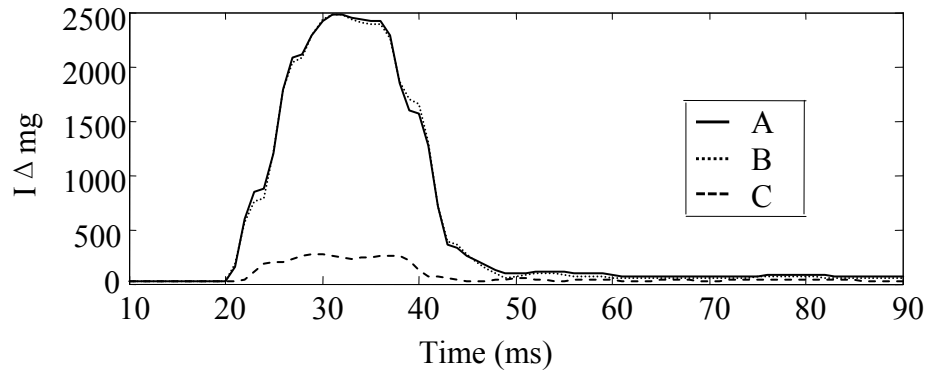


Figure 2.20: Waveforms from Rule S2 – Phase-A-B-ground permanent fault.

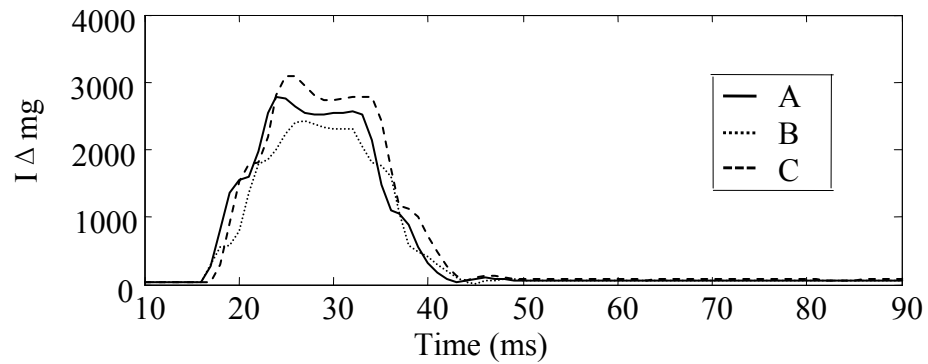


Figure 2.21: Waveforms from Rule S2 – Three-phase-ground permanent fault.

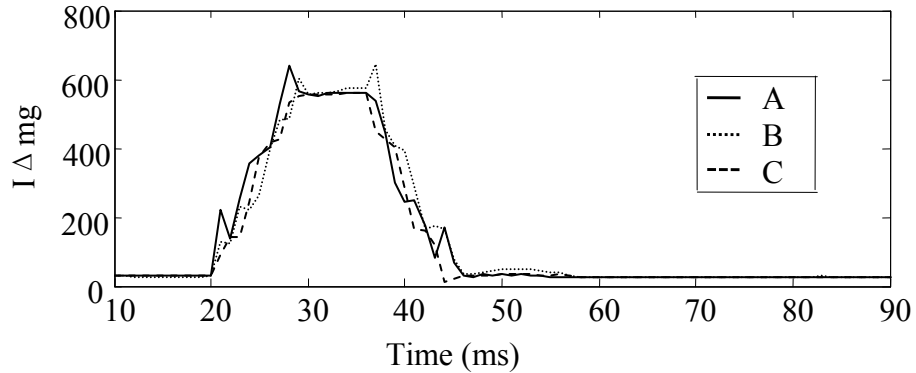


Figure 2.22: Waveforms from Rule S2 – Capacitor switching.

Apparently, when a transient occurs, the quantities obtained by Rule S1 would decrease to small values, on the other hand, the quantities obtained by Rule S2 would increase to large values. Then, this transient can be detected, however, only the transient type of SLG fault is considered and this fault type needs to be determined.

2.3.2 Selection of Faulty Phase

After the inception of the transient is detected, the faulty phase needs to be selected. By observing the waveforms obtained from Rule S2 in Figure 2.16-Figure 2.22, it is obviously shown in Figure 2.16 and Figure 2.17 that $I_{\Delta mg}$ of the faulty phase appears to be more than three times larger value compared to those of other two healthy phases when an SLG fault occurs. This phenomenon is especially unique for the SLG fault, which can be employed to select the faulty phase.

When the currents are sampled from the feeders or secondary side of transformer, Rule S3(a) is applied.

$$\begin{aligned}
 & MAX(I_{\Delta mg,j}) / MEDIUM(I_{\Delta mg,j}) > K_2 \quad j = A, B, C \\
 & Phase \ with \ MAX(I_{\Delta mg,j}) \ is \ Faulty \ Phase \quad - \ Rule \ S3(a)
 \end{aligned} \tag{2.12}$$

where $I_{\Delta mg}$ is the magnitude of the superimposed fault current, MAX is the maximum value, and $MEDIUM$ is the medium value in three-phase superimposed currents.

The Rule S3(a) can be applied for the situations where CTs are installed at the low side of transformer and feeders, and the transformer connections have no effect on this rule. However, when CTs are installed at the primary side of transformer, the selection rule needs to be modified accordingly.

When currents are sampled from the primary side of transformer and the transformer connection is Δ/Y_0 , $I_{\Delta mg}$ will have large changes in two phases in the case of SLG fault. And the changing degrees in two phases are almost same, shown in Figure 2.23. For other fault types, no similar phenomena can be observed.

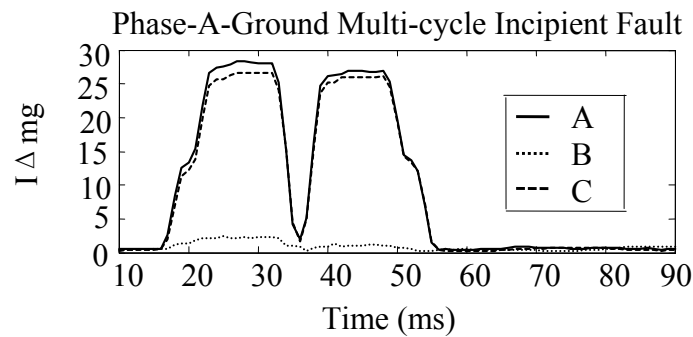


Figure 2.23: Waveforms of $I_{\Delta mg}$ (Phase-A-ground multi-cycle fault, primary side, Δ/Y_0).

Therefore, the selection rule can be defined in Equation (2.13) for the cases with the winding of Δ/Y_0 .

$$\begin{aligned}
 & MAX(I_{\Delta mg,j}) / MEDIUM(I_{\Delta mg,j}) < K_{23} \\
 & MEDIUM(I_{\Delta mg,j}) / MIN(I_{\Delta mg,j}) > K_{24} \quad j = A, B, C \\
 & \text{If } A \& B \text{ have larger values, Phase B is Faulty Phase} \\
 & \text{If } B \& C \text{ have larger values, Phase C is Faulty Phase - Rule S3(c)} \\
 & \text{If } C \& A \text{ have larger values, Phase A is Faulty Phase}
 \end{aligned} \tag{2.13}$$

where $I_{\Delta mg}$ is the magnitude of the superimposed fault current, and MAX , $MEDIUM$, MIN are the maximum, medium, and minimum values.

When currents are sampled from the primary side of transformer and the transformer connection is Y/Y_0 , $I_{\Delta mg}$ will have large changes for all three phases in the cases of SLG fault and three-phase-ground fault (3LG). And the changing degrees in three phases are almost same as shown in Figure 2.24. For other fault types, no similar phenomena can be observed.

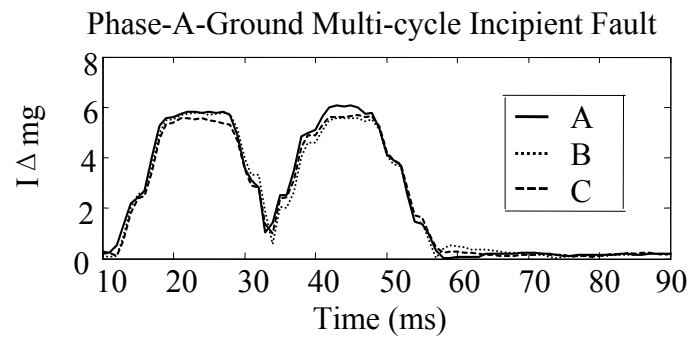


Figure 2.24: Waveforms of $I_{\Delta mg}$ (Phase-A-ground multi-cycle fault, primary side, Y/Y_0).

To further distinguish the SLG and 3LG, the amplitude of fault currents can be utilized. For a 3LG fault, the amplitudes of three-phase currents will change in the same direction shown in Figure 2.25, while the SLG fault will cause currents change in different directions shown in Figure 2.26.

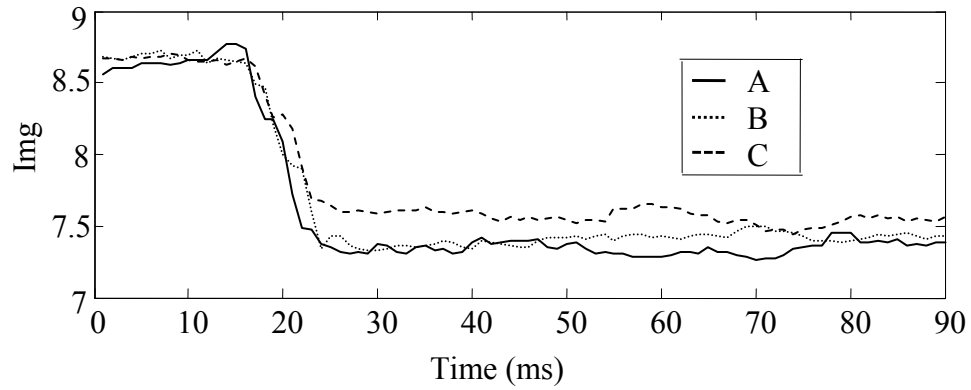


Figure 2.25: Amplitude of currents (3LG, primary side, Y/Y₀).

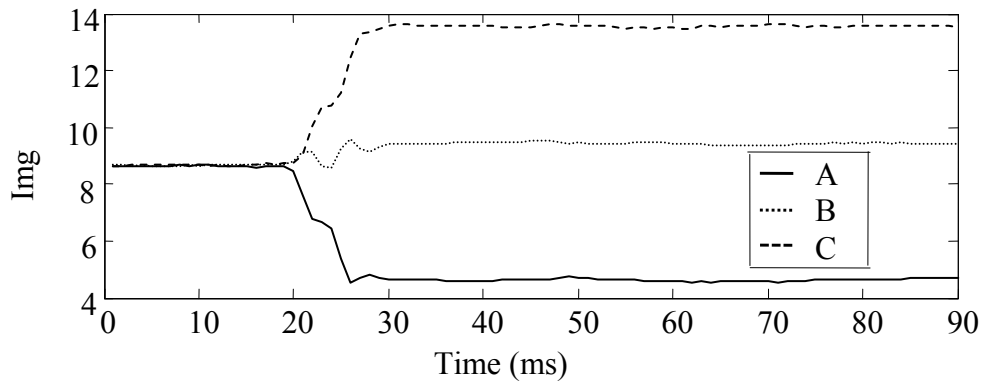


Figure 2.26: Amplitude of currents (SLG, primary side, Y/Y₀).

Therefore, the selection rule can be defined in Equation (2.14) for the cases with the windings of Y/Y₀.

$$\begin{aligned}
 &MAX(I_{\Delta mg,j})/MIN(I_{\Delta mg,j}) < K_{21} \\
 &MAX(I_{am,j})/MIN(I_{am,j}) > K_{22} \quad j = A, B, C \\
 &Phase\ with\ MIN(I_{am,j})\ is\ Faulty\ Phase \quad -\ Rule\ S3(b)
 \end{aligned} \tag{2.14}$$

where $I_{\Delta mg}$ is the magnitude of the superimposed fault current, I_{am} is the amplitude of the fault current, and MAX and MIN are the maximum and minimum values.

The rules for other common and theoretical connection windings can also be determined in the similar manner.

2.3.3 Classification

The event of SLG fault is already determined, so the final step is to discriminate the incipient fault from permanent fault. The process of classification is quite simple since it is only required to find whether the fault can last for up to 4 cycles, which can also be set to 5 cycles if considering the detection and classification delay.

$$\text{If } AMPCR = \left| \frac{I_{am,j}^{post} - I_{am,j}^{pre}}{I_{am,j}^{pre}} \right| < K_3 \quad j \text{ is faulty phase} \quad (2.15)$$

Then, Incipient fault is detected – Rule S4

where I_{am} is the amplitude of the prefault or post-fault current of the faulty phase at the power frequency.

2.3.4 Thresholds

The setting strategy and procedure is similar to the one explained in Section 2.2.4. There are two thresholds for detection, one for classification, and one or two for selection, which are all easily set. The meanings of the thresholds or behaviors of the rules are described below.

Rule S1 holds a large value at the normal situation, while it would decrease when a fault occurs. Then, K_{11} is set to a small value.

K_{12} in Rule S2 means a tolerance percentage that the superimposed fault current surpasses the normal current.

K_2 in Rule S3(a) demonstrates a minimum degree that the faulty phase is larger than the other two healthy phases.

K_{21} in Rule S3(b) denotes a maximum degree of the largest ratio among the superimposed currents and K_{22} denotes a minimum degree of the largest ratio among the faulty currents.

K_{23} in Rule S3(c) indicates a maximum degree of the ratio between the superimposed currents with the maximum and medium amplitude, while K_{24} indicates a minimum degree of the ratio between the superimposed currents with the medium and minimum amplitude.

K_3 in Rule S4 shows a range for which the amplitude of the faulty current may drop back after a certain period.

2.4 Simulations

2.4.1 Configuration of Simulation System

The simulation system includes two modules as illustrated in Figure 2.27. The first module is to simulate the test power systems and store the currents as COMTRADE [91] files in PSCAD/EMTDC. The simulations in this module cover the different events under various system and fault conditions. The detection algorithms are implemented in the second module where the data are analyzed in Matlab. The extra noise is also added into the original simulated signals.

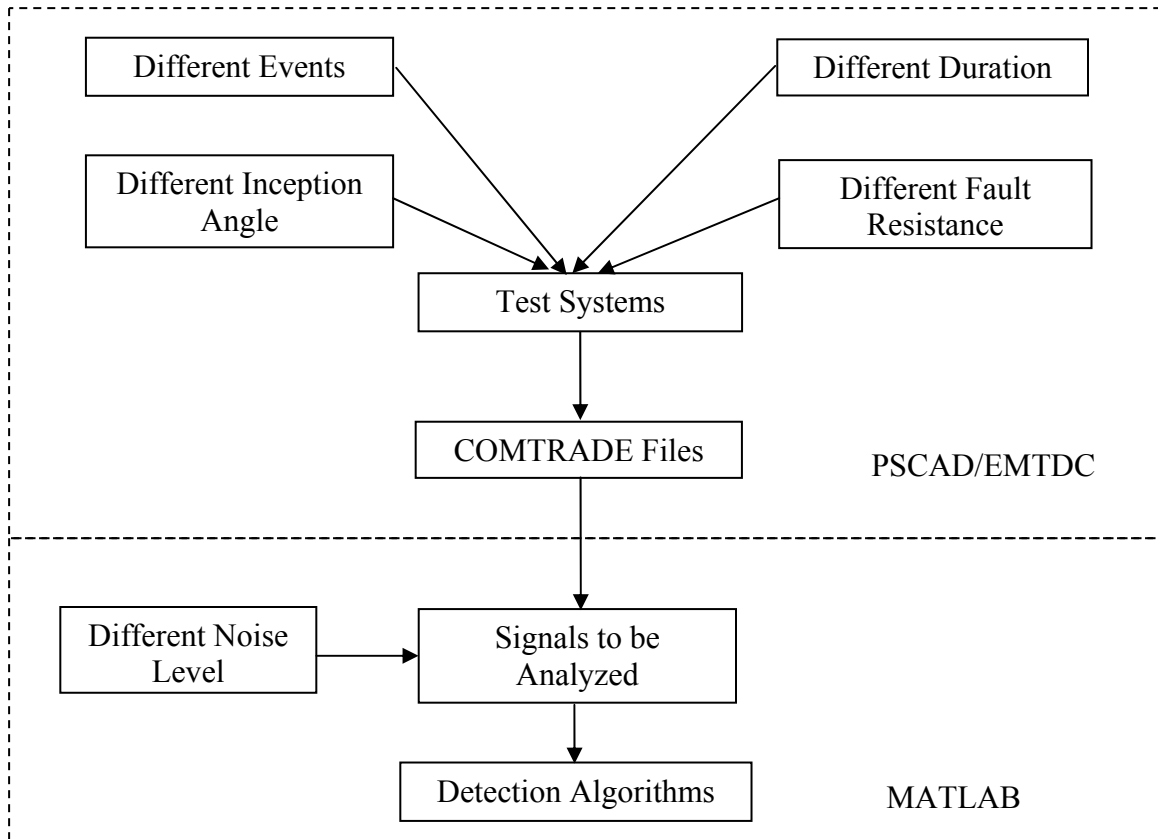


Figure 2.27: Configuration of simulation system.

2.4.2 Test Systems

Two distribution systems are selected for simulations. The first one is modified from a 110/10.5 kV distribution network [85], containing five underground cables, two overhead lines, and one combination of line and cable as shown in Figure 2.28.

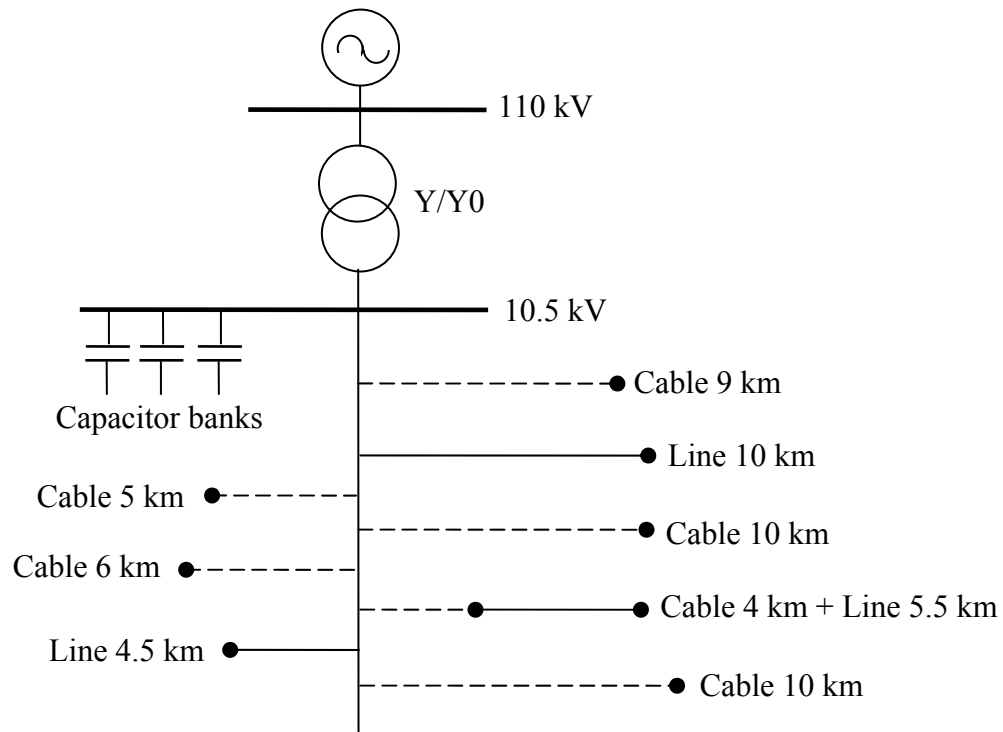


Figure 2.28: Test system 1.

The important system data include:

- 110kV grid: $V_n = 110kV$; $Z_{SC_POS} = 0.668 + j6.684 \Omega$.
- 110/10.5 kV transformer: $S_{rT} = 30MVA$; $u_k = 11.8\%$; $Yy0$.
- Overhead line: Al/St, 70/12, 19.5 km in total.
- Underground cable: NA2XS2Y, 3x1x185, 45 km in total.
- Capacitor bank: 2MVA, 3MVA, 5MVA.

The second test system is simplified from an IEEE 13-node test feeder [92], including two underground cables and eight overhead lines shown in Figure 2.29.

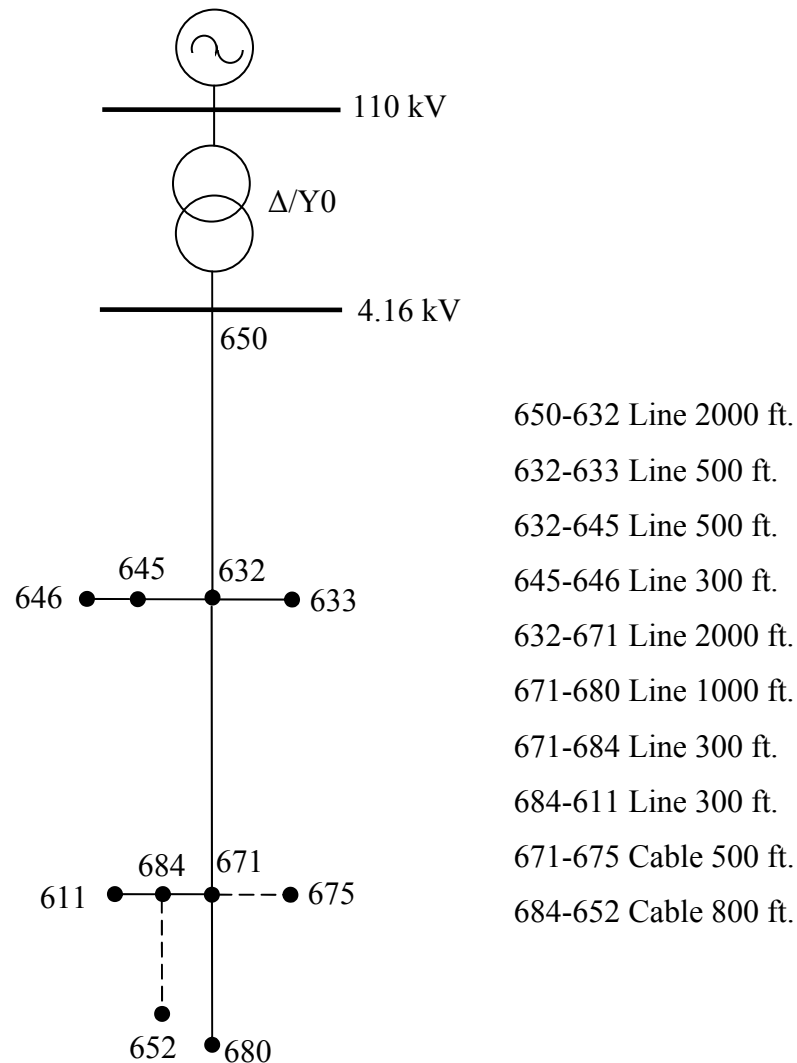


Figure 2.29: Test system 2.

The important system data can be referred to [92].

Several types of medium voltage level cables are used in two test systems. Since the semiconductive layers are not considered in PSCAD/EMTDC, the effect of the layers is approximated using procedures as discussed in [93].

2.4.3 Cases Studied

The studied cases involve the following variation of parameters and conditions:

- Noise levels, white noise are mixed into simulated data to make SNR (Signal-to-Noise Ratio) range from 8.8 to 44 dB;
- Fault distances, close-in terminal to far-end terminal in different feeders;
- Fault types, balanced and unbalanced, grounded and ungrounded;
- Fault resistances, zero to 50 ohm;
- Fault inception angles, 0-270 degree;
- CT locations, feeder, secondary and primary;
- Transformer windings;
- Capacitor and load switching;
- Relay auto-reclosure;
- Unbalanced/Balanced load;
- Faults in underground cables and overhead lines.

2.4.4 Simulation Results

2.4.4.1 Wavelet-based Scheme

Simulated in the wavelet-based scheme, this group of simulations concerns the various noise levels in the measured currents, different fault conditions, and other transient events. The total amount of 404 events is simulated and each event is simulated more than 300 times in a wide range of noise levels. The detection and classification results are given in Table 2.1.

It is evident that there is no false detection. Also it can be found that not all of the events can be detected correctly, nevertheless, it does not mean the proposed algorithm cannot obtain the desired performance. When SNR=44dB, 20 undetected sub-cycle faults and 12 undetected multi-cycle faults have the relatively high fault resistance, so the currents

have relatively small increment. In other SNR cases, the reason that causes the missing detection is exactly same. For example, the waveforms of two undetected events with high fault impedance are shown in Figure 2.30 and Figure 2.31.

Table 2.1: Detection and Classification Results (Wavelet-based Scheme)

Event	Event Amount	Correct Classified/Detected			
		SNR=44	SNR=33	SNR=20	SNR=8.8
Sub-Cycle	114	94/94	94/94	90/90	89/93
Multi-Cycle	114	102/102	102/102	102/102	102/102
Permanent	142	133/133	130/130	131/131	133/133
Cap. Switch	15	14/14	14/14	14/14	14/14
Load Change	19	9/10	9/10	9/10	9/11

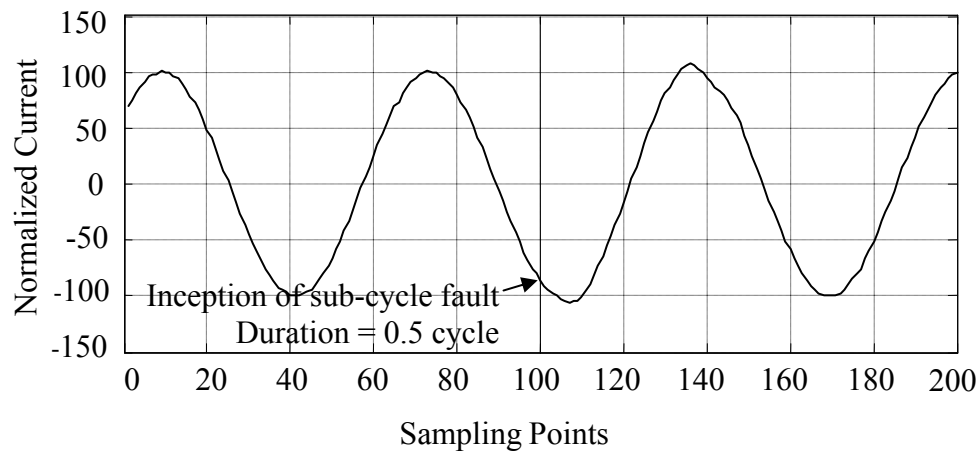


Figure 2.30: Undetected sub-cycle fault (30 ohm).

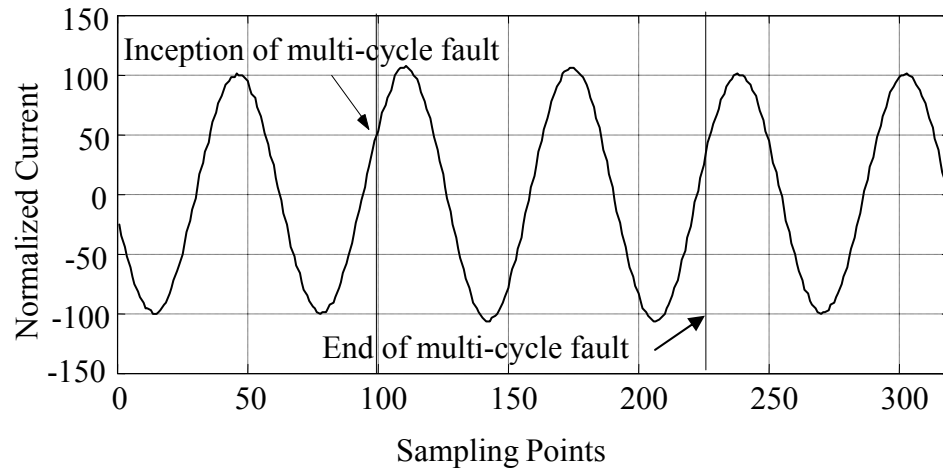


Figure 2.31: Undetected multi-cycle fault (50 ohm).

It should be mentioned that some events have the exactly same transient phenomena in voltages and currents, such as capacitor switching, load changing, and 3LG fault with high impedance, as shown in Figure 2.32. Therefore, only the general classification conclusion can be decided for these events with the similar phenomena. Actually, the detected events can be correctly classified when SNR is greater than 20dB, which is always satisfied in most measurements.

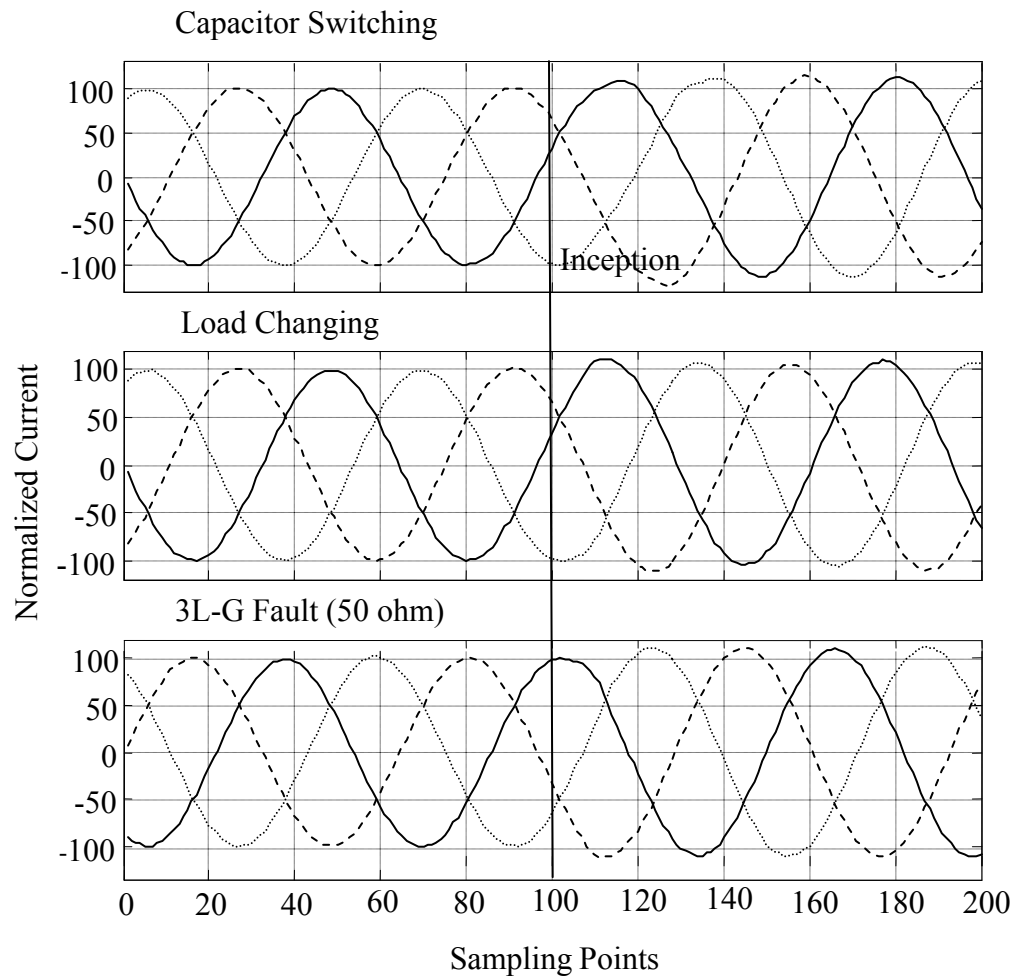


Figure 2.32: Events with similar changing.

One more group of simulations extends the simulations to consider the transformer windings and CT locations. With a few of the modifications of rules, both algorithms can be applied when the transformer has different windings or the currents are sampled from the different sides of transformer. The simulation results are similar to the previous ones.

2.4.4.2 Superimposed Components-based scheme

Similarly, same 404 events in two test systems are simulated, containing 177 SLG incipient faults and 90 of them have low (<5 ohm) or zero fault impedance. The SNR level is fixed to 44dB. The simulation results are shown in Table 2.2.

Table 2.2: Detection and Classification Results (Superimposed Components-based Scheme)

Amt. Of Event: 404 Amt. Of Incipient SLG: 177 Amt. Of Incipient SLG with low impedance: 90	CT Location	Detected (SLG/low impedance)	False Alarm	Incorrect Classification
	Primary	88/71	0	0
	Secondary	119/85	0	0
	Feeder	158/87	0	0

The missing detection is similarly resulted from the high fault impedance, small amplitude increment, or large threshold settings.

2.4.5 Results Using Field Recorded Data

Four multi-cycle cases and four sub-cycle cases, which were obtained from real systems, were also examined. All of them were correctly detected and classified by two proposed schemes. The detailed detection processes are illustrated by analyzing two types of incipient faults in Figure 2.33-Figure 2.36.

The top graph in Figure 2.33 is a sub-cycle incipient fault, and the currents are sampled from the secondary side of transformer. The incipient fault occurs at the time instant of 35.5ms and lasts for around 4ms. Due to the effect of the current summation of other feeders, the amplitude of the superimposed component is not large, about 60% of the maximum value of the prefault current in normal condition. Analyzed by the wavelet-based scheme, the fault is detected at 37.8ms, preliminarily classified as a sub-cycle incipient fault 26ms after the inception, and determinately confirmed 4 cycles after the detection.

Another sub-cycle incipient fault is processed in Figure 2.34 by the superimposed components-based method. The currents are measured in the feeder so that the faulty current reaches eight times larger than the regular peak value. The fault begins at 29.7ms and disappears at 36ms. The transient is instantly detected with 2ms delay and the faulty phase is selected simultaneously. It is classified correctly 4 cycles after the occurrence.

Figure 2.35 describes the analysis process of a 5-cycle incipient fault. As mentioned in Section 2.1.1, the multi-cycle incipient faults usually last one-quarter cycle to four cycles, however, both the frequency of fault occurrence and the duration of fault increase with time. In this situation, the larger margin for the detection delay can be adopted. The fault starts at 36.5ms and persists for next 89ms. Processed by the wavelet-based scheme, the fault is detected at 37.6ms, and pre-classified as a permanent fault or a multi-cycle incipient fault 1.5 cycles after the detection because both of them have the similar phoneme in the short period after the inception. The disappearance of fault is also detected at 126.2ms, and 2 cycles later, it is re-classified and verified as a multi-cycle incipient fault.

A 3-cycle incipient fault is shown in Figure 2.36 and analyzed by the superimposed components-based scheme. Commencing from 52.5ms, this fault vanishes at 105ms. It is initially caught at 55.6ms and finally classified at 139ms. The phase is selected at 60.8ms.

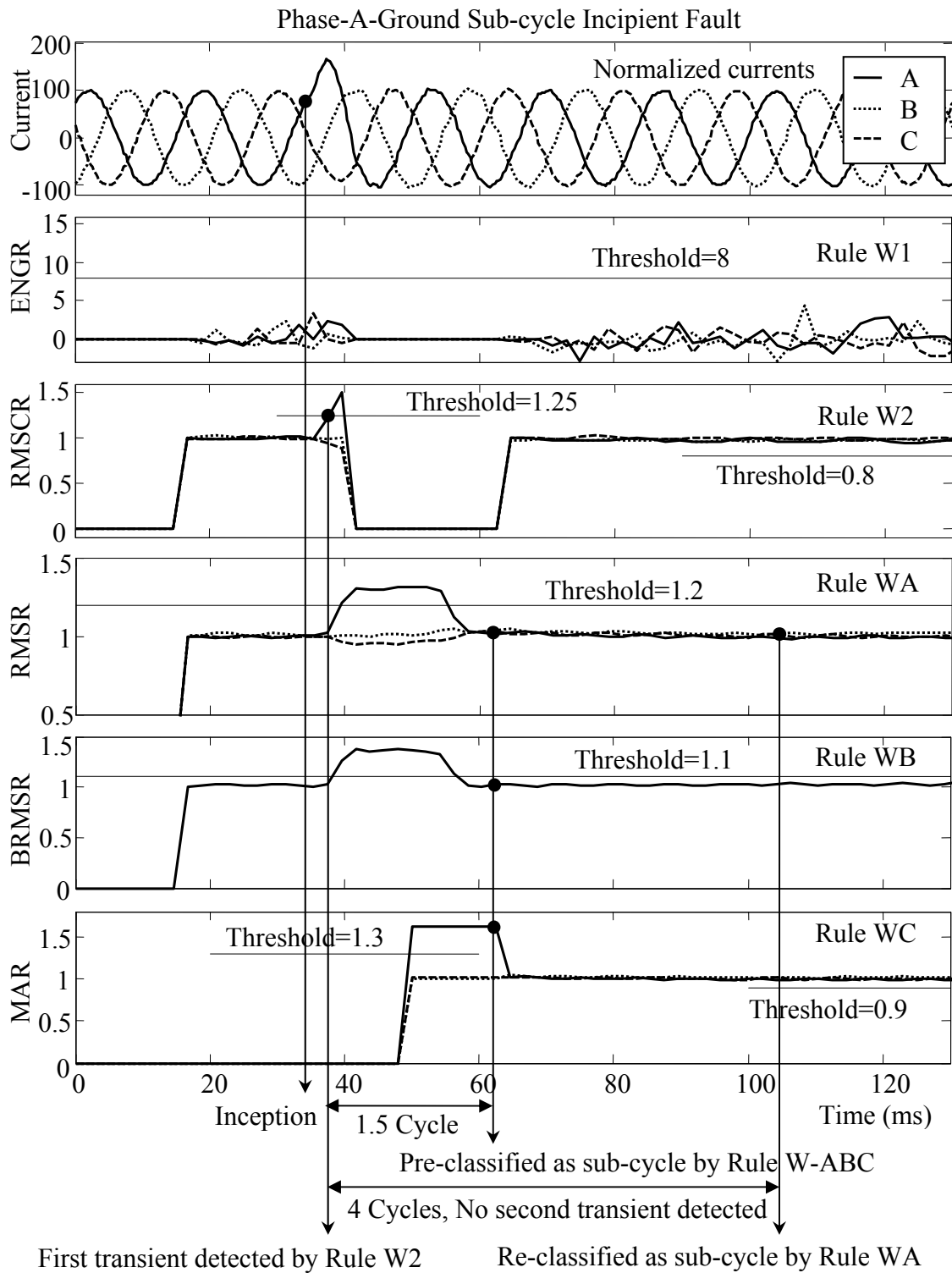


Figure 2.33: Analysis process of a sub-cycle incipient fault (Wavelet-based).

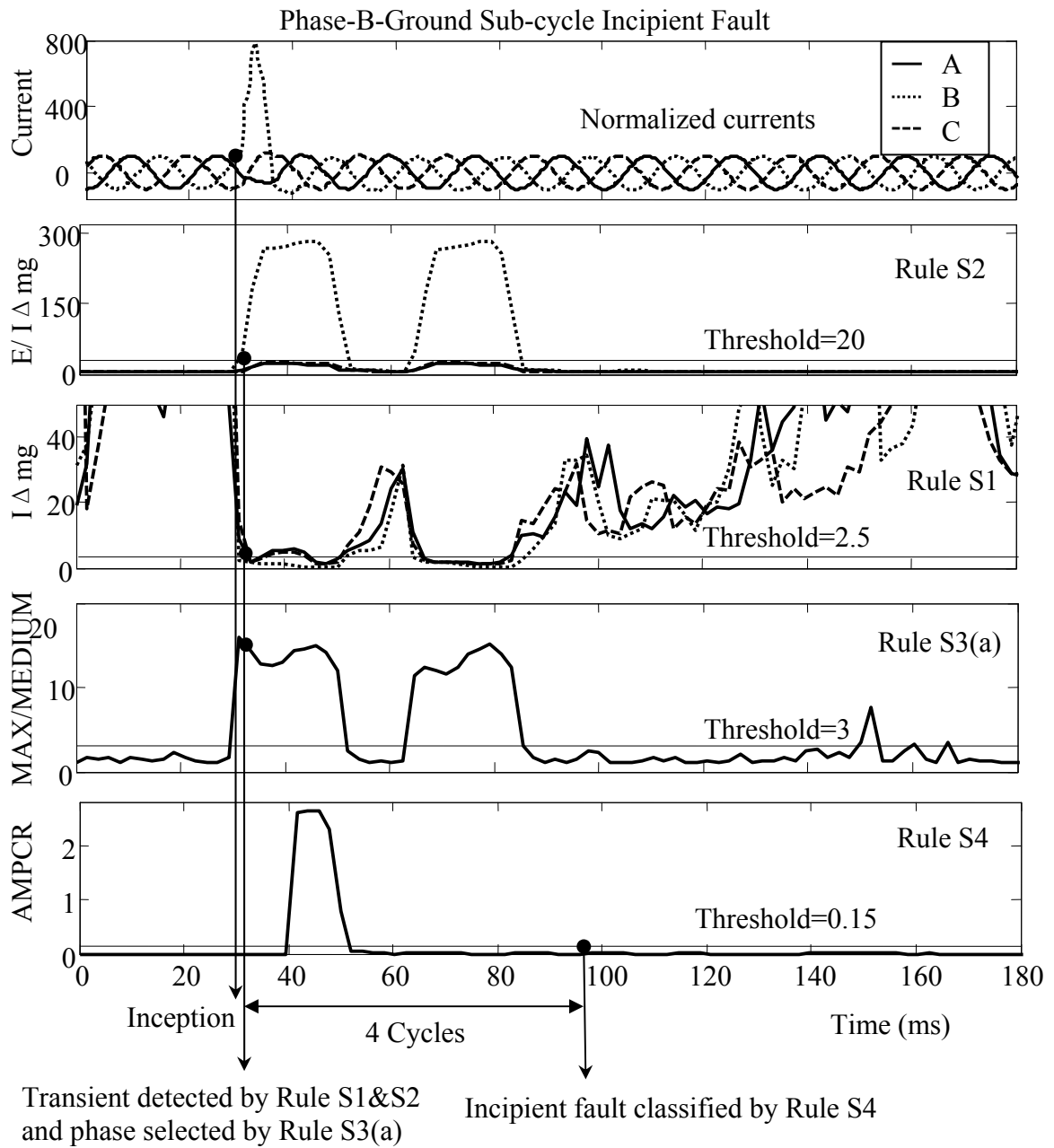


Figure 2.34: Analysis process of a sub-cycle incipient fault (Superimposed components-based).

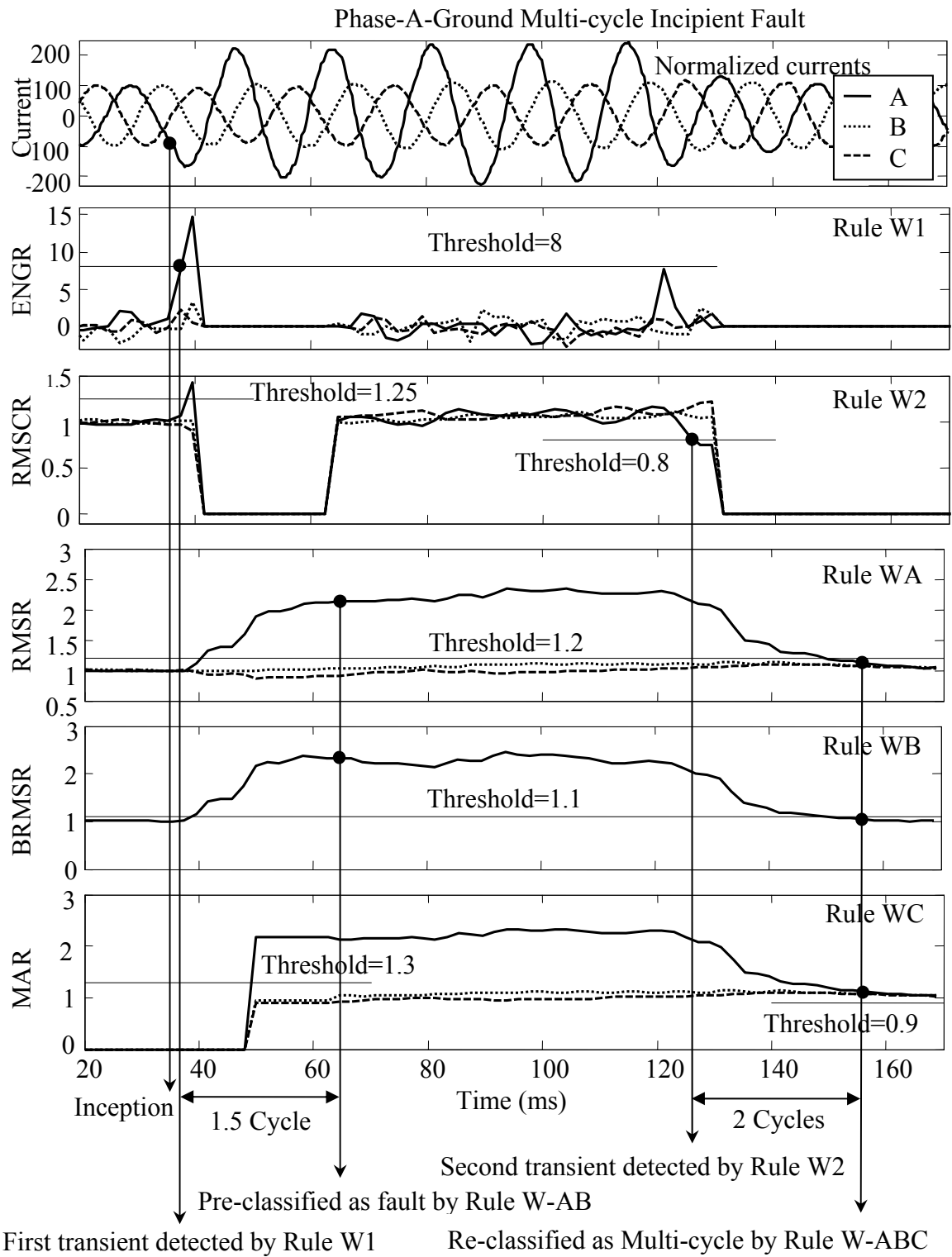


Figure 2.35: Analysis process of a multi-cycle incipient fault (Wavelet-based).

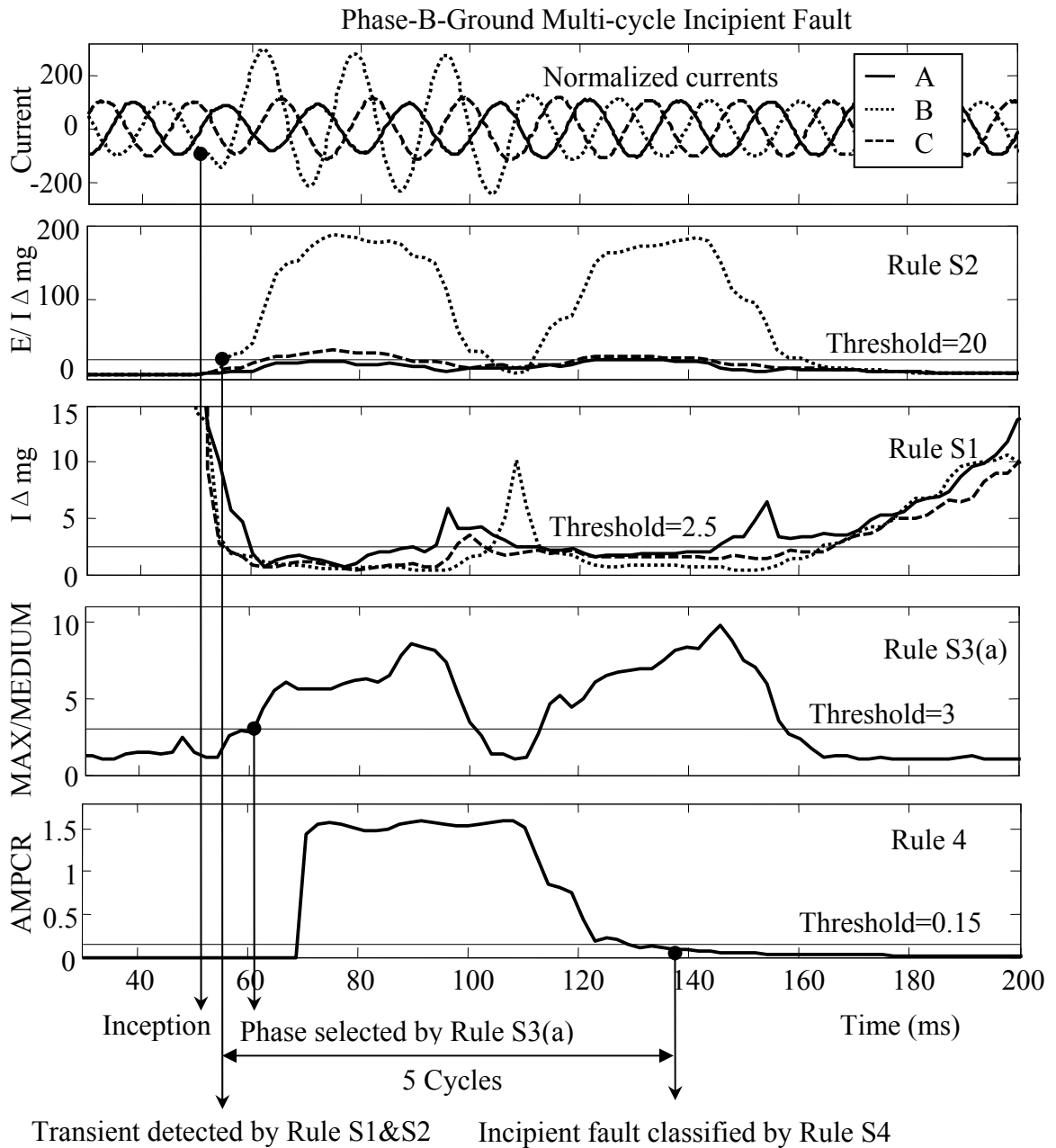


Figure 2.36: Analysis process of a multi-cycle incipient fault (Superimposed components-based).

It can be concluded from the above analysis of the field cases that, 1) the detection delay is less than 4ms, normally hovering around 2ms; 2) the classification delay is about 4-6

cycles after the detection; 3) the fault can be detected even if its duration is as short as 4ms; 4) the fault can be detected even if its superimposed amplitude is as less as 60% of the regular peak value. In addition, these conclusions are verified by the simulation cases in PSCAD/EMTDC.

Chapter 3

3 Fault Location Algorithms for Medium Voltage Cables

The fault location in underground cables is characterized as the technical difficulties due to the complexities in cables. Based on the direct circuit analysis, a set of location algorithms are proposed to locate the single phase related faults in the typical single-conductor cross-linked polyethylene (XLPE) cables rated at the medium voltage levels. A number of complex equations are effectively solved to find the fault distance and fault resistance. The algorithms only utilize the fundamental phasors of three-phase voltages and currents recorded at the substation. Particularly, the distinctive cable characteristics are considered, such as the effects of shunt capacitance, effects of metallic sheaths and common sheath bonding methods. The different fault scenarios are taken into account as well.

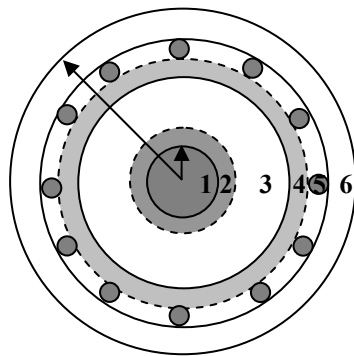
The background knowledge is first introduced, including the structure of a typical XLPE cable, the common sheath bonding methods, the complexities existing in fault location calculations for cables and the different fault scenarios. Then a two-layer π model is formulated to approximate the characteristics and behaviors of a typical MV XLPE cable. The principle and procedure of the location algorithms are specially explicated for a cable with sheaths grounded at the sending terminal. The differences and similarities of the algorithms for other bonding methods are compared and summarized as well. The estimation of load impedance is discussed for the constant impedance load model and static response load model respectively. The algorithms are examined on three types of MV cables with different fault types, fault resistances, fault distances and bonding methods in the last section of this chapter. The simulation studies demonstrate that the proposed algorithm can achieve the high accuracy under various system and fault conditions.

3.1 Background

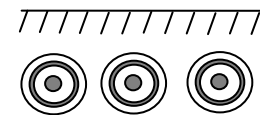
3.1.1 Structure of a Typical XLPE Cable

The typical structure of a widely used single-conductor cable is shown in Figure 3.1 and the each part numbered in the figure is explained as below:

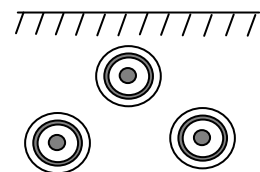
- 1 - Aluminum or copper stranded conductor.
- 2 - Semi-conducting conductor screen extruded around conductor.
- 3 - Insulation, XLPE are used in most modern MV and HV cables.
- 4 - Semi-conducting insulation screen. The semi-conducting swelling tapes wrapped around the insulation screen are considered as part of the insulation screen since the electrical properties of this layer are similar to those of the insulation screen.
- 5 - Copper wire sheath.
- 6 – Outer jacket, usually polyethylene (PE).



(a) Structure. 1: conductor, 2: conductor screen, 3: insulation of XLPE, 4: insulation screen, 5: wire sheath, 6: outer jacket of polyethylene (PE).



(b) Flat formation



(c) Trefoil formation

Figure 3.1: Structure of a typical single-conductor XLPE cable and laid formations of three-phase cables.

The cables could be directly buried or installed in an underground duct laid in the flat or trefoil formation. The choice depends on several factors like sheath bonding method, conductor area and available space for installation.

3.1.2 Sheath Bonding Methods

The magnetic field generated from the alternating current in the core conductor would induce a voltage in the metallic sheath linked to this field. Besides, the current flowing in the sheath of a cable would result in the extra power losses. Therefore for the sake of safe and economic operation, the sheath of a single-conductor cable must be bonded to the ground in different points to (1) reduce the sheath voltage, (2) reduce sheath current and sheath loss to a minimum, (3) maintain a continuous sheath circuit for fault current return and adequate lightning and switching surge protection, (4) decrease the possibility of the failure of outer jacket and sheath corrosion, and (5) possibly increase the load current carrying capacity.

The prevalent grounding methods contain the single point bonding at the sending terminal (SPBS), receiving terminal (SPBR), or middle point (SPBM); solid bonding at both ends (SBBE); and cross bonding (XB). Three of them are briefly introduced below and illustrated in Figure 3.2, and the details can be referred to [94].

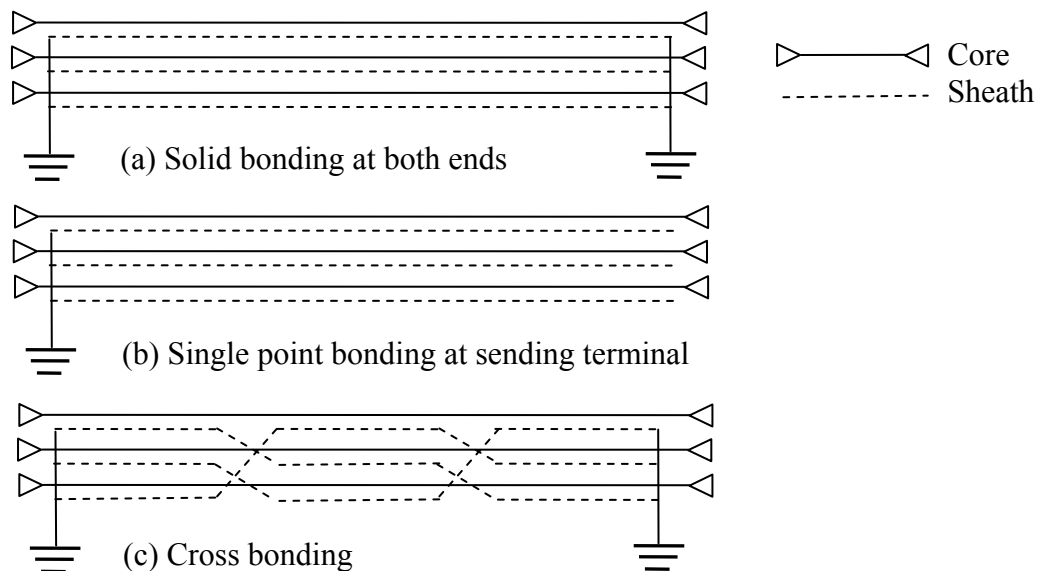


Figure 3.2: Sheath bonding methods.

The solid bonding method grounds sheaths at both ends, which can reduce the induced voltage. The disadvantages of this bonding method include that it provides the loop path for circulating currents at normal operation conditions, causes power losses in sheaths, and further reduces the cable ampacity. The single-point bonding method grounds sheaths at one point along the cable circuit, typically at one of the two terminals or at the middle point of a cable. Although there are no significant circulating currents flowing in sheaths, a voltage will be induced between the core conductor and sheath and between the sheath and earth. Therefore, the surge voltage limiters must be used to protect the floating end of sheaths from overvoltage danger. The cross bonding method grounds sheaths at both ends and sheaths are cross-connected at the joints by which the cable is sectionalized into three sections of equal length. The circulating currents and power losses are significantly reduced and the induced voltages are partially neutralized as well. The maximum induced voltage appears at the joint boxes.

3.1.3 Complexities in Fault Location for Cables

The location principles for underground cables are comparatively different from the ones for overhead transmission lines or distribution lines due to the following electrical characteristics of cables [95]-[99].

- The impedance per unit length of cables is less than that of lines.
- The series inductance of cables is typically 30~50% lower than that of lines.
- The shunt capacitance of cables is 30~40 times higher than that of lines.
- The zero-sequence impedance of cables is not constant and depends on many factors, such as bonding method, fault current, presence of parallel circuit and resistivity of ground.
- The zero-sequence impedance angle of cables is less than that of lines.
- The X/R ratio of cables is much lower than that of lines.

In addition to the differences in the electrical characteristics, the complexities of location techniques for cables also involve [9], [95]-[99]:

- The metallic sheath or shield of a single-conductor cable is bonded to ground in different points, which affect the return path of ground fault currents. The five most frequently applied methods are introduced in the previous subsection, i.e. SBBE, SPBS, SPBR, SPBM and XB. Therefore, the ground fault currents have the different return paths, such as through the sheath only, through the ground only, through the sheath and the ground in parallel, or through the ground and the sheaths of adjacent cables.
- The most commonly observed permanent faults in a single-conductor cable can be identified as the core-sheath-ground fault (CSGF), core-ground fault (CGF) and core-sheath fault (CSF).
- Three single-conductor cables have six conductors: three core conductors and three metallic sheaths. Usually, only voltages and currents of core conductors are measured. Although there might have few loop currents and small voltages along sheaths in the normal operating condition, the sheaths would cause distinct effect on the voltage and current along the core circuit in a faulty situation.
- For the reason that the series impedance matrix of cable is unsymmetrical, the direct application of the traditional modal transformations, like Fortescue [100] and Clarke [101], is improper [102], [103].
- Due to the different bonding methods, the reduction of neutral wires (sheaths) by the Kron's reduction [104] is also improper.

3.1.4 Fault Scenarios

The fault types in a single-conductor cable usually can be classified as the core-sheath-ground fault, core-ground fault and core-sheath fault, which are shown in Figure 3.3. The combination of values of three fault resistances is tabulated in Table 3.1 which can be used to decide the actual fault scenario.

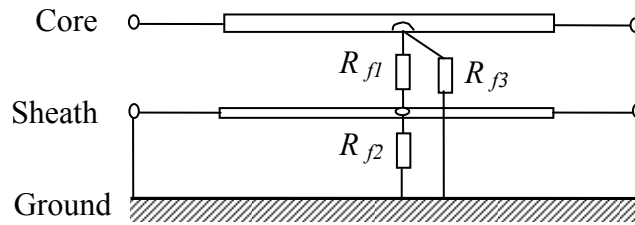


Figure 3.3: Fault scenarios.

Table 3.1: Decision of Fault Scenarios in Theory

Fault Scenarios	Fault Resistance		
	R_{f1}	R_{f2}	R_{f3}
Core-Sheath-Ground	X	X	∞
Core-Ground	∞	∞	X
Core-Sheath	X	∞	∞

It should be noted that X in Table 3.1 can be any practical non-negative real value.

3.2 Model of Cable

The cable models used in the EMTP (Electromagnetic Transients Program) can be divided into two categories: lumped parameter models and distributed parameter models [105], [106]. The lumped parameter models simplify the multiphase coupled circuits into the idealized electrical components, such as resistors, capacitors and inductors, constituting a π type circuit. The calculations are processed at a given frequency, normally power frequency, and the shunt conductance is usually ignored. The distributed characteristics of whole circuit can be approximately represented by cascading a series of identical π circuits into a ladder network. The distributed parameter models theoretically divide the whole circuit into infinitesimal elements, so the voltage at each node and current at each branch are not uniform. This model first decouples the differential equations in normal phase quantities into multiple separate differential equations in modal quantities or frequency quantities by transformation matrices, and solves the

decoupled equations in modal quantities or frequency quantities, then converts the results back to phase quantities.

The Frequency Dependent (Phase) model in the element library of PSCAD/EMTDC is claimed to be “the most numerically accurate and robust line/cable model available anywhere in the world” [107]. So this model is used for the simulation and the development of the algorithm. With the verification through the extensive simulations, a lumped parameter model, the two-layer π model, is formulated to accurately approximate the behaviors and characteristics of the frequency dependent model in PSCAD/EMTDC, especially for short cables. The model for three single-conductor cables is illustrated in Figure 3.4.

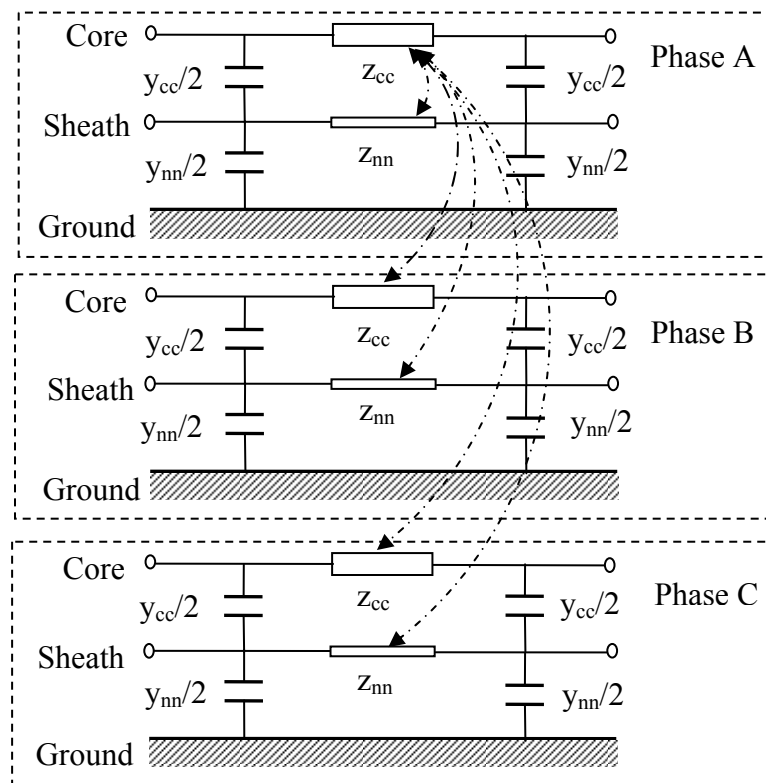


Figure 3.4: Model of three single-conductor XLPE cables. There exist the mutual impedances among all six conductors (Only the mutual impedances related to the core conductor of phase A are shown in the dash-dot lines above).

In the figure, z_{cc} is the self-impedance of core, z_{nn} is the self-impedance of sheath, y_{cn} is the admittance between the core and sheath, and y_{ng} is the admittance between the sheath and ground. It should be noted that there exist the mutual impedances among all six conductors and the sheaths are normally bonded to ground in some manner.

Based on the two-layer π model, the mathematical equations to represent the voltages and currents along the cable are expressed as,

$$\begin{bmatrix} V_{rc} \\ V_{rn} \end{bmatrix} = \begin{bmatrix} V_{sc} \\ V_{sn} \end{bmatrix} - L \begin{bmatrix} Z_{cc} & Z_{cn} \\ Z_{nc} & Z_{nn} \end{bmatrix} \left(\begin{bmatrix} I_{sc} \\ I_{sn} \end{bmatrix} - \frac{L}{2} \begin{bmatrix} Y_{cc} & Y_{cn} \\ Y_{nc} & Y_{nn} \end{bmatrix} \begin{bmatrix} V_{sc} \\ V_{sn} \end{bmatrix} \right) \quad (3.1)$$

$$\begin{bmatrix} I_{rc} \\ I_{rn} \end{bmatrix} = \begin{bmatrix} I_{sc} \\ I_{sn} \end{bmatrix} - \frac{L}{2} \begin{bmatrix} Y_{cc} & Y_{cn} \\ Y_{nc} & Y_{nn} \end{bmatrix} \begin{bmatrix} V_{sc} + V_{rc} \\ V_{sn} + V_{rn} \end{bmatrix} \quad (3.2)$$

where,

$$V_{rc} = \begin{bmatrix} V_{rc}^A & V_{rc}^B & V_{rc}^C \end{bmatrix}^T; \quad V_{rn} = \begin{bmatrix} V_{rn}^A & V_{rn}^B & V_{rn}^C \end{bmatrix}^T;$$

$$V_{sc} = \begin{bmatrix} V_{sc}^A & V_{sc}^B & V_{sc}^C \end{bmatrix}^T; \quad V_{sn} = \begin{bmatrix} V_{sn}^A & V_{sn}^B & V_{sn}^C \end{bmatrix}^T;$$

$$I_{rc} = \begin{bmatrix} I_{rc}^A & I_{rc}^B & I_{rc}^C \end{bmatrix}^T; \quad I_{rn} = \begin{bmatrix} I_{rn}^A & I_{rn}^B & I_{rn}^C \end{bmatrix}^T;$$

$$I_{sc} = \begin{bmatrix} I_{sc}^A & I_{sc}^B & I_{sc}^C \end{bmatrix}^T; \quad I_{sn} = \begin{bmatrix} I_{sn}^A & I_{sn}^B & I_{sn}^C \end{bmatrix}^T;$$

$$Z_{cc} = \begin{bmatrix} z_{cc}^{AA} & z_{cc}^{AB} & z_{cc}^{AC} \\ z_{cc}^{BA} & z_{cc}^{BB} & z_{cc}^{BC} \\ z_{cc}^{CA} & z_{cc}^{CB} & z_{cc}^{CC} \end{bmatrix}; \quad Z_{nn} = \begin{bmatrix} z_{nn}^{AA} & z_{nn}^{AB} & z_{nn}^{AC} \\ z_{nn}^{BA} & z_{nn}^{BB} & z_{nn}^{BC} \\ z_{nn}^{CA} & z_{nn}^{CB} & z_{nn}^{CC} \end{bmatrix};$$

$$Z_{cn} = \begin{bmatrix} z_{cn}^{AA} & z_{cn}^{AB} & z_{cn}^{AC} \\ z_{cn}^{BA} & z_{cn}^{BB} & z_{cn}^{BC} \\ z_{cn}^{CA} & z_{cn}^{CB} & z_{cn}^{CC} \end{bmatrix}; \quad Z_{nc} = Z_{cn};$$

$$Y_{cc} = \begin{bmatrix} y_{cc}^{AA} & 0 & 0 \\ 0 & y_{cc}^{BB} & 0 \\ 0 & 0 & y_{cc}^{CC} \end{bmatrix}; \quad Y_{nn} = \begin{bmatrix} y_{nn}^{AA} & 0 & 0 \\ 0 & y_{nn}^{BB} & 0 \\ 0 & 0 & y_{nn}^{CC} \end{bmatrix};$$

$$Y_{nc} = Y_{cn} = -Y_{cc}$$

and,

$$z_{cc}^{AA} = z_{cc}^{BB} = z_{cc}^{CC}; \quad z_{cn}^{AA} = z_{cn}^{BB} = z_{cn}^{CC}; \quad z_{nn}^{AA} = z_{nn}^{BB} = z_{nn}^{CC};$$

$$\begin{aligned} z_{cc}^{AB} &= z_{cc}^{BA} = z_{cc}^{BC} = z_{cc}^{CB} = z_{cn}^{AB} = z_{cn}^{BA} = z_{cn}^{BC} = z_{cn}^{CB} \\ &= z_{nn}^{AB} = z_{nn}^{BA} = z_{nn}^{BC} = z_{nn}^{CB}; \end{aligned}$$

$$y_{cc}^{AA} = y_{cc}^{BB} = y_{cc}^{CC}; \quad y_{nn}^{AA} = y_{nn}^{BB} = y_{nn}^{CC}$$

where V without the superscript is the voltage phasor vector, V with the superscript is the voltage phasor of a single phase, I without the superscript is the current phasor vector, I with the superscript is the current phasor of a single phase, Z is the series impedance matrix, Y is the shunt admittance matrix, and L is the length of cable. The capital subscripts denote the phase A , B , or C . The lowercase subscript s means quantities at the sending terminal, similarly, r at the receiving terminal, c for the core conductor and n for the sheath. Taking z_{cn}^{AB} as an example, it indicates the mutual impedance per unit length between core A and sheath B, while giving one more example, z_{cc}^{BB} expresses the self-impedance per unit length of core B, and so forth.

3.3 Location Algorithm for Cables with SPBS

3.3.1 Problem Formulation

This subsection is to propose a location algorithm for cables with the configuration of the single point bonding at the sending terminal (SPBS). Assuming a core-sheath-ground fault (CSGF) occurs in phase A of three single-conductor cables with SPBS, as illustrated in Figure 3.5.

The fault equations describing the circuit section from the sending terminal to the fault point are formulated as,

$$\begin{bmatrix} V_{fc} \\ V_{fn} \end{bmatrix} = \begin{bmatrix} V_{sc} \\ V_{sn} \end{bmatrix} - D \begin{bmatrix} Z_{cc} & Z_{cn} \\ Z_{nc} & Z_{nn} \end{bmatrix} \left(\begin{bmatrix} I_{sc} \\ I_{sn} \end{bmatrix} - \frac{D}{2} \begin{bmatrix} Y_{cc} & Y_{cn} \\ Y_{nc} & Y_{nn} \end{bmatrix} \begin{bmatrix} V_{sc} \\ V_{sn} \end{bmatrix} \right) \quad (3.3)$$

$$\begin{bmatrix} I_{fc} \\ I_{fn} \end{bmatrix} = \begin{bmatrix} I_{sc} \\ I_{sn} \end{bmatrix} - \frac{D}{2} \begin{bmatrix} Y_{cc} & Y_{cn} \\ Y_{nc} & Y_{nn} \end{bmatrix} \begin{bmatrix} V_{sc} + V_{fc} \\ V_{sn} + V_{fn} \end{bmatrix} \quad (3.4)$$

The fault equations describing the circuit section from the fault point to the receiving terminal are established as,

$$\begin{bmatrix} V_{rc} \\ V_{rn} \end{bmatrix} = \begin{bmatrix} V_{fc} \\ V_{fn} \end{bmatrix} - (L-D) \begin{bmatrix} Z_{cc} & Z_{cn} \\ Z_{nc} & Z_{nn} \end{bmatrix} \left(\begin{bmatrix} I_{f1c} \\ I_{f1n} \end{bmatrix} - \frac{L-D}{2} \begin{bmatrix} Y_{cc} & Y_{cn} \\ Y_{nc} & Y_{nn} \end{bmatrix} \begin{bmatrix} V_{fc} \\ V_{fn} \end{bmatrix} \right) \quad (3.5)$$

$$\begin{bmatrix} I_{rc} \\ I_{rn} \end{bmatrix} = \begin{bmatrix} I_{f1c} \\ I_{f1n} \end{bmatrix} - \frac{L-D}{2} \begin{bmatrix} Y_{cc} & Y_{cn} \\ Y_{nc} & Y_{nn} \end{bmatrix} \begin{bmatrix} V_{fc} + V_{rc} \\ V_{fn} + V_{rn} \end{bmatrix} \quad (3.6)$$

The fault equations at the fault point are formed as,

$$I_{fc}^B = I_{f1c}^B, \quad I_{fc}^C = I_{f1c}^C \quad (3.7)$$

$$I_{fn}^B = I_{f1n}^B, \quad I_{fn}^C = I_{f1n}^C \quad (3.8)$$

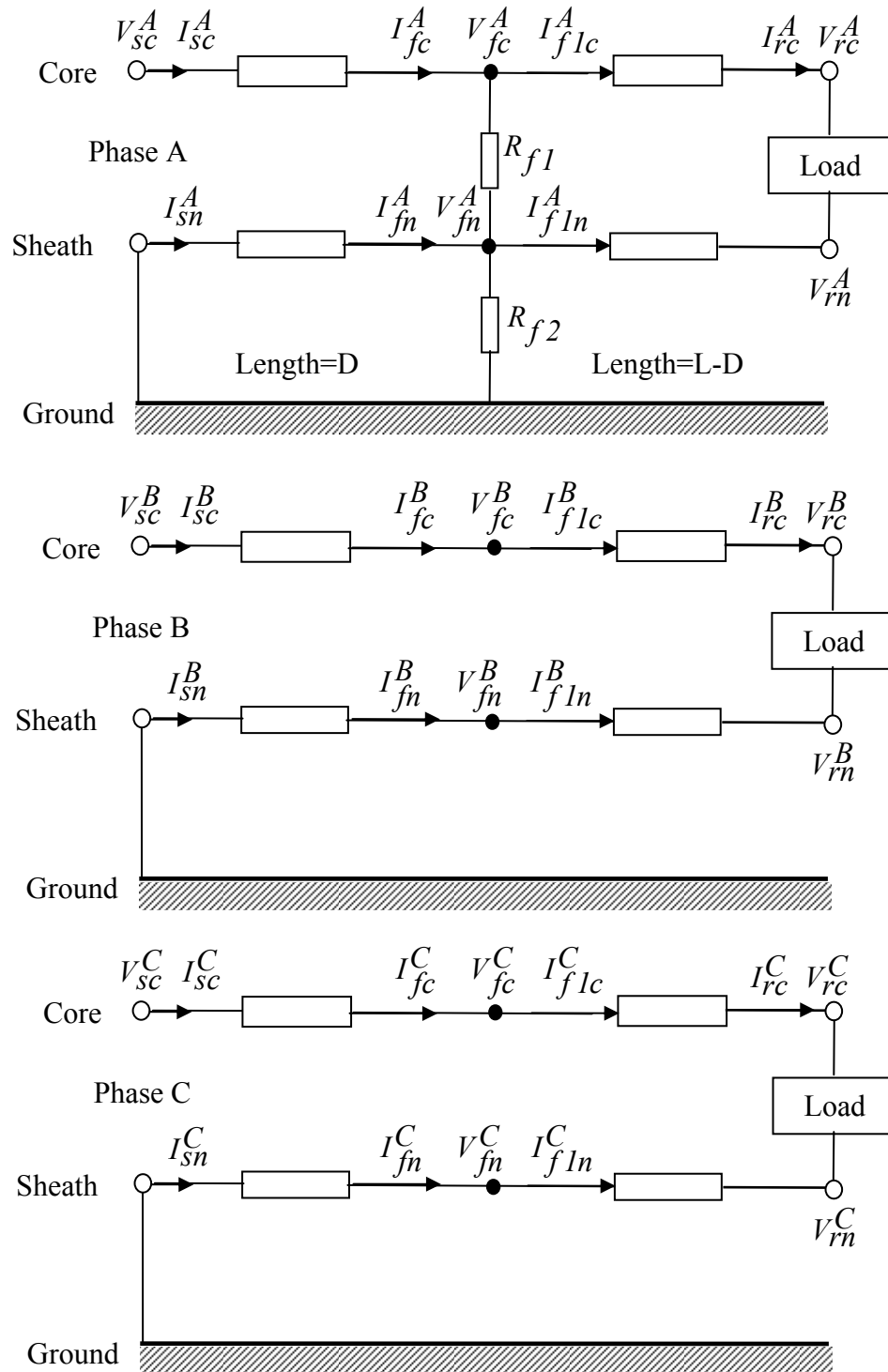


Figure 3.5: A CSGF in cable with SPBS.

$$R_{f1} = \frac{V_{fc}^A - V_{fn}^A}{I_{fc}^A - I_{f1c}^A} \quad (3.9)$$

$$R_{f2} = \frac{V_{fn}^A}{I_{fc}^A - I_{f1c}^A + I_{fn}^A - I_{f1n}^A} \quad (3.10)$$

where R_{f1} is the fault resistance between the core and sheath, and R_{f2} is the fault resistance between the sheath and ground.

At the receiving terminal, the loads are modeled as the constant impedance, and there exists the following relation,

$$V_{rc} = Z_{load} I_{rc} \quad (3.11)$$

where Z_{load} is the load impedance matrix.

The boundary conditions due to the grounding of sheaths are given as,

$$V_{sn} = 0; \quad I_{rn} = 0 \quad (3.12)$$

The whole cable circuit during the fault is represented by Equations (3.3)-(3.12). The known variables and preconditions in the above equations are summarized as follows.

- Six measurements comprise three-phase voltages (V_{sc}) and three-phase currents (I_{sc}) of the core conductors recorded at the substation.
- Cable parameter matrices (Z and Y) would be well documented in the database of utility companies, obtained from the datasheet of the manufacturers, calculated by the EMTP software, or estimated by the classical equations [108]-[110].
- The length of cable, L , is known.
- Six preconditions of voltages and currents in Equation (3.12) are known as zeros due to the fact that the sheaths are grounded at the sending terminal.

- Fault resistances (R_{f1} and R_{f2}) are non-negative real numbers.
- The load is modeled as the constant impedance or assumed that the load impedance would not change during 1-2 cycles right after the inception of a fault. The impedance can be estimated by the prefault voltage and current, which is explained in Section 3.9.1.1. In addition, the application of a more general load model is investigated in Section 3.9.2 as well.

The unknown variables need to be determined is the fault distance, and if required, the fault resistance as well.

For such a fault situation illustrated in Figure 3.5 and formulated in Equations (3.3)-(3.12), there have 75 unknown real variables and 78 real equations as listed in Table 3.2 and Table 3.3.

Table 3.2: List of Unknown Variables – SPBS & CSGF

	Variable Name	Number of Real Variables
Sending End	V_{sn}, I_{sn}	$2*3*2=12$
Fault Point	$V_{fc}, V_{fn}, I_{fi}, I_{fn}, I_{f1i}, I_{f1n}$	$6*3*2=36$
Receiving End	$V_{rc}, V_{rn}, I_{rc}, I_{rn}$	$4*3*2=24$
Real Variable	R_{f1}, R_{f2}, D	3
Total		75

Table 3.3: List of Equations – SPBS & CSGF

	Equation Index	Number of Real Equations
All Sections	(3.3)-(3.6)	$4*2*3*2=48$
Current at Fault Point	(3.7)-(3.8)	$2*2*2=8$
Bonding	(3.12)	$2*3*2=12$
Load	(3.11)	$1*3*2=6$
Fault Resistance	(3.9)-(3.10)	$2*2=4$
Total		78

However, it is impractical and time-consuming to solve this set of equations by directly using some mathematic solving tools, such as the solving functions in Matlab [111]. The fast solving algorithm would be proposed in the next subsection.

3.3.2 Locating Core-Sheath-Ground Fault

The proposed algorithm in this subsection is to locate the single-phase core-sheath-ground fault (CSGF) in three single-conductor cables, especially with sheaths only grounded at the sending terminal.

It is doubtless that all variables in Equations (3.3)-(3.12) would be definitely solved provided that the sheath currents (I_{sn}) and fault distance (D) were known. There are six real variables for I_{sn} , which values are time-varying and the range is hardly predictable. Nonetheless, there is only one real variable for D with a known range, i.e. from 0 to the length of cable, L . Therefore, a conceptual framework is proposed that a set of fault distances are first assumed, and then, the related sheath currents at the sending terminal are estimated for each assumed distance, subsequently all unknown quantities are solved by Equations (3.3)-(3.12), finally the exact fault point is accurately pinpointed.

3.3.2.1 Estimation of Sheath Currents of Healthy Cables

First, a fault distance (D) is assumed and three-phase sheath currents at the sending terminal (I_{sn}) are initially set to zeros or assigned to the values calculated from the estimation for the previous assumed distance.

The voltages at the fault point are calculated by,

$$\begin{bmatrix} V_{fc} \\ V_{fn} \end{bmatrix} = \begin{bmatrix} V_{sc} \\ 0 \end{bmatrix} - D \begin{bmatrix} Z_{cc} & Z_{cn} \\ Z_{nc} & Z_{nn} \end{bmatrix} \left(\begin{bmatrix} I_{sc} \\ I_{sn} \end{bmatrix} - \frac{D}{2} \begin{bmatrix} Y_{cc} & Y_{cn} \\ Y_{nc} & Y_{nn} \end{bmatrix} \begin{bmatrix} V_{sc} \\ 0 \end{bmatrix} \right) \quad (3.13)$$

The currents at the immediate left side of the fault point are formulated as,

$$\begin{bmatrix} I_{fc} \\ I_{fn} \end{bmatrix} = \begin{bmatrix} I_{sc} \\ I_{sn} \end{bmatrix} - \frac{D}{2} \begin{bmatrix} Y_{cc} & Y_{cn} \\ Y_{nc} & Y_{nn} \end{bmatrix} \begin{bmatrix} V_{sc} + V_{fc} \\ V_{fn} \end{bmatrix} \quad (3.14)$$

The voltages and currents at the receiving terminal are represented as,

$$I_{rc} = M^{-1} \left(V_{fn} - N V_{fc} \right) \quad (3.15)$$

$$V_{rn} = J^{-1} \left(V_{fc} - K I_{rc} \right) \quad (3.16)$$

$$V_{rc} = Z_{load} I_{rc} \quad (3.17)$$

where,

$$J = \frac{(L-D)^2}{2} Z_{cc} Y_{cn} + \frac{(L-D)^2}{2} Z_{cn} Y_{nn};$$

$$K = Z_{load} + (L-D) Z_{cc} + \frac{(L-D)^2}{2} Z_{cc} Y_{cc} Z_{load} \\ + \frac{(L-D)^2}{2} Z_{cn} Y_{nc} Z_{load};$$

$$M = -J^{-1} K + (L-D) Z_{nc} + \frac{(L-D)^2}{2} Z_{nc} Y_{cc} Z_{load} \\ - \frac{(L-D)^2}{2} Z_{nc} Y_{cn} J^{-1} K + \frac{(L-D)^2}{2} Z_{nn} Y_{nc} Z_{load} \\ - \frac{(L-D)^2}{2} Z_{nn} Y_{nn} J^{-1} K;$$

$$N = J^{-1} + \frac{(L-D)^2}{2} Z_{nc} Y_{cn} J^{-1} + \frac{(L-D)^2}{2} Z_{nn} Y_{nn} J^{-1};$$

$$Z_{load} = \begin{bmatrix} Z_{load}^A & 0 & 0 \\ 0 & Z_{load}^B & 0 \\ 0 & 0 & Z_{load}^C \end{bmatrix}$$

Based on the results from Equations (3.13), (3.15)-(3.17), the currents at the immediate right side of the fault point are described as,

$$\begin{bmatrix} I_{f1c} \\ I_{f1n} \end{bmatrix} = \begin{bmatrix} I_{rc} \\ 0 \end{bmatrix} + \frac{L-D}{2} \begin{bmatrix} Y_{cc} & Y_{cn} \\ Y_{nc} & Y_{nn} \end{bmatrix} \begin{bmatrix} V_{fc} + V_{rc} \\ V_{fn} + V_{rn} \end{bmatrix} \quad (3.18)$$

It is apparent that the core and sheath currents at the immediate left side and immediate right side of the fault point are exactly same in the healthy phases, i.e. phase B and C in this case. Thus, on the assumption that the currents of sheaths A and C are unchanged, a certain value of the current of sheath B can minimize the condition in Equation (3.19) when changing the real part and imaginary part of I_{sn}^B .

$$Cone^B = \left| I_{fn}^B - I_{f1n}^B \right|^2 \quad (3.19)$$

where I_{fn}^B and I_{f1n}^B can be calculated by Equations (3.14) and (3.18) respectively.

The above process is illustrated in Figure 3.6, where the vertex of the cone is related to the minimal point for the condition in Equation (3.19) and its x-y coordinates correspond to the real part and imaginary part of the desired current of sheath B.

The equation of a general conical surface can be represented as,

$$\frac{(x-x_0)^2}{a^2} + \frac{(y-y_0)^2}{b^2} = (z-z_0)^2 \quad (3.20)$$

Comparing with the conical surface in Figure 3.6, x_0 corresponds to $Real(I_{sn}^B)$ and y_0 to $Imag(I_{sn}^B)$, z_0 is very close to 0 and can be ignored, z^2 is the condition in Equation (3.19).

If assuming several pairs of x and y and calculating the relative z , the unknown coefficients a , b , x_0 and y_0 can be solved readily.

Based on the equation of the conical surface in such a shape, the simple solving procedure is explained in the following steps.

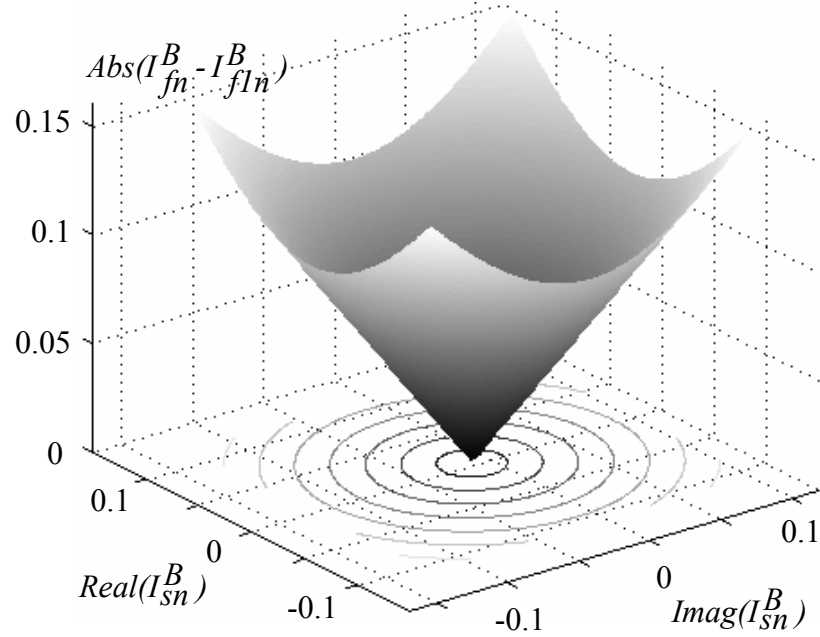


Figure 3.6: Conical surface to estimate current of the healthy sheath.

- Step 1: Assuming that the currents of sheaths A and C (I_{sn}^A and I_{sn}^C) are unchanged, which can be zeros or the values from the estimation for the previous assumed fault distance.
- Step 2: Setting $I_{sn}^A = 0, 1, -1, j, -j$, and calculating $Cone^B = C_1^B, C_2^B, C_3^B, C_4^B, C_5^B$ respectively using Equations (3.13)-(3.19).
- Step 3: The x-y coordinates of the vertex can be simply obtained by

$$I_{sn}^B = \frac{C_2^B - C_4^B}{2(C_1^B - C_2^B - C_4^B)} + j \frac{C_3^B - C_5^B}{2(C_1^B - C_3^B - C_5^B)} \quad (3.21)$$

The estimation of the sheath current of the healthy phase C has the very similar process, differentiating in the condition below:

$$Cone^C = \left| I_{fn}^C - I_{f1n}^C \right|^2 \quad (3.22)$$

3.3.2.2 Estimation of Sheath Current of Faulty Cable

Hitherto, a fault distance is assumed and the currents in the healthy sheaths have been estimated. In order to solve all variables in the circuit, it is necessary to estimate the sheath current in the faulty phase.

The known precondition of the faulty phase at the fault point is the fault resistance has the non-negative real number. Therefore, with changing of the real part and imaginary part of the current of sheath A, the three-dimensional shape of the imaginary part of the calculated fault resistances can be observed to find any hints for estimating a suitable sheath current, as shown in Figure 3.7 where the inclined plane represents the imaginary part of R_{f1} and the curved surface shows the imaginary part of R_{f2} .

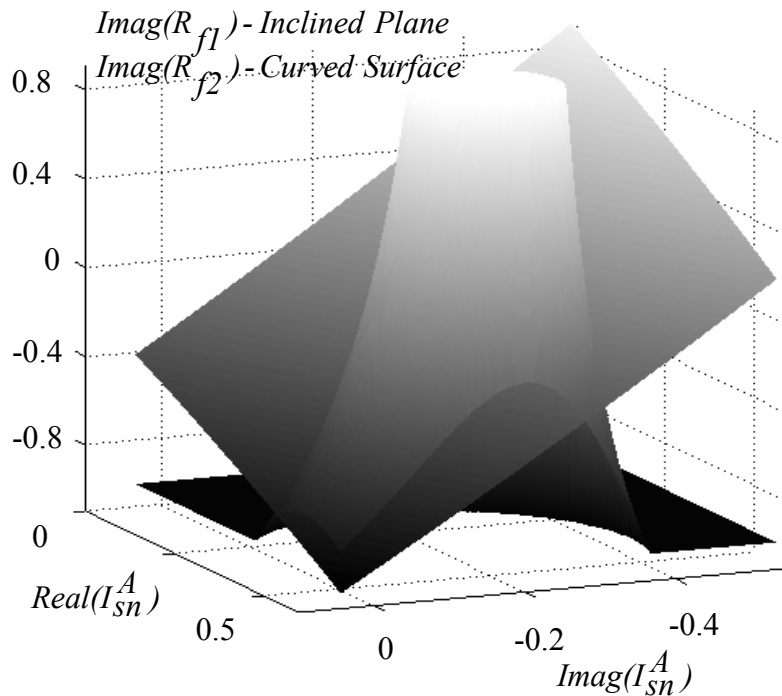


Figure 3.7: Three-dimensional illustration to estimate current of the faulty sheath.

Since the imaginary part of the fault resistance is zero, the three-dimensional surface is contoured to a two-dimensional plane in Figure 3.8 in which the contour of $Imag(R_{f2})=0$ is a circle and the one of $Imag(R_{f1})=0$ is a straight line. Apparently, two crossing dots, the square one and round one, are associated with the current of sheath A satisfying the zero value of the imaginary parts of the fault resistances. As the fault resistance has the non-negative value, the round dot is selected as the desired estimation accordingly.

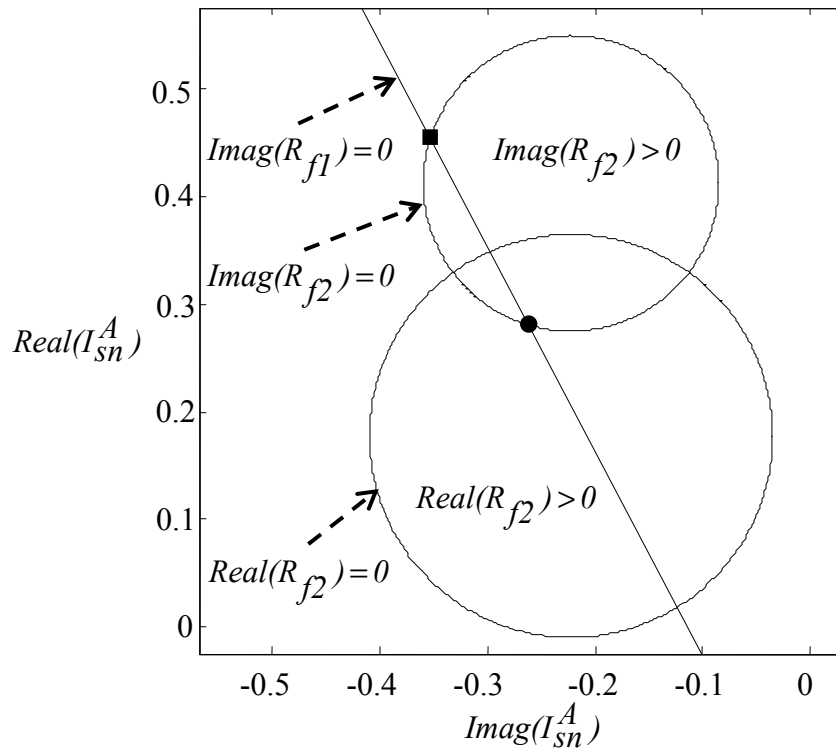


Figure 3.8: Contour of Figure 3.7 at zero planes.

In summary, the estimation process for sheath A can be concluded as the following steps.

- Step 1: Setting an initial current of sheath A (I_{sn}^A), which can be zero or the value from the estimation for the previous assumed fault distance.
- Step 2: Calculating the imaginary part of R_{f1} for several points around the initial current using Equations (3.13)-(3.18) and (3.9).

- Step 3: Finding the line equation by using the least square error technique.
- Step 4: Calculating the imaginary part of R_{f2} to find one in-circle point and three out-circle points using Equation (3.10).
- Step 5: Finding the circle equation by three points on the circle, which are iteratively calculated by four points obtained in Step 4.
- Step 6: Solving the line equation and the circle equation to find the crossing points and selecting the one with the non-negative fault resistance as the estimated current of the faulty sheath.

3.3.2.3 Pinpoint the Exact Fault Location

The currents of three sheaths have been estimated, therefore, the unknown variables in Equations (3.3)-(3.12) can be solved. However, the above results are based on a set of assumed fault distances, which will accordingly find a set of estimated sheath currents, as the round dots representing the estimated currents of sheath A, shown in Figure 3.9.

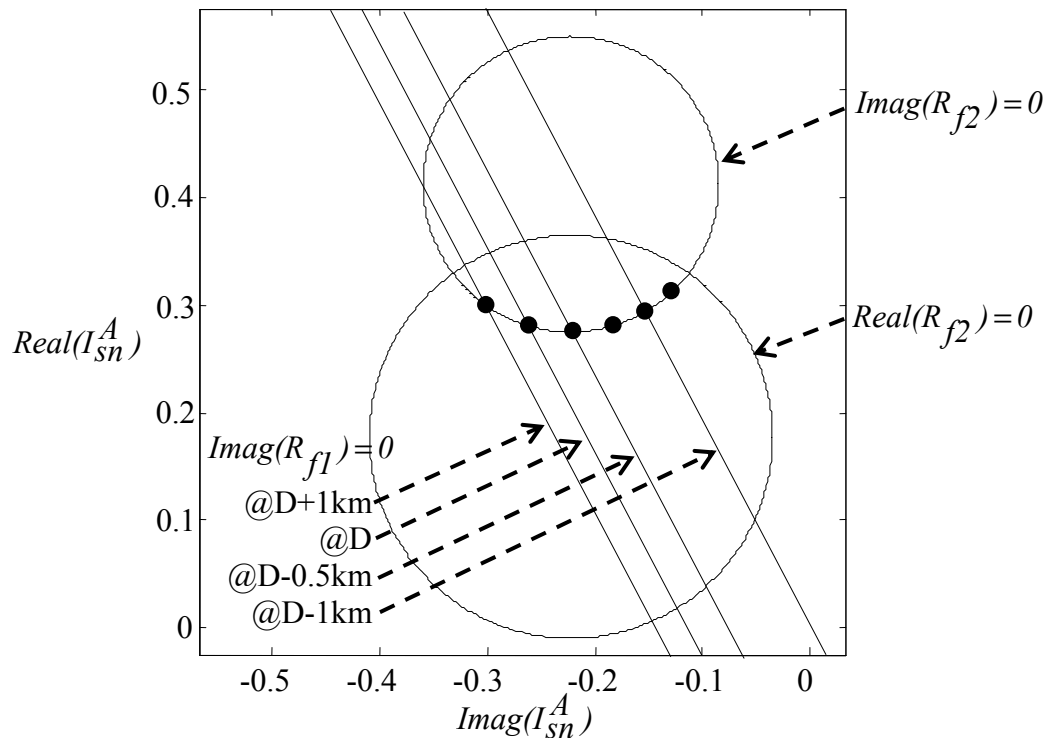


Figure 3.9: A set of estimated currents of sheath A marked as round dots.

Considering the consistent behavior of the healthy phases at the fault point, the correct distance could be pinpointed by one or combination of the following four criteria.

$$\begin{aligned}
 & 1. \min\left(\text{abs}\left(I_{fc}^B - I_{f1c}^B\right)\right); & 2. \min\left(\text{abs}\left(I_{fc}^C - I_{f1c}^C\right)\right); \\
 & 3. \max\left(\text{abs}\left(\frac{V_{fc}^B - V_{fn}^B}{I_{fc}^B - I_{f1c}^B}\right)\right); & 4. \max\left(\text{abs}\left(\frac{V_{fc}^C - V_{fn}^C}{I_{fc}^C - I_{f1c}^C}\right)\right)
 \end{aligned} \tag{3.23}$$

The four pinpoint criteria are shown in Figure 3.10 for a fault at 2 km of a 9 km cable, where the location results are quite accurate. The more accurate distance can be obtained by averaging the results from the calculations of more samples.

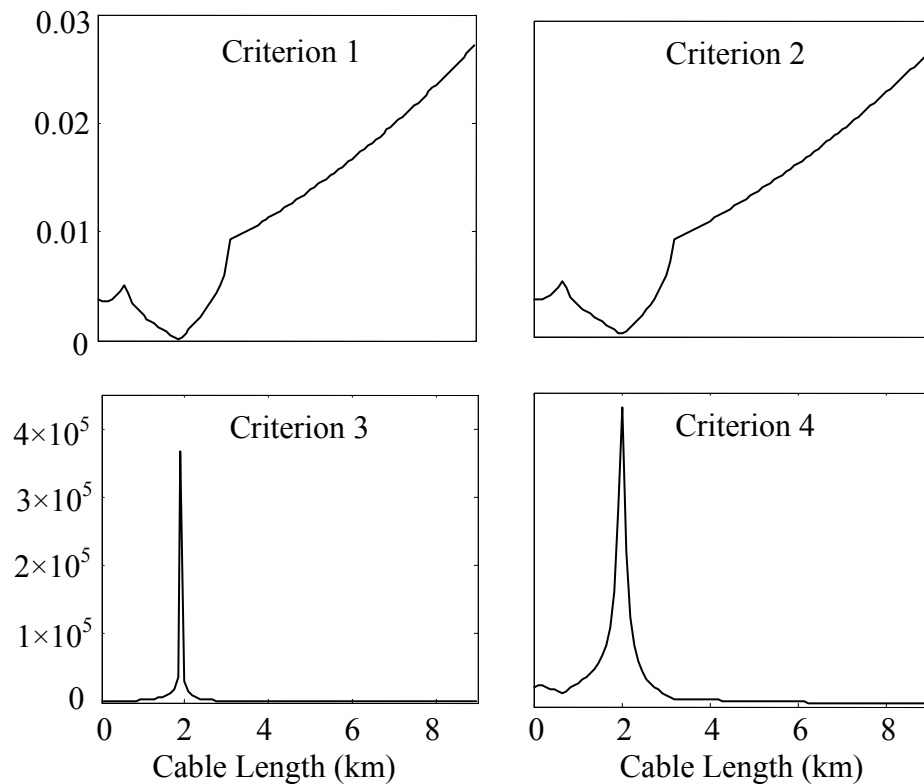


Figure 3.10: Example to show results of pinpoint criteria.

3.3.2.4 Location Procedure

Overall, the location procedure for CSGF is summarized in Figure 3.11. The whole procedure can be divided as two steps, the estimation step followed by the pinpoint step. The estimation step is to estimate the sheath currents at each assumed fault distance, and the pinpoint step is to find the exact fault point based on the results obtained in the first step.

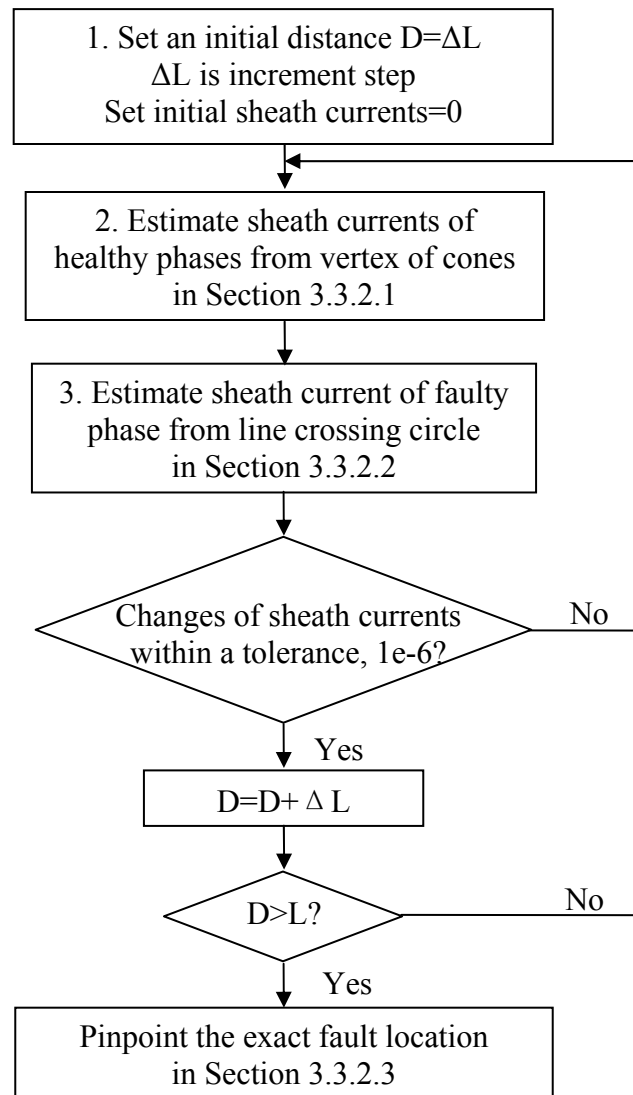


Figure 3.11: Location procedure for CSGF & SPBS.

3.3.3 Locating Core-Ground Fault

The core-ground fault (CGF) only has one fault resistance shown in Figure 3.3 and defined in Equation (3.24), thus there is no crossing point to estimate the current of sheath A.

$$R_{f3} = \frac{V_{fc}^A}{I_{fc}^A - I_{f1c}^A} \quad (3.24)$$

However, the current of sheath A has no change at the fault point which is similar to the situation for sheaths B and C, i.e.,

$$I_{fn}^A = I_{f1n}^A \quad (3.25)$$

So the similar estimation condition applied for sheaths B and C in Equations (3.19) and (3.22) can be employed to estimate the current of sheath A, shown in Equation (3.26).

$$Cone^A = \left| I_{fn}^A - I_{f1n}^A \right|^2 \quad (3.26)$$

Consequently, the estimation process for the current of sheath A is similar to the one for currents of sheaths B and C, which is discussed in the previous subsection. The location procedure in Figure 3.11 can also be used except that the Block 3 should change to “Estimate sheath current of faulty phase from vertex of cone.” The same pinpoint criteria can be used as well.

Besides, there have 74 unknown real variables and 78 real equations in such a situation as listed in Table 3.4 and Table 3.5.

Table 3.4: List of Unknown Variables – SPBS & CGF

	Variable Name	Number of Real Variables
Sending End	V_{sn}, I_{sn}	$2*3*2=12$
Fault Point	$V_{fc}, V_{fn}, I_{fi}, I_{fn}, I_{f1i}, I_{f1n}$	$6*3*2=36$
Receiving End	$V_{rc}, V_{rn}, I_{rc}, I_{rn}$	$4*3*2=24$
Real Variable	R_{f3}, D	2
Total		74

Table 3.5: List of Equations – SPBS & CGF

	Equation Index	Number of Real Equations
All Sections	(3.3)-(3.6)	$4*2*3*2=48$
Current at Fault Point	(3.7)-(3.8), (3.25)	$(2*2+1)*2=10$
Bonding	(3.12)	$2*3*2=12$
Load	(3.11)	$1*3*2=6$
Fault Resistance	(3.24)	$1*2=2$
Total		78

3.3.4 Locating Core-Sheath Fault

With respect to the core-sheath fault (CSF), the only fault resistance exists between the core and sheath denoted by R_{f1} in Equation (3.9), which can be alternatively represented as,

$$R'_{f1} = \frac{V_{fn}^A - V_{fc}^A}{I_{fn}^A - I_{f1n}^A} \quad (3.27)$$

It has been observed that the contour of $\text{Imag}(R'_{f1}) = 0$ is a circle and the one of $\text{Imag}(R_{f1}) = 0$ is a straight line. Therefore, the very similar location procedure in Figure 3.11 can be applied.

Besides, there have 75 unknown real variables and 79 real equations to express the situation of CSF as listed in Table 3.6 and Table 3.7.

Table 3.6: List of Unknown Variables – SPBS & CSF

	Variable Name	Number of Real Variables
Sending End	V_{sn}, I_{sn}	$2*3*2=12$
Fault Point	$V_{fc}, V_{fn}, I_{fi}, I_{fn}, I_{f1i}, I_{f1n}$	$6*3*2=36$
Receiving End	$V_{rc}, V_{rn}, I_{rc}, I_{rn}$	$4*3*2=24$
Real Variable	R_{f1}, R_{f1}', D	3
Total		75

Table 3.7: List of Equations – SPBS & CSF

	Equation Index	Number of Real Equations
All Sections	(3.3)-(3.6)	$4*2*3*2=48$
Current at Fault Point	(3.7)-(3.8)	$2*2*2=8$
Bonding	(3.12)	$2*3*2=12$
Load	(3.11)	$1*3*2=6$
Fault Resistance	(3.9), (3.27)	$2*2=4$
Extra Equation	$R_{f1}=R_{f1}'$	1
Total		79

3.3.5 General Location Scheme

A general location scheme for all fault scenarios is described in Figure 3.12. Upon the occurrence of a fault, all three location algorithms are applied to find the fault. The fault resistances, R_{f1} , R_{f1}' , R_{f2} , and R_{f3} , at the pinpointed fault distance are calculated by Equations (3.9), (3.27), (3.10), and (3.24) respectively. Then the specific fault type is obtained by the rules in Table 3.8, where X is a practical non-negative value, X_R and X_I could be any value.

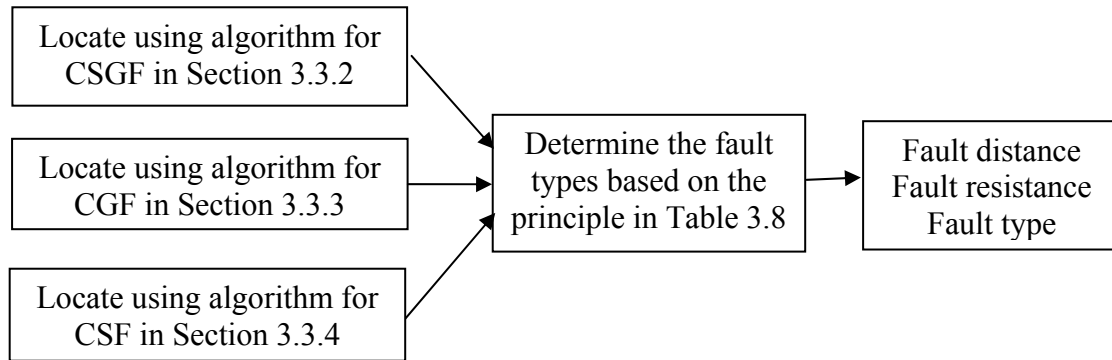


Figure 3.12: General location scheme - SPBS.

Table 3.8: Decision of Fault Scenarios in Practice

Fault Scenarios	Fault Resistance			
	R_{f1}	R_{f1}'	R_{f2}	R_{f3}
CSGF	$X+j0$	X_R+jX_I	$X+j0$	X_R+jX_I
CGF	X_R+jX_I	X_R+jX_I	X_R+jX_I	$X+j0$
CSF	$X+j0$	$\approx R_{f1}$	X_R+jX_I	X_R+jX_I

The location algorithm for SPBS has been explicated in this section, thus the location algorithms for other bonding methods will be compared with this algorithm unless otherwise specified.

3.4 Location Algorithm for Cables with SPBR

The location algorithm for cables with the configuration of the single point bonding at the receiving terminal (SPBR) is very similar to the one for SPBS. The differences and similarities between two algorithms will be discussed respectively in this subsection.

3.4.1 Differences from SPBS

There are four main differences in the algorithm for SPBR from the one for SPBS, i.e. bonding conditions, quantities to be estimated, load estimation and calculation equations.

- Due to the different bonding points, the sheath currents at the sending terminal are zeros and the sheath voltages at the receiving terminal are zeros. The fault equations describing the faulty section in the situation of CSGF are same as Equations (3.3)-(3.11), except that the boundary conditions in Equation (3.12) are changed to,

$$I_{sn} = 0; \quad V_{rn} = 0 \quad (3.28)$$

- The quantities to be estimated in the location algorithm are accordingly changed to the sheath voltages at the sending terminal (V_{sn}).
- The process of the load impedance estimation will be introduced in Section 3.9.1.2.
- The most different point is the calculation equations to describe the relations at the sending terminal, fault point and receiving terminal. Similarly, a fault distance (D) is assumed and three-phase sheath voltages (V_{sn}) are initially set to zeros or assigned to the values from the estimation for the previous assumed distance.

The voltages at the fault point are calculated by,

$$\begin{bmatrix} V_{fc} \\ V_{fn} \end{bmatrix} = \begin{bmatrix} V_{sc} \\ V_{sn} \end{bmatrix} - D \begin{bmatrix} Z_{cc} & Z_{cn} \\ Z_{nc} & Z_{nn} \end{bmatrix} \left(\begin{bmatrix} I_{sc} \\ 0 \end{bmatrix} - \frac{D}{2} \begin{bmatrix} Y_{cc} & Y_{cn} \\ Y_{nc} & Y_{nn} \end{bmatrix} \begin{bmatrix} V_{sc} \\ V_{sn} \end{bmatrix} \right) \quad (3.29)$$

The currents at the immediate left side of the fault point are formulated as,

$$\begin{bmatrix} I_{fc} \\ I_{fn} \end{bmatrix} = \begin{bmatrix} I_{sc} \\ 0 \end{bmatrix} - \frac{D}{2} \begin{bmatrix} Y_{cc} & Y_{cn} \\ Y_{nc} & Y_{nn} \end{bmatrix} \begin{bmatrix} V_{sc} + V_{fc} \\ V_{sn} + V_{fn} \end{bmatrix} \quad (3.30)$$

The voltages and currents at the receiving terminal are represented as,

$$I_{rc} = M^{-1} \begin{pmatrix} V_{fc} - NV_{fn} \end{pmatrix} \quad (3.31)$$

$$I_{rn} = J^{-1} \begin{pmatrix} V_{fn} - KI_{rc} \end{pmatrix} \quad (3.32)$$

$$V_{rc} = Z_{load} I_{rc} \quad (3.33)$$

where,

$$M = Z_{load} + (L-D) \left(Z_{cc} - Z_{cn} Z_{nn}^{-1} Z_{nc} \right) \left(IU + \frac{L-D}{2} Y_{cc} Z_{load} \right);$$

$$N = Z_{cn} Z_{nn}^{-1};$$

$$J = (L-D) Z_{nn};$$

$$K = (L-D) Z_{nc} \left(IU + \frac{L-D}{2} Y_{cc} Z_{load} \right) + \frac{(L-D)^2}{2} Z_{nn} Y_{nc} Z_{load};$$

$$Z_{load} = \begin{bmatrix} Z_{load}^A & 0 & 0 \\ 0 & Z_{load}^B & 0 \\ 0 & 0 & Z_{load}^C \end{bmatrix}$$

Then, the currents at the immediate right side of the fault point are described as,

$$\begin{bmatrix} I_{f1c} \\ I_{f1n} \end{bmatrix} = \begin{bmatrix} I_{rc} \\ I_{rn} \end{bmatrix} + \frac{L-D}{2} \begin{bmatrix} Y_{cc} & Y_{cn} \\ Y_{nc} & Y_{nn} \end{bmatrix} \begin{bmatrix} V_{fc} + V_{rc} \\ V_{fn} \end{bmatrix} \quad (3.34)$$

Comparing with the location procedure for SPBS, Equations (3.29)-(3.34) are used for solving problem in the case of SPBR instead of Equations (3.13)-(3.18) used for SPBS.

3.4.2 Similarities with SPBS

The similar issues between the algorithms for SPBR and SPBS are summarized as below.

- The known variables and preconditions in the calculation equations are almost same except for the boundary conditions.

- Similarly, there have 75 unknown real variables and 78 real equations for CSGF & SPBR, 74 unknown real variables and 78 real equations for CGF & SPBR, and 75 unknown real variables and 79 real equations for CSF & SPBR.
- The principle and procedure are basically similar in estimating sheath quantities of the healthy cables.
- The principle and procedure are quite similar in estimating sheath quantities of the faulty cable.
- The pinpoint criteria are completely same.
- The location principles for CSF and CGF are similar.
- The general location scheme and the fault type decision logic are exactly same.

3.5 Location Algorithm for Cables with SPBM

The cable with sheaths grounded at the middle point (SPBM) can be regarded as two cable sections, one equivalent to SPBR and the other to SPBS. It is clear that the algorithms presented in the previous subsections can be respectively applied for each section. However, the presence of one cable section would affect the calculations for the other section.

3.5.1 Fault in the First Half Section

3.5.1.1 Problem Formulation

The first half section with SPBM (SPBM-1) can be considered as a cable with SPBR. It is illustrated in Figure 3.13 where a CSGF occurs in SPBM-1.

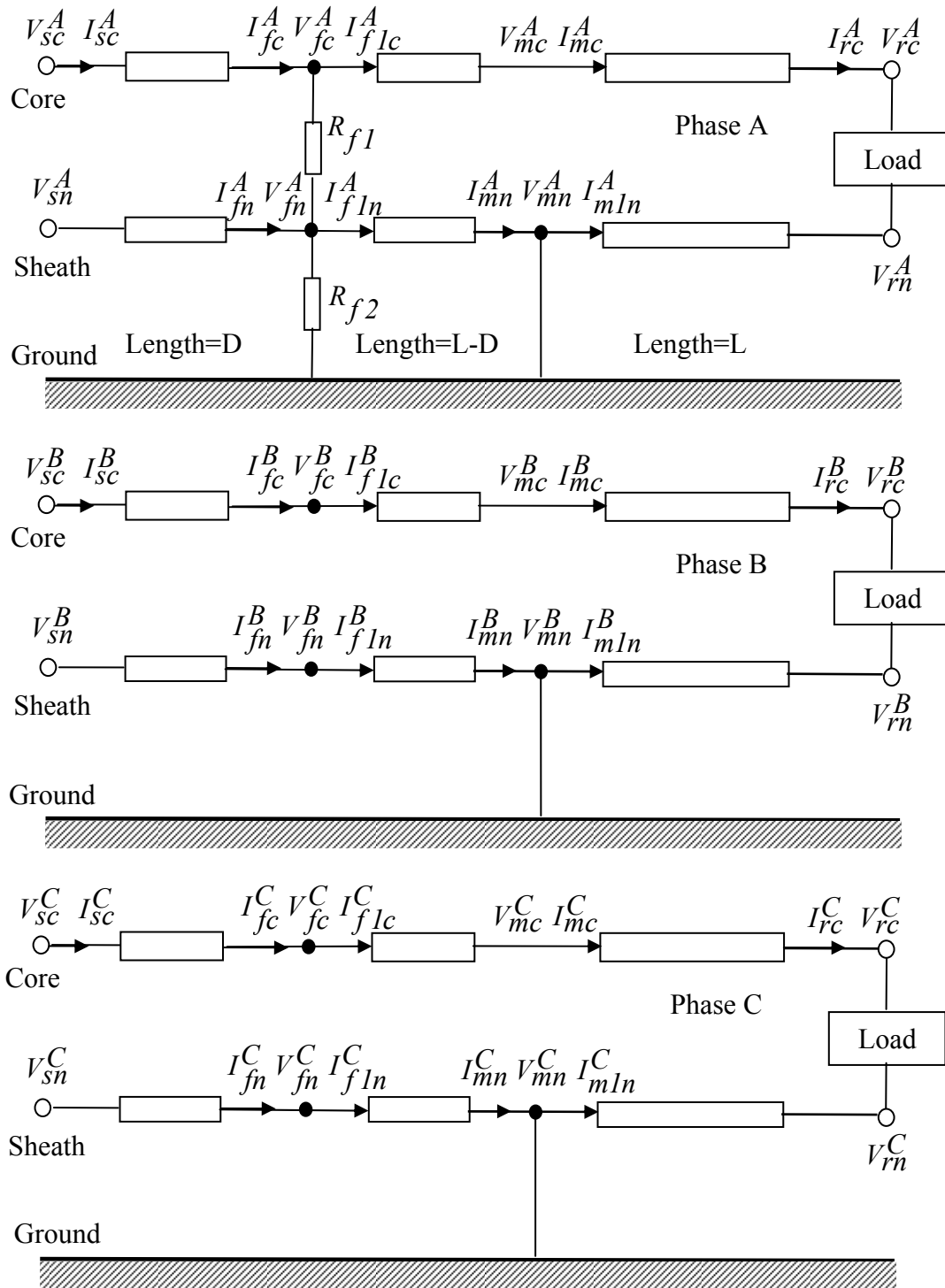


Figure 3.13: A CSGF in cable with SPBM-1.

The fault equations describing the circuit section from the sending terminal to the fault point are formulated as,

$$\begin{bmatrix} V_{fc} \\ V_{fn} \end{bmatrix} = \begin{bmatrix} V_{sc} \\ V_{sn} \end{bmatrix} - D \begin{bmatrix} Z_{cc} & Z_{cn} \\ Z_{nc} & Z_{nn} \end{bmatrix} \left(\begin{bmatrix} I_{sc} \\ I_{sn} \end{bmatrix} - \frac{D}{2} \begin{bmatrix} Y_{cc} & Y_{cn} \\ Y_{nc} & Y_{nn} \end{bmatrix} \begin{bmatrix} V_{sc} \\ V_{sn} \end{bmatrix} \right) \quad (3.35)$$

$$\begin{bmatrix} I_{fc} \\ I_{fn} \end{bmatrix} = \begin{bmatrix} I_{sc} \\ I_{sn} \end{bmatrix} - \frac{D}{2} \begin{bmatrix} Y_{cc} & Y_{cn} \\ Y_{nc} & Y_{nn} \end{bmatrix} \begin{bmatrix} V_{sc} + V_{fc} \\ V_{sn} + V_{fn} \end{bmatrix} \quad (3.36)$$

The fault equations describing the circuit section from the fault point to the middle point m are established as,

$$\begin{bmatrix} V_{mc} \\ V_{mn} \end{bmatrix} = \begin{bmatrix} V_{fc} \\ V_{fn} \end{bmatrix} - (L-D) \begin{bmatrix} Z_{cc} & Z_{cn} \\ Z_{nc} & Z_{nn} \end{bmatrix} \left(\begin{bmatrix} I_{f1c} \\ I_{f1n} \end{bmatrix} - \frac{L-D}{2} \begin{bmatrix} Y_{cc} & Y_{cn} \\ Y_{nc} & Y_{nn} \end{bmatrix} \begin{bmatrix} V_{fc} \\ V_{fn} \end{bmatrix} \right) \quad (3.37)$$

$$\begin{bmatrix} I_{mc} \\ I_{mn} \end{bmatrix} = \begin{bmatrix} I_{f1c} \\ I_{f1n} \end{bmatrix} - \frac{L-D}{2} \begin{bmatrix} Y_{cc} & Y_{cn} \\ Y_{nc} & Y_{nn} \end{bmatrix} \begin{bmatrix} V_{fc} + V_{mc} \\ V_{fn} + V_{mn} \end{bmatrix} \quad (3.38)$$

The fault equations describing the circuit section from the middle point to the receiving terminal are presented as,

$$\begin{bmatrix} V_{rc} \\ V_{rn} \end{bmatrix} = \begin{bmatrix} V_{mc} \\ V_{mn} \end{bmatrix} - L \begin{bmatrix} Z_{cc} & Z_{cn} \\ Z_{nc} & Z_{nn} \end{bmatrix} \left(\begin{bmatrix} I_{mc} \\ I_{m1n} \end{bmatrix} - \frac{L}{2} \begin{bmatrix} Y_{cc} & Y_{cn} \\ Y_{nc} & Y_{nn} \end{bmatrix} \begin{bmatrix} V_{mc} \\ V_{mn} \end{bmatrix} \right) \quad (3.39)$$

$$\begin{bmatrix} I_{rc} \\ I_{rn} \end{bmatrix} = \begin{bmatrix} I_{mc} \\ I_{m1n} \end{bmatrix} - \frac{L}{2} \begin{bmatrix} Y_{cc} & Y_{cn} \\ Y_{nc} & Y_{nn} \end{bmatrix} \begin{bmatrix} V_{rc} + V_{mc} \\ V_{rn} + V_{mn} \end{bmatrix} \quad (3.40)$$

The fault equations at the fault point are formed as,

$$I_{fc}^B = I_{f1c}^B, \quad I_{fc}^C = I_{f1c}^C \quad (3.41)$$

$$I_{fn}^B = I_{f1n}^B, I_{fn}^C = I_{f1n}^C \quad (3.42)$$

$$R_{f1} = \frac{V_{fc}^A - V_{fn}^A}{I_{fc}^A - I_{f1c}^A} \quad (3.43)$$

$$R_{f2} = \frac{V_{fn}^A}{I_{fc}^A - I_{f1c}^A + I_{fn}^A - I_{f1n}^A} \quad (3.44)$$

The boundary conditions due to the grounding of sheaths are given as,

$$I_{sn} = 0; I_{rn} = 0; V_{mn} = 0 \quad (3.45)$$

At the receiving terminal, the loads are modeled as the constant impedance, and there exists the following relation,

$$V_{rc} = Z_{load} I_{rc} \quad (3.46)$$

The whole cable circuit during the fault is represented by Equations (3.35)-(3.46). The known variables, preconditions and unknown variables in the equations are similar to the ones in Section 3.3.1.

For such a fault situation illustrated in Figure 3.13 and formulated in Equations (3.35)-(3.46), there have 105 unknown real variables and 108 real equations as listed in Table 3.9 and Table 3.10.

Table 3.9: List of Unknown Variables – SPBM-1 & CSGF

	Variable Name	Number of Real Variables
Sending End	V_{sn}, I_{sn}	$2*3*2=12$
Fault Point	$V_{fc}, V_{fn}, I_{fi}, I_{fn}, I_{f1i}, I_{f1n}$	$6*3*2=36$
Middle Point	$V_{mc}, V_{mn}, I_{mc}, I_{mn}, I_{m1n}$	$5*3*2=30$
Receiving End	$V_{rc}, V_{rn}, I_{rc}, I_{rn}$	$4*3*2=24$
Real Variable	R_{f1}, R_{f2}, D	3
Total		105

Table 3.10: List of Equations – SPBM-1 & CSGF

	Equation Index	Number of Real Equations
All Sections	(3.35)-(3.40)	6*2*3*2=72
Current at Fault Point	(3.41)-(3.42)	2*2*2=8
Bonding	(3.45)	3*3*2=18
Load	(3.46)	1*3*2=6
Fault Resistance	(3.43)-(3.44)	2*2=4
Total		108

3.5.1.2 Comparison with SPBR

There are two differences between the algorithm for SPBM-1 and the one for SPBR, i.e. the calculation equations and the process of load impedance estimation.

The voltages at the fault point are calculated by,

$$\begin{bmatrix} V_{fc} \\ V_{fn} \end{bmatrix} = \begin{bmatrix} V_{sc} \\ V_{sn} \end{bmatrix} - D \begin{bmatrix} Z_{cc} & Z_{cn} \\ Z_{nc} & Z_{nn} \end{bmatrix} \left(\begin{bmatrix} I_{sc} \\ 0 \end{bmatrix} - \frac{D}{2} \begin{bmatrix} Y_{cc} & Y_{cn} \\ Y_{nc} & Y_{nn} \end{bmatrix} \begin{bmatrix} V_{sc} \\ V_{sn} \end{bmatrix} \right) \quad (3.47)$$

The currents at the immediate left side of the fault point are formulated as,

$$\begin{bmatrix} I_{fc} \\ I_{fn} \end{bmatrix} = \begin{bmatrix} I_{sc} \\ 0 \end{bmatrix} - \frac{D}{2} \begin{bmatrix} Y_{cc} & Y_{cn} \\ Y_{nc} & Y_{nn} \end{bmatrix} \begin{bmatrix} V_{sc} + V_{fc} \\ V_{sn} + V_{fn} \end{bmatrix} \quad (3.48)$$

The voltages and currents at the receiving terminal are represented as,

$$I_{rc} = M^{-1} F \left(V_{fc} - N V_{fn} \right) \quad (3.49)$$

$$V_{rc} = Z_{load} I_{rc} \quad (3.50)$$

$$V_{rn} = D E I_{rc} \quad (3.51)$$

where,

$$M = Z_{load} - F \left(K + \frac{L}{2} KY_{cc} Z_{load} + \frac{L}{2} KY_{cn} DE \right) + LZ_{cc} + \frac{L^2}{2} Z_{cc} Y_{cc} Z_{load} \\ + \frac{L^2}{2} Z_{cc} Y_{cn} DE + \frac{L^2}{2} Z_{cn} Y_{nc} Z_{load} + \frac{L^2}{2} Z_{cn} Y_{nn} DE$$

$$F = \left(IU - \frac{L}{2} KY_{cc} - \frac{(L-D)}{2} KY_{cc} \right)^{-1};$$

$$N = Z_{cn}^{-1} Z_{nn};$$

$$D = \left(IU + \frac{L^2}{2} Z_{nc} Y_{cn} + \frac{L^2}{2} Z_{nn} Y_{nn} \right)^{-1};$$

$$E = - \left(LZ_{nc} + \frac{L^2}{2} Z_{nc} Y_{cc} Z_{load} + \frac{L^2}{2} Z_{nn} Y_{nc} Z_{load} \right);$$

$$K = (L-D) Z_{cn} Z_{nn}^{-1} Z_{nc} - (L-D) Z_{cc};$$

$$Z_{load} = \begin{bmatrix} Z_{load}^A & 0 & 0 \\ 0 & Z_{load}^B & 0 \\ 0 & 0 & Z_{load}^C \end{bmatrix}$$

Then, the voltages at the middle joint are described as,

$$\begin{bmatrix} V_{mc} \\ 0 \end{bmatrix} = \begin{bmatrix} V_{rc} \\ V_{rn} \end{bmatrix} + L \begin{bmatrix} Z_{cc} & Z_{cn} \\ Z_{nc} & Z_{nn} \end{bmatrix} \left(\begin{bmatrix} I_{rc} \\ 0 \end{bmatrix} + \frac{L}{2} \begin{bmatrix} Y_{cc} & Y_{cn} \\ Y_{nc} & Y_{nn} \end{bmatrix} \begin{bmatrix} V_{rc} \\ V_{rn} \end{bmatrix} \right) \quad (3.52)$$

The currents at the middle joint are described as,

$$\begin{bmatrix} I_{mc} \\ I_{m1n} \end{bmatrix} = \begin{bmatrix} I_{rc} \\ 0 \end{bmatrix} + \frac{L}{2} \begin{bmatrix} Y_{cc} & Y_{cn} \\ Y_{nc} & Y_{nn} \end{bmatrix} \begin{bmatrix} V_{mc} + V_{rc} \\ V_{rn} \end{bmatrix} \quad (3.53)$$

The sheath currents at the immediate left side of the joint point are described as,

$$I_{mn} = JV_{fn} - RI_{mc} - WV_{mn} \quad (3.54)$$

where,

$$J = \frac{1}{L-D} Z_{nn}^{-1},$$

$$R = Z_{nn}^{-1} Z_{nc};$$

$$W = \frac{L-D}{2} Z_{nn}^{-1} Z_{nc} Y_{cn} + \frac{L-D}{2} Y_{cn}$$

Finally, the currents at the immediate right side of the fault point are described as,

$$\begin{bmatrix} I_{f1c} \\ I_{f1n} \end{bmatrix} = \begin{bmatrix} I_{mc} \\ I_{mn} \end{bmatrix} + \frac{L-D}{2} \begin{bmatrix} Y_{cc} & Y_{cn} \\ Y_{nc} & Y_{nn} \end{bmatrix} \begin{bmatrix} V_{fc} + V_{mc} \\ V_{fn} \end{bmatrix} \quad (3.55)$$

Comparing with the location procedure for SPBR, Equations (3.47)-(3.55) are used for SPBM-1 instead of Equations (3.29)-(3.34) for SPBR. The load impedance estimation will be described in Section 3.9.1.3.

The similarities between the algorithm for SPBM-1 and the one for SPBR are concluded as below.

- The known variables and preconditions in the calculation equations are almost same except for the boundary conditions in Equation (3.45).
- As mentioned above, there have 105 unknown real variables and 108 real equations for a situation with CSGF & SPBM-1, similarly, 104 unknown real variables and 108

real equations for CGF & SPBM-1, and 105 unknown real variables and 109 real equations for CSF & SPBM-1.

- The following aspects are basically similar to the algorithm for SPBR.
 - Principle and procedure of estimating sheath quantities of the healthy cables;
 - Principle and procedure of estimating sheath quantities of the faulty cable;
 - Pinpoint criteria;
 - Location principles for CSF and CGF;
 - General location scheme for the first section;
 - Fault type decision logic.

3.5.2 Fault in the Second Half Section

The second half section with SPBM (SPBM-2) can be considered as a cable with SPBS and the algorithm for SPBS can be directly used if the core voltages (V_{mc}) and currents (I_{mc}) at the middle point are known.

Assuming a fault occurs in SPBM-2 in Figure 3.13, the fault equations describing the circuit section from the sending terminal to the middle point are formulated as,

$$\begin{bmatrix} V_{mc} \\ 0 \end{bmatrix} = \begin{bmatrix} V_{sc} \\ V_{sn} \end{bmatrix} - L \begin{bmatrix} Z_{cc} & Z_{cn} \\ Z_{nc} & Z_{nn} \end{bmatrix} \left(\begin{bmatrix} I_{sc} \\ 0 \end{bmatrix} - \frac{L}{2} \begin{bmatrix} Y_{cc} & Y_{cn} \\ Y_{nc} & Y_{nn} \end{bmatrix} \begin{bmatrix} V_{sc} \\ V_{sn} \end{bmatrix} \right) \quad (3.56)$$

$$\begin{bmatrix} I_{mc} \\ I_{mn} \end{bmatrix} = \begin{bmatrix} I_{sc} \\ 0 \end{bmatrix} - \frac{L}{2} \begin{bmatrix} Y_{cc} & Y_{cn} \\ Y_{nc} & Y_{nn} \end{bmatrix} \begin{bmatrix} V_{sc} + V_{mc} \\ V_{sn} \end{bmatrix} \quad (3.57)$$

The unknown variables in the above two equations are V_{mc} , I_{mc} , I_{mn} and V_{sn} . The amount of equations is exactly same as the amount of the unknown variables, so all variables can be solved, and V_{sn} is given as,

$$V_{sn} = J^{-1} \left(MI_{sc} - NV_{sc} \right) \quad (3.58)$$

where,

$$J = IU + \frac{L^2}{2} Z_{nc} Y_{cn} + \frac{L^2}{2} Z_{nn} Y_{nn};$$

$$M = LZ_{nc};$$

$$N = \frac{L^2}{2} Z_{nc} Y_{cc} + \frac{L^2}{2} Z_{nn} Y_{nc}$$

It is obvious that the location problem here is equivalent to the one for SPBS after V_{mc} and I_{mc} are estimated by Equations (3.56)-(3.58). Hitherto, the location algorithm for SPBS in Section 3.3 can be used completely.

3.5.3 Location Scheme for Entire Cable

The location scheme for entire cable is described in Figure 3.14. The first half section is examined by the algorithm for SPBM-1. If the obtained fault distance (DI) is very close to the middle point, the algorithm for SPBM-2 is applied then. Otherwise, the distance DI is the true fault distance and the location process stops here. If the located distance ($D2$) is close to the joint point again, the real fault distance would be around the joint point. Otherwise, the distance $D2$ is the true fault distance.

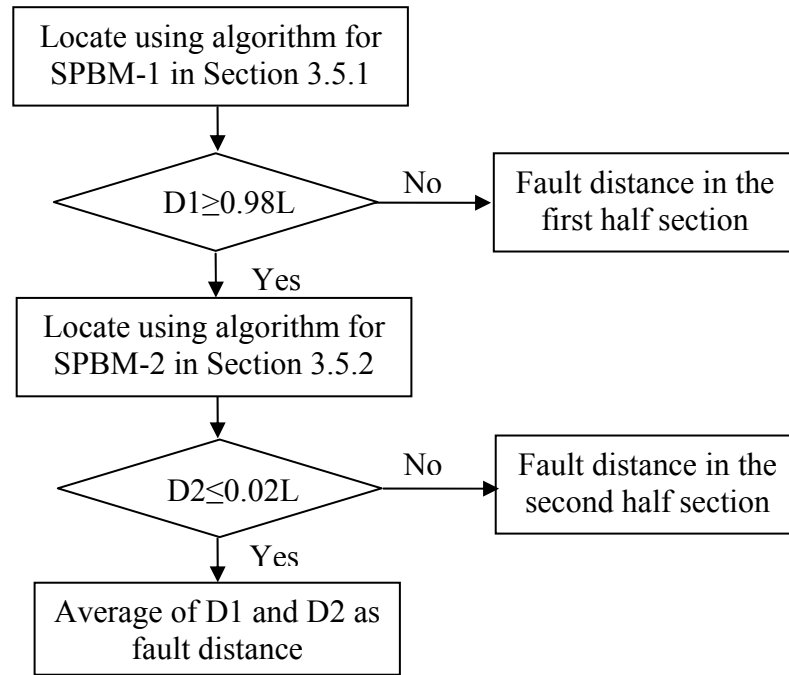


Figure 3.14: Location scheme for entire cable - SPBM.

3.6 Location Algorithm for Cables with SBBE

The location algorithm for cables with the configuration of the solid bonding at both ends (SBBE) is very similar to the one for SPBS.

3.6.1 Differences from SPBS

There are three main differences in the algorithm for SBBE from the one for SPBS, i.e. bonding conditions, calculation equations and load estimation.

- Due to the different bonding conditions, the sheath voltages at both terminals are zeros. The fault equations describing the faulty section in the situation of CSGF are same as Equations (3.3)- (3.11), except that the boundary conditions in Equation (3.12) are changed to,

$$V_{Sn} = 0; \quad V_{rn} = 0 \quad (3.59)$$

- The process of the load impedance estimation will be introduced in Section 3.9.1.4.
- The most different point is the calculation equations to describe the relations at the sending terminal, fault point and receiving terminal. Similarly, a fault distance (D) is assumed and three-phase current voltages (I_{sn}) are initially set to zeros or assigned to the values from the estimation for the previous assumed distance.

The voltages at the fault point are calculated by,

$$\begin{bmatrix} V_{fc} \\ V_{fn} \end{bmatrix} = \begin{bmatrix} V_{sc} \\ 0 \end{bmatrix} - D \begin{bmatrix} Z_{cc} & Z_{cn} \\ Z_{nc} & Z_{nn} \end{bmatrix} \left(\begin{bmatrix} I_{sc} \\ I_{sn} \end{bmatrix} - \frac{D}{2} \begin{bmatrix} Y_{cc} & Y_{cn} \\ Y_{nc} & Y_{nn} \end{bmatrix} \begin{bmatrix} V_{sc} \\ 0 \end{bmatrix} \right) \quad (3.60)$$

The currents at the immediate left side of the fault point are formulated as,

$$\begin{bmatrix} I_{fc} \\ I_{fn} \end{bmatrix} = \begin{bmatrix} I_{sc} \\ I_{sn} \end{bmatrix} - \frac{D}{2} \begin{bmatrix} Y_{cc} & Y_{cn} \\ Y_{nc} & Y_{nn} \end{bmatrix} \begin{bmatrix} V_{sc} + V_{fc} \\ V_{fn} \end{bmatrix} \quad (3.61)$$

The voltages and currents at the receiving terminal are represented as,

$$\begin{bmatrix} I_{rc} \\ I_{rn} \end{bmatrix} = \begin{bmatrix} M_{11} & M_{12} \\ M_{21} & M_{22} \end{bmatrix}^{-1} \begin{bmatrix} V_{fc} \\ V_{fn} \end{bmatrix} \quad (3.62)$$

$$V_{rc} = Z_{load} I_{rc} \quad (3.63)$$

where,

$$\begin{aligned} M_{11} = & Z_{load} + (L-D)Z_{cc} + \frac{(L-D)^2}{2} Y_{cc} Z_{cc} Z_{load} \\ & + \frac{(L-D)^2}{2} Y_{nc} Z_{cn} Z_{load}; \end{aligned}$$

$$\begin{aligned}
M_{12} &= (L-D)Z_{cn}; \\
M_{21} &= (L-D)Z_{nc} + \frac{(L-D)^2}{2}Y_{cc}Z_{nc}Z_{load} + \frac{(L-D)^2}{2}Y_{nc}Z_{nn}Z_{load}; \\
M_{22} &= (L-D)Z_{nn};
\end{aligned}$$

$$Z_{load} = \begin{bmatrix} Z_{load}^A & 0 & 0 \\ 0 & Z_{load}^B & 0 \\ 0 & 0 & Z_{load}^C \end{bmatrix}$$

Then, the currents at the immediate right side of the fault point are described as,

$$\begin{bmatrix} I_{f1c} \\ I_{f1n} \end{bmatrix} = \begin{bmatrix} I_{rc} \\ I_{rn} \end{bmatrix} + \frac{L-D}{2} \begin{bmatrix} Y_{cc} & Y_{cn} \\ Y_{nc} & Y_{nn} \end{bmatrix} \begin{bmatrix} V_{fc} + V_{rc} \\ V_{fn} \end{bmatrix} \quad (3.64)$$

Comparing with the location procedure for SPBS, Equations (3.60)-(3.64) are used for SBBE instead of Equations (3.13)-(3.18) used for SPBS.

3.6.2 Similarities with SPBS

The similar issues between the algorithms for SPBS and SBBE are summarized as below.

- The known variables and preconditions in the calculation equations are same except for the boundary conditions in Equation (3.59).
- Similarly, for a situation with CSGF & SBBE formulated in Equations (3.3)-(3.11) and (3.59), there have 75 unknown real variables and 78 real equations, 74 unknown real variables and 78 real equations for CGF & SBBE, and 75 unknown real variables and 79 real equations for CSF & SBBE.
- The following aspects are basically similar to the algorithm for SPBS.
 - Quantities to be estimated: sheath currents;
 - Principle and procedure of estimating sheath quantities of the healthy cables;

- Principle and procedure of estimating sheath quantities of the faulty cable;
- Pinpoint criteria;
- Location principles for CSF and CGF;
- General location scheme;
- Fault type decision logic.

3.7 Location Algorithm for Cables with XB

A cable with the cross bonding (XB) is divided into three sections of equal length and the sheaths are cross-connected at the joints. The first section is similar to SPBS at the starting terminal of the first section, but there have voltages and currents in sheaths at the ending terminal of the first section. The middle section has the voltages and currents in sheaths at both starting and ending terminals of this section. The last section is similar to SPBR at the ending terminal of the last section, but there have voltages and currents in sheaths at the starting terminal of the last section.

3.7.1 Fault in the First Section

3.7.1.1 Problem Formulation

A CSGF occurs in the first section with XB (XB-1), as illustrated in Figure 3.15.

The fault equations describing the circuit section from the sending terminal to the fault point are formulated as,

$$\begin{bmatrix} V_{fc} \\ V_{fn} \end{bmatrix} = \begin{bmatrix} V_{sc} \\ V_{sn} \end{bmatrix} - D \begin{bmatrix} Z_{cc} & Z_{cn} \\ Z_{nc} & Z_{nn} \end{bmatrix} \left(\begin{bmatrix} I_{sc} \\ I_{sn} \end{bmatrix} - \frac{D}{2} \begin{bmatrix} Y_{cc} & Y_{cn} \\ Y_{nc} & Y_{nn} \end{bmatrix} \begin{bmatrix} V_{sc} \\ V_{sn} \end{bmatrix} \right) \quad (3.65)$$

$$\begin{bmatrix} I_{fc} \\ I_{fn} \end{bmatrix} = \begin{bmatrix} I_{sc} \\ I_{sn} \end{bmatrix} - \frac{D}{2} \begin{bmatrix} Y_{cc} & Y_{cn} \\ Y_{nc} & Y_{nn} \end{bmatrix} \begin{bmatrix} V_{sc} + V_{fc} \\ V_{sn} + V_{fn} \end{bmatrix} \quad (3.66)$$

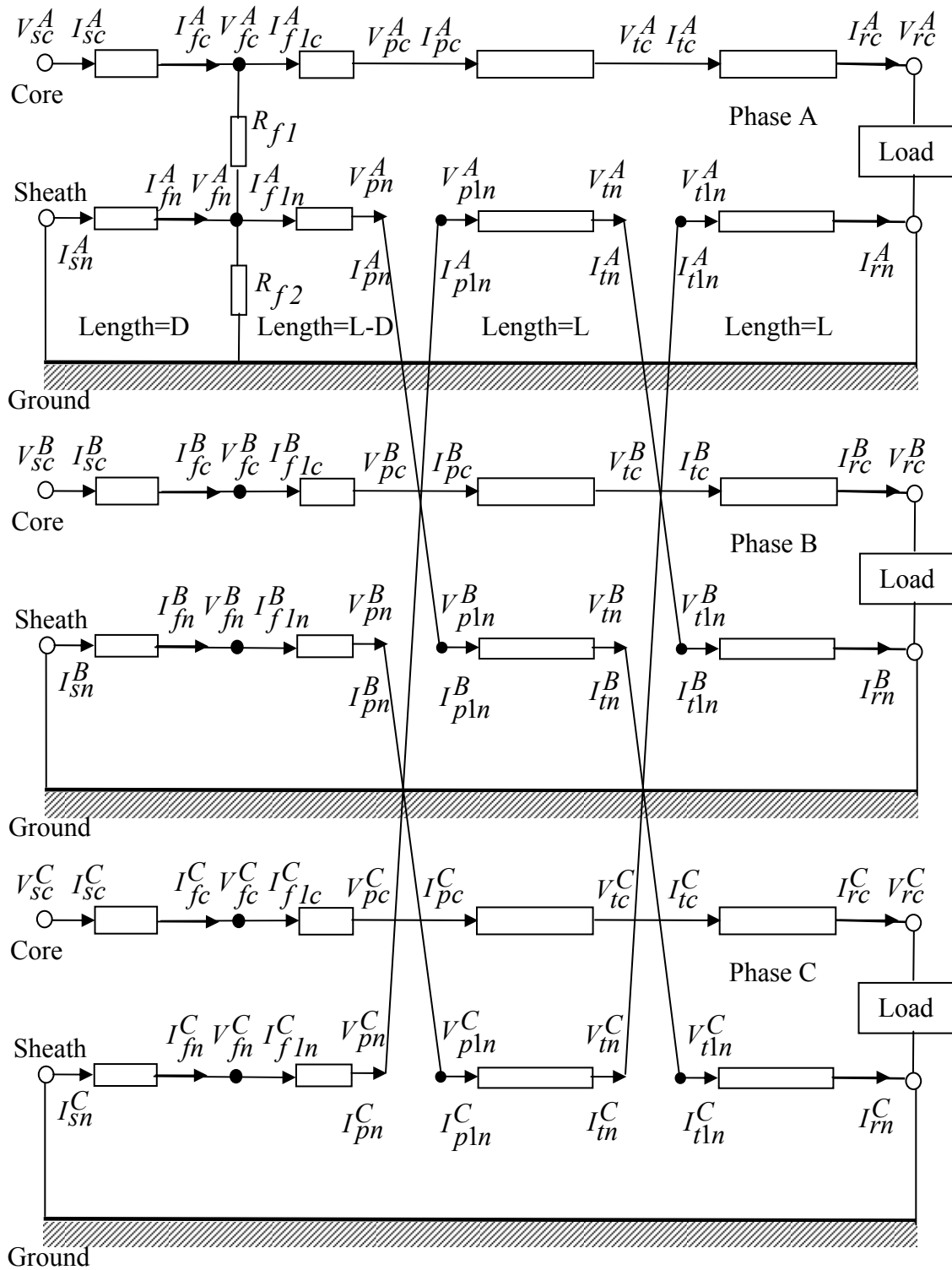


Figure 3.15: A CSGF in cable with XB-1.

The fault equations describing the circuit section from the fault point to the first joint point p are established as,

$$\begin{bmatrix} V_{pc} \\ V_{pn} \end{bmatrix} = \begin{bmatrix} V_{fc} \\ V_{fn} \end{bmatrix} - (L-D) \begin{bmatrix} Z_{cc} & Z_{cn} \\ Z_{nc} & Z_{nn} \end{bmatrix} \left(\begin{bmatrix} I_{f1c} \\ I_{f1n} \end{bmatrix} - \frac{L-D}{2} \begin{bmatrix} Y_{cc} & Y_{cn} \\ Y_{nc} & Y_{nn} \end{bmatrix} \begin{bmatrix} V_{fc} \\ V_{fn} \end{bmatrix} \right) \quad (3.67)$$

$$\begin{bmatrix} I_{pc} \\ I_{pn} \end{bmatrix} = \begin{bmatrix} I_{f1c} \\ I_{f1n} \end{bmatrix} - \frac{L-D}{2} \begin{bmatrix} Y_{cc} & Y_{cn} \\ Y_{nc} & Y_{nn} \end{bmatrix} \begin{bmatrix} V_{fc} + V_{pc} \\ V_{fn} + V_{pn} \end{bmatrix} \quad (3.68)$$

The fault equations describing the circuit section from the first joint point p to the second joint point t are presented as,

$$\begin{bmatrix} V_{tc} \\ V_{tn} \end{bmatrix} = \begin{bmatrix} V_{pc} \\ V_{pn} \end{bmatrix} - L \begin{bmatrix} Z_{cc} & Z_{cn} \\ Z_{nc} & Z_{nn} \end{bmatrix} \left(\begin{bmatrix} I_{pc} \\ I_{pn} \end{bmatrix} - \frac{L}{2} \begin{bmatrix} Y_{cc} & Y_{cn} \\ Y_{nc} & Y_{nn} \end{bmatrix} \begin{bmatrix} V_{pc} \\ V_{pn} \end{bmatrix} \right) \quad (3.69)$$

$$\begin{bmatrix} I_{tc} \\ I_{tn} \end{bmatrix} = \begin{bmatrix} I_{pc} \\ I_{pn} \end{bmatrix} - \frac{L}{2} \begin{bmatrix} Y_{cc} & Y_{cn} \\ Y_{nc} & Y_{nn} \end{bmatrix} \begin{bmatrix} V_{tc} + V_{pc} \\ V_{tn} + V_{pn} \end{bmatrix} \quad (3.70)$$

The fault equations describing the circuit section from the second joint point to the receiving terminal are presented as,

$$\begin{bmatrix} V_{rc} \\ V_{rn} \end{bmatrix} = \begin{bmatrix} V_{tc} \\ V_{tn} \end{bmatrix} - L \begin{bmatrix} Z_{cc} & Z_{cn} \\ Z_{nc} & Z_{nn} \end{bmatrix} \left(\begin{bmatrix} I_{tc} \\ I_{tn} \end{bmatrix} - \frac{L}{2} \begin{bmatrix} Y_{cc} & Y_{cn} \\ Y_{nc} & Y_{nn} \end{bmatrix} \begin{bmatrix} V_{tc} \\ V_{tn} \end{bmatrix} \right) \quad (3.71)$$

$$\begin{bmatrix} I_{rc} \\ I_{rn} \end{bmatrix} = \begin{bmatrix} I_{tc} \\ I_{tn} \end{bmatrix} - \frac{L}{2} \begin{bmatrix} Y_{cc} & Y_{cn} \\ Y_{nc} & Y_{nn} \end{bmatrix} \begin{bmatrix} V_{rc} + V_{tc} \\ V_{rn} + V_{tn} \end{bmatrix} \quad (3.72)$$

The fault equations at the fault point are formed as,

$$I_{fc}^B = I_{f1c}^B, \quad I_{fc}^C = I_{f1c}^C \quad (3.73)$$

$$I_{fn}^B = I_{f1n}^B, \quad I_{fn}^C = I_{f1n}^C \quad (3.74)$$

$$R_{f1} = \frac{V_{fc}^A - V_{fn}^A}{I_{fc}^A - I_{f1c}^A} \quad (3.75)$$

$$R_{f2} = \frac{V_{fn}^A}{I_{fc}^A - I_{f1c}^A + I_{fn}^A - I_{f1n}^A} \quad (3.76)$$

The boundary conditions due to the grounding of sheaths are given as,

$$V_{sn} = 0; \quad V_{rn} = 0 \quad (3.77)$$

The conditions at the first joint are given as,

$$V_{pn}^A = V_{p1n}^B; \quad V_{pn}^B = V_{p1n}^C; \quad V_{pn}^C = V_{p1n}^A \quad (3.78)$$

$$I_{pn}^A = I_{p1n}^B; \quad I_{pn}^B = I_{p1n}^C; \quad I_{pn}^C = I_{p1n}^A \quad (3.79)$$

The conditions at the second joint are given as,

$$V_{tn}^A = V_{t1n}^B; \quad V_{tn}^B = V_{t1n}^C; \quad V_{tn}^C = V_{t1n}^A \quad (3.80)$$

$$I_{tn}^A = I_{t1n}^B; \quad I_{tn}^B = I_{t1n}^C; \quad I_{tn}^C = I_{t1n}^A \quad (3.81)$$

At the receiving terminal, the loads are modeled as the constant impedance, and there exists the following relation,

$$V_{rc} = Z_{load} I_{rc} \quad (3.82)$$

The whole cable circuit during the fault is represented by Equations (3.65)-(3.82). The known variables, preconditions and unknown variables in the equations are similar with the ones in Section 3.3.1.

For such a fault situation illustrated in Figure 3.15 and formulated in Equations (3.65)-(3.82), there have 147 unknown real variables and 150 real equations as listed in Table 3.11 and Table 3.12.

Table 3.11: List of Unknown Variables – XB & CSGF

	Variable Name	Number of Real Variables
Sending End	V_{sn}, I_{sn}	$2*3*2=12$
Fault Point	$V_{fc}, V_{fn}, I_{fi}, I_{fn}, I_{f1i}, I_{f1n}$	$6*3*2=36$
First Joint	$V_{pc}, V_{pn}, V_{p1n}, I_{pc}, I_{pn}, I_{p1n}$	$6*3*2=36$
Second Joint	$V_{tc}, V_{tn}, V_{t1n}, I_{tc}, I_{tn}, I_{t1n}$	$6*3*2=36$
Receiving End	$V_{rc}, V_{rn}, I_{rc}, I_{rn}$	$4*3*2=24$
Real Variable	R_{f1}, R_{f2}, D	3
Total		147

Table 3.12: List of Equations – XB & CSGF

	Equation Index	Number of Real Equations
All Sections	(3.65)-(3.72)	$8*2*3*2=96$
Current at Fault Point	(3.73)-(3.74)	$2*2*2=8$
Bonding	(3.77)	$2*3*2=12$
Joint Point	(3.78)-(3.81)	$4*3*2=24$
Load	(3.82)	$1*3*2=6$
Fault Resistance	(3.75)-(3.76)	$2*2=4$
Total		150

3.7.1.2 Calculation Equations

First, a transformation matrix T is defined to associate the quantities at each joint point.

$$T = \begin{bmatrix} 1 & 0 & 0 & 0 & 0 & 0 \\ 0 & 1 & 0 & 0 & 0 & 0 \\ 0 & 0 & 1 & 0 & 0 & 0 \\ 0 & 0 & 0 & 0 & 0 & 1 \\ 0 & 0 & 0 & 1 & 0 & 0 \\ 0 & 0 & 0 & 0 & 1 & 0 \end{bmatrix} \quad T^{-1} = \begin{bmatrix} 1 & 0 & 0 & 0 & 0 & 0 \\ 0 & 1 & 0 & 0 & 0 & 0 \\ 0 & 0 & 1 & 0 & 0 & 0 \\ 0 & 0 & 0 & 0 & 1 & 0 \\ 0 & 0 & 0 & 0 & 0 & 1 \\ 0 & 0 & 0 & 1 & 0 & 0 \end{bmatrix} \quad (3.83)$$

With the help of the transformation matrix, the relations at the joints in Equations (3.78)-(3.81) can be represented as,

$$V_{p1} = \begin{bmatrix} V_{pc}^A \\ V_{pc}^B \\ V_{pc}^C \\ V_{p1n}^A \\ V_{p1n}^B \\ V_{p1n}^C \end{bmatrix} = TV_p = T \begin{bmatrix} V_{pc}^A \\ V_{pc}^B \\ V_{pc}^C \\ V_{pn}^A \\ V_{pn}^B \\ V_{pn}^C \end{bmatrix} \quad I_{p1} = \begin{bmatrix} I_{pc}^A \\ I_{pc}^B \\ I_{pc}^C \\ I_{p1n}^A \\ I_{p1n}^B \\ I_{p1n}^C \end{bmatrix} = TI_p = T \begin{bmatrix} I_{pc}^A \\ I_{pc}^B \\ I_{pc}^C \\ I_{pn}^A \\ I_{pn}^B \\ I_{pn}^C \end{bmatrix} \quad (3.84)$$

$$V_{t1} = \begin{bmatrix} V_{tc}^A \\ V_{tc}^B \\ V_{tc}^C \\ V_{t1n}^A \\ V_{t1n}^B \\ V_{t1n}^C \end{bmatrix} = TV_t = T \begin{bmatrix} V_{tc}^A \\ V_{tc}^B \\ V_{tc}^C \\ V_{tn}^A \\ V_{tn}^B \\ V_{tn}^C \end{bmatrix} \quad I_{t1} = \begin{bmatrix} I_{tc}^A \\ I_{tc}^B \\ I_{tc}^C \\ I_{t1n}^A \\ I_{t1n}^B \\ I_{t1n}^C \end{bmatrix} = TI_t = T \begin{bmatrix} I_{tc}^A \\ I_{tc}^B \\ I_{tc}^C \\ I_{tn}^A \\ I_{tn}^B \\ I_{tn}^C \end{bmatrix} \quad (3.85)$$

The voltages at the fault point are calculated by,

$$V_f = V_s - DZ \left(I_s - \frac{D}{2} YV_s \right) \quad (3.86)$$

The currents at the immediate left side of the fault point are formulated as,

$$I_f = I_s - \frac{D}{2} Y (V_s + V_f) \quad (3.87)$$

The voltages and currents at the receiving terminal are represented as,

$$I_r = M^{-1} V_f \quad (3.88)$$

$$V_r = Z_{load} I_r \quad (3.89)$$

where,

$$M = T^{-1} N + (L - D) Z \left(T^{-1} J + \frac{(L - D)}{2} Y A^{-1} N \right);$$

$$N = \left(LZ T^{-1} + \frac{L^2}{2} Z T^{-1} Y Z_{load} + T^{-1} \left(Z_{load} + LZ + \frac{L^2}{2} Z Y Z_{load} \right) \right);$$

$$J = T^{-1} \left(IU + LY Z_{load} + \frac{L^3}{4} Y Z Y Z_{load} \right)$$

$$+ \frac{L}{2} Y \left(N + T^{-1} \left(Z_{load} + LZ + \frac{L^2}{2} Z Y Z_{load} \right) \right);$$

$$Z_{load} = \begin{bmatrix} Z_{load}^A & 0 & 0 & 0 & 0 & 0 \\ 0 & Z_{load}^B & 0 & 0 & 0 & 0 \\ 0 & 0 & Z_{load}^C & 0 & 0 & 0 \\ 0 & 0 & 0 & 0 & 0 & 0 \\ 0 & 0 & 0 & 0 & 0 & 0 \\ 0 & 0 & 0 & 0 & 0 & 0 \end{bmatrix}$$

The voltages and currents at the sending end of the last section are described as,

$$V_{t1} = V_r + LZ \left(I_r + \frac{Y}{2} V_r \right) \quad (3.90)$$

$$I_{t1} = I_r + \frac{L}{2} Y (V_r + V_{t1}) \quad (3.91)$$

The voltages and currents at the receiving end of the middle section are described as,

$$V_t = T^{-1} V_{t1} \quad (3.92)$$

$$I_t = T^{-1} I_{t1} \quad (3.93)$$

The voltages and currents at the sending end of the middle section are described as,

$$V_{p1} = V_t + LZ \left(I_t + \frac{Y}{2} V_t \right) \quad (3.94)$$

$$I_{p1} = I_t + \frac{L}{2} Y (V_t + V_{p1}) \quad (3.95)$$

The voltages and currents at the receiving end of the first section are described as,

$$V_p = T^{-1} V_{p1} \quad (3.96)$$

$$I_p = T^{-1} I_{p1} \quad (3.97)$$

Then, the currents at the immediate right side of the fault point are described as,

$$I_{f1} = I_p + \frac{(L-D)}{2} Y (V_f + V_p) \quad (3.98)$$

3.7.2 Fault in the Middle Section

The middle cable section with XB (XB-2) is different with all situation discussed in the previous subsections since there exist the voltages and currents in sheaths at both ends of

this section. The formulation is similar to the one in Equations (3.65)-(3.82) except that the fault occurs in the middle section.

3.7.2.1 Calculation Equations

The voltages and currents at the receiving end of the first section are calculated by,

$$V_p = V_s - LZ \left(I_s - \frac{L}{2} Y V_s \right) \quad (3.99)$$

$$I_p = I_s - \frac{L}{2} Y (V_s + V_p) \quad (3.100)$$

The voltages and currents at the sending end of the middle section are calculated by,

$$V_{p1} = T V_p \quad (3.101)$$

$$I_{p1} = T I_p \quad (3.102)$$

The voltages at the fault point are calculated by,

$$V_f = V_{p1} - DZ \left(I_{p1} - \frac{D}{2} Y V_{p1} \right) \quad (3.103)$$

The currents at the immediate left side of the fault point are formulated as,

$$I_f = I_{p1} - \frac{D}{2} Y (V_{p1} + V_f) \quad (3.104)$$

The voltages and currents at the receiving terminal are represented as,

$$I_r = M^{-1} V_f \quad (3.105)$$

$$V_r = Z_{load} I_r \quad (3.106)$$

where,

$$M = (L-D)ZT^{-1} + \frac{(L-D)L}{2}ZT^{-1}YZ_{load} + NT^{-1} \left(Z_{load} + LZ + \frac{L^2}{2}ZYZ_{load} \right);$$

$$N = IU + \frac{(L-D)L}{2}ZT^{-1}YT + \frac{(L-D)^2}{2}ZY;$$

$$Z_{load} = \begin{bmatrix} Z_{load}^A & 0 & 0 & 0 & 0 & 0 \\ 0 & Z_{load}^B & 0 & 0 & 0 & 0 \\ 0 & 0 & Z_{load}^C & 0 & 0 & 0 \\ 0 & 0 & 0 & 0 & 0 & 0 \\ 0 & 0 & 0 & 0 & 0 & 0 \\ 0 & 0 & 0 & 0 & 0 & 0 \end{bmatrix}$$

The voltages and currents at the sending end of the last section are described as,

$$V_{t1} = V_r + LZ \left(I_r + \frac{Y}{2}V_r \right) \quad (3.107)$$

$$I_{t1} = I_r + \frac{L}{2}Y(V_r + V_{t1}) \quad (3.108)$$

The voltages and currents at the receiving end of the middle section are described as,

$$V_t = T^{-1}V_{t1} \quad (3.109)$$

$$I_t = T^{-1}I_{t1} \quad (3.110)$$

Then, the currents at the immediate right side of the fault point are described as,

$$I_{f1} = I_t + \frac{(L-D)}{2}Y(V_f + V_t) \quad (3.111)$$

3.7.3 Fault in the Last Section

The last cable section with XB (XB-3) has voltages and currents in sheaths at the starting terminal of the last section. The formulation is similar to the one in Equations (3.65)-(3.82) except that the fault occurs in the last section.

3.7.3.1 Calculation Equations

The voltages and currents at the receiving end of the first section are calculated by,

$$V_p = V_s - LZ \left(I_s - \frac{L}{2} Y V_s \right) \quad (3.112)$$

$$I_p = I_s - \frac{L}{2} Y (V_s + V_p) \quad (3.113)$$

The voltages and currents at the sending end of the middle section are calculated by,

$$V_{p1} = T V_p \quad (3.114)$$

$$I_{p1} = T I_p \quad (3.115)$$

The voltages and currents at the receiving end of the middle section are calculated by,

$$V_t = V_p - LZ \left(I_p - \frac{L}{2} Y V_p \right) \quad (3.116)$$

$$I_t = I_p - \frac{L}{2} Y (V_p + V_t) \quad (3.117)$$

The voltages and currents at the sending end of the last section are calculated by,

$$V_{t1} = T V_t \quad (3.118)$$

$$I_{t1} = T I_t \quad (3.119)$$

The voltages at the fault point are calculated by,

$$V_f = V_{t1} - DZ \left(I_{t1} - \frac{D}{2} Y V_{t1} \right) \quad (3.120)$$

The currents at the immediate left side of the fault point are formulated as,

$$I_f = I_{t1} - \frac{D}{2} Y \left(V_{t1} + V_f \right) \quad (3.121)$$

The voltages and currents at the receiving terminal are represented as,

$$I_r = M^{-1} V_f \quad (3.122)$$

$$V_r = Z_{load} I_r \quad (3.123)$$

where,

$$M = (L-D)Z + \left(Z_{load} + \frac{(L-D)^2}{2} Z Y Z_{load} \right);$$

$$Z_{load} = \begin{bmatrix} Z_{load}^A & 0 & 0 & 0 & 0 & 0 \\ 0 & Z_{load}^B & 0 & 0 & 0 & 0 \\ 0 & 0 & Z_{load}^C & 0 & 0 & 0 \\ 0 & 0 & 0 & 0 & 0 & 0 \\ 0 & 0 & 0 & 0 & 0 & 0 \\ 0 & 0 & 0 & 0 & 0 & 0 \end{bmatrix}$$

Then, the currents at the immediate right side of the fault point are described as,

$$I_{f1} = I_r + \frac{(L-D)}{2} Y \left(V_f + V_r \right) \quad (3.124)$$

3.7.4 Other Issues

Comparing with the detailed principle and procedure for SPBS, the similarity issues for all three XB methods are summarized as below.

- The known variables and preconditions in the calculation equations are same except for the boundary conditions in Equation (3.77).
- There have 147 unknown real variables and 150 real equations for CSGF & XB, 146 unknown real variables and 150 real equations for CGF & XB, and 147 unknown real variables and 151 real equations for CSF & XB.
- The following aspects are basically similar to the algorithm for SPBS.
 - Quantities to be estimated: sheath currents;
 - Principle and procedure of estimating sheath quantities of the healthy cables;
 - Principle and procedure of estimating sheath quantities of the faulty cable;
 - Pinpoint criteria;
 - Location principles for CSF and CGF;
 - General location scheme for each section
 - Fault type decision logic.

Besides, the process of the load impedance estimation will be introduced in Section 3.9.1.5.

3.7.5 Location Scheme for Entire Cable

Similar to the location scheme for SPBM, the location scheme for entire cable with XB is described in Figure 3.16.

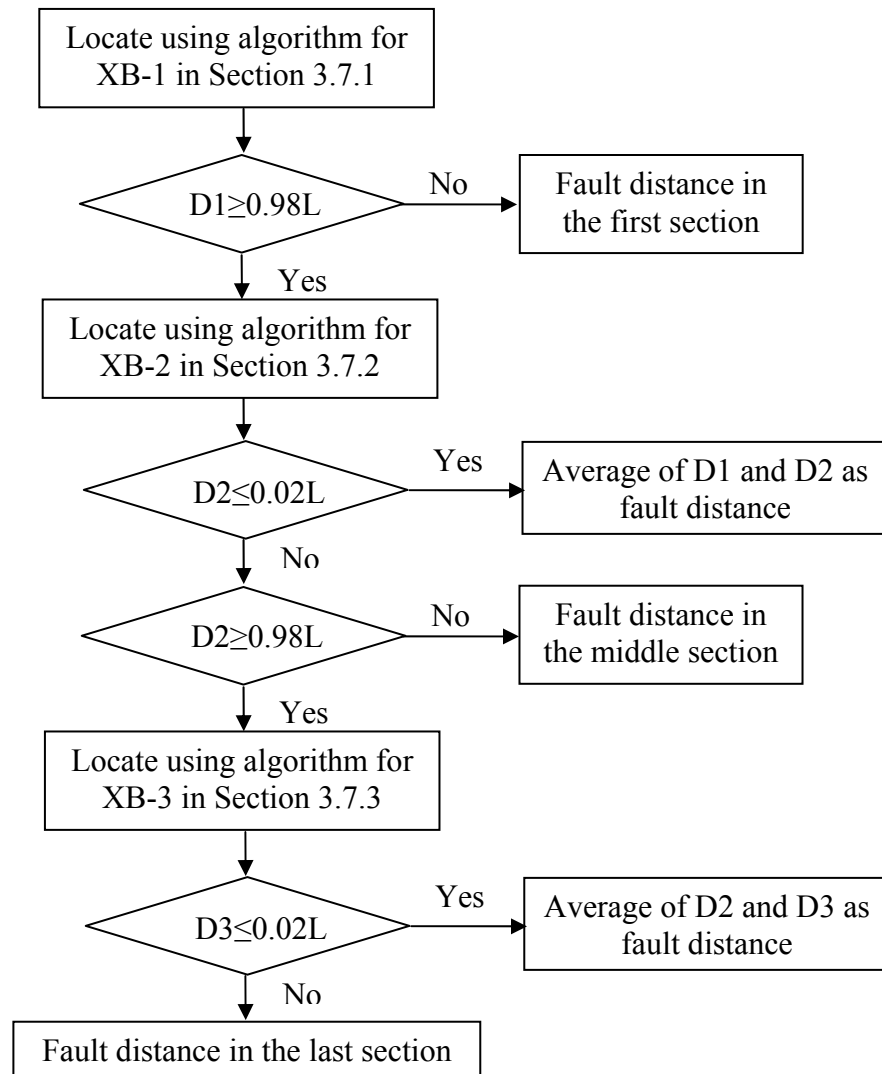


Figure 3.16: Location scheme for entire cable - XB.

3.8 Summary of Location Algorithms

The principle and procedure of the proposed algorithms for all bonding methods are summarized in Table 3.13 and Table 3.14.

Table 3.13: Summary of Algorithms for Single Point Bonding

		SPBS	SPBR	SPBM		
				First Half	Second Half	
Formulation equations		(3.3)-(3.12)	(3.3)-(3.11) (3.28)	(3.35)-(3.46)	(3.56)-(3.58) (3.3)-(3.11) (3.45)	
Number of real Variables	CSGF	75	75	105	105	
	CGF	74	74	104	104	
	CSF	75	75	105	105	
Number of real Equations	CSGF	78	78	108	108	
	CGF	78	78	108	108	
	CSF	79	79	109	109	
Bonding condition		(3.12)	(3.28)	(3.45)		
Calculation equations		(3.13)-(3.18)	(3.29)-(3.34)	(3.47)-(3.55)	(3.56)-(3.58) (3.13)-(3.18)	
Estimation	Quantity to be estimated		Sheath Current	Sheath Voltage	Sheath Voltage	Sheath Current
	Healthy Sheaths	Cone Equation	(3.19), (3.22)			
	Faulty Sheath (CSGF&CSF)	CSGF Line	(3.9) $\text{Imag}(R_{f1})=0$			
		CSGF Circle	(3.10) $\text{Imag}(R_{f2})=0$			
		CSF Line	(3.9) $\text{Imag}(R_{f1})=0$			
		CSF Circle	(3.27) $\text{Imag}(R_{f1}')=0$			
	Faulty Sheath (CGF)	Cone Equation	(3.26)			
		R_{f3}	(3.24)			
Pinpoint criteria		(3.23)				

Table 3.14: Summary of Algorithms for Solid and Cross Bonding

		SBBE	XBB		
			First	Middle	Last
Formulation equations		(3.3)-(3.11) (3.59)	(3.65)-(3.82)	Similar to (3.65)-(3.82)	Similar to (3.65)-(3.82)
Number of real variables	CSGF	75	147	147	147
	CGF	74	146	146	146
	CSF	75	147	147	147
Number of real equations	CSGF	78	150	150	150
	CGF	78	150	150	150
	CSF	79	151	151	151
Bonding condition		(3.59)	(3.77)		
Calculation equations		(3.60)-(3.64)	(3.86)-(3.98)	(3.99)-(3.111)	(3.112)- (3.124)
Estimation	Quantity to be estimated		Sheath Current	Sheath Current	
	Healthy Sheaths	Cone Equation	(3.19), (3.22)		
	Faulty Sheath (CSGF& CSF)	CSGF Line	(3.9) $\text{Imag}(R_{f1})=0$		
		CSGF Circle	(3.10) $\text{Imag}(R_{f2})=0$		
		CSF Line	(3.9) $\text{Imag}(R_{f1})=0$		
		CSF Circle	(3.27) $\text{Imag}(R_{f1}')=0$		
	Faulty Sheath (CGF)	Cone Equation	(3.26)		
R_{f3}		(3.24)			
Pinpoint criteria		(3.23)			

Although there need twenty four sub-algorithms in total to cover all five bonding methods and three fault scenarios, actually, the very basic principle and procedure are very similar. With respect to a specific system where the bonding method is already assigned, the major difference is just to employ the related calculation equations.

3.9 Load Impedance Estimation

3.9.1 Constant Impedance Load Model

The load used in the location algorithms is modeled as the constant impedance which will keep unchanged during the fault. Since the voltages and currents at the load terminal are not available, the load impedance should be estimated based on the prefault voltages and currents recorded at the substation. In addition, the accurate estimation should take the effect of sheaths and bonding methods into account.

3.9.1.1 SPBS

The following procedure describes the load impedance estimation for a cable with SPBS.

- Step 1: Based on Equations (3.1), (3.2) and (3.12), the sheath currents at the sending terminal are calculated.

$$I_{sn} = D^{-1}(EV_{sc} + FI_{sc}) \quad (3.125)$$

where,

$$D = IU + \frac{L^2}{2}Y_{nc}Z_{cn} + \frac{L^2}{2}Y_{nn}Z_{nn};$$

$$E = \frac{L}{2}Y_{nc} \left(2IU + \frac{L^2}{2}Z_{cc}Y_{cc} + \frac{L^2}{2}Z_{cn}Y_{nc} \right) + \frac{L}{2}Y_{nn} \left(\frac{L^2}{2}Z_{nc}Y_{cc} + \frac{L^2}{2}Z_{nn}Y_{nc} \right);$$

$$F = -\frac{L^2}{2}Y_{nc}Z_{cc} - \frac{L^2}{2}Y_{nn}Z_{nc}$$

- Step 2: The voltages (V_{rc}) and currents (I_{rc}) at the receiving terminal are obtained by Equations (3.1), (3.2), and (3.12).
- Step 3: The load impedance is then found by,

$$\begin{aligned}
Z_{load}^A &= V_{rc}^A / I_{rc}^A \\
Z_{load}^B &= V_{rc}^B / I_{rc}^B \\
Z_{load}^C &= V_{rc}^C / I_{rc}^C
\end{aligned} \tag{3.126}$$

3.9.1.2 SPBR

The following procedure describes the load impedance estimation for a cable with SPBR.

- Step 1: Based on Equations (3.1), (3.2) and (3.28), the sheath voltages at the sending terminal are calculated.

$$V_{sn} = D^{-1}(EV_{sc} + FI_{sc}) \tag{3.127}$$

where,

$$D = IU + \frac{L^2}{2} Z_{nc} Y_{cn} + \frac{L^2}{2} Z_{nn} Y_{nn};$$

$$E = -\frac{L^2}{2} Z_{nc} Y_{cc} - \frac{L^2}{2} Z_{nn} Y_{nc};$$

$$F = LZ_{nc}$$

- Step 2: The voltages (V_{rc}) and currents (I_{rc}) at the receiving terminal are obtained by Equations (3.1), (3.2), and (3.28).
- Step 3: Similar to the step 3 in Section 3.9.1.1.

3.9.1.3 SPBM

The load estimation for SPBM can be divided into two steps, one for SPBR followed by the other for SPBS.

- Step 1: Based on Equations (3.56)-(3.58), the core voltages and currents at the middle points are estimated.

- The rest steps are same as the steps 1-3 used for SPBS in Section 3.9.1.1.

3.9.1.4 SBBE

Since the sheath voltages at both ends are zeros, the estimation for load impedance is quite simple in such situation.

- Step 1: Based on Equations (3.1), (3.2) and (3.59), the sheath currents at the sending terminal are calculated.

$$I_{sn} = EV_{sc} + FI_{sc} \quad (3.128)$$

where,

$$E = \frac{L}{2}Y_{nc} + \frac{L^3}{2}Z_{nn}Z_{nc}Y_{cc};$$

$$F = -L^2Z_{nn}Z_{nc}$$

- Step 2: The voltages (V_{rc}) and currents (I_{rc}) at the receiving terminal are obtained by Equations (3.1), (3.2), and (3.59).
- Step 3: Similar to the step 3 in Section 3.9.1.1.

3.9.1.5 XB

The cable with XB has negligible circulating currents in sheaths and the sheath voltages at both ends are zeros, so the effect of the sheath can be ignored at the normal condition. The load impedance can be calculated by the voltage and current estimated below.

$$V_{rc} = V_{sc} - 3LZ_{cc} \left(I_{sc} - \frac{3L}{2}Y_{cc}V_{sc} \right) \quad (3.129)$$

$$I_{rc} = I_{sc} - \frac{3L}{2}Y_{cc} \left(V_{sc} + V_{rc} \right) \quad (3.130)$$

3.9.2 Static Response Load Model

The proposed algorithms employ the constant impedance load model. The application of the static response type models discussed in Section 1.3.3 is investigated. The static response load model is rewritten below,

$$Y = G_r \left| \frac{V}{V_0} \right|^{n_p - 2} + jB_r \left| \frac{V}{V_0} \right|^{n_q - 2} \quad (3.131)$$

where Y is the load admittance, V is the voltage at the load point, V_0 is the nominal voltage, n_p and n_q are the response parameters for the active and reactive components of the load, G_r and B_r are the constants proportional to load conductance and load susceptance.

To find the load admittance, the voltage at the load point during fault and the values of G_r and B_r need to be determined.

The G_r and B_r can be estimated by the prefault voltage and current in Equation (3.132).

$$Y_r = \frac{I_r}{V_r} = G_r \left| \frac{V_r}{V_0} \right|^{n_p - 2} + jB_r \left| \frac{V_r}{V_0} \right|^{n_q - 2} \quad (3.132)$$

where I_r and V_r are the current and voltage at the load terminal, which can be estimated by the algorithms discussed in Section 3.9.1.

The voltage V in Equation (3.131) is the voltage at the load terminal during fault, which can be estimated based on the fact that the voltage drop along the circuit is small and almost proportional to the circuit length. Therefore, V can be approximately estimated by,

$$|V| = |V_f| - \frac{L-D}{L} \left(|V_s^{pre}| - |V_r^{pre}| \right) \quad (3.133)$$

where D is the fault distance, L is the cable length, V_s^{pre} is the prefault voltage measured at the sending terminal, V_r^{pre} is the prefault voltage at the receiving terminal estimated by algorithms in Section 3.9.1, and V_f is the fault voltage calculated in the location process.

3.10 Simulations

3.10.1 Test Cases

To validate the effectiveness and functionality of the proposed algorithms, the extensive simulation cases are carried out in PSCAD/EMTDC, involving the following variation of parameters and conditions:

- Three types of MV cables are modeled, one 8 km N2XS2Y-1*185-25/20kV, one 9 km NA2XS2Y-1*400-35/20kV and one 9 km N2XS2Y-1*185-25/20kV.
- Fault distances are distributed along the whole cable, from the first 50 meter to the last 50 meter.
- Fault resistances range from zero to 50 Ω .
- Three fault scenarios are involved, i.e. core-sheath-ground fault, core-ground fault and core-sheath fault.
- Five bonding methods are considered, including single point bonding at the sending, receiving, or middle point; solid bonding at both the sending and receiving ends; and cross bonding.

3.10.2 Simulation Results

The location error is defined in [35] as,

$$error = \frac{Estimated\ Distance - Exact\ Distance}{Total\ Line\ Length} \times 100\% \quad (3.134)$$

And the average of absolute values of location errors of the simulation results are concluded in Table 3.15.

Table 3.15: Average of Absolute Values of Location Errors

	Core-Sheath-Ground	Core-Ground	Core-Sheath	Average
Solid Bonding	0.044%	0.045%	0.048%	0.046% 3.68m of 8km
Single Point @ Sending	0.058%	0.051%	0.11%	0.072% 6.48m of 9km
Single Point @ Receiving	0.15%	0.047%	0.25%	0.15% 13.5m of 9km
Single Point @ Middle	0.17%	0.036%	0.52%	0.24% 21.6m of 9km
Cross Bonding	0.069%	0.072%	0.058%	0.066% 5.94m of 9km

In all simulations, the computation is first processed for 100 points along a cable with equal interval. After a suitable range is detected using the pinpoint criteria, the step length of five meters are applied to further find the more accurate fault point. In average, the computation time for eight samples in one cycle is less than one minute in an ordinary personal computer. The final fault distance is given as the average of eight calculations in one cycle, which will reduce, to certain extent, errors caused by the factors such as, phasor measurement errors and dynamic change of the fault resistance. Some of the simulation cases are selected for more discussion below.

3.10.2.1 Effect of Fault Type

Three fault types are examined for the five bonding methods respectively. The first scenario is to examine the effect of the different fault types at the condition with SPBS. A set of cases are investigated with the following conditions and the location errors are shown in Figure 3.17.

- Fault distance: 0.05, 1, 2, 3.2, 4.5, 5.2, 6, 7, 8, 8.95 km.
- Bonding method: Single-point bonding at the sending terminal.
- Fault resistances: (1) $R_{f1}=0\Omega$, $R_{f2}=0\Omega$ for core-sheath-ground fault; (2) $R_{f1}=0\Omega$ for core-sheath fault; (3) $R_{f3}=0\Omega$ for core-ground fault.

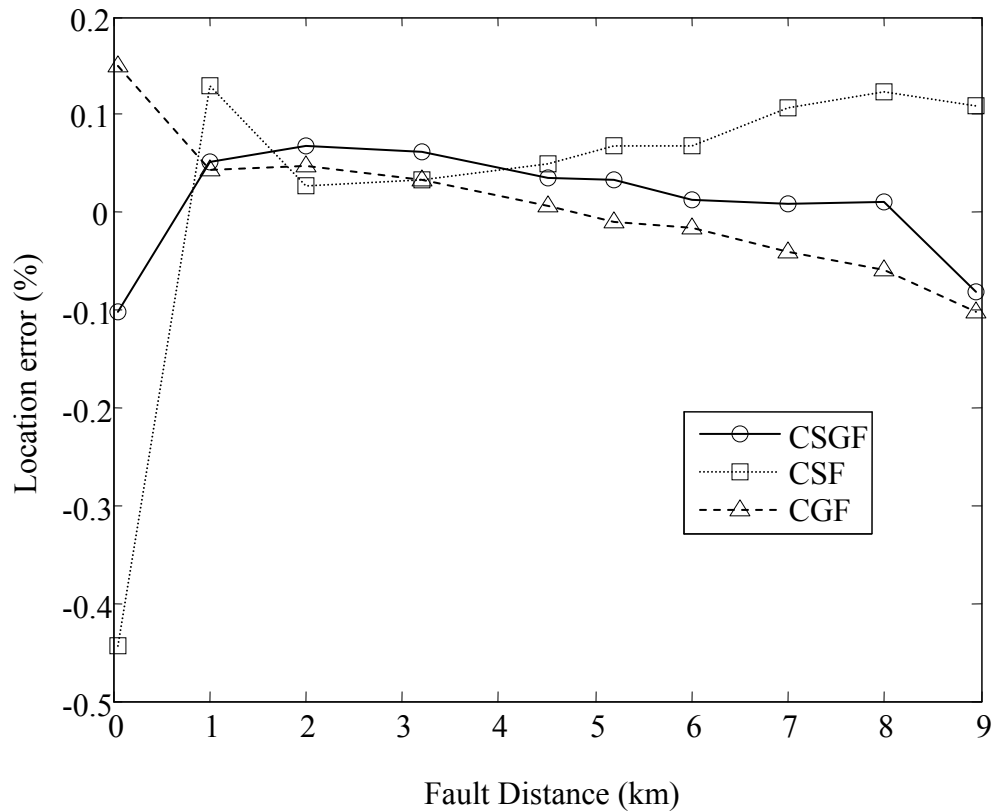


Figure 3.17: Effect of fault type - SPBS.

It can be observed that there is an error increase for the faults at the close-in point, which is owing to the effect of fault distance and will be discussed in Section 3.10.2.3.

Basically, the fault type has no effect on the location accuracy for the bonding method of SPBS.

The second scenario is to examine the effect of the different fault types at the condition with SPBR. A set of cases are investigated with the following conditions and the location errors are shown in Figure 3.18.

- Fault distance: 0.05, 1, 2, 3.2, 4.5, 5.2, 6, 7, 8, 8.95 km.
- Bonding method: Single-point bonding at the receiving terminal.

- Fault resistances: (1) $R_{f1}=0\Omega$, $R_{f2}=0\Omega$ for core-sheath-ground fault; (2) $R_{f1}=0\Omega$ for core-sheath fault; (3) $R_{f3}=0\Omega$ for core-ground fault.

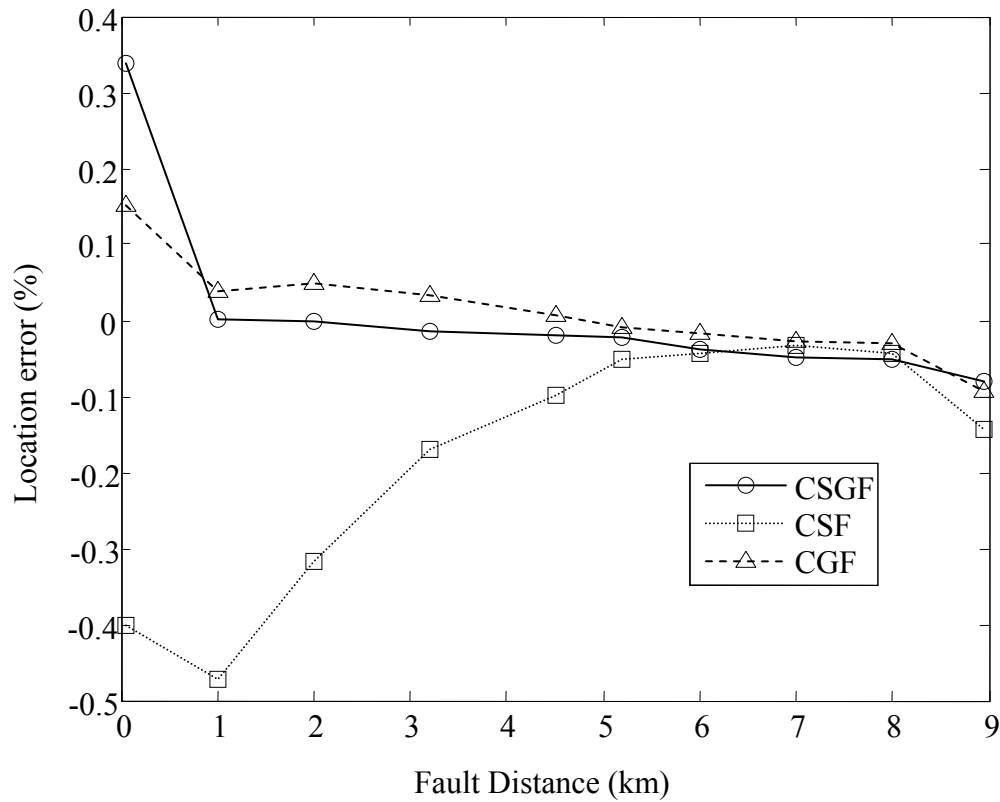


Figure 3.18: Effect of fault type - SPBR.

It can be observed that the CSF has the relatively large error at the first third section.

The third scenario is to examine the effect of the different fault types at the condition with SPBM. A set of cases are investigated with the following conditions and the location errors are shown in Figure 3.19.

- Fault distance: 0.05, 1, 2.5, 3.5, 4.5, 5.2, 6, 7, 8, 8.95 km.
- Bonding method: Single-point bonding at the middle point.

- Fault resistances: (1) $R_{f1}=0\Omega$, $R_{f2}=0\Omega$ for core-sheath-ground fault; (2) $R_{f1}=0\Omega$ for core-sheath fault; (3) $R_{f3}=0\Omega$ for core-ground fault.

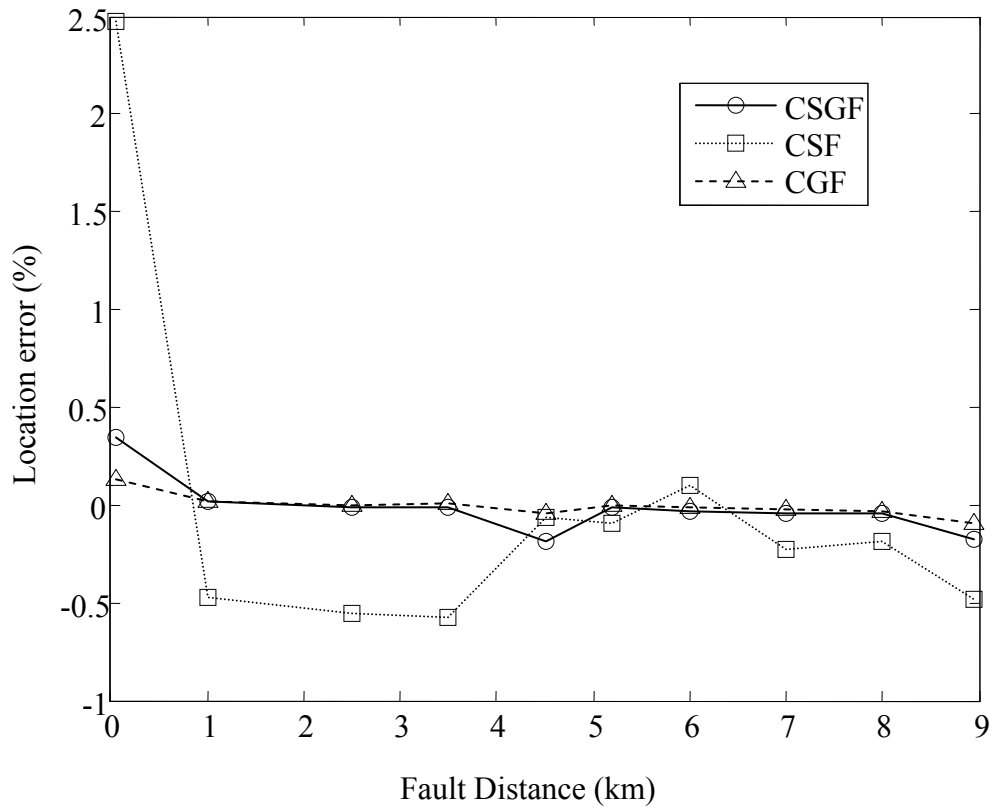


Figure 3.19: Effect of fault type - SPBM.

Similarly, the close-in faults will result in an error increase. However, the location error is especially high for the CSF type when faults occur at the first half section. It should be mentioned that the location error at the middle point is normal.

The fourth scenario is to examine the effect of the different fault types at the condition with SBBE. A set of cases are investigated with the following conditions and the location errors are shown in Figure 3.20.

- Fault distance: 0.05, 1, 2, 3, 3.9, 4.1, 5, 6, 7, 7.95 km.

- Bonding method: Solid bonding at both sending end and receiving end.
- Fault resistances: (1) $R_{f1}=0\Omega$, $R_{f2}=0\Omega$ for core-sheath-ground fault; (2) $R_{f1}=0\Omega$ for core-sheath fault; (3) $R_{f3}=0\Omega$ for core-ground fault.

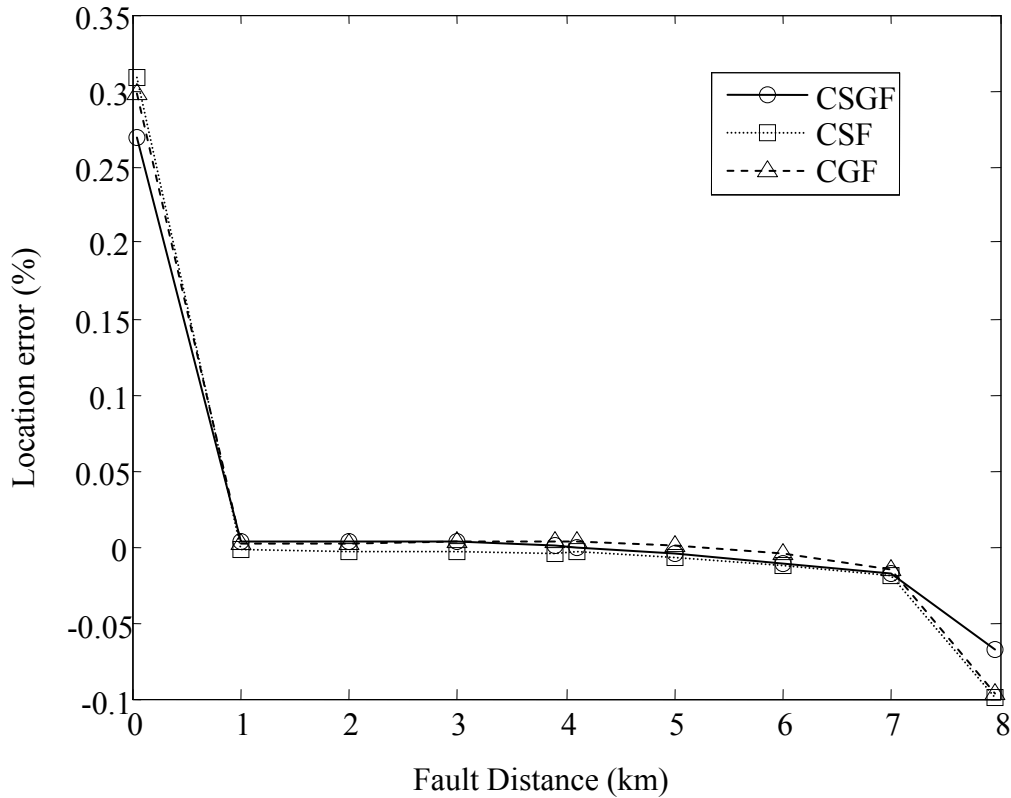


Figure 3.20: Effect of fault type - SBBE.

Basically, the fault types have no effect on the location accuracy at the situation with SBBE except that there is a bit high error for close-in and far-end faults.

The fifth scenario is to examine the effect of the different fault types at the condition with XB. A set of cases are investigated with the following conditions and the location errors are shown in Figure 3.21.

- Fault distance: 0.05, 1, 2, 3, 4, 5, 6, 7, 8, 8.95 km.

- Bonding method: Cross bonding.
- Fault resistances: (1) $R_{f1}=0\Omega$, $R_{f2}=0\Omega$ for core-sheath-ground fault; (2) $R_{f1}=0\Omega$ for core-sheath fault; (3) $R_{f3}=0\Omega$ for core-ground fault.

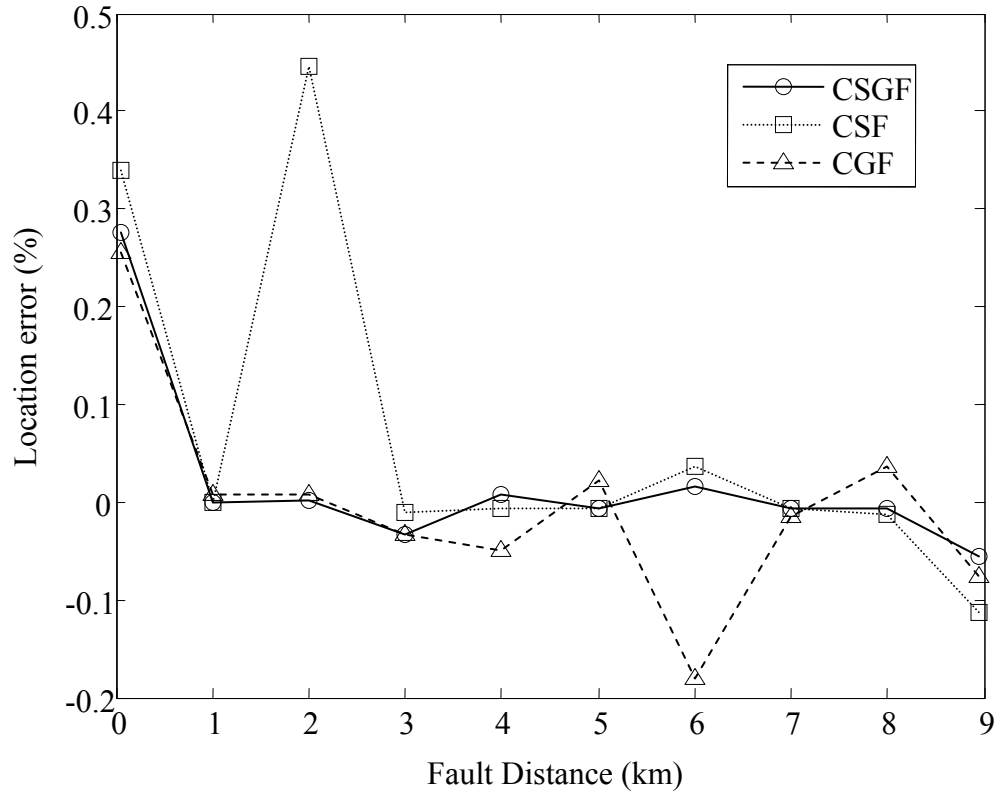


Figure 3.21: Effect of fault type - XB.

There is an error increase for the faults at the close-in, far-end, and crossing points. Basically, the fault type has no effect on the location accuracy for the cross bonding method.

3.10.2.2 Effect of Bonding Method

Five bonding methods are examined for the three fault types respectively. The first scenario is to examine the effect of the different bonding methods at the fault condition of

CSGF. A set of cases are investigated with the following conditions and the location errors are shown in Figure 3.22.

- Ten fault distances, from the first 50 m to the last 50 m.
 - SBBE: 0.05, 1, 2, 3, 3.9, 4.1, 5, 6, 7, 7.95 km.
 - SPBS, SPBR: 0.05, 1, 2, 3.2, 4.5, 5.2, 6, 7, 8, 8.95 km.
 - SPBM: 0.05, 1, 2.5, 3.5, 4.5, 5.2, 6, 7, 8, 8.95 km.
 - XB: 0.05, 1, 2, 3, 4, 5, 6, 7, 8, 8.95 km.
- Fault type: Core-sheath-ground at phase A.
- Fault resistance: $R_{f1}=10\Omega$, $R_{f2}=5\Omega$.

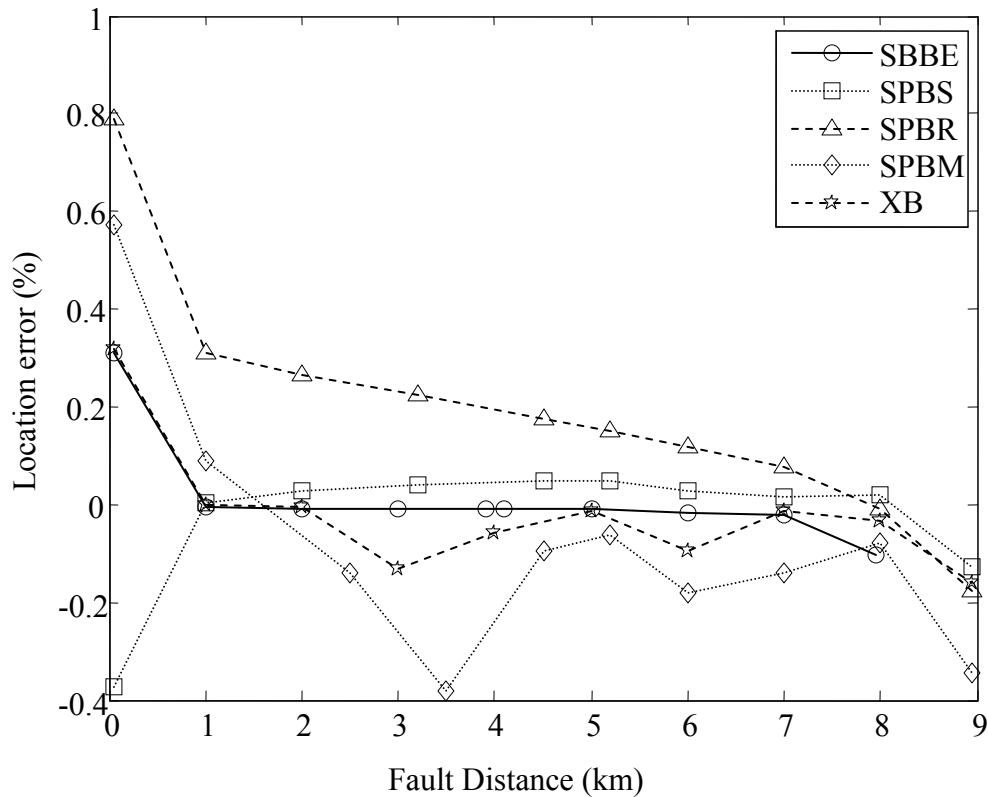


Figure 3.22: Effect of bonding method - CSGF.

In the situation of CSGF, there is the relatively large error for the cases with SPBR and SPBM. The other bonding methods have no effect on the location accuracy.

The second scenario is to examine the effect of the different bonding methods at the fault condition of CSF. A set of cases are investigated with the following conditions and the location errors are shown in Figure 3.23.

- Ten fault distances, from the first 50 m to the last 50 m.
 - SBBE: 0.05, 1, 2, 3, 3.9, 4.1, 5, 6, 7, 7.95 km.
 - SPBS, SPBR: 0.05, 1, 2, 3.2, 4.5, 5.2, 6, 7, 8, 8.95 km.
 - SPBM: 0.05, 1, 2.5, 3.5, 4.5, 5.2, 6, 7, 8, 8.95 km.
 - XB: 0.05, 1, 2, 3, 4, 5, 6, 7, 8, 8.95 km.
- Fault type: Core-sheath at phase A.
- Fault resistance: $R_{f1}=10\Omega$.

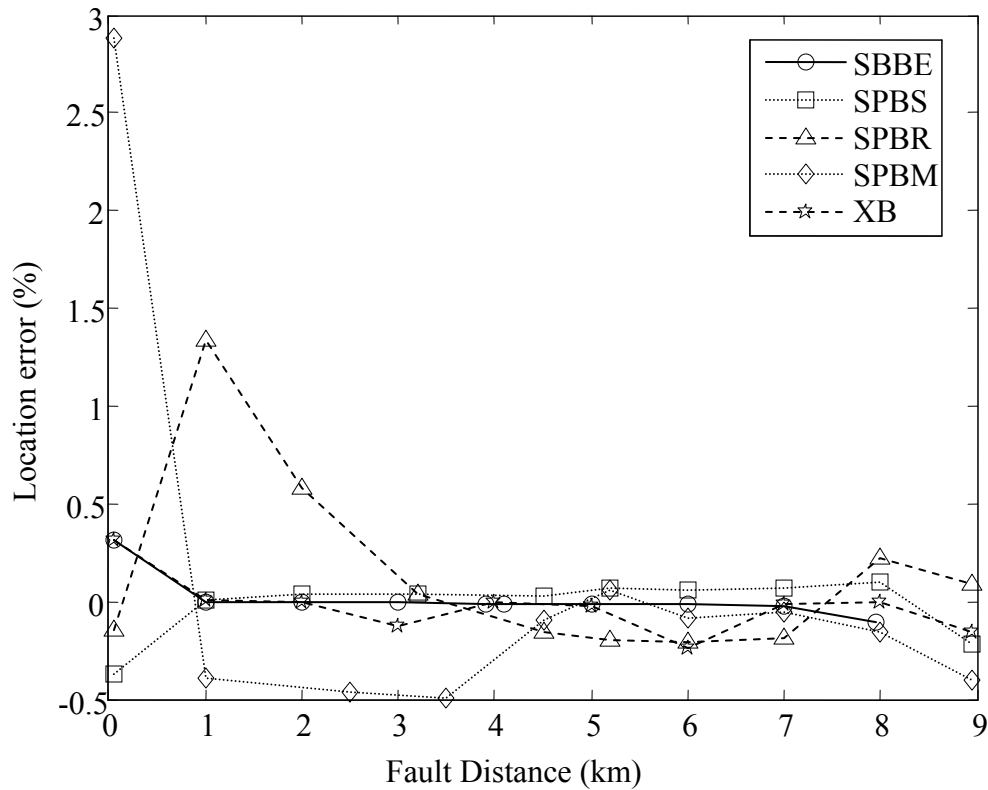


Figure 3.23: Effect of bonding method - CSF.

In the situation of CSF, there is the relatively large error for the cases with SPBR and SPBM, especially at the first third section. The other bonding methods have no effect on the location accuracy.

The third scenario is to examine the effect of the different bonding methods at the fault condition of CGF. A set of cases are investigated with the following conditions and the location errors are shown in Figure 3.24.

- Ten fault distances, from the first 50 m to the last 50 m.
 - SBBE: 0.05, 1, 2, 3, 3.9, 4.1, 5, 6, 7, 7.95 km.
 - SPBS, SPBR: 0.05, 1, 2, 3.2, 4.5, 5.2, 6, 7, 8, 8.95 km.

- SPBM: 0.05, 1, 2.5, 3.5, 4.5, 5.2, 6, 7, 8, 8.95 km.
- XB: 0.05, 1, 2, 3, 4, 5, 6, 7, 8, 8.95 km.
- Fault type: Core-ground at phase A.
- Fault resistance: $R_{f3}=10\Omega$.

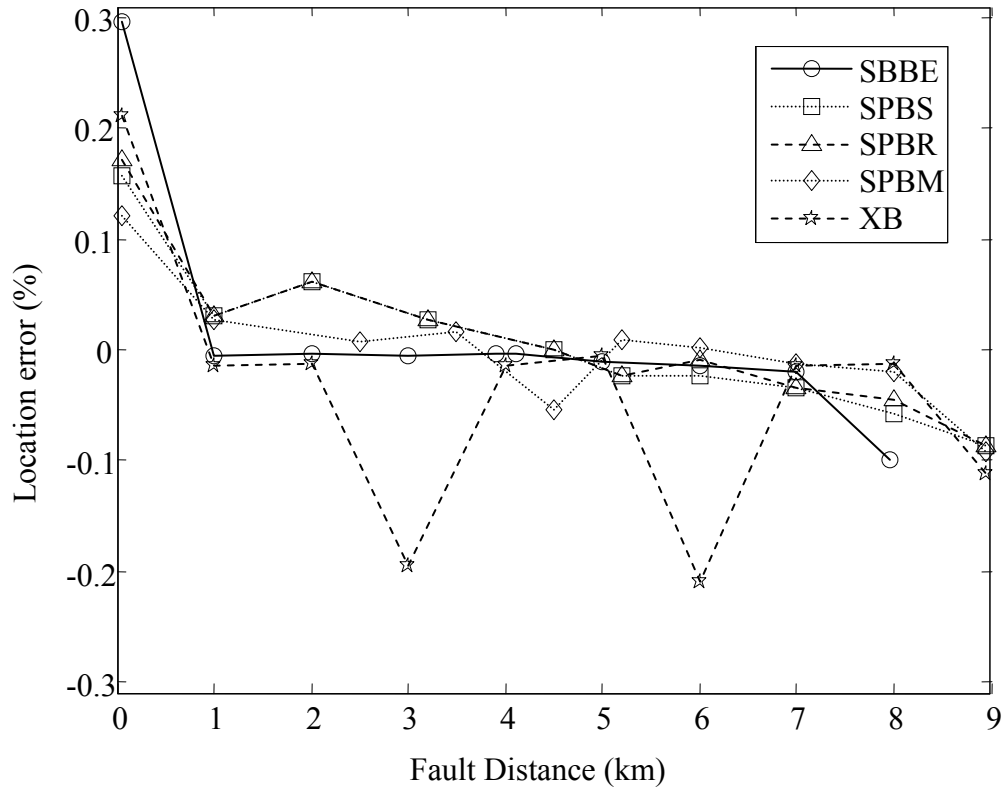


Figure 3.24: Effect of bonding method - CGF.

Basically, the bonding methods have no effect on the location accuracy in the case of CGF. The large errors are affected by the fault distance.

3.10.2.3 Effect of Fault Distance

In order to analyze the effect of the variety of fault distance on the performance of the proposed algorithms, three bonding methods combined with three fault types are selected

to examine the effect of fault distance. The first scenario is to examine the effect of the different fault distance at the condition with SBBE and CSGF. A set of cases are investigated with the following conditions and the location errors are shown in Figure 3.25.

- Fault distance: 0.05, 1, 2, 3, 3.9, 4.1, 5, 6, 7, 7.95 km or 0.1, 1, 2, 3, 3.9, 4.1, 5, 6, 7, 7.9 km.
- Fault type: Core-sheath-ground at phase A.
- Bonding method: Solid bonding at both terminals.
- Fault resistance: (1) $R_{f1}=10\Omega$, $R_{f2}=5\Omega$; (2) $R_{f1}=10\Omega$, $R_{f2}=0\Omega$; (3) $R_{f1}=0\Omega$, $R_{f2}=5\Omega$; (4) $R_{f1}=0\Omega$, $R_{f2}=0\Omega$.

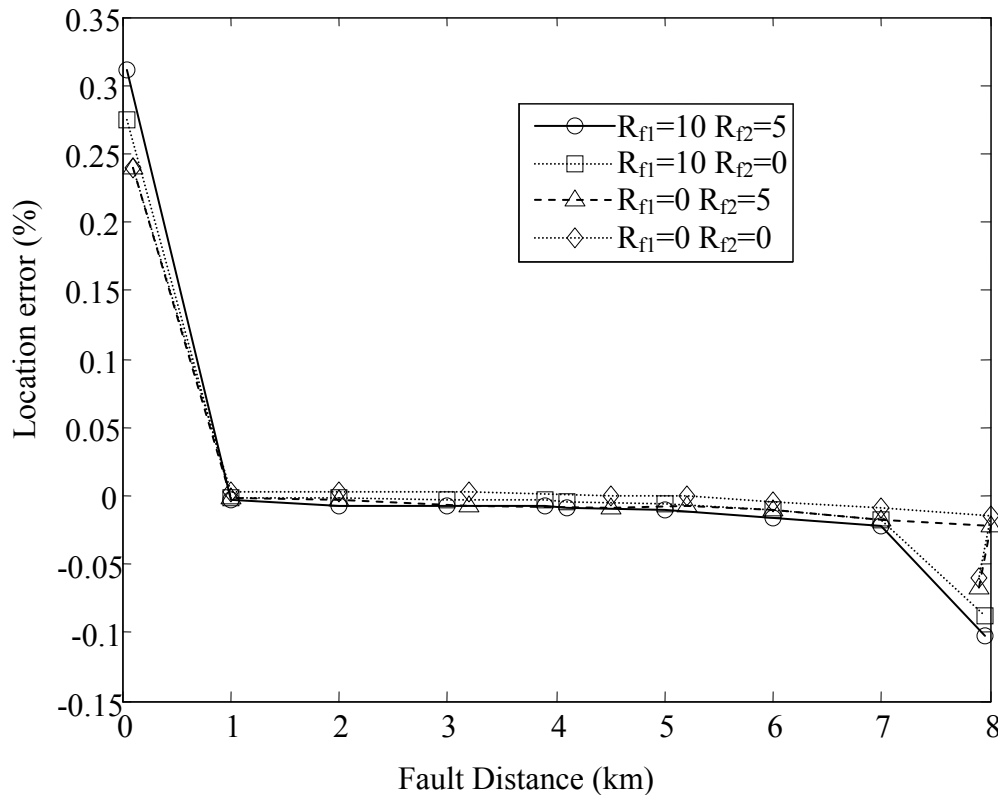


Figure 3.25: Effect of fault distance – SBBE&CSGF.

It can be clearly observed that the higher error occurs if the fault is close to two terminals, especially to close-in terminal. Besides, the location error is negligible for faults occurring in most section of the cable.

The second scenario is to examine the effect of the different fault distance at the condition with XB and CGF. A set of cases are investigated with the following conditions and the location errors are shown in Figure 3.26.

- Fault distance: 0.05, 1, 2, 3, 4, 5, 6, 7, 8, 8.95 km.
- Fault type: Core-ground at phase A.
- Bonding method: Cross bonding.
- Fault resistance: (1) $R_{f1}=10\Omega$; (2) $R_{f1}=0\Omega$.

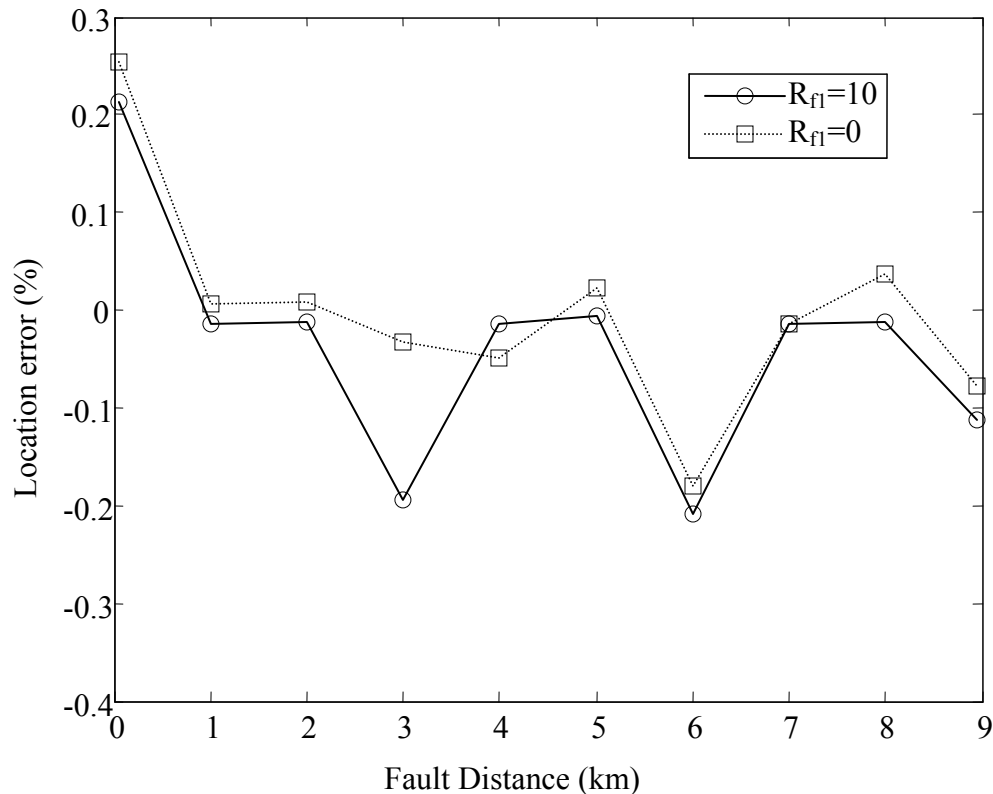


Figure 3.26: Effect of fault distance – XB&CGF.

Similarly, the higher error occurs if the fault is close to two terminals and crossing points. Besides, the location error is negligible for faults occurring in most section of the cable.

The third scenario is to examine the effect of the different fault distance at the condition with SPBM and CSF. A set of cases are investigated with the following conditions and the location errors are shown in Figure 3.27.

- Fault distance: 0.05, 1, 2.5, 3.5, 4.5, 5.2, 6, 7, 8, 8.95 km.
- Fault type: Core-sheath at phase A.
- Bonding method: Single point bonding at the middle point.
- Fault resistance: (1) $R_{f1}=10\Omega$; (2) $R_{f1}=0\Omega$.

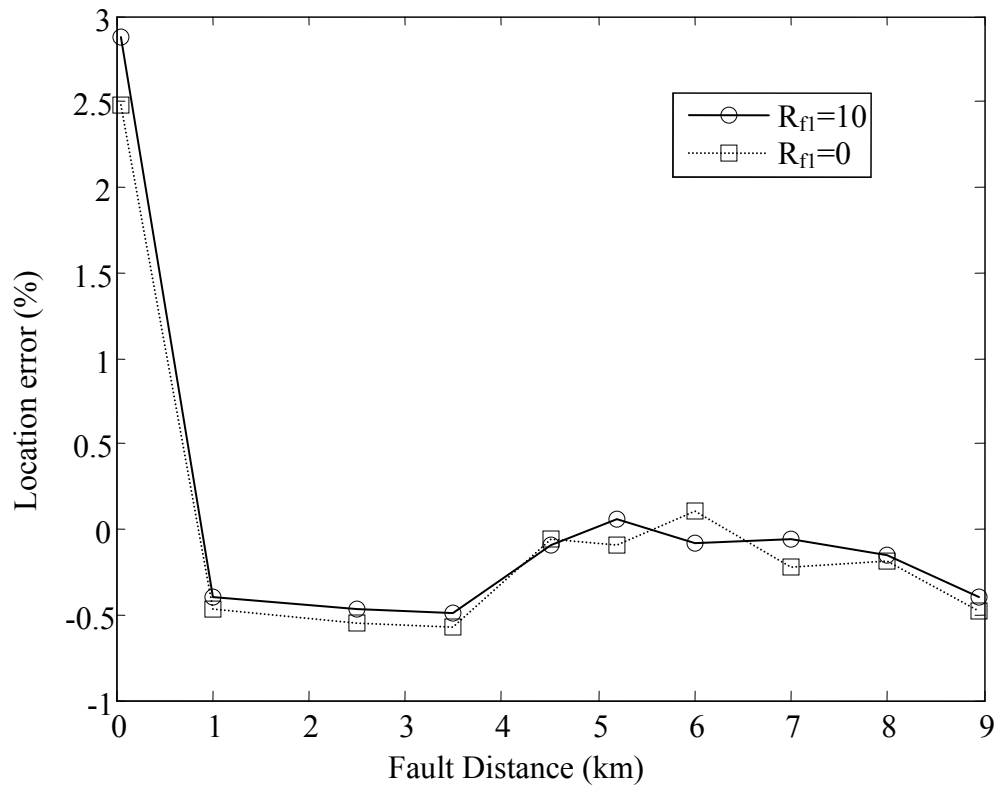


Figure 3.27: Effect of fault distance – SPBM&CSF.

The much higher error occurs if the fault is at the first third section. Besides, the relatively large errors in other situations are caused by the bonding method of SPBM.

It has been observed that there has error increase for faults located around the close-in, far-end and crossing points in simulations. This phenomenon is caused by the cable model and setting of the simulation software rather than the location algorithm itself. The PSCAD/EMTDC software requires the simulation time step should be less than the one tenth of the traveling time of the shortest cable length for better accuracy if the frequency dependent (phase) cable model is used. The traveling time of a 50 meter cable section is around 333.33 nanoseconds in theory. However, the traveling time for the same length cable is calculated as 31.8 nanoseconds in PSCAD/EMTDC, so the simulation time step should be set as low as 3.18 nanoseconds, which in turn would result in the very long simulation time for a single fault case.

3.10.2.4 Effect of Fault Resistance

Similarly to the investigation in the previous subsection, three bonding methods combined with three fault types are selected to examine the effect of fault resistance. The first scenario is to examine the effect of the different fault resistance at the condition with SPBS and CSGF. A set of cases are investigated with the following conditions and the location errors are shown in Figure 3.28.

- Fault distance: 0.05, 1, 2, 3.2, 4.5, 5.2, 6, 7, 8, 8.95 km.
- Fault type: Core-sheath-ground at phase A.
- Bonding method: Single-point bonding at the sending terminal.
- Fault resistance: (1) $R_{f1}=10\Omega$, $R_{f2}=5\Omega$; (2) $R_{f1}=10\Omega$, $R_{f2}=0\Omega$; (3) $R_{f1}=0\Omega$, $R_{f2}=5\Omega$; (4) $R_{f1}=0\Omega$, $R_{f2}=0\Omega$; (5) $R_{f1}=50\Omega$, $R_{f2}=25\Omega$.

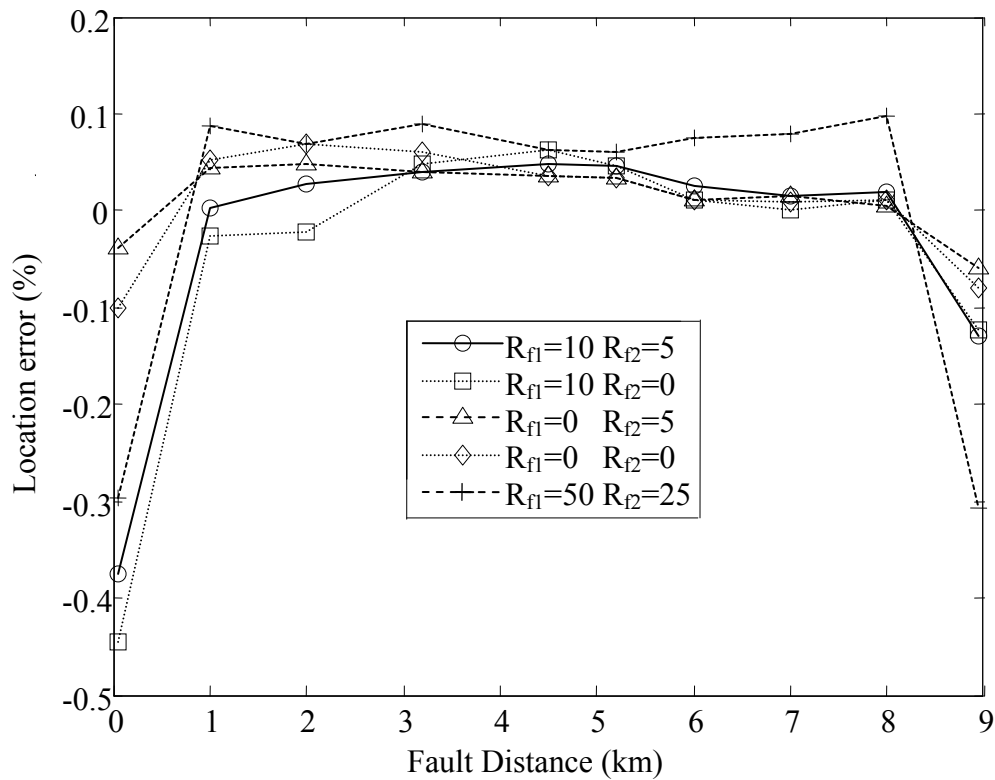


Figure 3.28: Effect of fault resistance – SPBS&CSGF.

It is apparent that the location accuracy is independent of the fault resistance.

The second scenario is to examine the effect of the different fault resistance at the condition with SBBE and CGF. A set of cases are investigated with the following conditions and the location errors are shown in Figure 3.29.

- Fault distance: 0.05, 1, 2, 3, 3.9, 4.1, 5, 6, 7, 7.95 km.
- Fault type: Core-ground at phase A.
- Bonding method: Solid bonding at both terminals.
- Fault resistance: (1) $R_{f3}=10\Omega$; (2) $R_{f3}=0\Omega$.

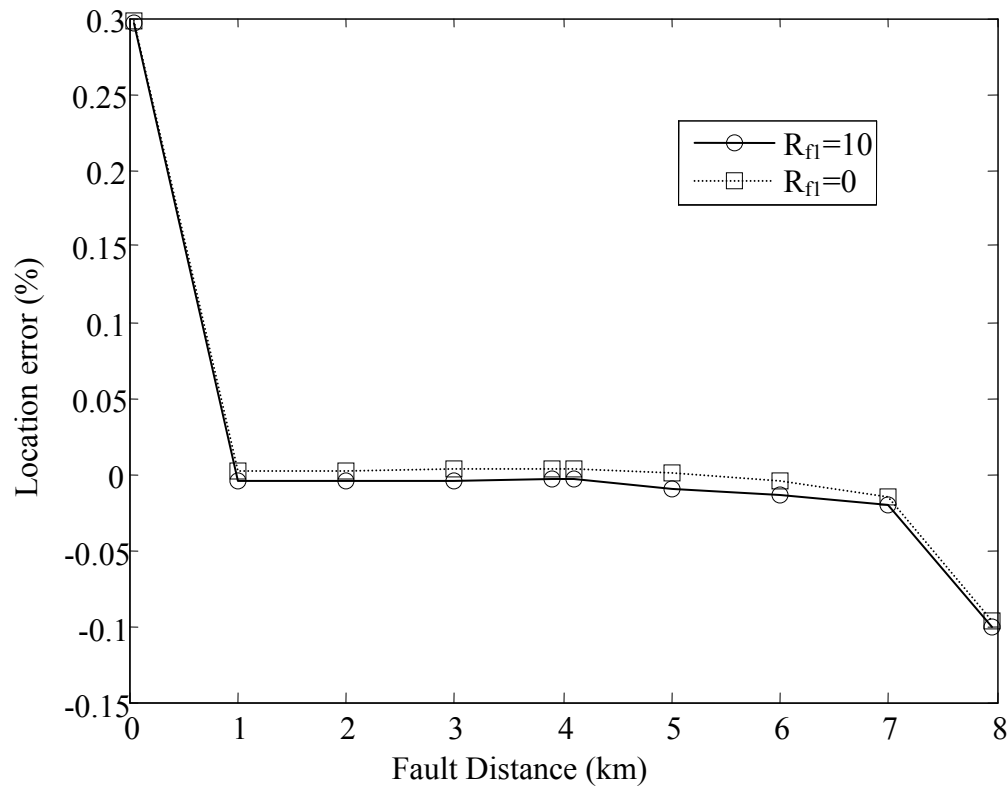


Figure 3.29: Effect of fault resistance – SBBE&CGF.

It can be observed that the location accuracy is independent of the fault resistance.

The third scenario is to examine the effect of the different fault resistance at the condition with XB and CSF. A set of cases are investigated with the following conditions and the location errors are shown in Figure 3.30.

- Fault distance: 0.05, 1, 2, 3, 4, 5, 6, 7, 8, 8.95 km.
- Fault type: Core-sheath at phase A.
- Bonding method: Cross bonding.
- Fault resistance: (1) $R_{f1}=10\Omega$; (2) $R_{f1}=0\Omega$.

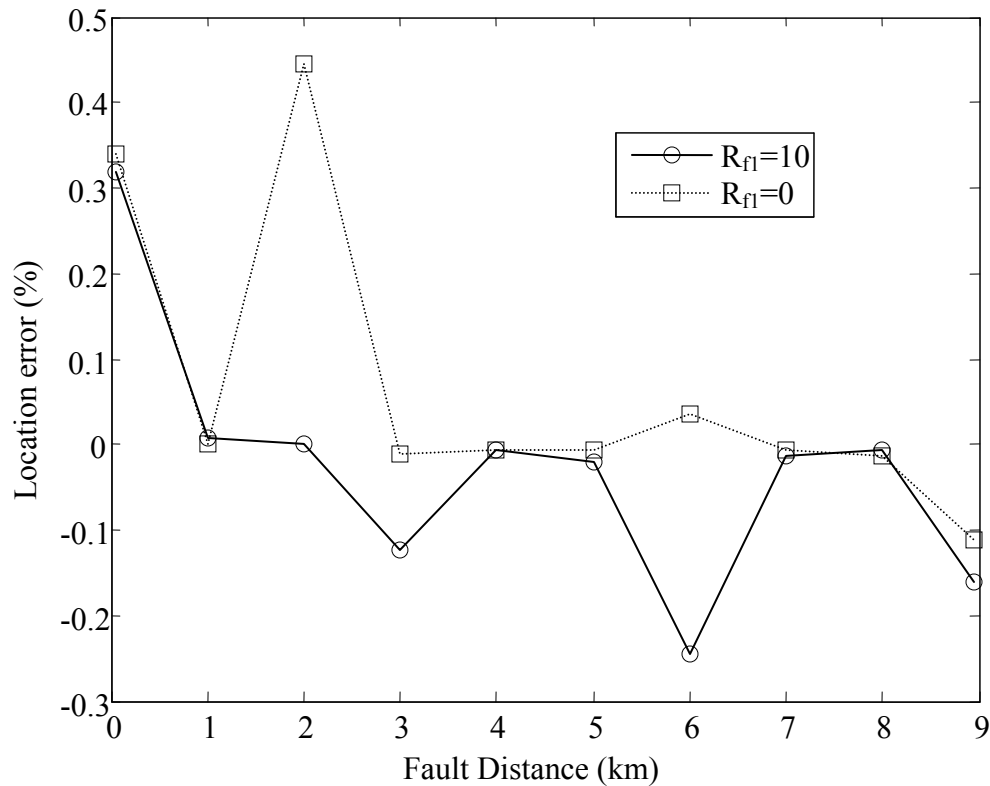


Figure 3.30: Effect of fault resistance – XB&CSF.

The location accuracy is independent of the fault resistance.

3.10.2.5 Effect of Changes of Cable Parameters

To investigate the effect of changes of cable parameters, the true cable parameters in series impedance matrix Z and shunt admittance matrix Y are randomly perturbed within a range of $\pm 20\%$. A series of cases is investigated with the following conditions:

- Fault distance: 0.1, 1, 2, 3, 3.9, 4.1, 5, 6, 7, 7.9 km.
- Bonding method: Solid bonding at both ends.
- Cable parameters: 100 groups of cable parameters randomly perturbed within a range of $\pm 20\%$.

The distribution of absolute values of location errors (DAE) is defined in Equation (3.135) and the results are listed in Table 3.16.

$$DAE = \frac{\text{Number of faults in an absolute error range}}{\text{Total number of faults}} \times 100\% \quad (3.135)$$

Table 3.16: Distribution of Absolute Values of Location Errors

Error range	0~1%	1~2.5%	2.5~5%	5~10%	>10%
Core-Sheath-Ground	32.30%	22.35%	20.55%	16.82%	7.98%
Core-Ground	33.75%	20.85%	20.60%	16.80%	8.00%
Core-Sheath	33.70%	20.95%	20.55%	16.80%	8.00%
All cases	33.01%	21.63%	20.56%	16.81%	7.99%

Around 54% faults can be located with the error less than 2.5%, equivalently 200 meters in this set of cases. It should be mentioned that an online parameter estimation method would be helpful to reduce the location error.

3.10.2.6 Calculation of Fault Resistance

The fault resistances can also be accurately calculated except for the cases of close-in and far-end faults, which could be affected by the ground bonding. The first scenario is to calculate the fault resistance at different fault conditions with SPBR. A set of cases are investigated with the following conditions and the fault resistances are shown in Figure 3.31.

- Fault distance: 0.05, 1, 2, 3.2, 4.5, 5.2, 6, 7, 8, 8.95 km.
- Fault type: (1) Core-sheath-ground; (2) Core-ground; (3) Core-sheath.
- Bonding method: Single point bonding at the receiving terminal.
- Fault resistance: (1) $R_{f1}=10\Omega$, $R_{f2}=5\Omega$ for CSGF; (2) $R_{f1}=10\Omega$ for CGF; (3) $R_{f3}=10\Omega$ for CSF.

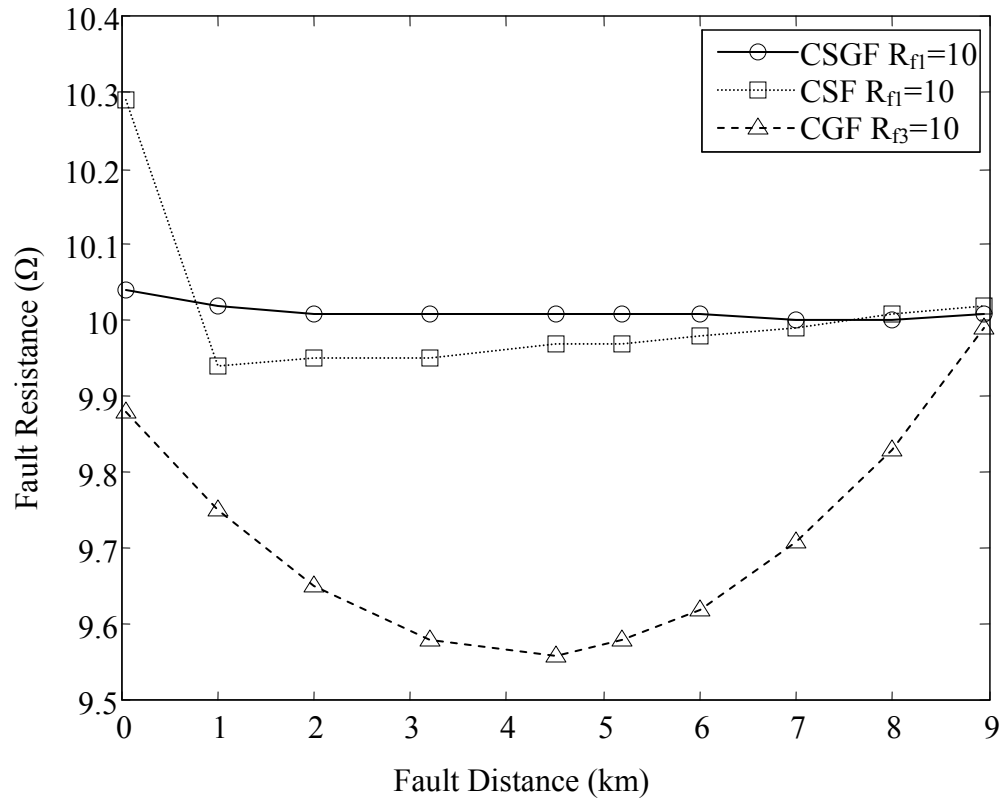


Figure 3.31: Calculation of fault resistance – SPBR.

It has been shown that the core-related fault resistance can be accurately estimated, which is independent of the fault distance. The relatively large errors occur for the case of CGF.

The second scenario is to calculate the fault resistance at CSGF fault condition with SBBE. A set of cases are investigated with the following conditions and the fault resistances are shown in Figure 3.32.

- Fault distance: 0.05, 1, 2.5, 3.5, 4.5, 5.2, 6, 7, 8, 8.95 km.
- Fault type: Core-sheath-ground.
- Bonding method: Single point bonding at the middle point.
- Fault resistance: (1) $R_{f1}=10\Omega$, $R_{f2}=5\Omega$; (2) $R_{f1}=0\Omega$, $R_{f2}=5\Omega$.

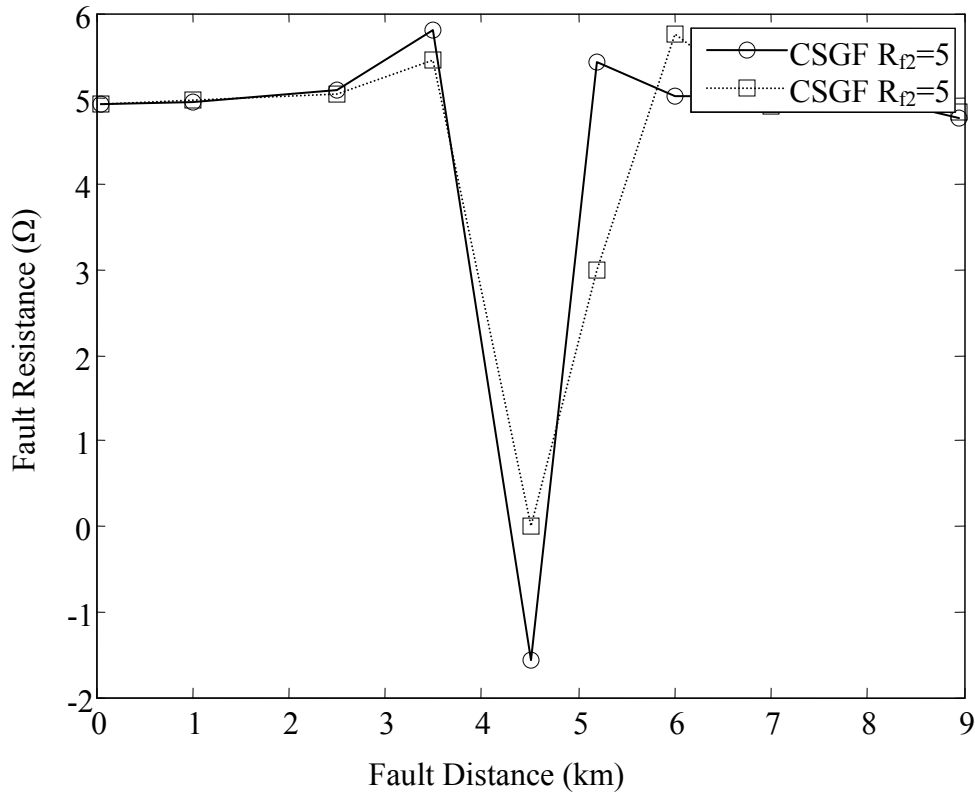


Figure 3.32: Calculation of fault resistance – SPBM.

Normally, the sheath-ground fault resistance can be accurately estimated for the faults occurring away from the bonding point. The ground bonding would result in the large error when faults are close to the bonding point due to the changing of the fault current path.

The third scenario is to calculate the fault resistance at different fault conditions with XB. A set of cases are investigated with the following conditions and the fault resistances are shown in Figure 3.33.

- Fault distance: 0.05, 1, 2, 3.2, 4.5, 5.2, 6, 7, 8, 8.95 km.
- Fault type: (1) Core-sheath-ground; (2) Core-ground; (3) Core-sheath.
- Bonding method: Single point bonding at the sending terminal.

- Fault resistance: (1) $R_{f1}=0\Omega$, $R_{f2}=0\Omega$ for CSGF; (2) $R_{f1}=0\Omega$ for CGF; (3) $R_{f3}=0\Omega$ for CSF.

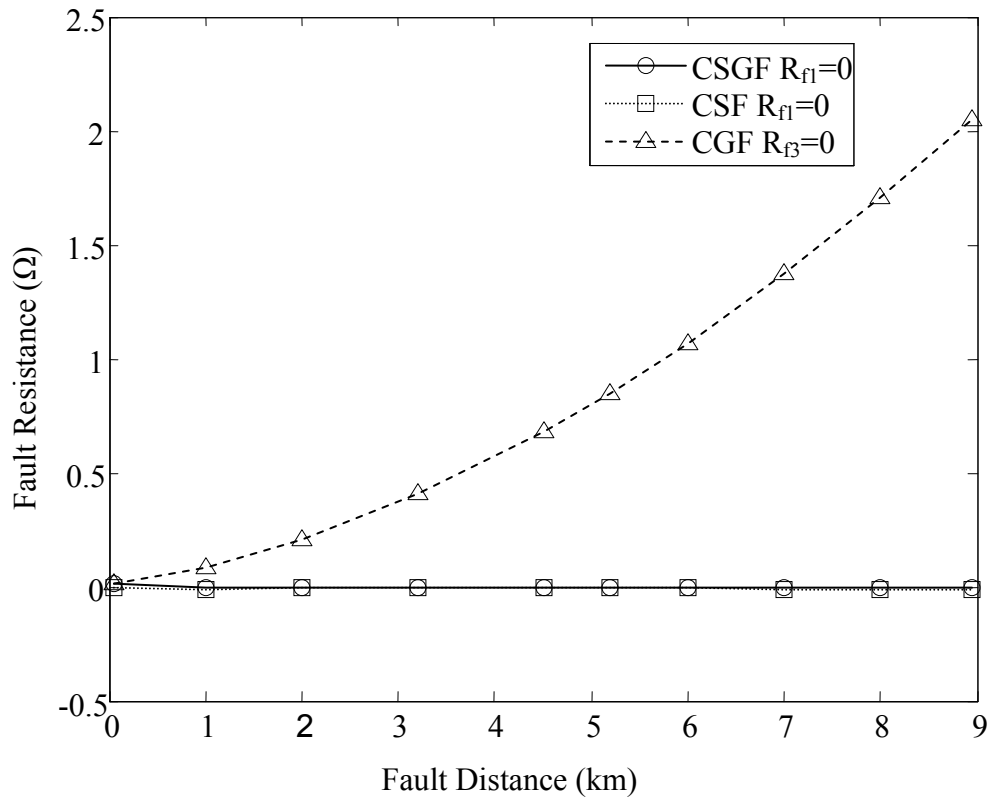


Figure 3.33: Calculation of fault resistance – SPBS.

The zero fault resistance can be accurately estimated in the cases of CSGF and CSF. However, there has relatively large error in the case of CGF owing to the fact that the fault resistance is not involved in the calculation of the CGF algorithm.

3.10.3 Summary of Effects

It has been tested that the fault resistance has no effect on the location accuracy. Basically, the fault distance has no effect on the location accuracy, except that there has an error increase for faults closed to the close-in, far-end and crossing points, which is caused by the model and setting in the simulation software. The changes of cable

parameters would result in the large increase of the location error, but it can be averted by an online parameter estimation method.

The effects of the bonding methods and fault types on the location accuracy are summarized in Table 3.17.

Table 3.17: Effects of Bonding Methods and Fault Types on Location Accuracy

	Core-Sheath-Ground	Core-Ground	Core-Sheath
Solid Bonding	No effect	No effect	No effect
Single Point @ Sending	No effect	No effect	No effect
Single Point @ Receiving	Relatively large	No effect	Relatively large at the first third section
Single Point @ Middle	Relatively large	No effect	Relatively large at the first half section
Cross Bonding	No effect	No effect	No effect

Chapter 4

4 Extension of the Proposed Fault Location Algorithms to Medium Voltage Cables in Distribution Networks

A set of the fault location algorithms for a plain cable with no laterals have been presented in Chapter 3. The extensive simulations have validated the accuracy and effectiveness of the proposed scheme. This chapter is to extend the proposed location algorithms to underground distribution networks. In order to ensure the effectiveness of location calculations, the voltages and currents at the sending terminal of the faulty cable section, and the seen impedance behind the faulty section should be accurately estimated. The power flow analysis or state estimation approach can provide the additional information required by the location algorithm. Taking account of the complexity and particularity of cable circuits in distribution networks, the state estimation for underground distribution systems is formulated as a nonlinear optimization problem that is solved by the sequential quadratic programming (SQP) technique. A section-by-section estimation algorithm combined with the backward/forward sweep algorithm is proposed to estimate the nodal voltage and branch current for each line section. The simulation studies indicate the proposed fault location algorithm and the state estimation algorithm can achieve good performance under different system and fault conditions.

The background knowledge is first introduced, including the complexities existing in fault location calculations for cables, complexities existing in the state estimation for distribution networks, problems emerging from the extension, and introduction to the SQP nonlinear programming. Then the details of the proposed state estimation method are discussed. A general location procedure combined with the proposed state estimation technique is described as well. The application of the static response load model is investigated. The algorithm is examined on a 31-node radial underground distribution network, with consideration of laterals, tapped loads, unbalanced loads, different fault types and fault distances.

4.1 Background

4.1.1 Complexities in Fault Location in Distribution Networks

The traditional fault analysis algorithms applied for transmission systems cannot effectively achieve the expected performance in distribution systems due to the following reasons.

- Existence of short and heterogeneous feeders, including various size and length lines and cables with different configurations.
- Presence of laterals along the main feeder.
- Presence of tapped loads distributed along the main feeder and laterals.
- Unbalanced loads due to the presence of single phase, double-phase and three-phase loads.
- Untransposed lines and cables.

4.1.2 Complexities in State Estimation for Distribution Networks

Similarly, the traditional state estimation or power flow analysis algorithms applied for transmission systems cannot be directly applied for distribution systems due to the following facts [112].

- Unbalanced system in nature, including laterals, tapped loads, and untransposed and heterogeneous feeders.
- Limited availability of real-time measurements.
- Large number of loads.

For the sake of the accurate estimation, the state estimation for underground distribution networks should consider the characteristics of cables, such as the relatively large capacitance, effect of metallic sheath, sheath bonding method and unbalance impedance matrix.

4.1.3 Emerging Issues Caused by Extension to Distribution Networks

It has been mentioned that the general logic principle in most of location algorithms is first to determine the fault point in a plain line or cable with no laterals. Subsequently, the location algorithm is extended to distribution networks taking account of the presence of laterals, tapped loads, unbalanced loads, heterogeneity of lines, etc. The extension of such a location algorithm for a plain line/cable into distribution networks causes three technical issues.

- How to obtain the voltage and current at the sending terminal of the faulty section?
- How to estimate the seen load impedance at the receiving terminal of the faulty section if the load impedance is required in calculations?
- How to resolve the multiple estimates for possible faulty points due to the existence of laterals? This problem specially exists in the impedance-based location algorithms.

Due to the limited availability of measurements, the voltages and currents are usually recorded at the substation in a distribution system. Therefore, the voltage and current can be simply obtained by lumping all upstream loads and laterals between the substation and faulty section, or gradually calculated node by node starting from the substation to the faulty section. To carry out the above calculations, one prerequisite is the information of laterals and tapped loads between the substation and faulty section should be available for calculations. Similarly, the data of laterals and tapped loads behind the faulty section should also be known to solve the second issue.

Overall, the load information prior to fault and during fault should be estimated for the purpose of the accurate location. The sequential quadratic programming technique is applied in this work to estimate the prefault voltage and load information of each node in distribution networks.

4.1.4 Introduction to Sequential Quadratic Programming

Sequential quadratic programming (SQP) algorithms have proved to be fast and robust for solving the general nonlinear optimization problem of the form [113],

$$\begin{aligned}
 & \text{Minimize } f(x) \\
 & \text{subject to,} \\
 & \quad l \leq x_m \leq u \quad m = 1, 2, \dots, n \\
 & \quad CI_i(x) \geq 0 \quad i = 1, 2, \dots, p \\
 & \quad CE_j(x) = 0 \quad j = 1, 2, \dots, q
 \end{aligned} \tag{4.1}$$

where $f(x)$, $CI(x)$ and $CE(x)$ are nonlinear smooth continuous functions which have continuous second partial derivatives. The nonlinear problem has one quadratic objective function $f(x)$, n variables x , p inequality constraints $CI(x)$, q equality constraints $CE(x)$. The notations l and u express the bound constraints on x .

The basic concept of SQP is to convert the nonlinear problem in Equation (4.1) into a sequence of quadratic programming (QP) subproblems in Equation (4.2) where the objective function is quadratic and the constraints are linear. Thus, SQP is converted to an iterative method which solves a QP problem at each iteration.

$$\begin{aligned}
 & \text{Minimize } f(x) \\
 & \text{subject to,} \\
 & \quad Ax = b \\
 & \quad Cx \geq d
 \end{aligned} \tag{4.2}$$

where $f(x)$ is the quadratic objective function, and the matrices of A and C and the vectors of b and d compose the linear constraints.

The solving procedure of SQP is available in many numerical optimization books such as [113] and [114], free third party software, such as SQPlab [115], and commercial mathematical tools, such as Matlab.

4.2 Development of State Estimation Algorithm

4.2.1 Problem Formulation

The state estimation for distribution networks can be used for different needs, such as voltage monitoring and control at each bus, load control and service restoration for individual loads, nodal pricing for aggregated loads, and fault location as suggested in this work. Considering an underground distribution network, the known quantities and preconditions can be summarized as follows.

- Limited measurements, including three-phase voltages and three-phase currents of the core conductors recorded at the substation, and other sparse measurements placed in feeder transformers or important loads where voltage, current and/or power quantities can be measured.
- Load information can be acquired from the analysis of load forecast, documented in the historical database, or analyzed from the load profiles.
- Cable configuration and parameter would be stored in the database of utility companies or obtained by other ways mentioned in Section 3.3.1. The information includes the cable length, series impedance matrix, shunt admittance matrix and sheath bonding method.

Owing to the availability of measurements and the uncertainty of load information, the problem of the distribution state estimation can be formulated as a constrained nonlinear optimization problem that incorporates the operating and loading constraints. The voltages at each node are firstly estimated by solving the optimization problem, and subsequently the loads are calculated based on the estimated voltages.

4.2.2 State Estimation Algorithm

The formulation of the state estimation is described as a constrained nonlinear programming given as,

$$\underset{V}{\text{Minimize}} \|W(z - f(V))\|_2 \quad (4.3)$$

subject to,

$$|V_n|^{min} \leq |V_n| \leq |V_n|^{max} \quad (4.4)$$

$$\theta_n^{min} \leq \theta_n \leq \theta_n^{max} \quad (4.5)$$

$$PLB_n \leq \frac{P_n^{est} - P_n^{ini}}{P_n^{ini}} \leq PUB_n \quad (4.6)$$

$$QLB_n \leq \frac{Q_n^{est} - Q_n^{ini}}{Q_n^{ini}} \leq QUB_n \quad \text{for each node } n \quad (4.7)$$

In the objective function (4.3), the voltage vector V is the set of state variables. The vector z is the set of measurements. The function $f(V)$ is the measurement function, where the estimated measurements are calculated from the state variables. The matrix W is the diagonal weighing matrix to rank different types of measurements with different emphasis. The notation $\| \cdot \|_2$ denotes the Euclidean norm to evaluate the fitness of weighted measurement residuals.

In the voltage constraints (4.4) and (4.5), the magnitude of the state variable V at each node would be limited into a range from $|V|^{min}$ to $|V|^{max}$. Similarly, the angle of the state variable V at each node would be limited into a range from θ^{min} to θ^{max} .

In the loading constraints (4.6) and (4.7), the injected real power and reactive power P^{est} and Q^{est} at each node are estimated by $f(V)$. The initial real power and reactive power at each node P^{ini} and Q^{ini} are obtained from the initial load information in advance. The relative error between them should be in a range bounded by $[PLB, PUB]$ and $[QLB, QUB]$.

4.2.2.1 Objective Function

The objective of the formulated optimization problem is to minimize the weighted errors between the measurements (z) and the calculated results from the measurement function

$f(V)$). Therefore, the estimated load flows can best fit measured load flows and adapt a balance between the initial load information and calculated load outcome.

The measurement vector z denotes the measurements of the real power and reactive power injected into each node, including the real-time measurements, zero-injection measurements and load pseudo measurements. The real-time measurements are physically sampled from sensors placed in networks sparsely. Since there have no enough real-time measurements for the calculations of estimation, the load pseudo measurements are introduced, which consider the known load information as a type of measurement with less accuracy. The zero-injection measurements particularly represent the zero injected power at the zero injection nodes and can also be regarded as the real-time measurements or highly accurate pseudo measurements. There have twelve measurements for a three-phase node, including three measurements of real part of real power, three measurements of imaginary part of real power, three measurements of real part of reactive power, and three measurements of imaginary part of reactive power. Similarly, there have eight measurements for a two-phase node, and four for a single phase node.

The measurement function $f(V)$ is to calculate the injected power at each node based on voltages at all adjacent nodes. For example, the injected power at node n can be calculated as,

$$S_n = \sum_{k \in A_n} S_{nk} = \sum_{k \in A_n} f_{nk}(V) \quad (4.8)$$

where S_n is the injected load flow at node n , S_{nk} is the power flowing out of node n to node k , and A_n is the set containing the nodes directly connected to node n . In the example shown in Figure 4.1, $A_n = \{m, s, t\}$. The function $f_{nk}(V)$ is to calculate the branch load flowing out of node n to node k based on the voltages at nodes n and k .

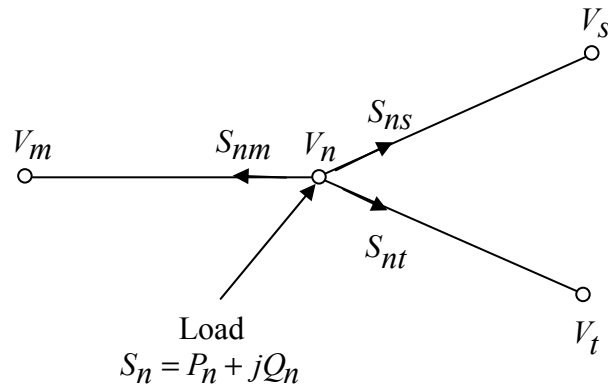


Figure 4.1: Example to calculate injected power.

Since the electrical characteristics and structural configurations of underground cables are different with those of overhead lines, the more accurate calculation of power flow for a cable circuit should consider the cable capacitance, effect of sheath and sheath grounding method. Taking three single-conductor cables with sheaths grounded at the sending terminal as an example, the power flow is calculated as below, where the mathematical description and cable model have been explained in Section 3.3.1.

$$f_{sr}(V) = S_{sr} = V_{sc} \cdot I_{sc}^* \quad (4.9)$$

$$I_{sc} = M^{-1}(NV_{sc} - RV_{rc}) \quad (4.10)$$

where,

$$M = LZ_{cc} + \Delta M$$

$$N = IU + \Delta N$$

$$R = IU + \Delta R$$

$$\Delta M = -\frac{L^3}{2} Z_{cn} U Y_{nn} Z_{nc}$$

$$\Delta N = \frac{L^2}{2} Z_{cc} Y_{cc} - LZ_{cn} T + \frac{L^2}{2} Z_{cn} Y_{nc}$$

$$\Delta R = \frac{L^2}{2} Z_{cn} U Y_{nc}$$

$$T = U \left(\frac{L}{2} Y_{nc} + \frac{L^3}{4} Y_{nn} Z_{nc} Y_{cc} + \frac{L^3}{4} Y_{nn} Z_{nn} Y_{nc} \right)$$

$$U = \left(IU + \frac{L^2}{2} Y_{nn} Z_{nn} \right)^{-1}$$

where V is the voltage phasor vector, I is the current phasor vector, Z is the series impedance matrix, Y is the shunt admittance matrix, IU is the identity matrix, and L is the length of cable. The symbol $*$ denotes the elementwise multiplication. The lowercase subscript s means quantities at the sending terminal, similarly, r at the receiving terminal, c for core conductor and n for sheath. Taking Z_{cn} as an example, it indicates the mutual impedance matrix per unit length between three cores and three sheaths, and so forth.

It is clear in Equation (4.10) that the power flow calculation for cables differs from the classical equation for lines in the fact that there have three correction factors, ΔM , ΔN and ΔR , which are caused by the particular characteristics and configurations of cables.

The matrix W in the objective function is the diagonal weighing matrix, which is determined by the accuracy of corresponding measurements. For example, the real-time measurements are most accurate and credible, so the largest weight values would be assigned to the residuals of them. The notation $\| \cdot \|_2$ denotes the Euclidean norm, which is defined as,

$$\|x\|_2 = \sqrt{x_1^2 + x_2^2 + \dots + x_n^2} \quad (4.11)$$

where the vector $x = \{x_1, x_2, \dots, x_n\}$.

4.2.2.2 Voltage Constraints

The voltage at each node will maintain in a limited range around the nominal rating in the normal operating condition. Therefore, this limited range can be used as the operating constraints in Equations (4.4) and (4.5) to restrict the search region. Normally, this range

can be uniformly set within the $\pm 3\sim 5\%$ of the voltages measured at the substation. The values of real part and imaginary part can also be used as constraints rather than the magnitude and angle. The state variables at each node contain six real variables for a three-phase node, four for a two-phase node or two for a single phase node.

4.2.2.3 Loading Constraints

As mentioned in the above subsection, the known load information is considered as the load pseudo measurements. However, this initial load information is obtained from the load forecast, historical database or load profile, so it cannot accurately represent the true load flow, which may be in a range around the initial load values. This range can be set as the constraints in Equations (4.6) and (4.7) to further narrow down the search region, which can also be expressed as,

$$P_n^{est} = P_n^{ini} + PB_n \cdot P_n^{ini} \quad (4.12)$$

$$PLB_n \leq PB_n \leq PUB_n \quad (4.13)$$

$$Q_n^{est} = Q_n^{ini} + QB_n \cdot Q_n^{ini} \quad (4.14)$$

$$QLB_n \leq QB_n \leq QUB_n \quad \text{for each node } n \quad (4.15)$$

where P_n^{est} and Q_n^{est} express the injected real and reactive power calculated by Equations (4.8)-(4.10), PB_n and QB_n are the load variation factors ranging from PLB_n and QLB_n to PUB_n and QUB_n respectively.

Hitherto, the state estimation problem formulated in Equation (4.3) is in fact similar to the general nonlinear optimization problem described in Equation (4.1), which can be solved by the sequential quadratic programming methods.

4.3 General Location Procedure Combined with State Estimation

The general location procedure combined with the state estimation is described in this section, which can be divided into four steps, i.e. prefault load estimation by DSE,

estimation of voltages and currents during fault, determination of faulty section, and fault location.

In order to explain each step more clearly, the procedure will be processed on a 31-node radial unbalanced underground distribution network shown in Figure 4.2. Besides, the simulation will also be carried out on this test system.

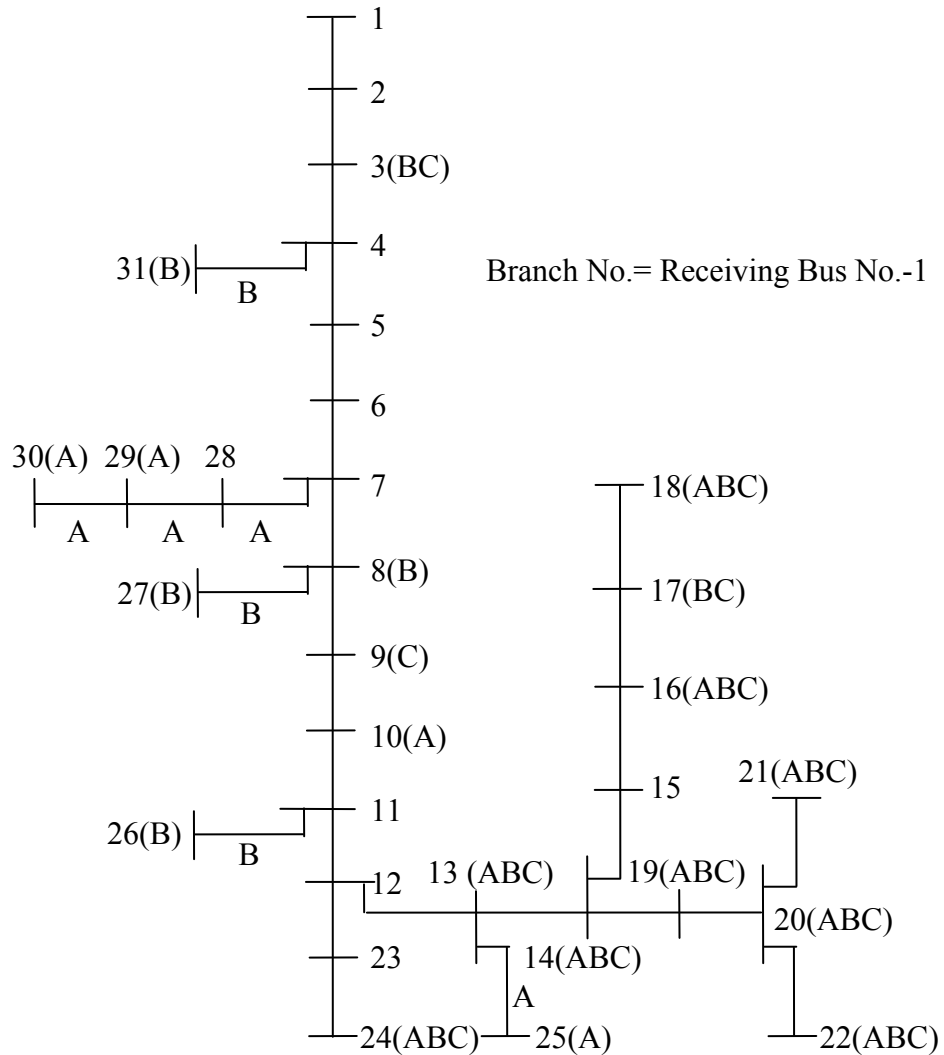


Figure 4.2: A radial unbalanced underground distribution network.

In the figure, the digits denote the bus number, the character *A*, *B*, and/or *C* in the bracket behind a bus number means the phase(s) of the tapped load(s) at that bus, the character *A*,

B , or C near a cable section expresses the phase of that lateral, and the section is a three-phase feeder or lateral if there is no character near that section. The branch number is equal to the receiving bus number minus one.

4.3.1 Prefault Load Estimation by DSE

The loads prior to the inception of a fault should be estimated in order to provide the real-time load information for the fault location algorithm. This estimation process can be regularly carried out in DMS, like every fifteen or thirty minutes. The results include the estimated voltage at each node. Also the following quantities can be calculated by Equations (4.8)-(4.10):

- Branch current of each branch.
- Branch real and reactive powers flowing in and out of a branch.
- Injected load at each node.
- Seen impedance behind each circuit section.

First, the initial load information can be acquired from the analysis of load forecast, documented in the historical database, or analyzed from the load profiles. The initial information can be used for two purposes:

- Composing the pseudo measurements.
- Calculating the voltage, $V_{profile}$, at each node related to this specific load profile. The applied algorithm is a section-by-section estimation algorithm combined with the backward/forward sweep algorithm (BFSA) [58], which will be introduced in Section 4.3.2.1.

Then, the state variables should be determined, including six real variables for each three-phase node, four for each two-phase node or two for each single phase node. For example, in the system in Figure 4.2, the total number of state variables is $(24-1) \times 6 + 7 \times 2 = 152$. It should be mentioned that the voltage at the substation bus is not counted as the state variable.

Next, the initial values of state variables are calculated by scaling as below.

$$V_{initial_i} = V_{initial_0} \left| \frac{V_{profile_i}}{V_{profile_0}} \right| \quad (4.16)$$

where $V_{profile_i}$ is the voltage at bus i estimated by the initial load profile. $V_{profile_0}$ is the voltage at the substation, which should be accurate for the corresponding load profile. $V_{initial_i}$ is the initial voltage at bus i used for solving SE. $V_{initial_0}$ is the voltage at the substation, which is measured in real-time.

The voltage constraints are easily to be set. Normally, the constraint at each node can be uniformly set within the $\pm 3\%$ of the $V_{initial_i}$ so that the voltage constraints can be rewritten as,

$$0.97 |V_{initial_i}| \leq |V_i| \leq 1.03 |V_{initial_i}| \quad (4.17)$$

$$0.97 \angle V_{initial_i} \leq \angle V_i \leq 1.03 \angle V_{initial_i} \quad (4.18)$$

where V_i is the voltage at bus i , and is regarded as the state variable.

The initial loads are chosen to close to the true loads; however the real biases between them are unknown. The loading constraints, PLB_n , QLB_n , PUB_n and QUB_n , can be uniformly set as the constants. That is, the lower boundaries, PLB_n and QLB_n , are set to a constant for all nodes, and the upper boundaries, PUB_n and QUB_n , are also set to a constant for all nodes. The values of constants depend on the accuracy of the initial load information. For example, if the initial load information is obtained from the load forecast, which is supposed to be more accurate, the upper constant can be set to 0.05 and the lower one to -0.05. And if the load is documented from a set of incomplete information, the upper constant can be set to a value in the range from 0.05 to 0.2 and the lower one could have the same value with the negative sign.

4.3.2 Estimation of Quantities during Fault

In order to apply the proposed location algorithm upon the occurrence of a fault, the following quantities have to be estimated:

- Nodal voltage at the sending terminal of the faulty section.
- Branch current of the faulty section at the sending terminal.
- Seen impedance behind the receiving terminal of the faulty section.

During a fault, the faulty section is first unknown, so every section would be assumed as the faulty section. The related voltage, current and seen impedance should be estimated for each cable section.

4.3.2.1 Estimation of Voltages and Currents

First, the loads are modeled as the constant impedance which would keep unchanged before and during the fault. The general load model will be discussed in Section 4.4. Therefore, the available information includes the voltages and currents measured at the substation and the load impedances at each injection node estimated by the state estimation algorithm.

A section-by-section estimation algorithm combined with the backward/forward sweep algorithm is proposed to estimate the nodal voltage and branch current for each line section. Before the explanation of the proposed estimation algorithm, some sub-algorithms (SA) are introduced first. For a general cable section between two nodes shown in Figure 4.3, the sub-algorithms can be categorized in Table 4.1.

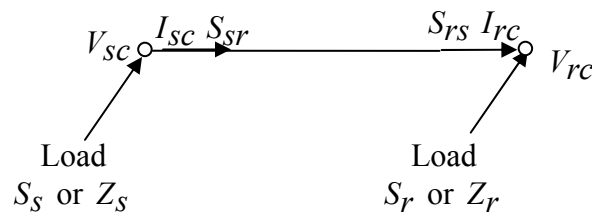


Figure 4.3: General circuit section to categorize sub-algorithms.

In the figure, V_{sc} and I_{sc} are the voltages and currents of core conductors at the sending terminal. V_{rc} and I_{rc} are the voltages and currents of core conductors at the receiving terminal. S_{sr} is the power flowing from node s to r , and S_{rs} is the power flowing from node r to s . S_s and Z_s are the injected power and load impedance at node s . S_r and Z_r are the injected power and load impedance at node r . Besides, V_{rn} and I_{sn} will be used, which represent the sheath voltage at the receiving terminal and sheath current at the sending terminal.

Table 4.1: Category of Sub-Algorithms

SA	Known Variables	Main variables to be calculated	Type
1	V_{sc}, I_{sc}	V_{rc}, I_{rc}	Analytical
2	V_{sc}, V_{rc}	S_{sr}, S_{rs}	Analytical
3	V_{rc}, I_{rc}	V_{sc}, I_{sc}	Analytical
4	V_{sc}, Z_r	V_{rc}, S_{sr}	Iterative
5	V_{sc}, S_{sr}	V_{rc}, S_{rs}	Analytical
6	V_{rc}, S_{rs}	V_{sc}, S_{sr}	Analytical

The calculation details of each sub-algorithm are explained below. It should be mentioned that the cable capacitance, sheath bonding method (SPBS in this case) and effect of sheath are considered in the calculations.

- SA1: $V_{sc}, I_{sc} \rightarrow V_{rc}, I_{rc}$

$$I_{sn} = D^{-1}(EV_{sc} + FI_{sc}) \quad (4.19)$$

$$\begin{bmatrix} V_{rc} \\ V_{rn} \end{bmatrix} = \begin{bmatrix} V_{sc} \\ 0 \end{bmatrix} - L \begin{bmatrix} Z_{cc} & Z_{cn} \\ Z_{nc} & Z_{nn} \end{bmatrix} \left(\begin{bmatrix} I_{sc} \\ I_{sn} \end{bmatrix} - \frac{L}{2} \begin{bmatrix} Y_{cc} & Y_{cn} \\ Y_{nc} & Y_{nn} \end{bmatrix} \begin{bmatrix} V_{sc} \\ 0 \end{bmatrix} \right) \quad (4.20)$$

$$\begin{bmatrix} I_{rc} \\ I_{rn} \end{bmatrix} = \begin{bmatrix} I_{sc} \\ I_{sn} \end{bmatrix} - \frac{L}{2} \begin{bmatrix} Y_{cc} & Y_{cn} \\ Y_{nc} & Y_{nn} \end{bmatrix} \begin{bmatrix} V_{sc} + V_{rc} \\ V_{sn} + V_{rn} \end{bmatrix} \quad (4.21)$$

where,

$$D = IU + \frac{L^2}{2} Y_{nc} Z_{cn} + \frac{L^2}{2} Y_{nn} Z_{nn}$$

$$E = \frac{L}{2} Y_{nc} (2IU + \frac{L^2}{2} Z_{cc} Y_{cc} + \frac{L^2}{2} Z_{cn} Y_{nc}) \\ + \frac{L}{2} Y_{nn} (\frac{L^2}{2} Z_{nc} Y_{cc} + \frac{L^2}{2} Z_{nn} Y_{nc})$$

$$F = -\frac{L^2}{2} Y_{nc} Z_{cc} - \frac{L^2}{2} Y_{nn} Z_{nc}$$

- SA2: $V_{sc}, V_{rc} \rightarrow S_{sr}, S_{rs}$

$$I_{sc} = X^{-1}(WV_{sc} + UV_{rc}) \quad (4.22)$$

$$I_{sn} = D^{-1}(EV_{sc} + FI_{sc}) \quad (4.23)$$

$$\begin{bmatrix} V_{rc} \\ V_{rn} \end{bmatrix} = \begin{bmatrix} V_{sc} \\ 0 \end{bmatrix} - L \begin{bmatrix} Z_{cc} & Z_{cn} \\ Z_{nc} & Z_{nn} \end{bmatrix} \left(\begin{bmatrix} I_{sc} \\ I_{sn} \end{bmatrix} - \frac{L}{2} \begin{bmatrix} Y_{cc} & Y_{cn} \\ Y_{nc} & Y_{nn} \end{bmatrix} \begin{bmatrix} V_{sc} \\ 0 \end{bmatrix} \right) \quad (4.24)$$

$$\begin{bmatrix} I_{rc} \\ I_{rn} \end{bmatrix} = \begin{bmatrix} I_{sc} \\ I_{sn} \end{bmatrix} - \frac{L}{2} \begin{bmatrix} Y_{cc} & Y_{cn} \\ Y_{nc} & Y_{nn} \end{bmatrix} \begin{bmatrix} V_{sc} + V_{rc} \\ V_{sn} + V_{rn} \end{bmatrix} \quad (4.25)$$

$$S_{sr} = V_{sc} I_{sc}^* \quad (4.26)$$

$$S_{rs} = V_{rc} I_{rc}^* \quad (4.27)$$

where,

$$X = LZ_{cc} - \frac{L^3}{2} Z_{cn} R Y_{nn} Z_{nc}$$

$$W = IU + \frac{L^2}{2} Z_{cc} Y_{cc} - LZ_{cn} M + \frac{L^2}{2} Z_{cn} Y_{nc}$$

$$U = -IU - \frac{L^2}{2} Z_{cn} R Y_{nc}$$

$$S = R \left(\frac{L}{2} Y_{nc} + \frac{L^3}{4} Y_{nn} Z_{nc} Y_{cc} + \frac{L^3}{4} Y_{nn} Z_{nn} Y_{nc} \right)$$

$$R = \left(IU + \frac{L^2}{2} Y_{nn} Z_{nn} \right)^{-1}$$

$$D = IU + \frac{L^2}{2} Y_{nc} Z_{cn} + \frac{L^2}{2} Y_{nn} Z_{nn}$$

$$E = \frac{L}{2} Y_{nc} (2IU + \frac{L^2}{2} Z_{cc} Y_{cc} + \frac{L^2}{2} Z_{cn} Y_{nc}) \\ + \frac{L}{2} Y_{nn} (\frac{L^2}{2} Z_{nc} Y_{cc} + \frac{L^2}{2} Z_{nn} Y_{nc})$$

$$F = -\frac{L^2}{2} Y_{nc} Z_{cc} - \frac{L^2}{2} Y_{nn} Z_{nc}$$

- SA3: $V_{rc}, I_{rc} \rightarrow V_{sc}, I_{sc}$

$$V_{rn} = D^{-1}(E V_{rc} + F I_{rc}) \quad (4.28)$$

$$\begin{bmatrix} V_{sc} \\ 0 \end{bmatrix} = \begin{bmatrix} V_{rc} \\ V_{rn} \end{bmatrix} + L \begin{bmatrix} Z_{cc} & Z_{cn} \\ Z_{nc} & Z_{nn} \end{bmatrix} \left(\begin{bmatrix} I_{rc} \\ 0 \end{bmatrix} + \frac{L}{2} \begin{bmatrix} Y_{cc} & Y_{cn} \\ Y_{nc} & Y_{nn} \end{bmatrix} \begin{bmatrix} V_{rc} \\ V_{rn} \end{bmatrix} \right) \quad (4.29)$$

$$\begin{bmatrix} I_{sc} \\ I_{sn} \end{bmatrix} = \begin{bmatrix} I_{rc} \\ I_{rn} \end{bmatrix} + \frac{L}{2} \begin{bmatrix} Y_{cc} & Y_{cn} \\ Y_{nc} & Y_{nn} \end{bmatrix} \begin{bmatrix} V_{sc} + V_{rc} \\ V_{rn} \end{bmatrix} \quad (4.30)$$

where,

$$D = IU + \frac{L^2}{2} Z_{nc} Y_{cn} + \frac{L^2}{2} Z_{nn} Y_{nn}$$

$$E = -\frac{L^2}{2} Z_{nc} Y_{cc} - \frac{L^2}{2} Z_{nn} Y_{nc}$$

$$F = -LZ_{nc}$$

- SA4: $V_{sc}, Z_r \rightarrow V_{rc}, S_{sr}$

This sub-algorithm is an iterative algorithm which is similar to the backward/forward sweep algorithm, as shown in Figure 4.4

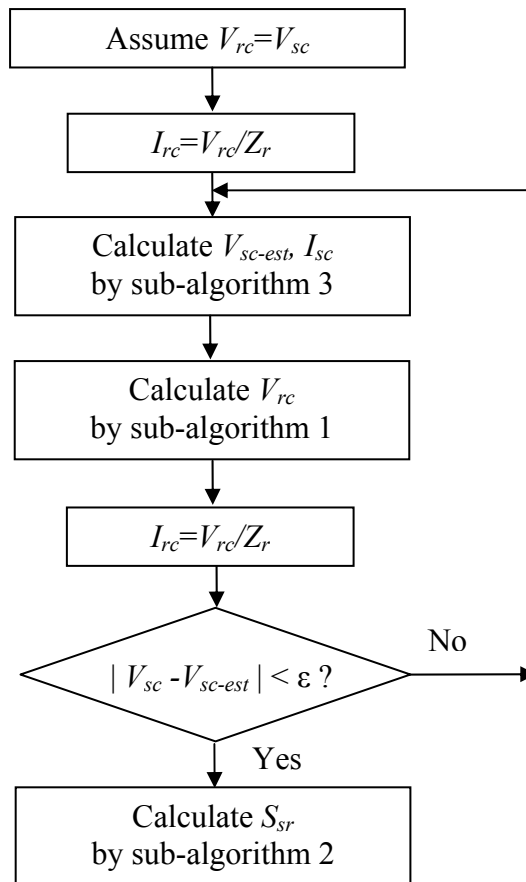


Figure 4.4: Flowchart of SA4.

- SA5: $V_{sc}, S_{sr} \rightarrow V_{rc}, S_{rs}$

$$I_{sc} = \left(\frac{S_{sr}}{V_{sc}} \right)^* \quad (4.31)$$

$$I_{sn} = D^{-1}(EV_{sc} + FI_{sc}) \quad (4.32)$$

$$\begin{bmatrix} V_{rc} \\ V_{rn} \end{bmatrix} = \begin{bmatrix} V_{sc} \\ 0 \end{bmatrix} - L \begin{bmatrix} Z_{cc} & Z_{cn} \\ Z_{nc} & Z_{nn} \end{bmatrix} \left(\begin{bmatrix} I_{sc} \\ I_{sn} \end{bmatrix} - \frac{L}{2} \begin{bmatrix} Y_{cc} & Y_{cn} \\ Y_{nc} & Y_{nn} \end{bmatrix} \begin{bmatrix} V_{sc} \\ 0 \end{bmatrix} \right) \quad (4.33)$$

$$\begin{bmatrix} I_{rc} \\ I_{rn} \end{bmatrix} = \begin{bmatrix} I_{sc} \\ I_{sn} \end{bmatrix} - \frac{L}{2} \begin{bmatrix} Y_{cc} & Y_{cn} \\ Y_{nc} & Y_{nn} \end{bmatrix} \begin{bmatrix} V_{sc} + V_{rc} \\ V_{sn} + V_{rn} \end{bmatrix} \quad (4.34)$$

where,

$$D = IU + \frac{L^2}{2} Y_{nc} Z_{cn} + \frac{L^2}{2} Y_{nn} Z_{nn}$$

$$\begin{aligned} E &= \frac{L}{2} Y_{nc} (2IU + \frac{L^2}{2} Z_{cc} Y_{cc} + \frac{L^2}{2} Z_{cn} Y_{nc}) \\ &\quad + \frac{L}{2} Y_{nn} (\frac{L^2}{2} Z_{nc} Y_{cc} + \frac{L^2}{2} Z_{nn} Y_{nc}) \end{aligned}$$

$$F = -\frac{L^2}{2} Y_{nc} Z_{cc} - \frac{L^2}{2} Y_{nn} Z_{nc}$$

- SA6: $V_{rc}, S_{rs} \rightarrow V_{sc}, S_{sr}$

$$I_{rc} = \left(\frac{S_{rs}}{V_{rc}} \right)^* \quad (4.35)$$

$$V_{rn} = D^{-1}(EV_{rc} + FI_{rc}) \quad (4.36)$$

$$\begin{bmatrix} V_{sc} \\ 0 \end{bmatrix} = \begin{bmatrix} V_{rc} \\ V_{rn} \end{bmatrix} + L \begin{bmatrix} Z_{cc} & Z_{cn} \\ Z_{nc} & Z_{nn} \end{bmatrix} \left(\begin{bmatrix} I_{rc} \\ 0 \end{bmatrix} + \frac{L}{2} \begin{bmatrix} Y_{cc} & Y_{cn} \\ Y_{nc} & Y_{nn} \end{bmatrix} \begin{bmatrix} V_{rc} \\ V_{rn} \end{bmatrix} \right) \quad (4.37)$$

$$\begin{bmatrix} I_{sc} \\ I_{sn} \end{bmatrix} = \begin{bmatrix} I_{rc} \\ I_{rn} \end{bmatrix} + \frac{L}{2} \begin{bmatrix} Y_{cc} & Y_{cn} \\ Y_{nc} & Y_{nn} \end{bmatrix} \begin{bmatrix} V_{sc} + V_{rc} \\ V_{rn} \end{bmatrix} \quad (4.38)$$

$$S_{sr} = V_{sc} I_{sc}^* \quad (4.39)$$

where,

$$D = IU + \frac{L^2}{2} Z_{nc} Y_{cn} + \frac{L^2}{2} Z_{nn} Y_{nn}$$

$$E = -\frac{L^2}{2} Z_{nc} Y_{cc} - \frac{L^2}{2} Z_{nn} Y_{nc}$$

$$F = -LZ_{nc}$$

Basically, the voltages and currents are estimated section by section starting from the substation. If there are laterals or tapped loads at one certain bus, four situations are involved and summarized as below. Assuming V_x and I_{xr} are known from the previous estimation, and the quantities at node $x+1$ need to be estimated.

- The bus x has no lateral and tapped load, as shown in Figure 4.5.

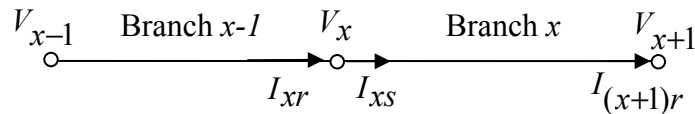


Figure 4.5: Node with no lateral and tapped load.

Since $I_{xs} = I_{xr}$, V_{x+1} and $I_{(x+1)r}$ can be estimated directly by SA1.

- The bus x has the tapped load but with no lateral, as shown in Figure 4.6.

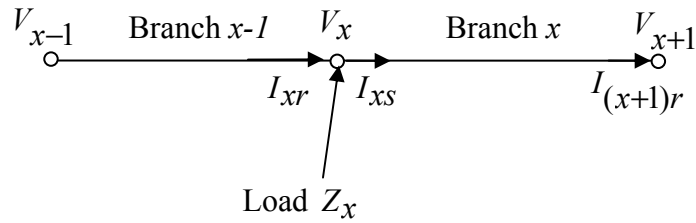


Figure 4.6: Node with tapped load and with no lateral.

Since $I_{xs} = I_{xr} - V_x/Z_x$, then V_{x+1} and $I_{(x+1)r}$ can be estimated directly by SA1.

- The bus x has the lateral but with no tapped load, as shown in Figure 4.7.

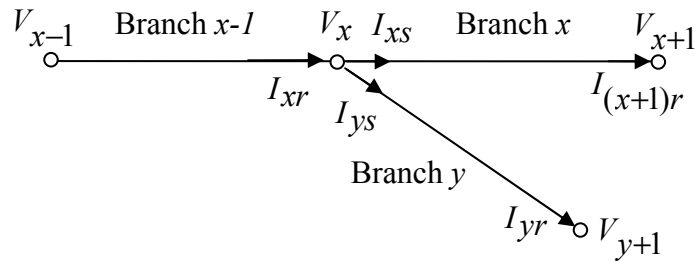


Figure 4.7: Node with lateral and with no tapped load.

First, I_{ys} is estimated by the backward/forward sweep algorithm where SA1-SA6 may be applied, then $I_{xs} = I_{xr} - I_{ys}$, V_{x+1} and $I_{(x+1)r}$ can be estimated directly by SA1.

- The bus x has both tapped load and lateral, as shown in Figure 4.8.

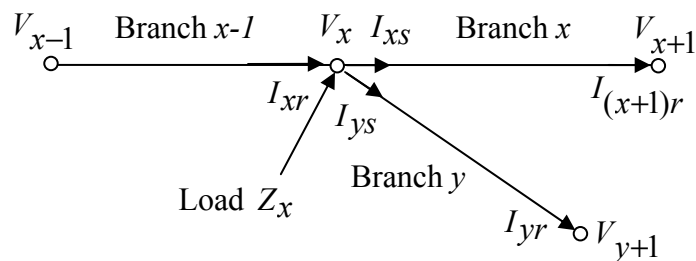


Figure 4.8: Node with lateral and tapped load.

First, I_{ys} is estimated by the backward/forward sweep algorithm where SA1-SA6 may be applied, then $I_{xs} = I_{xr} - V_x / Z_x - I_{ys}$, V_{x+1} and $I_{(x+1)r}$ can be estimated directly by SA1.

To explain the estimation algorithm more clearly, the estimation details for the system in Figure 4.2 are illustrated in Table 4.2.

In the table, V_x means the voltage at bus x . I_{xs} denotes the current flowing in branch x and I_{xr} denotes the current flowing out of branch x . The subscripts of apparent power S have the same denotation as the one for current I . Z_x is the injected load impedance at node x . The quantities with the bold font are the quantities needed for the location algorithm.

4.3.2.2 Estimation of Seen Impedance

The seen impedance behind the receiving terminal of the faulty section should be estimated as well for the purpose of the application of the location algorithm. The seen impedance estimated by the state estimation can be used here since the seen impedance is unchanged after the occurrence of fault, which is proven below.

Assuming there is a fault in the cable section between node $x-1$ and x , the cable section between node x and $x+1$ is behind the faulty section, as shown in Figure 4.9.

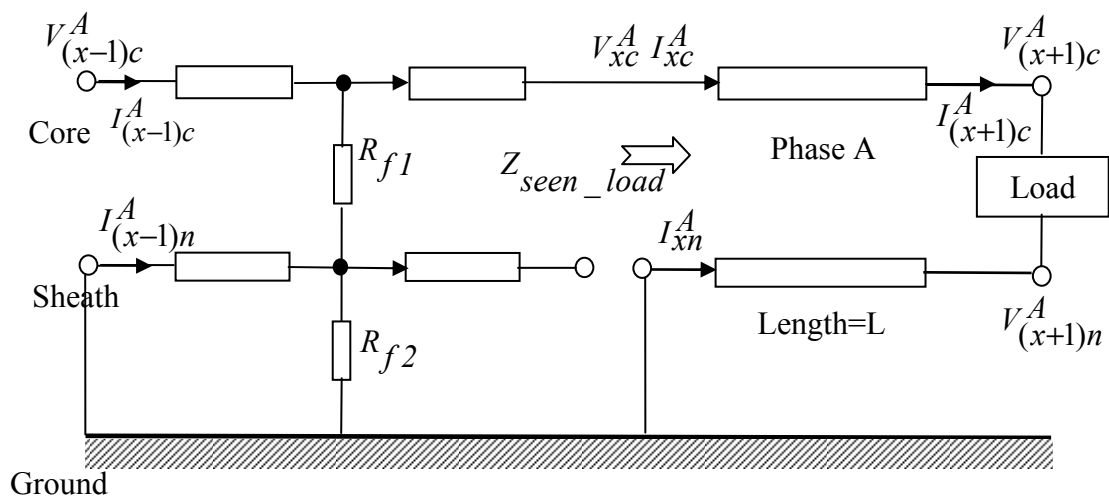


Figure 4.9: Calculation of seen impedance.

Table 4.2: Estimation of Nodal Voltages and Branch Currents

Faulty Branch No.	Known Variables	Variables to be calculated	Algorithm or Equations
1	V_1, I_{1s}	$V_2, I_{1r} (I_{2s})$	SA1
2	V_2, I_{2s}	V_3, I_{2r}	SA1
3	V_3, I_{2r}, Z_3	I_{3s}, V_4, I_{3r}	SA1
	V_4, Z_{31}	$V_{31}, S_{30s} \rightarrow I_{30s}$	SA4 on 30
4	V_4, I_{3r}, I_{30s}	$I_{4s}, V_5, I_{4r} (I_{5s})$	SA1
5	V_5, I_{5s}	$V_6, I_{5r} (I_{6s})$	SA1
6	V_6, I_{6s}	V_7, I_{6r}	SA1
	V_7, Z_{29}, Z_{30}	$V_{28}, V_{29}, V_{30}, I_{27s}$	BFSA on 27 28 29, SA3, SA1
7	V_7, I_{6r}, I_{27s}	I_{7s}, V_8, I_{7r}	SA1
	V_8, Z_{27}	$V_{27}, S_{26s} \rightarrow I_{26s}$	SA4 on 26
8	$V_8, I_{7r}, Z_8, I_{26s}$	I_{8s}, V_9, I_{8r}	SA1
9	V_9, I_{8r}, Z_9	I_{9s}, V_{10}, I_{9r}	SA1
10	V_{10}, I_{9r}, Z_{10}	I_{10s}, V_{11}, I_{10r}	SA1
	V_{11}, Z_{26}	$V_{26}, S_{25s} \rightarrow I_{25s}$	SA4 on 25
11	V_{11}, I_{10r}, I_{25s}	I_{11s}, V_{12}, I_{11r}	SA1
	V_{12}, Z_{24}	I_{22s}	BFSA on 22-23, SA6 SA5
12	V_{12}, I_{11r}, I_{22s}	I_{12s}, V_{13}, I_{12r}	SA1
	V_{13}, Z_{25}	$V_{25}, S_{24s} \rightarrow I_{24s}$	SA4 on 24
13	$V_{13}, I_{12r}, I_{24s}, Z_{13}$	I_{13s}, V_{14}, I_{13r}	SA1
	$V_{14}, Z_{16}, Z_{17}, Z_{18}$	I_{14s}	BFSA on 14-17, SA3 SA1
18	$V_{14}, I_{13r}, I_{14s}, Z_{14}$	I_{18s}, V_{19}, I_{18r}	SA1
19	V_{19}, I_{18r}, Z_{19}	I_{19s}, V_{20}, I_{19r}	SA1
	V_{20}, Z_{22}	$V_{22}, S_{21s} \rightarrow I_{21s}$	SA4 on 21
20	I_{19r}, I_{21s}, Z_{20}	I_{20s}	SA1
	V_{20}, Z_{21}	$V_{21}, S_{20s} \rightarrow I_{20s}$	SA4 on 20
21	I_{19r}, I_{20s}, Z_{20}	I_{21s}	SA1
	$V_{14}, Z_{19}, Z_{20}, Z_{21}, Z_{22}$	I_{18s}	BFSA on 18-21, SA3 SA1 SA4
14	$V_{14}, I_{13r}, I_{18s}, Z_{14}$	$I_{14s}, V_{15}, I_{14r} (I_{15s})$	SA1
15	V_{15}, I_{15s}	V_{16}, I_{15r}	SA1
16	V_{16}, I_{15r}, Z_{16}	I_{16s}, V_{17}, I_{16r}	SA1
17	V_{17}, I_{16r}, Z_{17}	I_{17s}, V_{18}	SA1
	$V_{12}, \text{All } Z \text{ between } 13-22$	I_{12s}	BFSA on 13-22, SA3 SA1 SA4
22 23	V_{12}, I_{11r}, I_{12s}	$I_{22s}, V_{23}, I_{22r} (I_{23s})$	SA1

The load impedance Z_{load} is estimated by the prefault quantities. The seen impedance Z_{seen_load} is required for locating the fault in the faulty section, which can be calculated by Equations (4.40)-(4.42).

$$\begin{bmatrix} V_{(x+1)c} \\ V_{(x+1)n} \end{bmatrix} = \begin{bmatrix} V_{xc} \\ 0 \end{bmatrix} - L \begin{bmatrix} Z_{cc} & Z_{cn} \\ Z_{nc} & Z_{nn} \end{bmatrix} \left(\begin{bmatrix} I_{xc} \\ I_{xn} \end{bmatrix} - \frac{L}{2} \begin{bmatrix} Y_{cc} & Y_{cn} \\ Y_{nc} & Y_{nn} \end{bmatrix} \begin{bmatrix} V_{xc} \\ 0 \end{bmatrix} \right) \quad (4.40)$$

$$\begin{bmatrix} I_{(x+1)c} \\ 0 \end{bmatrix} = \begin{bmatrix} I_{xc} \\ I_{xn} \end{bmatrix} - \frac{L}{2} \begin{bmatrix} Y_{cc} & Y_{cn} \\ Y_{nc} & Y_{nn} \end{bmatrix} \begin{bmatrix} V_{(x+1)c} + V_{xc} \\ V_{(x+1)n} \end{bmatrix} \quad (4.41)$$

$$Z_{seen_load} = \frac{V_{xc}}{I_{xc}} = \frac{Z_{load} M_M^{-1} M_G}{M_F Z_{load}^{-1} M_N} \quad (4.42)$$

where,

$$M_A = \left(-IU - \frac{L^2}{2} Y_{nn} Z_{nn} \right)^{-1}$$

$$M_B = M_A \left(-\frac{L}{2} Y_{nc} - \frac{L^3}{4} Y_{nn} Z_{nc} Y_{cc} - \frac{L^3}{4} Y_{nn} Z_{nn} Y_{nc} \right)$$

$$M_C = -\frac{L}{2} M_A Y_{nc}$$

$$M_D = \frac{L^2}{2} M_A Y_{nn} Z_{nc}$$

$$M_E = \left(IU + LZ_{cn} M_C \right)^{-1}$$

$$M_F = M_E \left(IU + \frac{L^2}{2} Z_{cc} Y_{cc} + \frac{L^2}{2} Z_{cn} Y_{nc} - LZ_{cn} M_B \right)$$

$$M_F = M_E \left(-LZ_{cc} - LZ_{cn} M_D \right)$$

$$M_H = \left(IU + \frac{L^2}{2} Z_{nc} Y_{cn} + \frac{L^2}{2} Z_{nn} Y_{nn} \right)^{-1}$$

$$M_J = M_H \left(-\frac{L^2}{2} Z_{nc} Y_{cc} - \frac{L^2}{2} Z_{nn} Y_{nc} \right)$$

$$M_K = -LM_H Z_{nc}$$

$$M_L = \left(IU + \frac{L}{2} Y_{cn} M_K \right)^{-1}$$

$$M_M = M_L \left(IU - \frac{L}{2} Y_{cc} M_G - \frac{L}{2} Y_{cn} M_J M_G \right)$$

$$M_N = M_L \left(-\frac{L}{2} Y_{cc} - \frac{L}{2} Y_{cc} M_F - \frac{L}{2} Y_{cn} M_J M_F \right)$$

In Equation (4.42), M_M , M_G , M_N , and M_F are constants, Z_{load} are estimated by the prefault voltage and current. Therefore, if the load is modeled as the constant impedance, three facts can be implied,

- The seen impedance behind the faulty section depends on the load impedance and circuit parameters and is independent of voltage and current, that is, the magnitudes of voltage and current have no impact on this seen impedance.
- The seen impedance can be calculated by the prefault voltages and currents obtained by the SE analysis.

- All downstream feeders, laterals and loads behind the faulty section can be lumped as the seen impedance by this way.

4.3.3 Determination of Faulty Section

So far, the voltage and current at the sending terminal of each section, and the seen impedance behind each section have been estimated. The proposed location algorithm can be applied for each cable section, starting from the source.

If the location calculation is processed on a healthy cable, one or more of the following phenomena could be observed:

- No line-circle crossing point when estimating the current of the faulty sheath;
- Multiple zigzags in the curves of the pinpoint criteria;
- Singular matrix in the process of calculations.

Therefore, the true faulty section is identified as the section with the definite line-circle crossing points, smooth curves of the pinpoint criteria, and well-conditioned matrix in calculation.

Based on the test system in Figure 4.2, three examples with CSGF are given to show the process of determination of the faulty section.

The first example shows a fault occurs at the branch 1 between node 1 and 2. As illustrated in Figure 4.10, there exists the line crossing circle zone along the cable, the pinpoint criteria are smooth, and the minimal point can be clearly found in the curve of the pinpoint criterion. However, these phenomena cannot be observed in Figure 4.11 where the location calculation is processed in the healthy branch 2. Other healthy branches have the similar problem. Therefore, the faulty section can be identified as the branch 1.

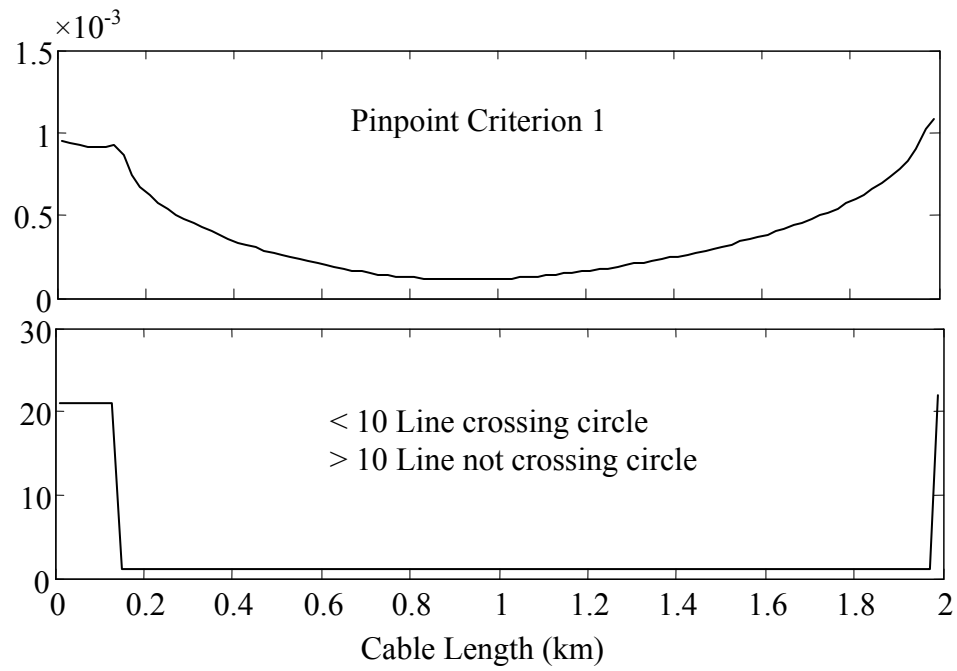


Figure 4.10: Calculation processed on branch 1 (CSGF at branch 1).

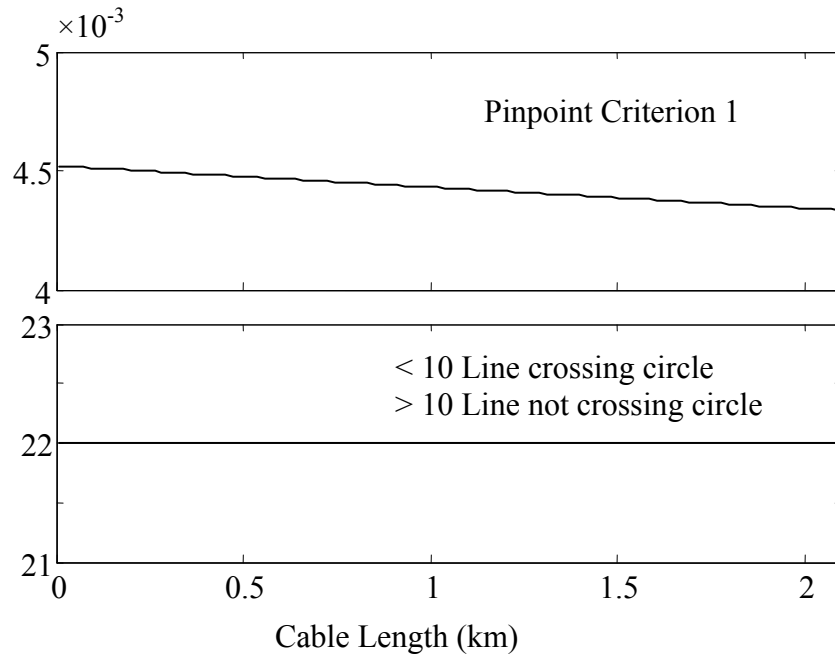


Figure 4.11: Calculation processed on branch 2 (CSGF at branch 1).

The second example shows a fault occurs at the branch 14 between node 14 and 15. The adjacent branches include the branch 13 between node 13 and 14, branch 15 between node 15 and 16, and branch 18 between node 14 and 19. As illustrated in Figure 4.12, there exists the line crossing circle zone along the cable, the pinpoint criteria are smooth, and the minimal point can be clearly found in the curve of the pinpoint criterion. However, these phenomena cannot be observed in Figure 4.13-Figure 4.15, where the location calculation is processed in the adjacent healthy branches. Other healthy branches have the similar problem. Therefore, the faulty section can be identified as the branch 14.

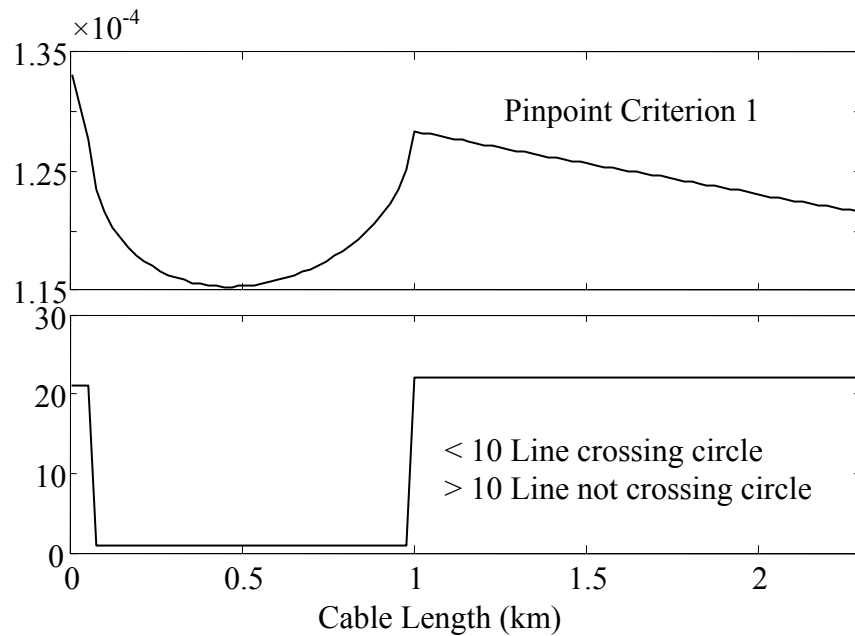


Figure 4.12: Calculation processed on branch 14 (CSGF at branch 14).

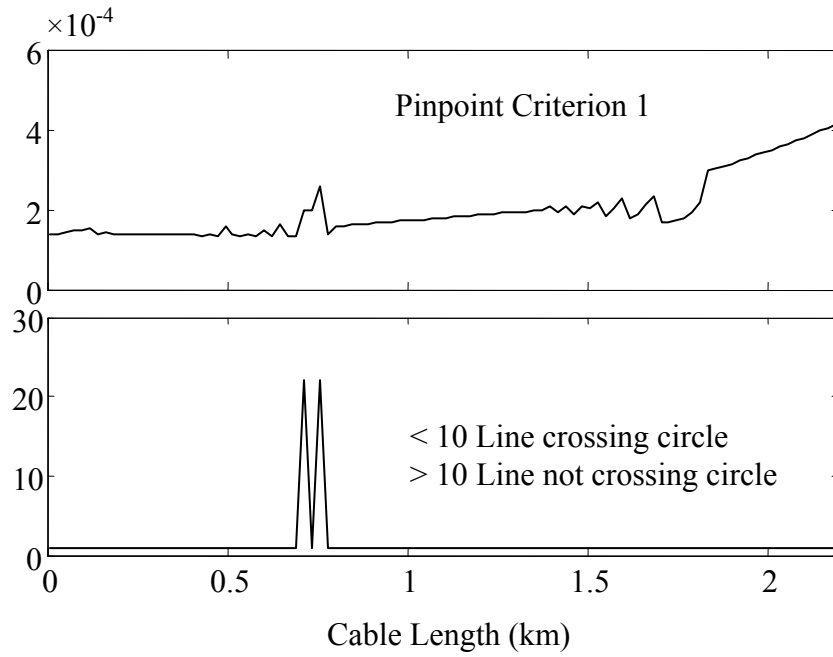


Figure 4.13: Calculation processed on branch 13 (CSGF at branch 14).

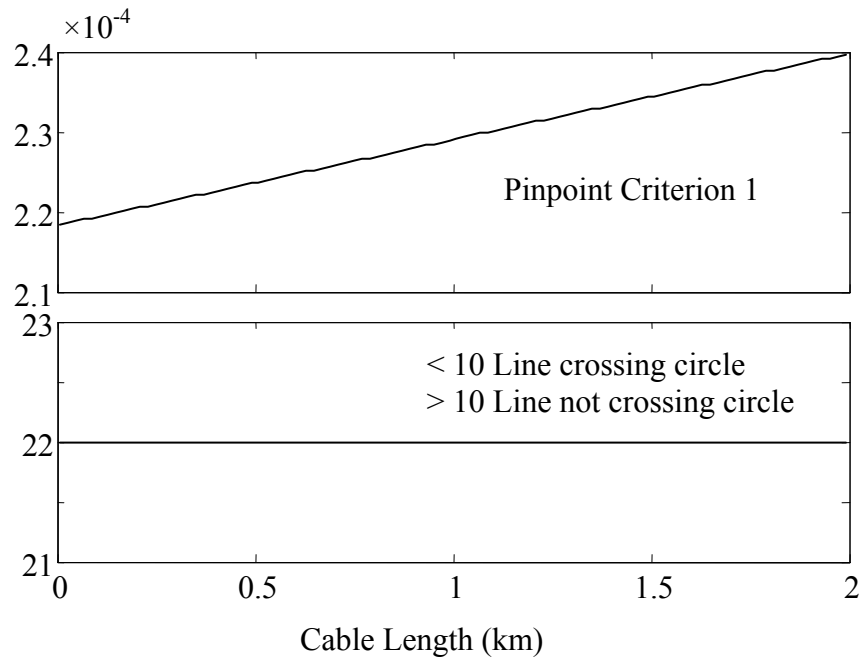


Figure 4.14: Calculation processed on branch 15 (CSGF at branch 14).

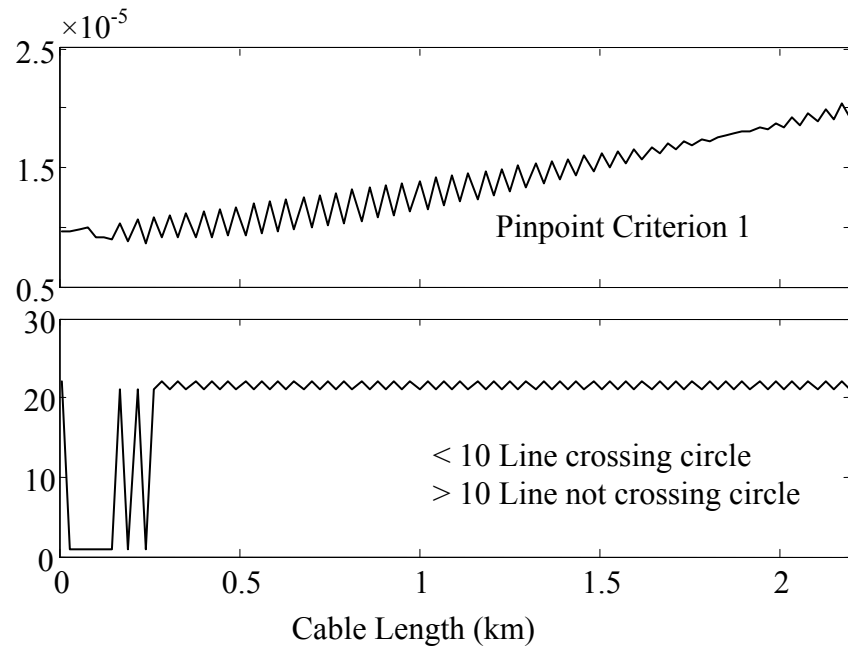


Figure 4.15: Calculation processed on branch 18 (CSGF at branch 14).

The third example shows a fault occurs at the branch 21 between node 20 and 22. The adjacent branches include the branch 19 between node 19 and 20, and branch 20 between node 20 and 21. As illustrated in Figure 4.16, there exists the line crossing circle zone along the cable, the pinpoint criteria are smooth, and the minimal point can be clearly found in the curve of the pinpoint criterion. However, these phenomena cannot be observed in Figure 4.17 and Figure 4.18, where the location calculation is processed in the adjacent healthy branches. Other healthy branches have the similar problem. Therefore, the faulty section can be identified as the branch 21.

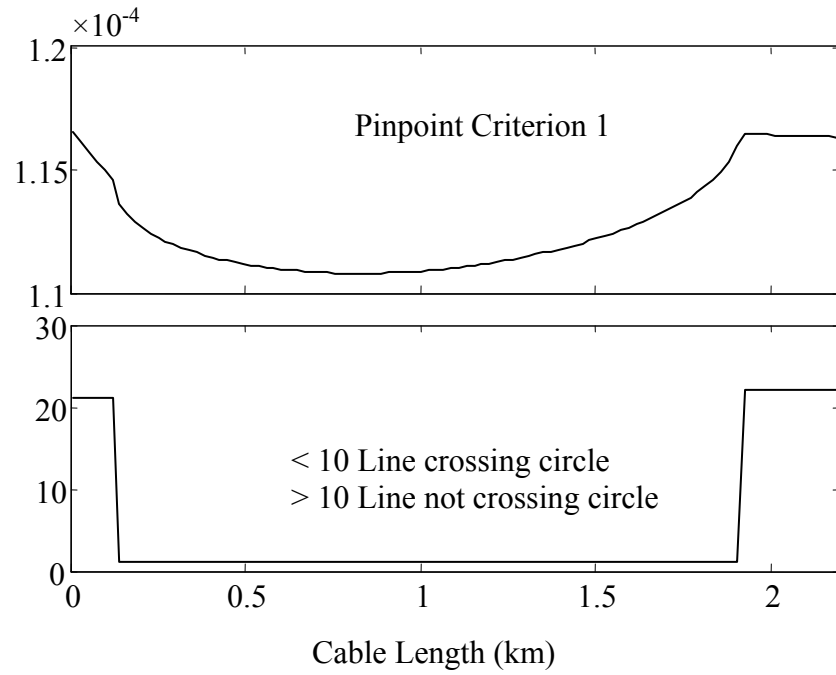


Figure 4.16: Calculation processed on branch 21 (CSGF at branch 21).

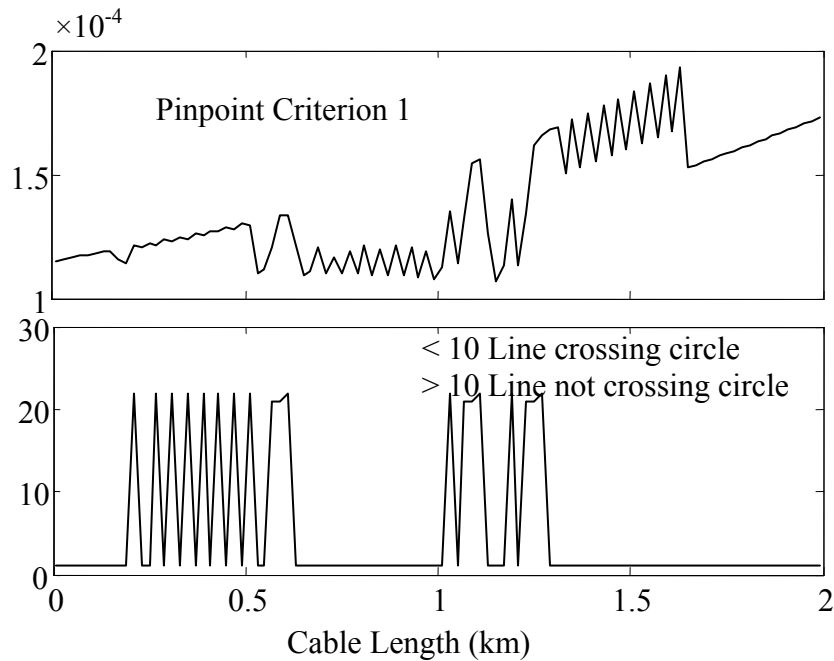


Figure 4.17: Calculation processed on branch 19 (CSGF at branch 21).

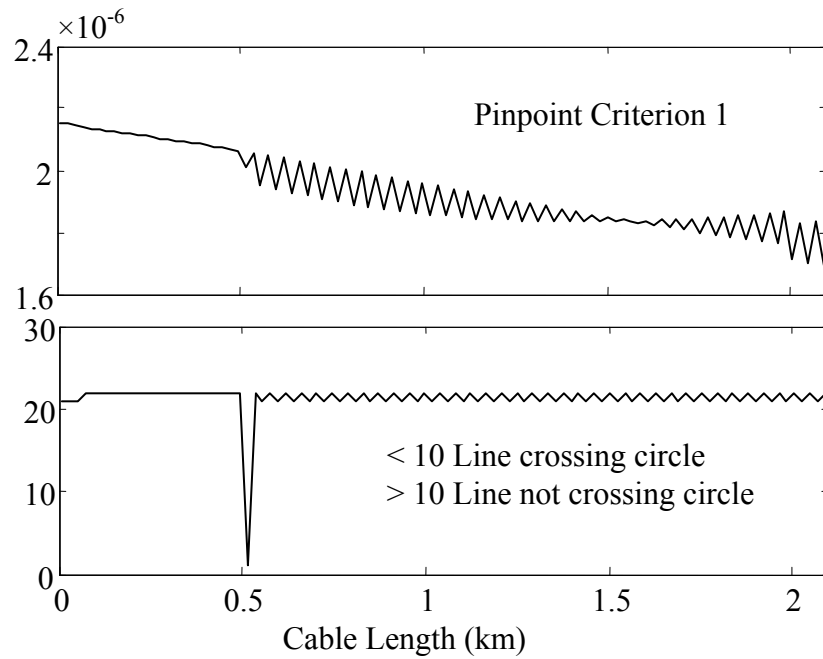


Figure 4.18: Calculation processed on branch 20 (CSGF at branch 21).

The same phenomena can also be observed in the calculation process for the cases of CSF. However, since the calculation of CG has no such crossing points, the faulty section can be determined by the uniform behavior of two criteria. Similarly, three examples are described in Figure 4.19 and Figure 4.20 for a CGF at branch 1, Figure 4.21-Figure 4.24 for a CGF at branch 14 and Figure 4.25-Figure 4.27 for a CGF at branch 21.

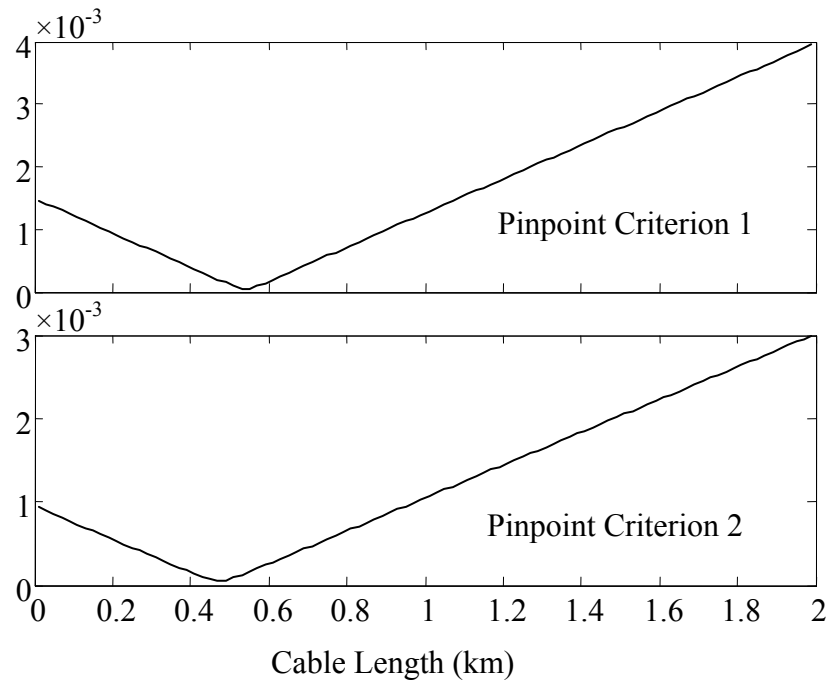


Figure 4.19: Calculation processed on branch 1 (CGF at branch 1).

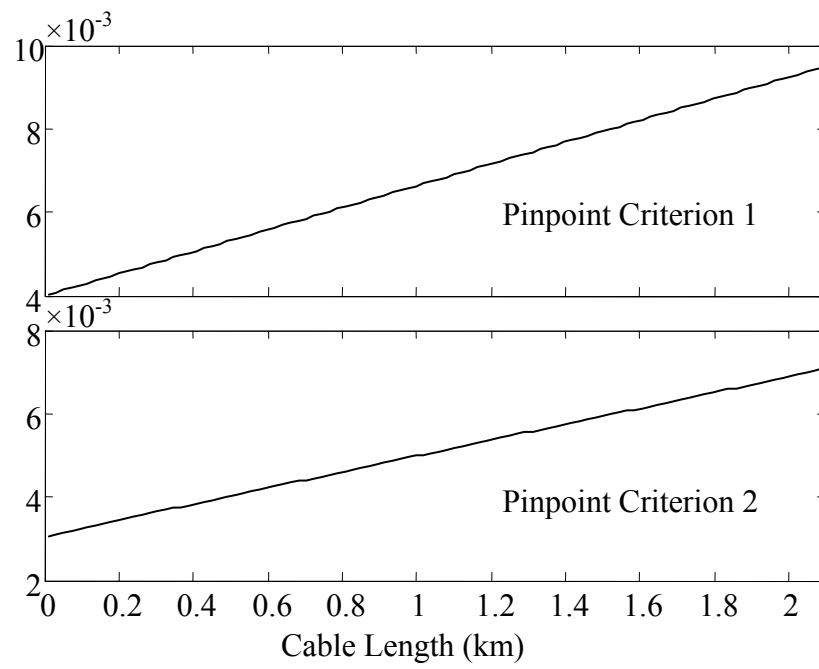


Figure 4.20: Calculation processed on branch 2 (CGF at branch 1).

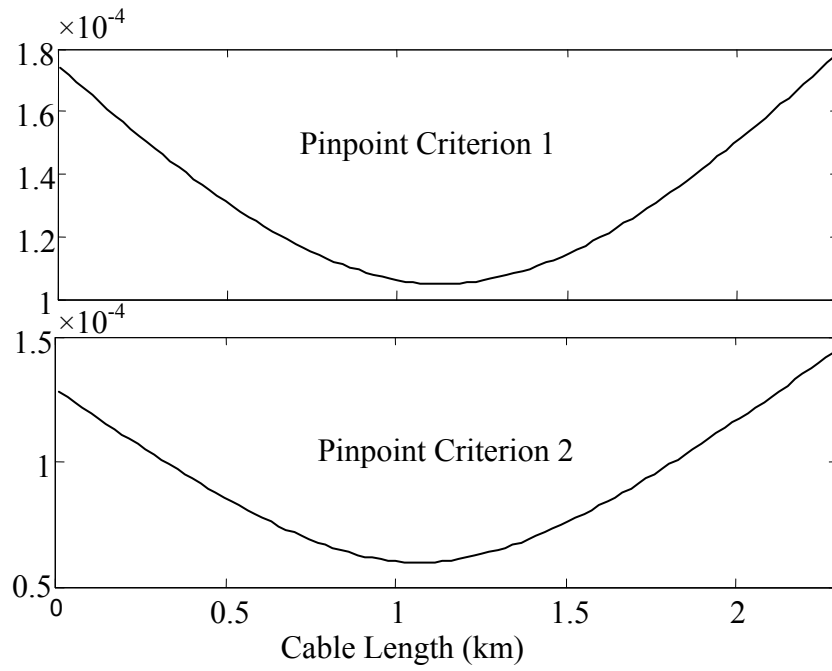


Figure 4.21: Calculation processed on branch 14 (CGF at branch 14).

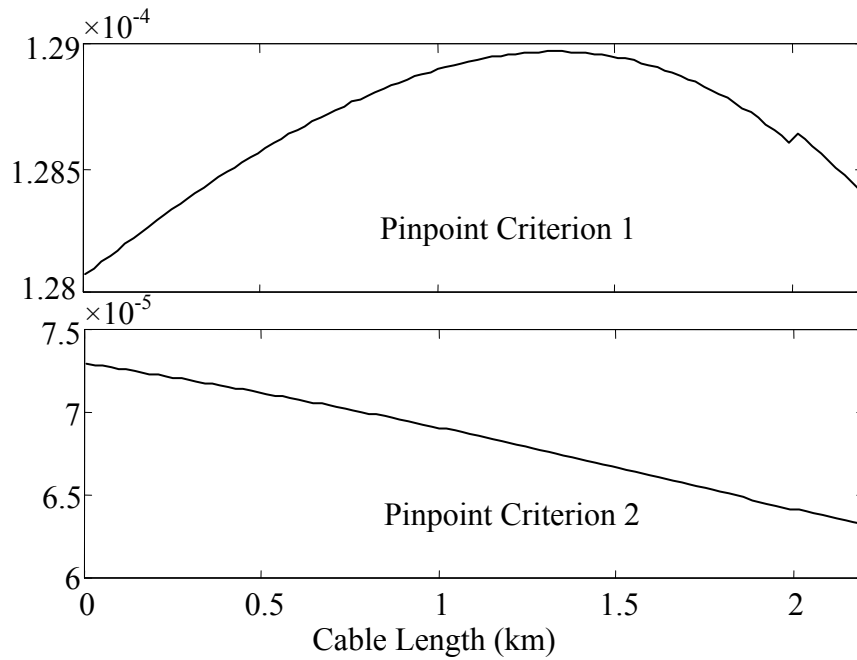


Figure 4.22: Calculation processed on branch 13 (CGF at branch 14).

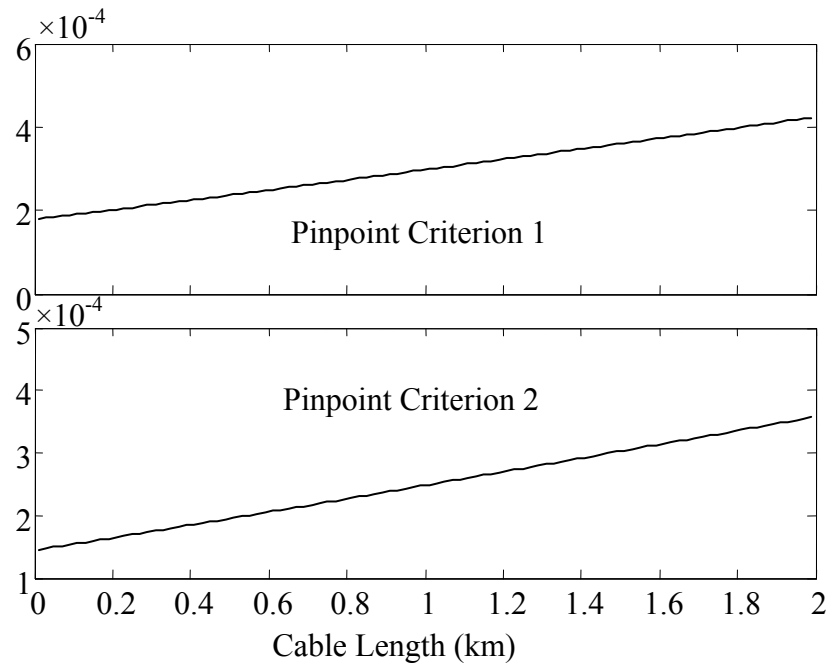


Figure 4.23: Calculation processed on branch 15 (CGF at branch 14).

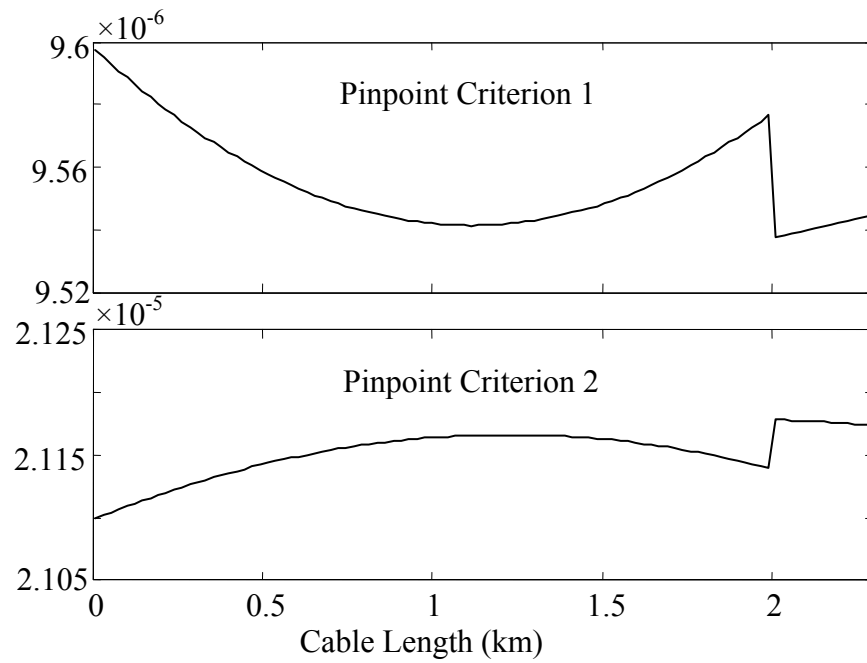


Figure 4.24: Calculation processed on branch 18 (CGF at branch 14).

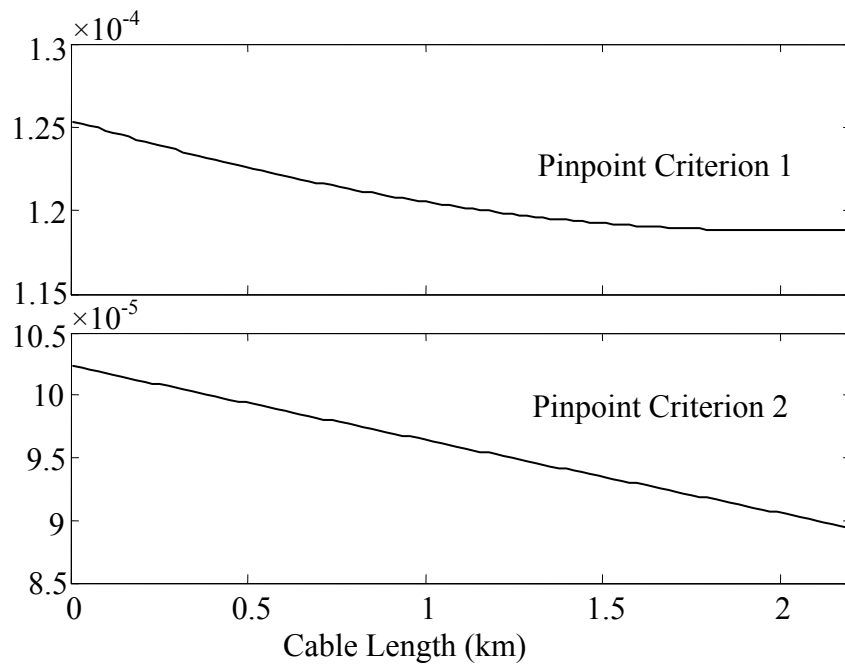


Figure 4.25: Calculation processed on branch 21 (CGF at branch 21).

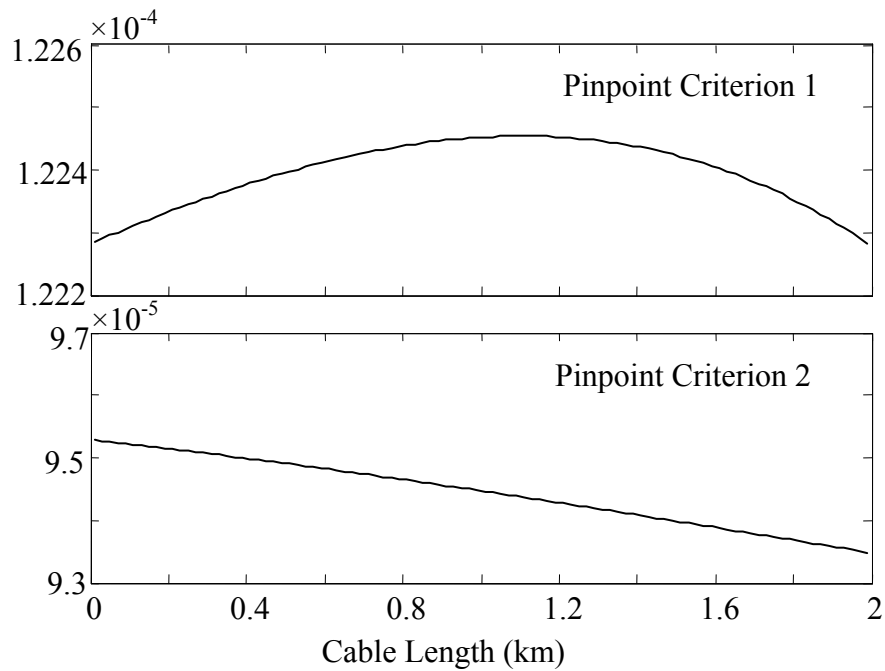


Figure 4.26: Calculation processed on branch 19 (CGF at branch 21).

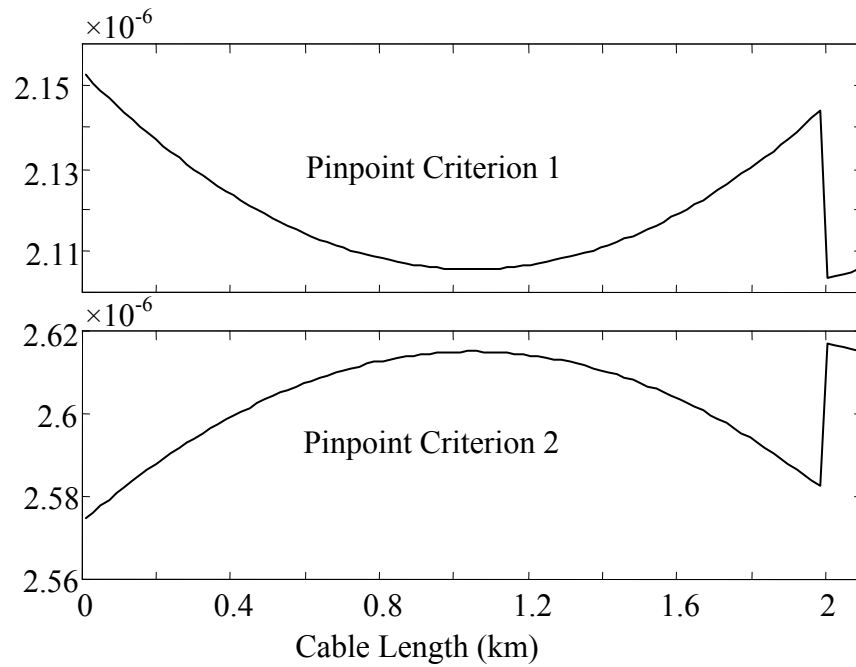


Figure 4.27: Calculation processed on branch 20 (CGF at branch 21).

The problem of multiple estimations is eliminated. The basic reason is that the proposed location algorithm is not based on the calculation of the apparent impedance, so the prerequisite that the multiple points have the same apparent impedance does not exist. Moreover, the availability of the line-circle crossing point and smoothness of pinpoint criteria for each circuit section can further identify the fault section.

4.3.4 Fault Location

The location algorithm can be applied for more samples in the determined faulty section and the final fault distance is the average of the results.

4.3.5 Summary of Location Procedure

Overall, the location procedure can be concluded as follows.

- Step 1: The state estimation problem is regularly solved by SQP methods in DMS, and the voltage at each node is estimated. Then the branch current of each branch, injected load at each node and seen impedance behind each circuit are calculated. This step is explained in Section 4.3.1.
- Step 2: Upon the occurrence of a fault, the voltages and currents at the sending terminal of each circuit section are estimated with the assumption that the fault may occur at this certain section. The employed quantities are the real measurements during the fault, and estimated load impedance at each node obtained in Step 1. This step is explained in Section 4.3.2.
- Step 3: The faulty section has been assumed, the voltage and current have been estimated in Step 2, and the seen impedance has been estimated in Step 1. The proposed location algorithm in Chapter 3 is applied for each cable section, starting from the source. The true faulty section would be selected. This step is explained in Section 4.3.3.
- Step 4: The location algorithm can be applied for more samples in the determined faulty section as mentioned in Section 4.3.4.

With respect to the three emerging issues mentioned in Section 4.1.3, the first issue is resolved in Step 2, the second one in Step 1 and the third one in Step 3.

4.4 Application of Static Response Load Model

The above algorithm is based on the assumption that the load model is the constant impedance. Similarly to Section 3.9.2, the effect of the static response type models will be investigated. This load model is introduced in Section 1.3.3 and [39], and given as,

$$Y = G_r \left| \frac{V}{V_0} \right|^{n_p - 2} + jB_r \left| \frac{V}{V_0} \right|^{n_q - 2} \quad (4.43)$$

The G_r and B_r can be estimated by the prefault voltage and current obtained from the state estimation.

The voltage V in Equation (4.43) is the voltage at the load terminal during fault, and its magnitude can be approximately estimated by,

$$|V| = \left(\left| V_f \right| - \frac{L-D}{L} \left(\left| V_s^{pre} \right| - \left| V_r^{pre} \right| \right) \right) \frac{\left| V_l^{pre} \right|}{\left| V_r^{pre} \right|} \quad (4.44)$$

where D is the fault distance, L is the cable length. V_s^{pre} is the pre-fault voltage at the sending terminal, V_r^{pre} is the pre-fault voltage at the receiving terminal, V_l^{pre} is the pre-fault voltage at the load point, all of them are estimated by the state estimation method. V_f is the fault voltage calculated in the location process.

Since the load impedance is changed during the fault, the seen impedance calculated by the pre-fault quantities cannot be used. However, it can be estimated by Equation (4.42) during the fault. Due to the large computation in such situation, the constant parameters used in the calculation can be preprocessed and stored in the database.

4.5 Simulations

4.5.1 Test System and Cases

A radial underground distribution network shown in Figure 4.2 is used to examine the state estimation algorithm and fault location algorithm. The test system has the following aspects:

- 31 buses.
- 23 three-phase feeders or laterals and 7 single-phase laterals.
- 9 three-phase, 2 double-phase and 9 single-phase loads.
- All circuits are composed of underground cables with sheaths grounded at the sending terminal of circuit sections.

- Only measurements of the voltage and current are available at the substation, i.e. bus 1. For other distribution systems, there may have more measurement points sparsely placed in the system.

The details of the test system are listed in Table 4.3.

Table 4.3: Details of Test System

Branch No.	Starting Node	Ending Node	Phase	Length (km)
1	1	2	ABC	2
2	2	3	ABC	2.1
3	3	4	ABC	9.8237
4	4	5	ABC	11.43
5	5	6	ABC	9.06
6	6	7	ABC	2.3
7	7	8	ABC	3.112
8	8	9	ABC	2
9	9	10	ABC	6.23
10	10	11	ABC	2.2
11	11	12	ABC	11.22
12	12	13	ABC	2
13	13	14	ABC	2.2
14	14	15	ABC	2.3
15	15	16	ABC	2
16	16	17	ABC	2.1
17	17	18	ABC	2.2
18	14	19	ABC	2.3
19	19	20	ABC	2
20	20	21	ABC	2.1
21	20	22	ABC	2.2
22	12	23	ABC	3
23	23	24	ABC	5
24	13	25	A	2.1
25	11	26	B	7.11
26	8	27	B	2.1
27	7	28	A	2.3
28	28	29	A	14.676
29	29	30	A	4.188
30	4	31	B	2.2

In order to apply the proposed state estimation technique, a set of initial load patterns (LP) should be assigned as the load pseudo measurements. Therefore, seven load patterns given below are introduced by uniformly or randomly perturbing the true loads within a range.

- LP1: higher within 4~6%.
- LP2: higher within 0~5%.
- LP3: higher within 5~10%.
- LP4: higher within 5~15%.
- LP5: within -5~5%.
- LP6: within -10~10%.
- LP7: within -20~20%.

The patterns LP1-LP4 demonstrate the uniform load profiles, which have a uniformly positive bias regarding to the true loads. The patterns LP5-LP7 represent the generic load profiles.

The fault cases involve the following variation of parameters and conditions:

- Faults occur at each three-phase cable.
- Fault distances are fixed at 25%, 50% and 75% length of each cable section.
- Fault resistances are fixed as 4 ohm.
- Three fault scenarios are respectively involved for each fault point.
- The location algorithm is processed for each load pattern.

4.5.2 Performance Indices

The fault location performance is evaluated by the relative location error defined in [35] as,

$$error = \frac{Estimated\ Distance - Exact\ Distance}{Length\ of\ Faulty\ Line} \times 100\% \quad (4.45)$$

The functionality of the state estimation algorithm is evaluated by three performance indices.

- Average voltage magnitude relative error (AVM)

$$AVM(\%) = \frac{1}{N_b} \sum_{i=1}^{N_b} \left| \frac{|V_{i,est}^k| - |V_{i,true}^k|}{|V_{i,true}^k|} \right| \times 100, \quad k = A, B, C \quad (4.46)$$

where N_b is the amount of buses, $V_{i,est}^k$ is the estimated voltage of phase k at bus i , similarly, $V_{i,true}^k$ is the true voltage of phase k at bus i .

- Average weighted real power load relative error (AWP)

$$AWP(\%) = \sum_{i=1}^{N_b} \left(w_i^k \left| \frac{P_{i,est}^k - P_{i,true}^k}{P_{i,true}^k} \right| \right) \times 100, \quad k = A, B, C \quad (4.47)$$

where $P_{i,est}^k$ is the estimated real power of phase k injected into node i , $P_{i,true}^k$ is the true real power of phase k injected into node i . w_i^k is the factor to weigh the ratio value of phase k at bus i and given as,

$$w_i^k = \frac{P_{i,true}^k}{\sum_{j=1}^{N_b} P_{j,true}^k}, \quad k = A, B, C \quad (4.48)$$

- Average weighted reactive power load relative error (AWQ)

$$AWQ(\%) = \sum_{i=1}^{N_b} \left(w_i^k \left| \frac{Q_{i,est}^k - Q_{i,true}^k}{Q_{i,true}^k} \right| \right) \times 100, \quad k = A, B, C \quad (4.49)$$

where $Q_{i,est}^k$ is the estimated reactive power of phase k injected into node i , $Q_{i,true}^k$ is the true reactive power of phase k injected into node i . w_i^k is given as

$$w_i^k = \frac{Q_{i,true}^k}{\sum_{j=1}^{N_b} Q_{j,true}^k}, \quad k = A, B, C \quad (4.50)$$

4.5.3 State Estimation Results

The performance indices for the seven initial load patterns are listed in Table 4.4. The seven load patterns are applied into the state estimation algorithm and the corresponding SQP problem is solved by the optimization function in Matlab. Accordingly, the performance indices for the estimated loads are shown in Table 4.5.

Table 4.4: Performance Indices for Initial Loads

Load Pattern	Phase	Error (%)		
		AVM	AWP	AWQ
LP1: 4~6%	A	0.540	3.783	3.528
	B	0.270	4.218	4.257
	C	0.319	4.297	4.136
LP2: 0~5%	A	0.348	2.238	2.885
	B	0.073	3.140	2.290
	C	0.312	2.739	2.264
LP3: 5~10%	A	0.870	6.243	5.162
	B	0.426	7.715	5.904
	C	0.430	7.269	4.949
LP4: 5~15%	A	1.057	5.617	9.573
	B	0.530	6.631	9.475
	C	0.646	5.950	9.990
LP5: -5~5%	A	0.406	2.621	2.347
	B	0.207	2.344	4.014
	C	0.289	2.277	2.467

Table 4.4: Performance Indices for Initial Loads (Continued)

Load Pattern	Phase	Error (%)		
		AVM	AWP	AWQ
LP6: -10~10%	A	0.685	5.143	4.782
	B	0.290	5.650	6.433
	C	0.688	4.390	6.375
LP7: -20~20%	A	0.214	11.493	10.087
	B	0.934	10.121	8.452
	C	0.879	11.644	6.097

Table 4.5: Performance Indices for Estimated Loads

Load Pattern	Phase	Error (%)		
		AVM	AWP	AWQ
LP1: 4~6%	A	0.025	0.667	0.814
	B	0.013	0.629	1.144
	C	0.017	0.977	0.629
LP2: 0~5%	A	0.043	1.455	1.850
	B	0.017	1.557	1.528
	C	0.044	1.728	1.144
LP3: 5~10%	A	0.011	1.571	1.762
	B	0.012	1.441	1.559
	C	0.016	1.325	1.241
LP4: 5~15%	A	0.069	1.504	2.576
	B	0.036	1.656	2.371
	C	0.022	1.333	2.318
LP5: -5~5%	A	0.018	2.576	2.400
	B	0.007	1.846	2.760
	C	0.014	1.586	2.042
LP6: -10~10%	A	0.077	4.159	3.699
	B	0.028	2.889	5.865
	C	0.066	5.253	4.064
LP7: -20~20%	A	0.051	8.087	9.937
	B	0.032	10.230	7.337
	C	0.049	8.244	6.619

The improvement can be evaluated by the factor of Percent Reduction in Error (PRE), which is defined in Equation (4.51). The results are listed in Table 4.6.

$$PRE = \frac{\text{Initial Error} - \text{New Error}}{\text{Initial Error}} \times 100\% \quad (4.51)$$

Table 4.6: Percent Reduction in Error - Load Estimation

Load Pattern	PRE (%)		
	AVM	AWP	AWQ
LP1	93.8	81.5	78.3
LP2	85.8	41.6	39.2
LP3	97.7	79.6	71.5
LP4	94.3	75.3	75.0
LP5	95.7	17.0	18.4
LP6	89.7	19.0	22.5
LP7	93.5	20.1	0.03

It can be observed that the voltages can be accurately estimated in all seven patterns. The estimation of real and reactive powers has the large improvement, especially for the uniform load profiles.

4.5.4 Fault Location Results

The average of absolute values of location errors of the simulation results are concluded in Table 4.7.

Table 4.7: Average of Absolute Values of Location Errors – Individual Load Pattern

Load Pattern	Core-Sheath-Ground	Core-Ground	Core-Sheath	Average
LP1	2.48% 66.2m	1.43% 35.8m	1.94% 52.7m	1.95% 51.6m
LP2	3.12% 95.7m	0.54% 13.0m	3.01% 82.6m	2.22% 63.8m
LP3	2.70% 79.8m	1.63% 41.1m	2.80% 73.9m	2.38% 64.9m
LP4	2.50% 76.7m	1.70% 42.8m	2.95% 83.3m	2.39% 67.6m
LP5	3.33% 112.7m	1.81% 45.5m	2.41% 68.4m	2.52% 75.5m
LP6	4.00% 135.1m	2.10% 50.6m	2.28% 62.9m	2.80% 82.9m
LP7	4.06% 137.4m	2.82% 66.5m	3.10% 90.9m	3.33% 98.3m
Average	3.17% 100.5m	1.72% 42.2m	2.64% 73.5m	2.51% 72.1m

The average relative error is 2.51% and the average absolute error is 72.1 meter. The generic load patterns LP5-LP7 have the relatively large error. Overall, the location errors are relatively larger than those in Section 3.10.2, but still in the acceptable range.

The distribution of absolute values of relative errors (DRE) is defined in Equation (4.52) and the results are listed in Table 4.8.

$$DRE = \frac{\text{Number of faults in a relative error range}}{\text{Total number of faults}} \times 100\% \quad (4.52)$$

Table 4.8: Distribution of Absolute Values of Relative Errors – Individual Load Pattern

Load Pattern	Fault	Relative Error Range			
		0~1%	1~2.5%	2.5~5%	5+%
LP1	CSGF	31.9	29.0	27.5	11.6
	CGF	39.1	53.6	4.4	2.9
	CSF	52.2	20.3	17.4	10.1
	Average	41.1	34.3	16.4	8.2
LP2	CSGF	23.2	30.4	21.8	24.6
	CGF	97.1	0	0	2.9
	CSF	27.6	30.4	27.5	14.5
	Average	49.3	20.3	16.4	14.0
LP3	CSGF	31.9	27.5	26.1	14.5
	CGF	39.1	31.9	27.5	1.5
	CSF	36.3	30.4	15.9	17.4
	Average	35.8	30.0	23.2	11.0
LP4	CSGF	33.3	29.0	24.7	13.0
	CGF	30.4	30.4	39.2	0
	CSF	31.9	26.1	23.2	18.8
	Average	31.9	28.5	29.0	10.6
LP5	CSGF	18.9	24.6	37.7	18.8
	CGF	34.8	23.2	42.0	0
	CSF	39.1	26.1	18.9	15.9
	Average	30.9	24.6	32.9	11.6
LP6	CSGF	5.8	36.2	26.1	31.9
	CGF	43.5	13.0	40.6	2.9
	CSF	39.1	26.1	21.8	13.0
	Average	29.5	25.1	29.5	15.9
LP7	CSGF	16.0	29.0	27.5	27.5
	CGF	37.7	18.8	29.0	14.5
	CSF	31.9	15.9	27.6	24.7
	Average	28.5	21.3	28.0	22.2
Average of All		35.3	26.3	25.0	13.4

It shows that more than 60 percent of faults can be located with the relative error less than 2.5%.

The distribution of absolute values of absolute errors (DAE) is defined in Equation (3.135) and the results are listed in Table 4.9.

Table 4.9: Distribution of Absolute Values of Absolute Errors – Individual Load Pattern

Load Pattern	Fault	Absolute Error Range			
		0~50m	50~100m	100~200m	200+m
LP1	CSGF	44.9	31.9	23.2	0
	CGF	85.5	11.6	2.9	0
	CSF	62.3	26.1	7.3	4.3
	Average	64.3	23.2	11.1	1.4
LP2	CSGF	34.8	26.1	29.0	10.1
	CGF	97.1	0	2.9	0
	CSF	40.6	30.4	24.6	43.4
	Average	57.5	18.9	18.8	4.8
LP3	CSGF	39.1	37.7	14.5	8.7
	CGF	55.1	42.0	2.9	0
	CSF	52.2	21.7	17.4	8.7
	Average	48.8	33.8	11.6	5.8
LP4	CSGF	44.9	29.0	23.2	2.9
	CGF	50.7	47.8	1.5	0
	CSF	42.0	24.6	26.1	7.3
	Average	45.9	33.8	16.9	3.4
LP5	CSGF	31.9	23.2	29.0	15.9
	CGF	52.2	47.8	0	0
	CSF	55.1	17.4	21.7	5.8
	Average	46.4	29.5	16.9	7.2
LP6	CSGF	26.1	21.7	27.6	24.6
	CGF	44.9	52.2	0	2.9
	CSF	50.7	29.0	17.4	2.9
	Average	40.6	34.3	15.0	10.1
LP7	CSGF	24.7	21.7	30.4	23.2
	CGF	47.8	34.8	14.5	2.9
	CSF	37.7	23.2	30.4	8.7
	Average	36.7	26.6	25.1	11.6
Average of All		48.6	28.6	16.5	6.3

It shows that 77.2 percent of faults can be located with the absolute error less than 100 m.

The effects of cable length, faulty section, load profile, fault distance and fault type on the location accuracy will be discussed in the following subsections.

4.5.4.1 Effect of Cable Length

The effect of cable length is examined in this subsection. The first scenario includes the following conditions and the location errors are shown in Figure 4.28.

- Cable length: All 23 three-phase feeders, ranging from 2-11.43 km.
- Load Profile: (1) LP5; (2) LP6.
- Fault distance: 25%.
- Fault type: CSGF.

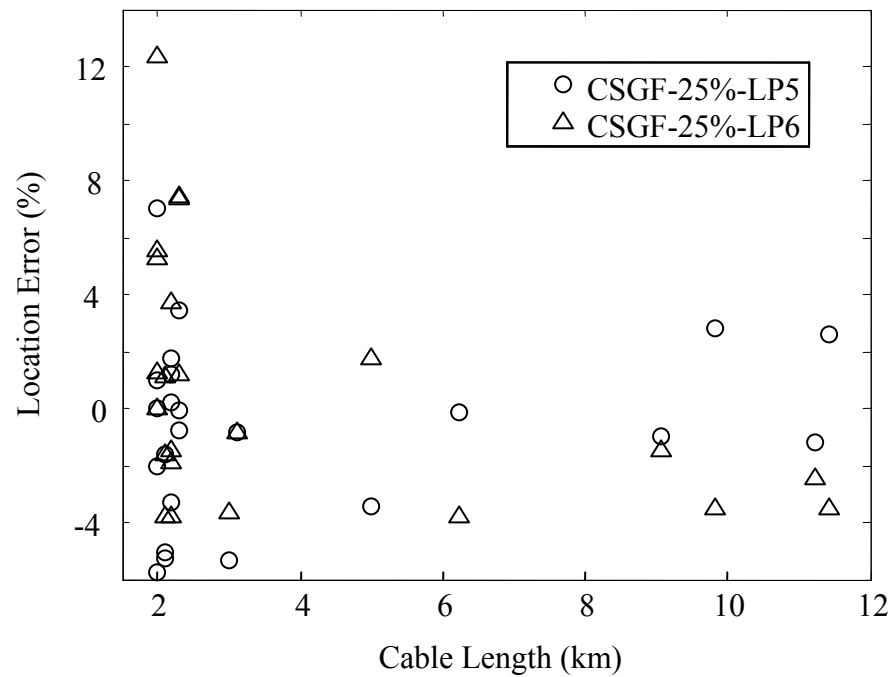


Figure 4.28: Effect of cable length (CSGF @25%).

The second scenario includes the following conditions and the location errors are shown in Figure 4.29.

- Cable length: All 23 three-phase feeders, ranging from 2-11.43 km.
- Load Profile: (1) LP5; (2) LP6.
- Fault distance: 50%.
- Fault type: CSF.

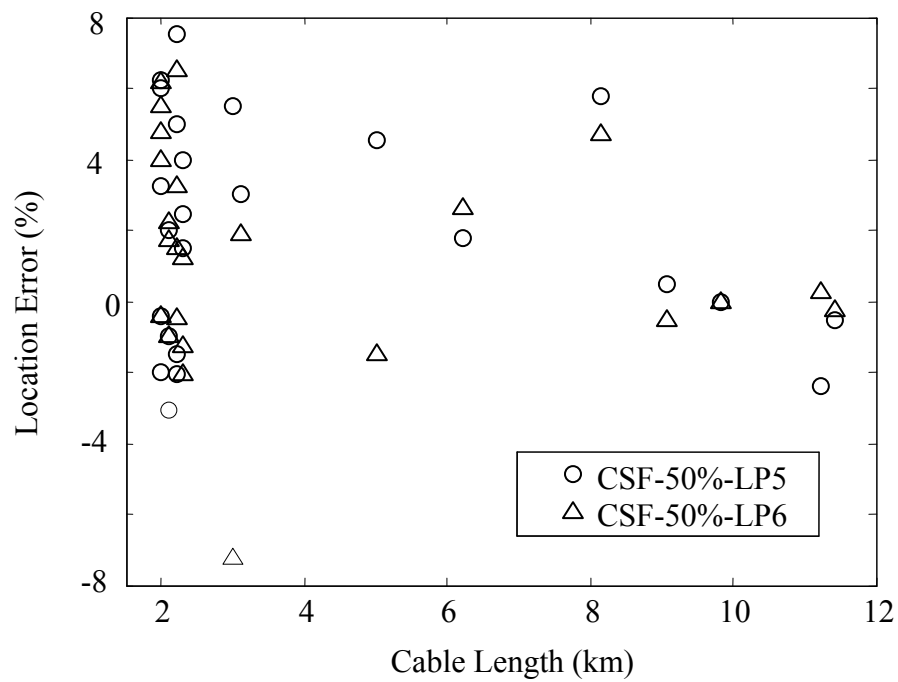


Figure 4.29: Effect of cable length (CSF @50%).

The third scenario includes the following conditions and the location errors are shown in Figure 4.30.

- Cable length: All 23 three-phase feeders, ranging from 2-11.43 km.
- Load Profile: (1) LP5; (2) LP6.

- Fault distance: 75%.
- Fault type: CGF.

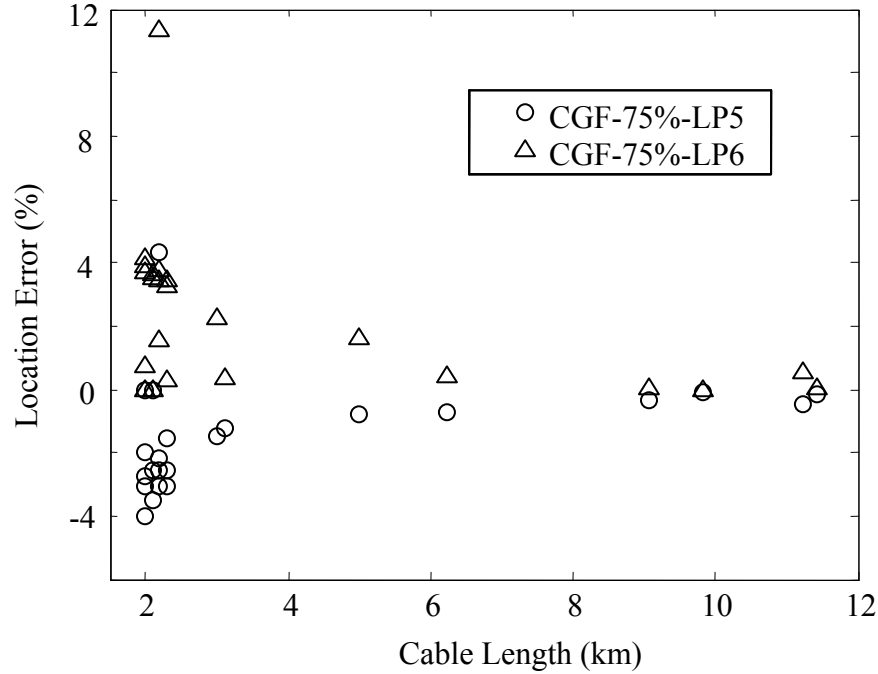


Figure 4.30: Effect of cable length (CGF @75%).

Although some relatively larger errors occur for faults on the shorter cables, as show in Figure 4.28-Figure 4.30, it cannot be concluded that the shorter cable is more likely to have the larger location error. This phenomenon is not solely caused by the variation of cable length, which will be discussed in the next subsection. Basically, the cable length itself has no effect on the location accuracy.

4.5.4.2 Effect of Faulty Section

The effect of the distance between the substation and the middle point of a cable section is investigated in this subsection. The first scenario includes the following conditions and the location errors are shown in Figure 4.31.

- Faulty section: Distance from middle point of 23 three-phase feeders to the substation, ranging from 1-73.176 km.
- Load Profile: LP4.
- Fault distance: 25%.
- Fault type: CSGF.

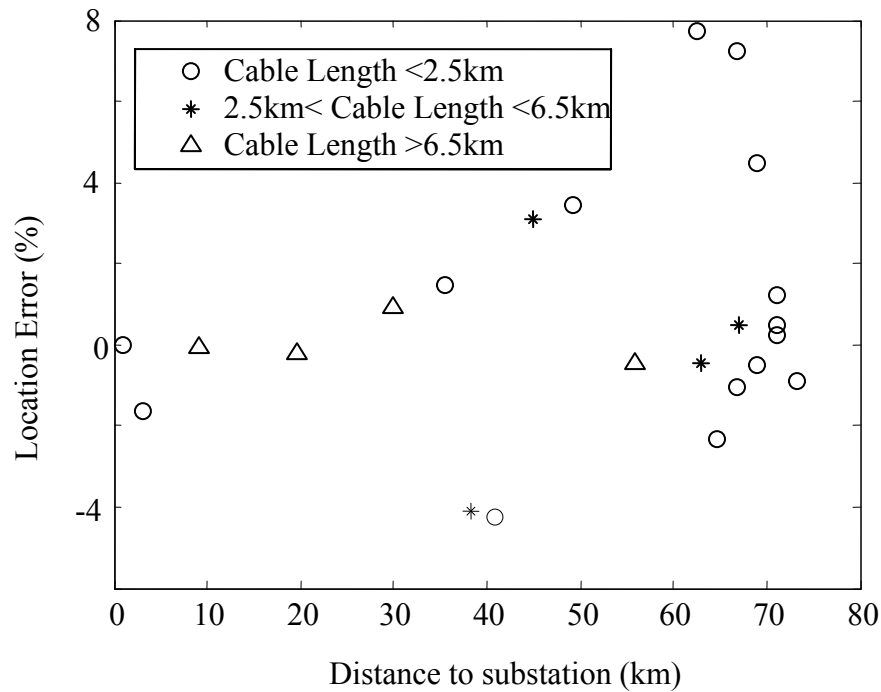


Figure 4.31: Effect of faulty section (CSGF @25%).

The second scenario includes the following conditions and the location errors are shown in Figure 4.32.

- Faulty section: Distance from middle point of 23 three-phase feeders to the substation, ranging from 1-73.176 km.
- Load Profile: LP4.

- Fault distance: 50%.
- Fault type: CSF.

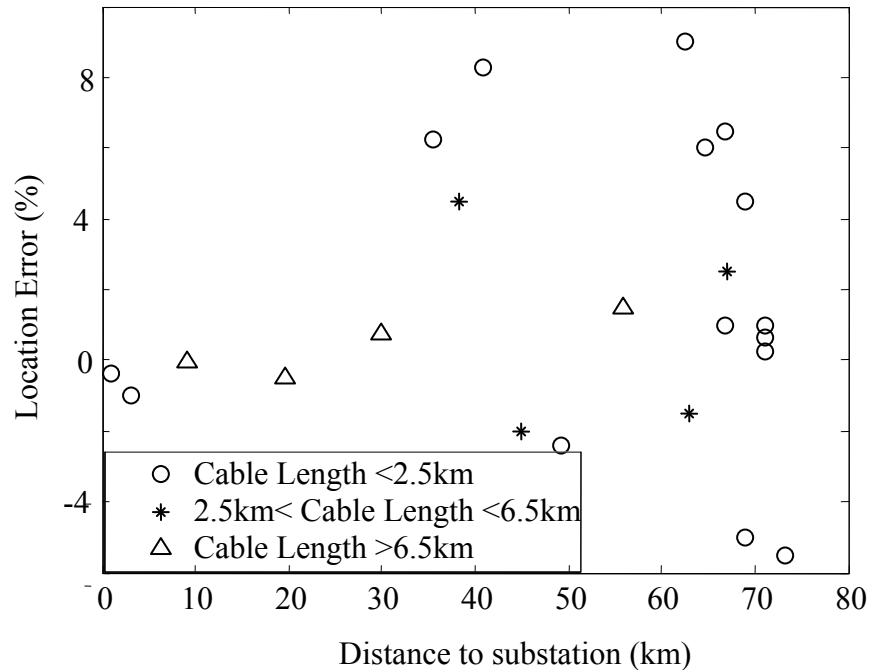


Figure 4.32: Effect of faulty section (CSF @50%).

The third scenario includes the following conditions and the location errors are shown in Figure 4.33.

- Faulty section: Distance from middle point of 23 three-phase feeders to the substation, ranging from 1-73.176 km.
- Load Profile: LP4.
- Fault distance: 75%.
- Fault type: CGF.

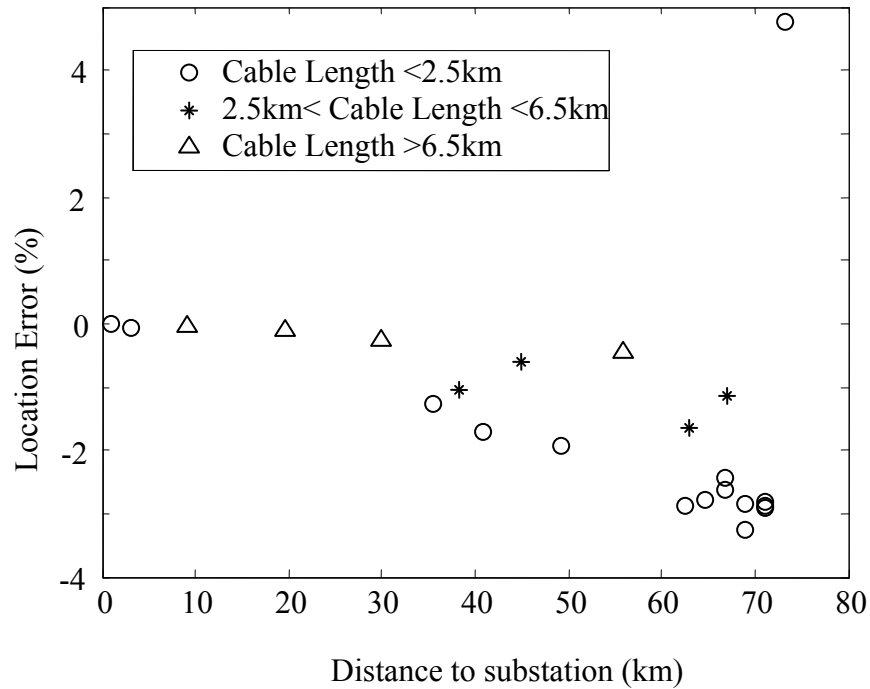


Figure 4.33: Effect of faulty section (CGF @75%).

It can be observed that the largest errors occur at cables with the short length and long distance to substation. However, this phenomenon cannot be concluded for all cables with the short length and long distance to substation. Otherwise, the distance from the faulty section to substation has no effect on the location accuracy.

4.5.4.3 Effect of Load Profile

The effect of load profile is investigated in this subsection. The first scenario includes the following conditions and the location errors are shown in Figure 4.34.

- Cable: All 23 three-phase cables.
- Load Profile: (1) LP5; (2) LP6; (3) LP7.
- Fault distance: 50%.
- Fault type: CSGF.

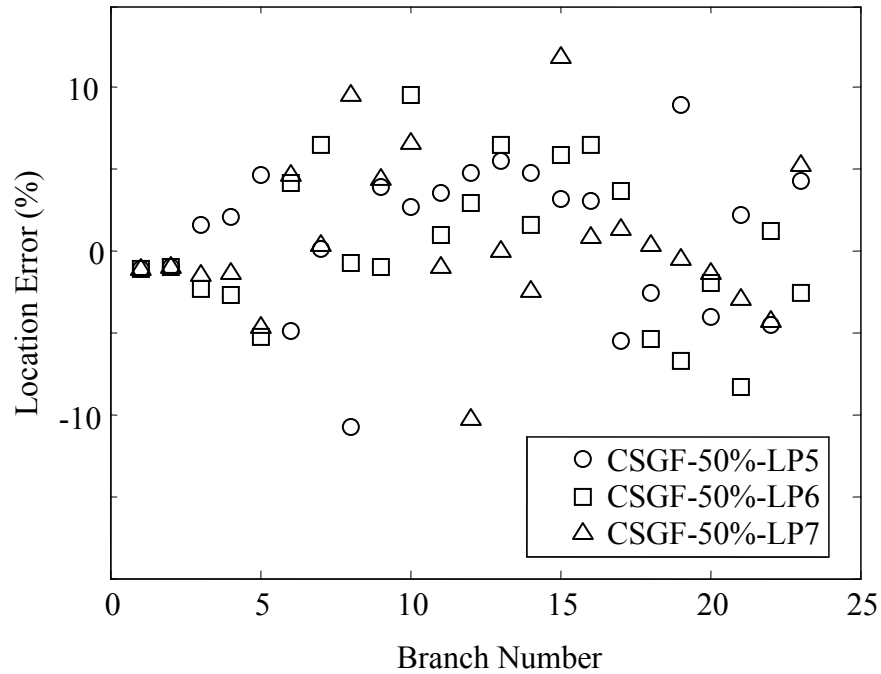


Figure 4.34: Effect of load profile (CSGF@50%, Generic profile).

The second scenario includes the following conditions and the location errors are shown in Figure 4.35.

- Cable: All 23 three-phase cables.
- Load Profile: (1) LP2; (2) LP3; (3) LP4.
- Fault distance: 50%.
- Fault type: CSGF.

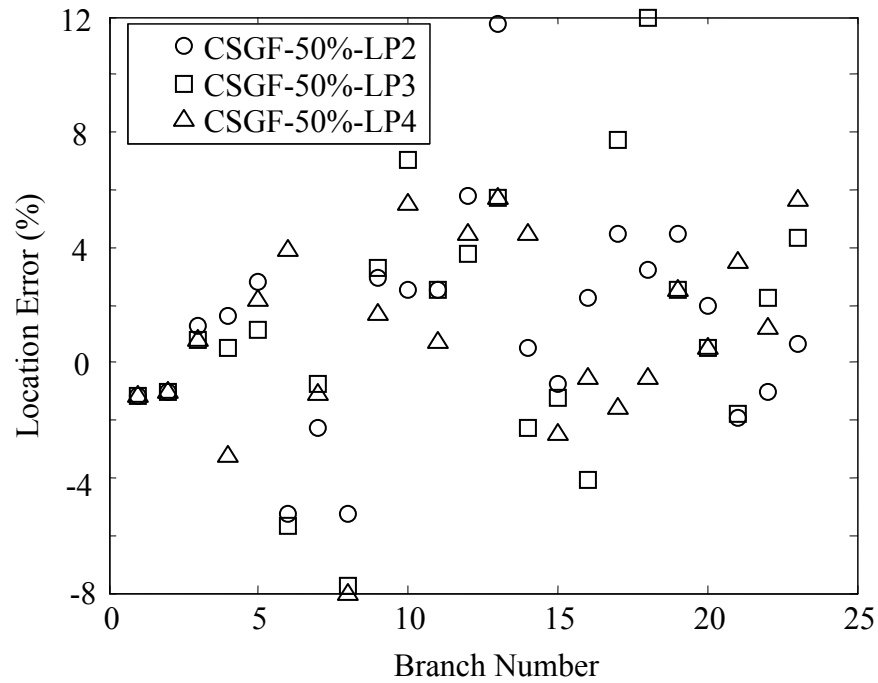


Figure 4.35: Effect of load profile (CSGF@50%, Uniform profile).

The third scenario includes the following conditions and the location errors are shown in Figure 4.36.

- Cable: All 23 three-phase cables.
- Load Profile: (1) LP5; (2) LP6; (3) LP7.
- Fault distance: 50%.
- Fault type: CGF.

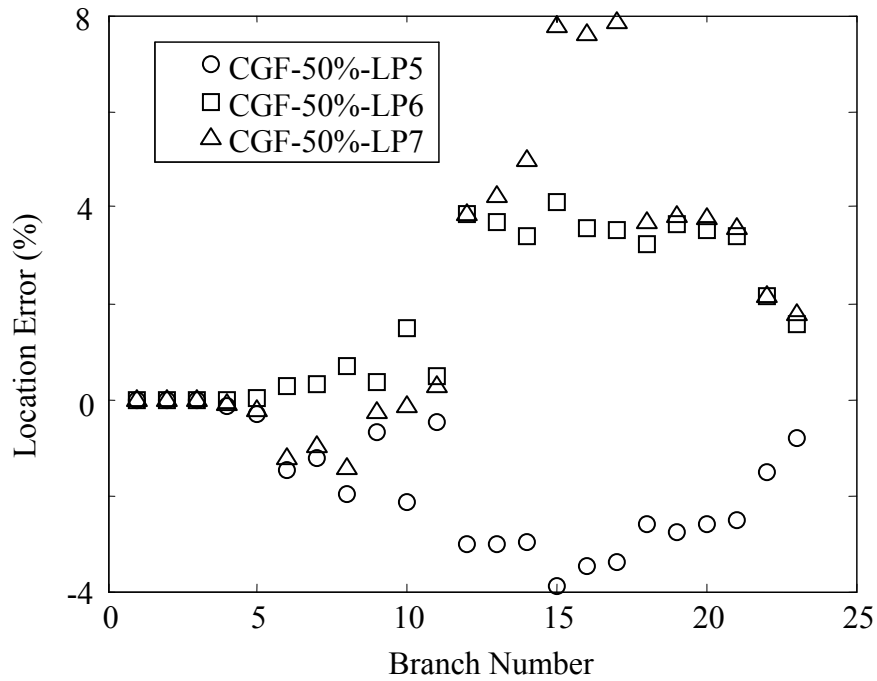


Figure 4.36: Effect of load profile (CGF@50%, Generic profile).

The fourth scenario includes the following conditions and the location errors are shown in Figure 4.37.

- Cable: All 23 three-phase cables.
- Load Profile: (1) LP2; (2) LP3; (3) LP4.
- Fault distance: 50%.
- Fault type: CGF.

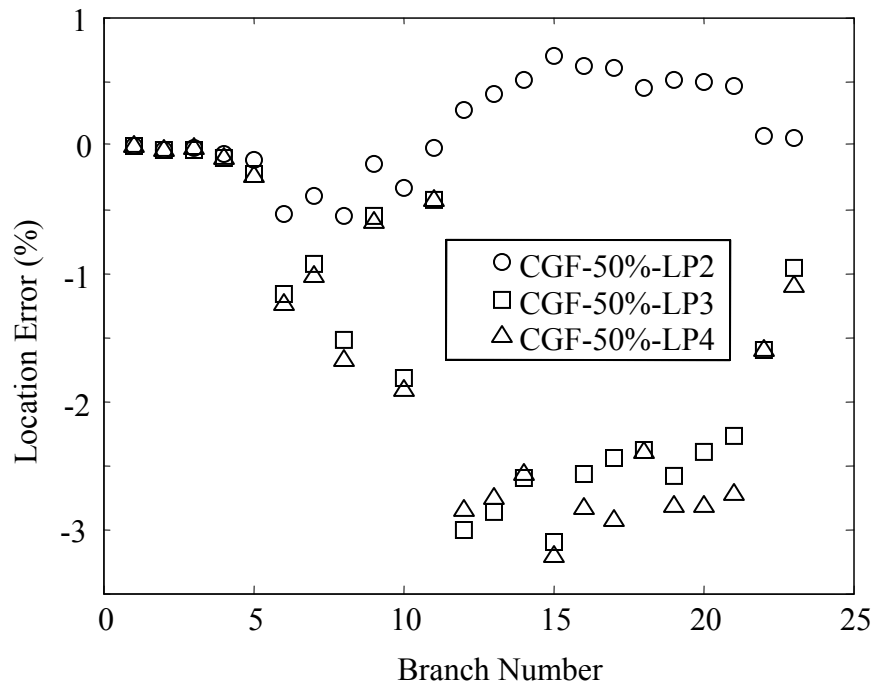


Figure 4.37: Effect of load profile (CGF@50%, Uniform profile).

Comparing the results obtained from the uniform load profiles and generic load profiles in Figure 4.34-Figure 4.37, it cannot be clearly concluded which one would result in the larger location error. However, the average data in Table 4.7 demonstrate the generic profile would lead to the relatively higher location error.

4.5.4.4 Effect of Fault Distance

The effect of fault distance is investigated in this subsection. The first scenario includes the following conditions and the location errors are shown in Figure 4.38.

- Cable: All 23 three-phase cables.
- Load Profile: LP1.
- Fault distance: (1) 25%; (2) 50%; (3) 75%.
- Fault type: CSGF.

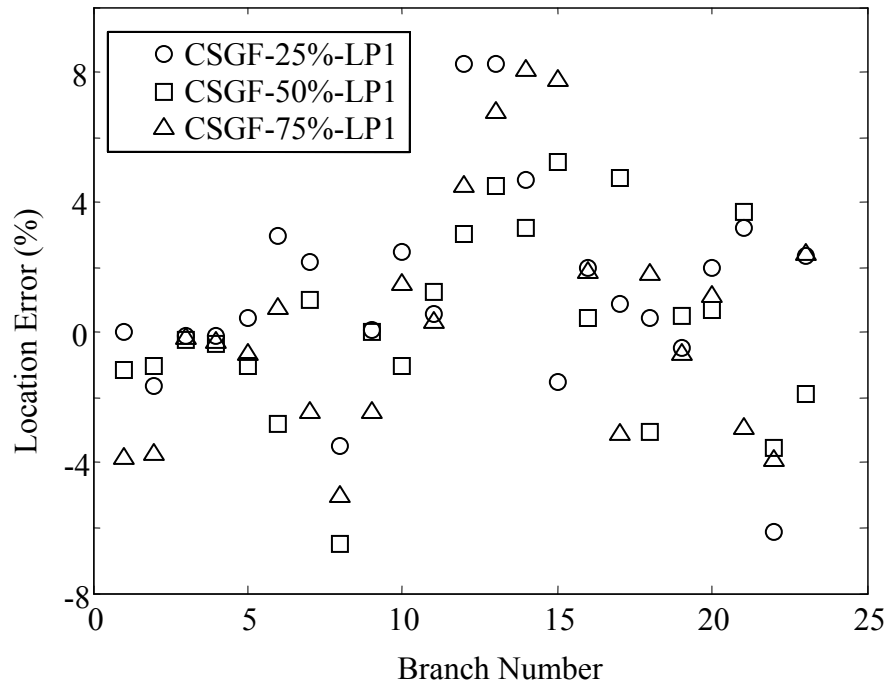


Figure 4.38: Effect of fault distance (CSGF, LP1).

The second scenario includes the following conditions and the location errors are shown in Figure 4.39.

- Cable: All 23 three-phase cables.
- Load Profile: LP1.
- Fault distance: (1) 25%; (2) 50%; (3) 75%.
- Fault type: CSF.

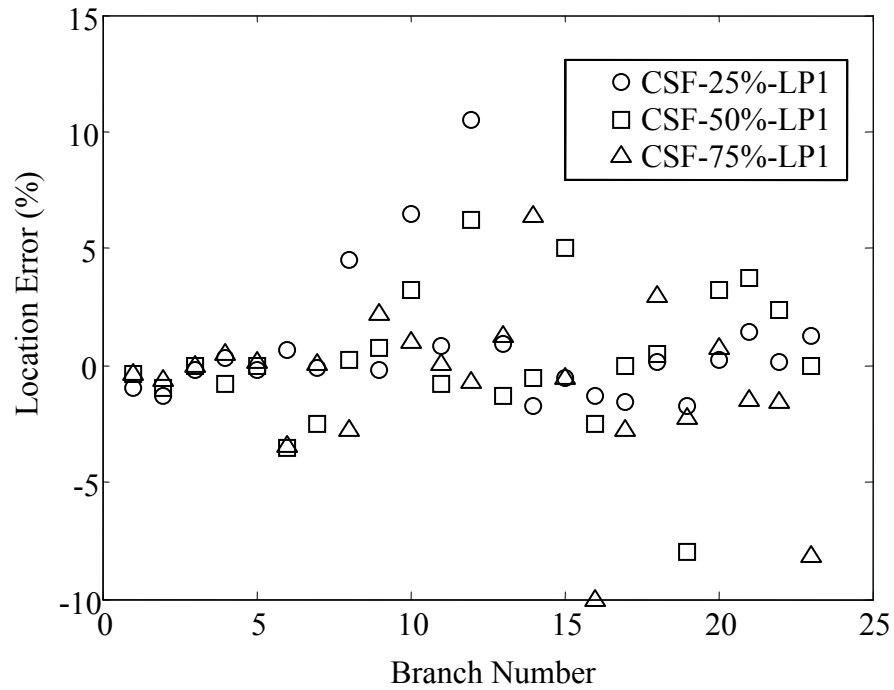


Figure 4.39: Effect of fault distance (CSF, LP1).

The third scenario includes the following conditions and the location errors are shown in Figure 4.40.

- Cable: All 23 three-phase cables.
- Load Profile: LP1.
- Fault distance: (1) 25%; (2) 50%; (3) 75%.
- Fault type: CGF.

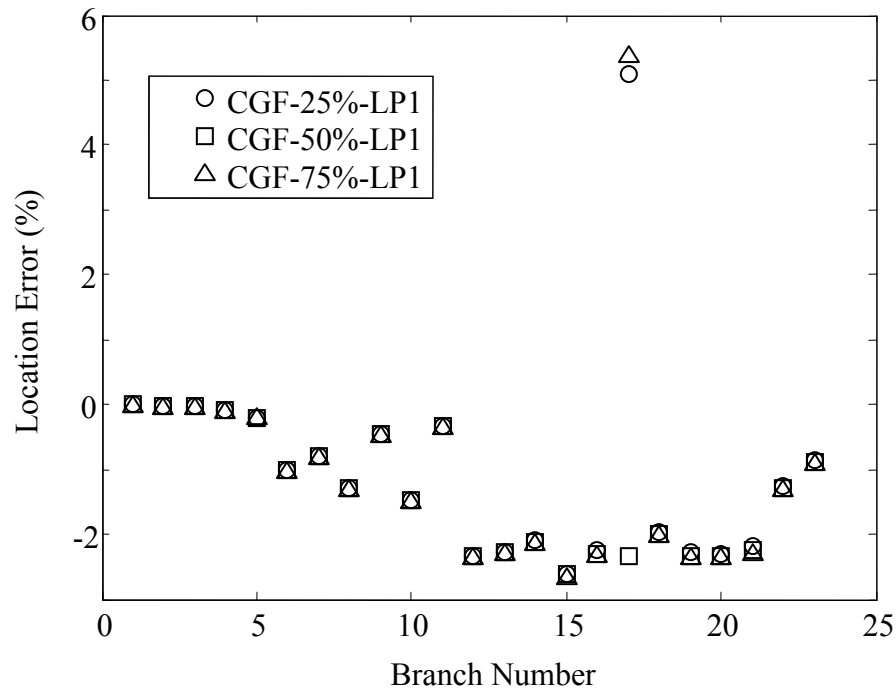


Figure 4.40: Effect of fault distance (CGF, LP1).

The location errors in Figure 4.38-Figure 4.40 are distributed randomly. Therefore, the fault distance has no effect on the location accuracy. Based on the analysis in Section 3.10.2.3, the error increase may be observed in close-in and far-end faults.

4.5.4.5 Effect of Fault Type

The effect of fault type is investigated in this subsection. The first scenario includes the following conditions and the location errors are shown in Figure 4.41.

- Cable: All 23 three-phase cables.
- Load Profile: LP2.
- Fault distance: 25%.
- Fault type: (1) CSGF; (2) CSF; (3) CGF.

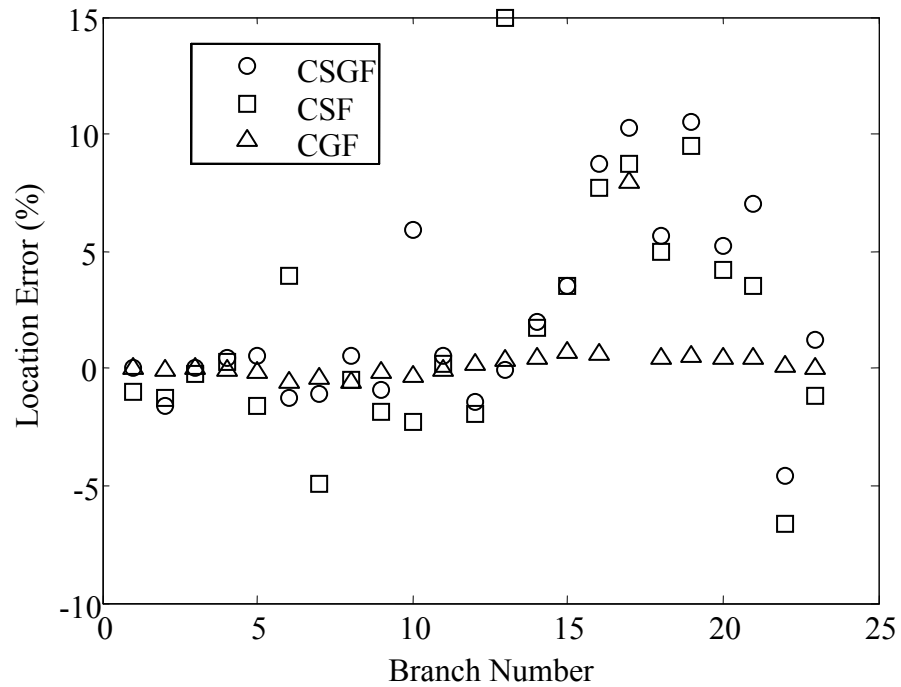


Figure 4.41: Effect of fault type (25%, LP2).

The second scenario includes the following conditions and the location errors are shown in Figure 4.42.

- Cable: All 23 three-phase cables.
- Load Profile: LP4.
- Fault distance: 50%.
- Fault type: (1) CSGF; (2) CSF; (3) CGF.

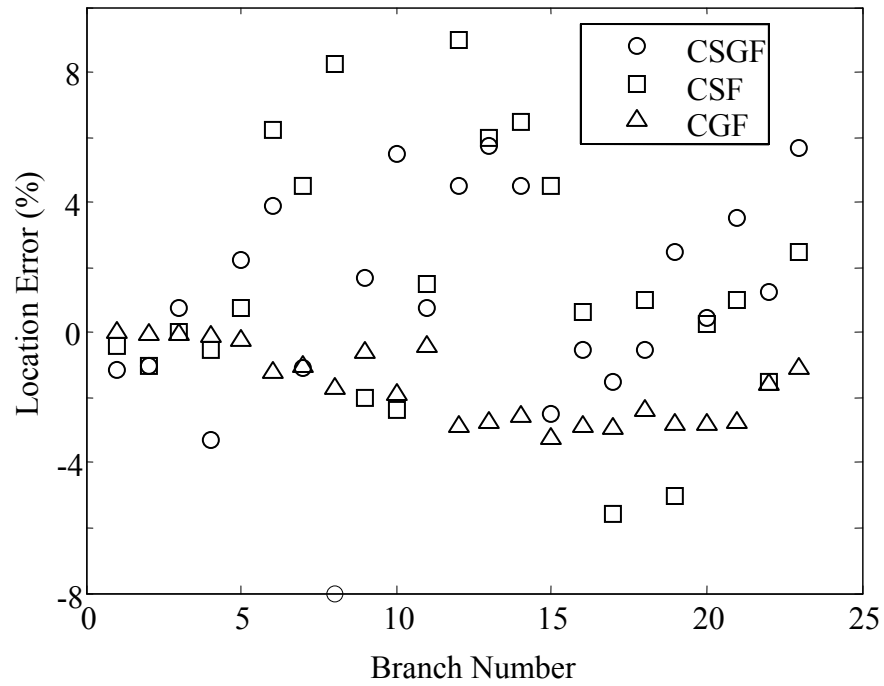


Figure 4.42: Effect of fault type (50%, LP4).

The third scenario includes the following conditions and the location errors are shown in Figure 4.43.

- Cable: All 23 three-phase cables.
- Load Profile: LP6.
- Fault distance: 75%.
- Fault type: (1) CSGF; (2) CSF; (3) CGF.

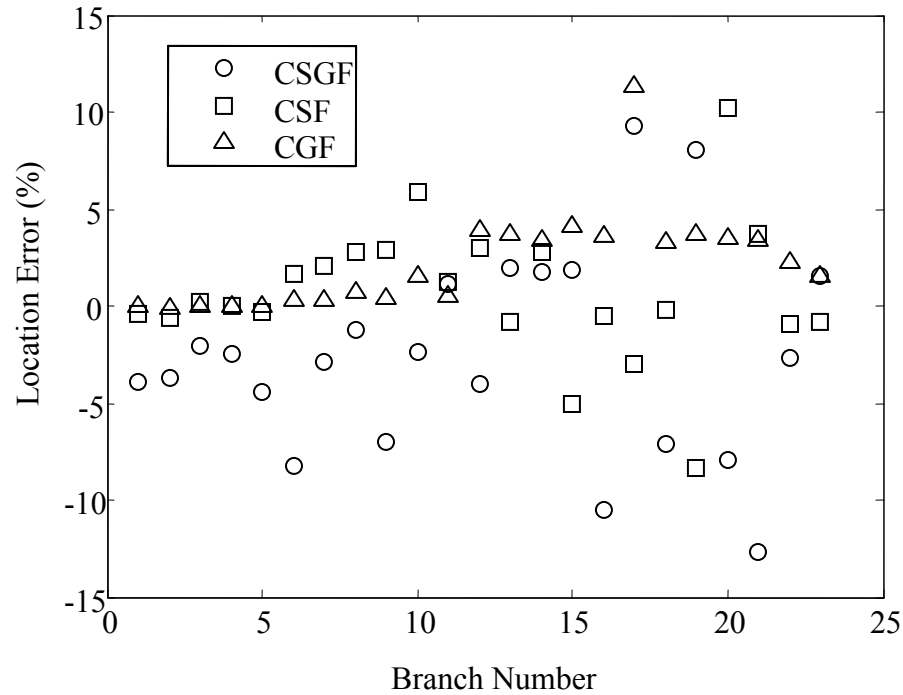


Figure 4.43: Effect of fault type (75%, LP6).

It is apparent that the CGF has the smallest errors, and the CSGF and CSF have the relatively large errors.

4.5.4.6 Summary of Effects

The following conclusion can be summarized from the above analysis:

- The large error may occur at cables with the short length and long distance to substation. Otherwise, the cable length and distance from the faulty section to substation have no effect on the location accuracy.
- The generic load profile would lead to the larger error than the uniform load profile.
- The fault distance has no effect on the location accuracy.
- The CGF has the smaller error than CSGF and CSF.

4.5.4.7 More Accurate Results

The above simulation results are based on one certain load profile individually. However, there may have several load profiles available for the state estimation and the most suitable one cannot be readily decided. Therefore, several available load profiles can be processed for the state estimation and fault location. The final results can be calculated by averaging.

Three groups are simulated, in which five load profiles are randomly selected from the seven load patterns. The average of absolute values of location errors of each group are concluded in Table 4.10.

Table 4.10: Average of Absolute Values of Location Errors – Combination of Load Patterns

Load Patterns	Core-Sheath-Ground	Core-Ground	Core-Sheath	Average
LP2, 4, 5, 6,7	2.02% 59.5m	0.63% 16.3m	1.65% 45.4m	1.43% 40.4m
LP2, 3, 4, 5, 6	1.94% 58.3m	1.14% 28.9m	1.4% 38.1m	1.49% 41.8m
LP1, 2, 3, 6, 7	2.08% 62.2m	0.68% 17.0m	1.37% 36.7m	1.38% 38.6m

The percent reduction in error is used to evaluate the improvement in location errors, as shown in Table 4.11. It can be found that, in average, both relative and absolute errors are reduced by more than 40%.

Table 4.11: Percent Reduction in Error – Combination of Load Patterns

Load Patterns	Error Type	Core-Sheath-Ground	Core-Ground	Core-Sheath	Average
LP2, 4, 5, 6,7	Relative	36.3	63.4	37.5	43.0
	Absolute	40.8	61.4	38.2	44.0
LP2, 3, 4, 5, 6	Relative	38.8	33.7	47.0	40.6
	Absolute	42.0	31.5	48.2	42.0
LP1, 2, 3, 6, 7	Relative	34.4	60.5	48.1	45.0
	Absolute	38.1	59.7	50.1	46.5

The distribution of absolute values of relative errors is tabulated in Table 4.12. It can be observed that more than 80% faults can be located with the relative error less than 2.5%, increasing from 61.6% using the individual load pattern.

Table 4.12: Distribution of Absolute Values of Relative Errors – Combination of Load Patterns

Load Pattern	Fault	Relative Error Range			
		0~1%	1~2.5%	2.5~5%	5+%
LP2, 4, 5, 6,7	CSGF	36.2	31.9	24.6	7.3
	CGF	89.9	7.3	0	2.9
	CSF	43.5	31.9	20.3	4.3
	Average	56.5	23.7	15.0	4.8
LP2, 3, 4, 5, 6	CSGF	39.1	34.8	17.4	8.7
	CGF	42.0	55.1	0	2.9
	CSF	56.5	27.5	10.2	5.8
	Average	45.9	39.1	9.2	5.8
LP1, 2, 3, 6, 7	CSGF	30.4	31.9	33.3	4.4
	CGF	92.8	4.3	0	2.9
	CSF	52.2	29.0	17.4	1.4
	Average	58.5	21.7	16.9	2.9

The distribution of absolute values of absolute errors is tabulated in Table 4.13. It is clear that more than 88% faults can be located with the absolute error less than 100 m, increasing from 77.2% using the individual load pattern.

Table 4.13: Distribution of Absolute Values of Absolute Errors – Combination of Load Patterns

Load Pattern	Fault	Absolute Error Range			
		0~50m	50~100m	100~200m	200+m
LP2, 4, 5, 6,7	CSGF	52.2	24.6	23.2	0
	CGF	97.1	0	2.9	0
	CSF	59.4	31.9	8.7	0
	Average	69.6	18.8	11.6	0
LP2, 3, 4, 5, 6	CSGF	59.4	20.3	18.8	1.5
	CGF	97.1	0	2.9	0
	CSF	73.9	17.4	8.7	0
	Average	76.8	12.6	10.1	0.5
LP1, 2, 3, 6, 7	CSGF	44.9	39.1	14.5	1.5
	CGF	97.1	0	2.9	0
	CSF	69.6	27.5	2.9	0
	Average	70.5	22.2	6.8	0.5

It should be noted that the application of the combination of load patterns would increase the computation time. This problem can be resolved by using two or more multi-core computers to process the algorithms in parallel.

Chapter 5

5 Conclusions and Future Works

Three schemes have been developed in this thesis, i.e. incipient fault detection for distribution cables based on the wavelet analysis and superimposed components, fault location for distribution cables based on the direct circuit analysis, and state estimation for underground distribution networks based on the sequential quadratic programming technique. Then, the proposed fault location algorithm and state estimation method have been applied together to locate faults in underground distribution networks.

5.1 Conclusions

Based on the methodology of wavelet transform and analysis of superimposed components, two schemes have been proposed to detect and classify the incipient faults in underground distribution cables. The following design goals have been achieved for the schemes.

- Easy implementation in the existing digital relays;
- High detection and classification accuracy;
- Low rate of missing detection, false alarm, and incorrect classification;
- Insensitive to fault type, fault location, fault resistance, and fault inception angle
- Less dead zone;
- Robust to noise, disturbance, and uncertainties;
- Configurable for different CT locations;
- Configurable for different transformer windings;
- Capable to detect and classify in real time.

The wavelet-based scheme has the following advantages in terms of the accuracy, detectability, and identifiability.

- Achieving higher detection accuracy, especially for high impedance incipient faults;
- Supervising almost entire length of cable, i.e., less detection dead zone;
- Detecting and classifying the different fault types;
- Detecting and classifying the other transients, such as cold load pickup and capacitor switching;
- Eliminating noise from signals.

The superimposed components-based scheme is particularly designed to detect SLG incipient faults. In other respects, this method has the following advantages in terms of the configuration and simplicity.

- Performing simple and less computation;
- Setting fewer thresholds;
- Implementing by easily upgrading firmware.

The wavelet-based scheme can obtain the low rate of missing detection and zero rate of false alarm in the presence of the various noise levels, fault conditions, transient types and system configurations. The superimposed components-based scheme is capable of achieving the zero rates of false alarm and misclassification. The advantages of both schemes indicate a technical feasibility for practical implementations.

Based on the direct circuit analysis of a two-layer π cable model, a set of fault location algorithms have been proposed to locate the single phase-related permanent faults in underground cables. The main characteristics of the location algorithms are concluded as follows.

- A two-layer π cable model has been formulated to approximate the behaviors and characteristics of cables and used to develop the location algorithms.
- The various cable characteristics have been taken into account, such as the shunt capacitance, metallic sheaths, heterogeneity and untransposition.
- A set of location algorithms have been developed to cover five bonding methods and three fault scenarios.
- A large number of complex equations in the location algorithms have been solved effectively and efficiently.
- Only fundamental voltage and current phasors measured at substation have been utilized.
- The estimation of load impedance has been proposed and the application of the static response type load model has been investigated.
- The location algorithms are capable to calculate fault resistance.
- The location algorithms are capable to determine fault type.
- The high location accuracy has been achieved.
- The location algorithms are insensitive to fault resistance.
- Basically, the location algorithms are insensitive to fault distance except that there has an error increase for faults closed to the close-in, far-end and crossing points, which is caused by the model and setting in the simulation software.
- There may have relatively large error for CSGF or CSF with SPBR or SPBM, otherwise, the bonding methods and fault scenarios have no effect on the location accuracy.
- The location algorithms are capable to locate in real time.

The state estimation for underground distribution networks has been formulated as a nonlinear optimization problem and solved by the sequential quadratic programming method. The proposed location algorithm incorporating with the proposed state estimation algorithm has the following characteristics.

- The state estimation for underground distribution networks has been formulated as a nonlinear optimization problem and solved by the SQP method.
- The shunt capacitance, effect of metallic sheath and bonding method have been taken into account for the development of the state estimation method.
- The laterals and tapped loads have been taken into account.
- A section-by-section estimation algorithm combined with the backward/forward sweep algorithm has been proposed to estimate the nodal voltage and branch current for each line section. Six sub-algorithms have been applied in the estimation algorithm.
- Only fundamental voltage and current phasors measured at substation have been utilized.
- The state estimation algorithm can accurately estimate the nodal voltages. The estimation accuracy of load flows is acceptable.
- The estimation of the seen impedance behind the faulty section has been discussed and the application of the static response type load model has been investigated.
- The state estimation algorithm can provide necessary information for the location algorithms.
- The faulty section can be determined.
- The location accuracy is acceptable.

- Basically , the location of the faulty section and the cable length have no effect on the location accuracy, however, faults in cables with short length and long distance to substation may have relatively large error.
- The generic patterns would lead to the relatively higher location error than the uniform load patterns.
- The fault distance has no effect on the location accuracy.
- The CGF has the smaller error than CSGF and CSF.
- A revised scheme has been proposed to increase the location accuracy.

5.2 Future Works

Nowadays, the fault location and state estimation for underground distribution networks are very challenging. This work may help in some degree to encourage further analytical and practical studies in the fields of fault location and state estimation for real underground distribution systems. The possibly interesting future works include,

- Formulation of a simple cable model or development of a modified transformation matrix. The cable model used in this work can accurately present the characteristics and behaviors of cables; however, its complexity limits the possible simplicity of the fault location algorithms.
- Online estimation of cable parameters. The cable parameters, especially the capacitance, may have a quite large change over age. An online estimation method using single end measurements can provide more accurate parameters for location algorithms and in turn improve the location accuracy.
- Application of the state estimation algorithm in large-scale networks. The proposed state estimation algorithm has been examined in a 31-node radial distribution system with one measurement point; however, the application in the large-scale system would result in the longer computation time and possibly larger estimation error.

Therefore, the state estimation algorithm should be modified by adapting more measurements and/or dividing the large system into small zones.

- Location of incipient faults. The permanent fault in cables would be averted if the incipient fault was located, which is significantly important for utility companies to have sufficient time to diagnosis the defective cable in advance. Considering the short duration of faults, the method using sample values would be one possible solution.

References

- [1] S. M. Miri, and A. Privette, "A survey of incipient fault detection and location techniques for extruded shielded power cables," in *Proc. the 26th Southeastern Symposium on System Theory*, pp. 402-405, March 20-22, 1994.
- [2] W. Charytoniuk, W. Lee, M. Chen, J. Cultrera, and T. Maffetone, "Arcing fault detection in underground distribution networks-feasibility study," *IEEE Trans. Industry Applications*, vol. 36, no. 6, pp. 1756-1761, 2000.
- [3] N. T. Stringer, L. A. Kojovic, "Prevention of underground cable splice failures," *IEEE Trans. Industry Applications*, vol. 37, no. 1, pp. 230-239, 2001.
- [4] T. T. Newton and L. Kojovic, "Detection of sub-cycle, self-clearing faults," U.S. Patent 6 198 401, Feb. 12, 1999.
- [5] B. Kasztenny, I. Voloh, C. G. Jones, and G. Baroudi, "Detection of incipient faults in underground medium voltage cables," in *Proc. 61st Annual Conference for Protective Relay Engineers*, pp. 349-366, April 1-3, 2008.
- [6] A. Edwards, H. Kang, and S. Subramanian, "Improved algorithm for detection of self-clearing transient cable faults," in *Proc. IET 9th International Conference on Developments in Power System Protection*, pp. 204-207, March 17-20, 2008.
- [7] K. L. Butler-Purry and J. Cardoso, "Characterization of underground cable incipient behavior using time-frequency multi-resolution analysis and artificial neural networks," in *Proc. Power and Energy Society General Meeting - Conversion and Delivery of Electrical Energy in the 21st Century*, pp. 1-11, July 20-24, 2008.
- [8] M. J. Mousavi, K. L. Butler-Purry, R. Gutierrez-Osuna, and M. Najafi, "Classification of load change transients and incipient abnormalities in underground cable using pattern analysis techniques," in *Proc. IEEE Power Engineering Society Transmission and Distribution Conference and Exposition*, pp. 175-180, Sept. 17-22, 2003.
- [9] "Underground cable fault location reference manual," Electric Power Research Institute, TR-105502, Nov. 1995.
- [10] E. C. Bascom III, D. W. Von Dollen, and H. W. Ng, "Computerized underground cable fault location expertise," in *Proc. IEEE Power Engineering Society Transmission and Distribution Conference*, pp. 376-382, Apr. 10-15, 1994.
- [11] K. K. Kuan and K. Warwick, "Real-time expert system for fault location on high voltage underground distribution cables," *IEE Proceedings C: Generation, Transmission and Distribution*, vol. 139, no. 3, pp. 235-240, May 1992.
- [12] H. Diaz and M. López, "Fault location techniques for electrical distribution networks: a literature survey," in *Proc. the Fifth IASTED International Conference*, pp. 311-318, June 15-17, 2005.

- [13] K. Zimmerman, and D. Costello, "Impedance-based fault location experience," in *Proc. Rural Electric Power Conference*, pp. 1-16, Feb. 18, 2005.
- [14] E. O. Schweitzer III, "A review of impedance-based fault locating experience," in *Proc. the Fourteen Annual Iowa-Nebraska System Protection Seminar*, pp. 1-31, Oct. 16, 1990.
- [15] A. D. Filomena, M. Resener, R. H. Salim, and A. S. Bretas, "Fault location for underground distribution feeders: An extended impedance-based formulation with capacitive current compensation," *Electrical Power and Energy Systems (31)*, pp. 489-496, 2009.
- [16] M. M. Saha, F. Provoost, and E. Rosolowski, "Fault location method for MV cable network," in *Proc. the Seventh International Conference on Developments in Power System Protection*, pp. 323-326, Apr. 9-12, 2001.
- [17] T. A. Kawady, A. I. Taalab, and M. El-Sad, "An accurate fault locator for underground distribution networks using modified apparent-impedance calculation," in *Proc. the tenth IET International Conference on Developments in Power System Protection*, pp. 1-5, Mar. 29-Apr. 1, 2010.
- [18] S. Jamali and V. Talavat, "Fault location method for distribution networks using 37-buses distributed parameter line model," in *Proc. the Eighth IEE International Conference on Developments in Power System Protection*, pp. 216-219, Apr. 5-8, 2004.
- [19] T. Takagi, Y. Yamakoshi, M. Yamaura, R. Kondou, and T. Matsushima, "Development of a new type fault locator using the one-terminal voltage and current data," *IEEE Trans. Power Apparatus and Systems*, vol. PAS-101, no. 8, pp. 2892-2898, Aug. 1982.
- [20] X. Yang, M. S. Choi, S. J. Lee, C. W. Ten, and S. I. Lim, "Fault location for underground power cable using distributed parameter approach," *IEEE Trans. Power System*, vol. 23, no. 4, pp. 1809-1816, Nov. 2008.
- [21] M. M. A. Aziz, E. S. T. El Din, D. K.L Ibrahim, and M. Gilany, "A phasor-based double ended fault location scheme for aged power cables," *Electric Power Components and Systems*, vol. 34, pp. 417-432, 2006.
- [22] D. D. Sabin, C. Dimitriu, D. Santiago, and G. Baroudi, "Overview of an automatic underground distribution fault location system," in *Proc. IEEE Power & Energy Society General Meeting*, pp. 1-5, July 26-30, 2009.
- [23] F. Provoost and W. Van Buijtenen, "Practical experience with fault location in MV cable networks," in *Proc. 20th International Conference on Electricity Distribution*, Paper no. 0527, June 8-11, 2009.
- [24] P. M. Van Oirsouw and F. Provoost, "Fault localization in an MV distribution network," in *Proc. 17th International Conference on Electricity Distribution*, pp. 2-6, May 12-15, 2003.
- [25] L. V. Bewley, "Traveling waves on transmission systems," *Trans. of the American Institute of Electrical Engineers*, vol. 50, no. 2, pp. 532-550, 1931.

- [26] P. F. Gale, P. A. Crossley, B. Xu, Y. Ge, B. J. Cory, and J. R. G. Barker, "Fault location based on travelling waves," in *Proc. Fifth International Conference on Developments in Power System Protection*, pp. 54-59, Mar. 30-Apr. 1, 1993.
- [27] Z. Q. Bo, R. K. Aggarwal, A. T. Johns, and P. J. Moore, "Accurate fault location and protection scheme for power cable using fault generated high frequency voltage transients," in *Proc. the Eight Mediterranean Electro-technical Conference, Industrial Applications in Power Systems*, pp. 777-780, May 1996.
- [28] Z. Chen, Z. Q. Bo, F. Jiang, X. Z. Dong, G. Weller, and N. F. Chin, "Wavelet transform based accurate fault location and protection technique for cable circuits," in *Proc. International Conference on Advances in Power System Control, Operation and Management*, pp. 59-63, Oct. 30-Nov. 1, 2000.
- [29] W. Zhao, Y. H. Song, and W. R. Chen, "Improved GPS travelling wave fault locator for power cables by using wavelet analysis," *Electrical Power System Research* (23), pp. 403-411, 2001.
- [30] M. Gilany, D. Ibrahim, and E. S. Tag Eldin, "Traveling-wave-based fault-location scheme for multiend-aged underground cable system," *IEEE Trans. Power Delivery*, vol. 22, no. 1, pp. 82-89, Jan. 2010.
- [31] H. Hizam, P. A. Crossley, P. F. Gale, and G. Bryson, "Fault section identification and location on a distribution feeder using travelling waves," in *Proc. IEEE Power & Energy Society Summer Meeting*, vol. 3, pp. 1107-1112, July 25, 2002.
- [32] J. Sadeh and H. Afradi, "A new and accurate fault location algorithm for combined transmission lines using adaptive network-based fuzzy inference system," *Electrical Power System Research* (79), pp. 1538-1545, 2009.
- [33] J. Moshtagh and R. K. Aggarwal, "A new approach to ungrounded fault location in a three-phase underground distribution system using combined neural networks & wavelet analysis," in *Proc. Canadian Conference on Electrical and Computer Engineering*, pp. 376-381, May 2006.
- [34] "Distribution Fault Location," Electric Power Research Institute, 1012438, Dec. 2006.
- [35] *IEEE Guide for Determining Fault Location on AC Transmission and Distribution Lines*, IEEE Standard C37.114-2004, June 2005.
- [36] J. Mora-Flórez, J. Meléndez, and G. Carrillo-Caicedo, "Comparison of impedance based fault location methods for power distribution systems," *Electrical Power System Research* (78), pp. 657-666, 2008.
- [37] T. Short, J. Kim, and C. Melhorn, "Update on distribution system fault location technologies and effectiveness," in *Proc. 20th International Conference and Exhibition on Electricity Distribution - Part 1*, paper no. 0973, June 8-11, 2009.
- [38] M. Lehtonen, "Novel techniques for fault location in distribution networks," in *Proc. Power Quality and Supply Reliability Conference*, pp. 1-6, Aug. 27-29, 2008.

- [39] K. Srinivasan and A. St.-Jacques, "A new fault location algorithm for radial transmission lines with loads," *IEEE Trans. Power Delivery*, vol. 4, no. 3, pp. 1676-1682, July 1989.
- [40] A. A. Girgis, C. M. Fallon, and D. L. Lubkeman, "A fault location technique for rural distribution feeders," *IEEE Trans. Industry Application*, vol. 29, no. 6, pp. 1170-1175, Nov. 1993.
- [41] J. Zhu, D. L. Lubkeman, and A. A. Girgis, "Automated fault location and diagnosis on electric power distribution feeders," *IEEE Trans. on Power Delivery*, vol. 12, no. 2, pp. 801-809, April 1997.
- [42] R. Aggarwal, Y. Aslan, and A. Johns, "New concept in fault location for overhead distribution systems using superimposed components," *IEE Proc. Generation, Transmission and Distribution*, vol. 144, no. 3, pp. 309-316, May 1997.
- [43] Y. Aslan and R. K. Aggarwal, "An alternative approach to fault location on main line feeders and laterals in low voltage overhead distribution networks," in *Proc. IET 9th International Conference on Developments in Power System Protection*, pp. 354-359, mar. 17-20, 2008.
- [44] R. Das, "Determining the locations of faults in distribution systems," Ph.D. thesis, Dept. Elec. Eng., Univ. Saskatchewan, 1998.
- [45] R. Das, M.S. Sachdev, and T. S. Sidhu, "A fault locator for radial subtransmission and distribution lines," in *Proc. IEEE Power & Energy Society Summer Meeting*, vol. 1, pp. 443-448, 2000.
- [46] D. Novosel, D. Hart, Y. Hu, and J. Myllymaki, "System for locating faults and estimating fault resistance in distribution networks with tapped loads," U.S. Patent 5 839 093, Nov. 17, 1998.
- [47] S. Santoso, R. C. Dugan, J. Lamoree, and A. Sundaram, "Distance estimation technique for single line-to-ground faults in a radial distribution system," in *Proc. IEEE Power & Energy Society Winter Meeting*, pp. 2551-2555, Jan. 23-27, 2000.
- [48] M. Saha and E. Rosolowski, "Method and device of fault location for distribution networks," U.S. Patent 6 483 435, Nov. 19, 2002.
- [49] M. Saha, E. Rosolowski, and J. Izykowski, "ATP-EMTP investigation for fault location in medium voltage networks," in *Proc. International Conference on Power Systems Transients*, paper no. IPST05-220, June 19-23, 2005.
- [50] S.-J. Lee, M.-S. Choi, S.-H. Kang, B.-G. Jin, D.-S. Lee, B.-S. Ahn, N.-S. Yoon, H.-Y. Kim, and S.-B. Wee, "An intelligent and efficient fault location and diagnosis scheme for radial distribution systems," *IEEE Trans. Power Delivery*, vol. 19, no. 2, pp. 524-532, Apr. 2004.
- [51] E. C. Senger, G. Jr. Manassero, C. Goldemberg, and E. L. Pellini, "Automated fault location system for primary distribution networks," *IEEE Trans. Power Delivery*, vol. 20, no. 2, pp. 1332-1340, April 2005.

- [52] R. H. Salim, M. Resener, A. D. Filomena, K. R. C. de Oliveira, and A. S. Bretas, "Extended fault-location formulation for power distribution systems," *IEEE Trans. Power Delivery*, vol. 24, no. 2, pp. 508-516, April 2009.
- [53] R. A. F. Pereira, L. G. W. da Silva, M. Kezunovic, and J. R. S. Mantovani, "Improved fault location on distribution feeders based on matching during-fault voltage sags," *IEEE Trans. Power Delivery*, vol. 24, no. 2, pp. 852-866, April 2009.
- [54] G. Morales-Espana, J. Mora-Florez, and H. Vargas-Torres, "Elimination of multiple estimation for fault location in radial power systems by using fundamental single-end measurements," *IEEE Trans. Power Delivery*, vol. 24, no. 3, pp. 1382-1389, July 2009.
- [55] M. M. Alamuti, H. Nouri, N. Makhoul, and M. Montakhab, "Developed single end low voltage fault location using distributed parameter approach," in *Proc. the 44th International Universities Power Engineering Conference*, pp. 1-5, Sept. 1-4, 2009.
- [56] M. A. Mirzai and A. A. Afzalian, "A novel fault-locator system; algorithm, principle and practical implementation," *IEEE Trans. on Power Delivery*, vol. 25, no. 1, pp. 35-46, Jan. 2010.
- [57] Y. Liao, "Generalized fault-location methods for overhead electric distribution systems," *IEEE Trans. on Power Delivery*, vol. 26, no. 1, pp. 53-64, Jan. 2011.
- [58] W. H. Kersting, *Distribution System Modeling and Analysis*. Boca Raton, FL: CRC, 2002.
- [59] C. S. Cheng and D. Shirmohammadi, "A three-phase power flow method for real-time distribution system analysis," *IEEE Trans. Power System*, vol. 10, no. 2, pp. 671-679, May 1995.
- [60] W. H. Kersting and W. H. Phillips, "Distribution feeder line models," *IEEE Trans. Industry Applications*, vol. 31, no. 4, pp. 715-720, July/Aug. 1995.
- [61] J. J. Grainger and W. D. Stevenson Jr., *Power system analysis*, New York: McGraw-Hill, 1994.
- [62] K. Srinivasan, C. T. Nguyen, Y. Robichaud, A. St. Jacques, and G. J. Rogers, "Load response coefficients monitoring system: Theory and field experience," *IEEE Trans. Power Apparatus and Systems*, vol. PAS-100, no. 8, pp. 3818-3827, Aug. 1981.
- [63] C. A. Reineri and C. Alvarez, "Load research for fault location in distribution feeders," *IEE Proc. Generation, Transmission and Distribution*, vol. 146, no. 2, pp. 115-120, May 1999.
- [64] J. Wan, "Nodal load estimation for electric power distribution systems," Ph.D. thesis, Dept. Elec. Eng., Drexel Univ., 2003.
- [65] J. Wan and K. N. Miu, "Weighted least squares methods for load estimation in distribution networks," *IEEE Trans. Power System*, vol. 18, no. 4, pp. 1338-1345, Nov. 2003.

- [66] M. Baran and A. W. Kelley, "State estimation for real time monitoring of distribution systems," *IEEE Trans. Power System*, vol. 9, no. 3, pp. 1601-1609, Aug. 1994.
- [67] M. E. Baran and A. W. Kelley, "A branch-current-based state estimation method for distribution systems" *IEEE Trans. Power System*, vol. 10, no. 1, pp. 483-491, Feb. 1995.
- [68] W.-M. Lin, J.-H. Teng, and S.-J. Chen, "A highly efficient algorithm in treating current measurements for the branch-current-based distribution state estimation," *IEEE Trans. Power Delivery*, vol. 16, no. 3, pp. 433-439, July 2001.
- [69] M. R. Irving and C. N. Macqueen, "Robust algorithm for load estimation in distribution networks," *IEE Proc. Generation, Transmission and Distribution*, vol. 145, no. 5, pp. 499-504, Sept. 1998.
- [70] M. K. Celik and W. H. E. Liu, "A practical distribution state calculation algorithm," in *Proc. IEEE Power & Energy Society Winter Meeting*, vol. 1, pp. 442-447, 1999.
- [71] A. Gomez Esposito and E. Romero Ramos, "Reliable load flow technique for radial distribution networks," *IEEE Trans. Power System*, vol. 14, no. 3, pp. 1063-1069, Aug. 1999.
- [72] J.-H. Teng and C.-Y. Chang, "A novel and fast three-phase load flow for unbalanced radial distribution systems" *IEEE Trans. Power System*, vol. 17, no. 4, pp. 1238-1244, Nov. 2002.
- [73] R. A. Jabr, "Radial distribution load flow using conic programming," *IEEE Trans. Power System*, vol. 21, no. 3, pp. 1458-1459, Aug. 2006.
- [74] R. Ross, "Inception and propagation mechanisms of water treeing," *IEEE Trans. Dielectrics and Electrical Insulation*, vol. 5, no. 5, pp. 660-680, Oct. 1998.
- [75] G. Chen and C. H. Tham, "Electrical treeing characteristics in XLPE power cable insulation in frequency range between 20 and 500 Hz," *IEEE Trans. Dielectrics and Electrical Insulation*, vol. 16, no. 1, pp. 179-188, Feb. 2009.
- [76] M. S. Mashikian and A. Szatkowski, "Medium voltage cable defects revealed by off-line partial discharge testing at power frequency," *IEEE Electrical Insulation Magazine*, vol. 22, no. 4, pp. 24-32, July/Aug. 2006.
- [77] J. Densley, "Ageing mechanisms and diagnostics for power cables - an overview," *IEEE Electrical Insulation Magazine*, vol. 17, no. 1, pp. 14-22, Jan./Feb. 2001.
- [78] B. Koch, and Y. Carpentier, "Manhole explosion due to arcing faults on underground secondary distribution cables in ducts," *IEEE Trans. Power Delivery*, vol. 7, no. 3, pp. 1425-1433, July 1992.
- [79] A. Hamel, A. Gaudreau, and M. Côté, "Intermittent arcing fault on underground low-voltage cables," *IEEE Trans. Power Delivery*, vol. 19, no. 4, pp. 1862-1868, Oct. 2004.
- [80] *IEEE Guide for Performing Arc-Flash Hazard Calculations*, IEEE Standard 1584-2002.

- [81] R. Wilkins, M. Allison, and M. Lang, "Improved method for arc flash hazard analysis – calculating hazards," *IEEE Ind. Application Magazine*, vol. 11, no. 3, pp. 40–48, 2005.
- [82] T. Gammon and J. Matthews, "The historical evolution of arcing-fault models for low-voltage systems," in *Proc. Industrial and Commercial Power Systems Technical Conference*, pp. 1-6, Aug. 1999.
- [83] H. A. Darwish and N. I. Elkalashy, "Universal arc representation using EMTP," *IEEE Trans. Power Delivery*, vol. 20, no. 2, pp. 772–779, Apr. 2000.
- [84] U. Habedank, "Application of a new arc model for the evaluation of short-circuit breaking tests," *IEEE Trans. Power Delivery*, vol. 8, no. 4, pp. 1921–1925, Oct. 1993.
- [85] M. Kizilcay, and P. La Seta, "Digital simulation of fault arcs in medium-voltage distribution networks," in *Proc. 15th Power Systems Computation Conference*, session 36, paper 3, pp. 1-7, August 22-26, 2005.
- [86] G. I. Ospina, D. Cubillos, and L. Ibanez, "Analysis of arcing fault models," in *Proc. IEEE Power Engineering Society Transmission and Distribution Conference and Exposition: Latin America*, pp. 1-5, Aug. 13-15, 2008
- [87] D.C. Robertson, O.I. Camps, J.S. Mayer, and W.B. Gish, "Wavelets and electromagnetic power system transients," *IEEE Trans. Power Delivery*, vol. 11, no. 2, pp. 1050-1058, Apr. 1996.
- [88] N.S.D. Brito, B.A. Souza, and F.A.C. Pires, "Daubechies wavelets in quality of electrical power," in *Proc. 8th International Conference on Harmonics and Quality of Power*, pp. 511-515, Oct 14-16, 1998.
- [89] I. Daubechies, *Ten Lectures on Wavelets*, SIAM, 1992.
- [90] A. V. Oppenheim, R.W. Schafer, and J. R. Buck, *Discrete-time signal processing*, 2nd ed., Prentice-Hall, 1998.
- [91] *IEEE Standard Common Format for Transient Data Exchange (COMTRADE) for Power Systems*, IEEE Std. 37.111-1991.
- [92] W.H. Kersting, "Radial distribution test feeders," in *Proc. IEEE Power & Energy Society Winter Meeting*, vol. 2, pp. 908-912, Jan. 28-Feb. 1, 2001.
- [93] B. Gustavsen, "Panel session on data for modeling system transients insulated cables," in *Proc. IEEE Power & Energy Society Winter Meeting*, vol. 2, pp. 718-723, Jan. 28-Feb. 1, 2001.
- [94] *IEEE Guide for Application of Sheath-Bonding Methods for Single-Conductor Cables and the Calculation of Induced Voltages and Currents in Cable Sheaths*, IEEE Standard 575-988, March 1986.
- [95] D. A. Tziouvaras, "Protection of high-voltage AC cables," in *Proc. Power Systems Conference: Advanced Metering, Protection, Control, Communication and Distributed Resources*, pp 316-328, Mar. 14-17, 2006.

- [96] J. Zipp, "Protective relaying considerations for transmission lines with high voltage AC cables," *IEEE Trans. on Power Delivery*, vol. 12, no. 1, pp. 83-96, Jan. 1997.
- [97] B. Kasztenny, I. Voloh, and J. G. Hubertus, "Applying distance protection to cable circuits," in *Proc. 57th Annual Conference for Protective Relay Engineers*, pp. 46-69, Mar. 30-Apr. 1, 2004.
- [98] V. Leitloff, X. Bourgeat, and G. Duboc, "Setting constraints for distance protection on underground lines," in *Proc. Seventh International Conference on Developments in Power System Protection*, pp. 467-470, Apr. 9-12, 2001.
- [99] J. Vargas, A. Guzmán, and J. Robles, "Underground/submarine cable protection using a negative-sequence directional comparison scheme," [Online]. Available: www2.selinc.com/techpprs/underground.pdf.
- [100] C. L. Fortescue, "Method of symmetrical co-ordinates applied to the solution of polyphase networks," *Trans. of American Institute of Electrical Engineers*, vol. XXXVII, no. 2, pp. 1027-1140, July, 1918.
- [101] E. Clarke, *Circuit Analysis of AC Power Systems*, vol. I. New York: Wiley, 1950.
- [102] J. A. Brandao Faria and J. H. Briceno Mendez, "Modal analysis of untransposed bilateral three-phase lines - a perturbation approach," *IEEE Trans. on Power Delivery*, vol. 12, no. 1, pp. 497-504, Jan. 1997.
- [103] A. J. do Prado, J. P. Filho, S. Kurokawa, and E. F. Bovolato, "Correction procedure applied to a single real transformation matrix -untransposed three-phase transmission line cases," in *Proc. IEEE Power Engineering Society Transmission & Distribution Conference and Exposition: Latin America*, pp. 1-6, Aug. 15-18, 2006.
- [104] G. Kron, *Tensor analysis of networks*, New York: Wiley, 1939.
- [105] L. Marti, "Simulation of electromagnetic transients in underground cables using the EMTP," in *Proc. the 2nd International Conference on Advances in Power System Control, Operation and Management*, pp. 147-152, Dec. 7-10, 1993.
- [106] L. Marti, "Simulation of transients in underground cables with frequency-dependent modal transformation matrices," *IEEE Trans. on Power Delivery*, vol. 3, no. 3, pp. 1099-1110, July 1988.
- [107] "PSCAD/EMTDC User's Guide," Manitoba HVDC Research Center, 2004.
- [108] J. R. Carson, "Wave propagation in overhead wires with ground return," *Bell System Technical Journal*, vol. 5, pp. 539-554, 1926.
- [109] L. M. Wedepohl and D. J. Wilcox, "Transient analysis of underground power-transmission systems. System-model and wave-propagation characteristics," *Proceedings of the Institution of Electrical Engineers*, vol. 120, no. 2, pp. 253-260, Feb. 1973.
- [110] G. C. Stone and S. A. Boggs, "Propagation of partial discharge pulses in shielded power cable," in *Proc. Annual Report of the Conference on Electrical Insulation and Dielectric Phenomena*, pp. 275-280, 1982.

- [111] The Mathworks, Inc., Mathworks Matlab [Online]. Available: <http://www.mathworks.com>.
- [112] M. E. Baran, "Challenges in state estimation on distribution systems," in *Proc. IEEE Power & Energy Society Summer Meeting*, vol. 1, pp. 429-433, 2001.
- [113] J. F. Bonnans, J. C. Gilbert, C. Lemarechal, and C. A. Sagastizábal, *Numerical optimization: Theoretical and practical aspects*, 2nd ed., New York: Springer, 2006.
- [114] A. Antoniou and W.-S. Lu, *Practical optimization algorithms and engineering applications*, New York: Springer, 2007.
- [115] J. C. Gilbert, SQPlab: A Matlab software for solving nonlinear optimization problems and optimal control problems. [Online]. Available: <http://www-rocq.inria.fr/~gilbert/preprint/u02-sqplab.pdf>.

Appendices

Appendix A: Illustration of Traveling Wave

A single phase to ground fault occurs at 50 km of a 140 km transmission line and the fault currents are shown in Figure A.1.

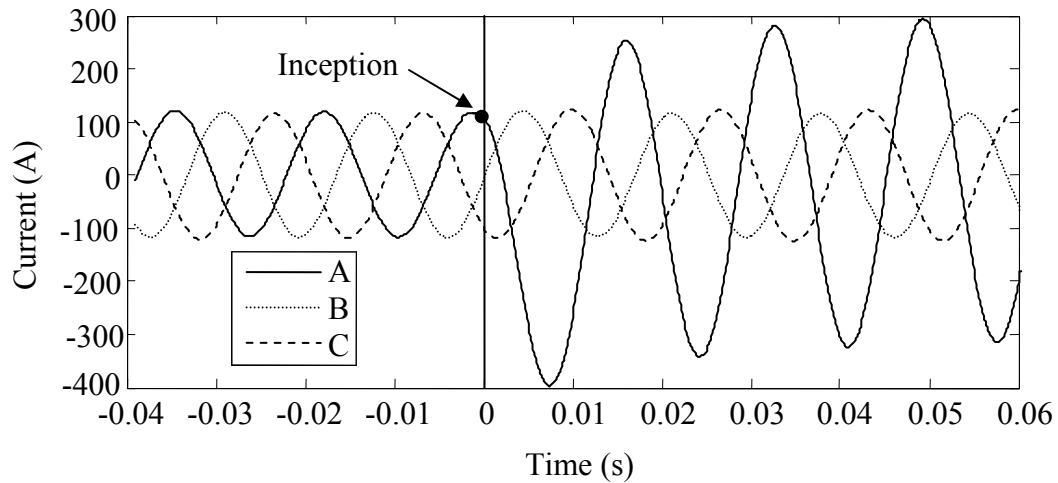


Figure A.1: Fault currents.

It is apparent that there is no any special phenomenon can be observed in the fault currents in addition to the increasing magnitude. However, if the fault current of phase A is zoomed in around the occurrence instant of fault at the resolution of microseconds, the wavefronts of the traveling waves can be clearly observed, as shown in Figure A.2. The current has no changes at the inception instant in the monitor point which is located at the sending terminal, 50 km far to the fault point. The wavefront (1) is the initial wave directly caused by the fault, taking 169 μ s and traveling 50 km after the occurrence of the fault. The propagation velocity is 295.86m/ μ s, which is close to the light speed. The wavefront (1) is reflected back to the line and reflected again at the fault point towards the sending terminal, which is detected as the wavefront (2). The initial wave at the fault point also propagates towards the receiving terminal, reflects there, transmits through the

fault point, arrives at the sending terminal, and forms the wavefront (3). Similar to the formation of the wavefront (2), the wavefront (4) is formed by two reflections of the wavefront (2) at the sending terminal and fault point.

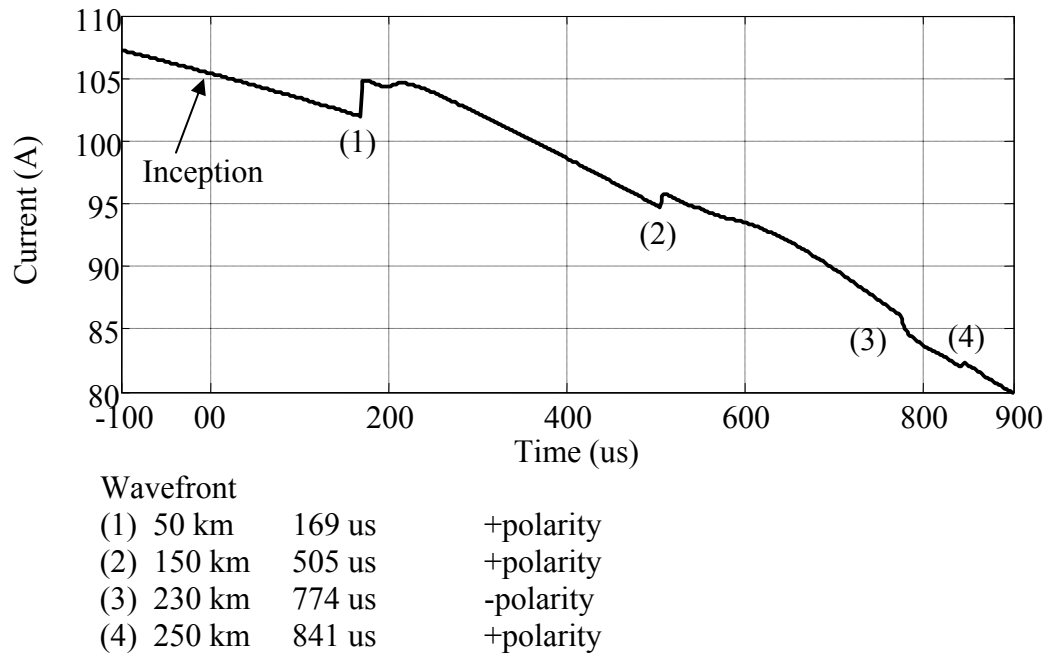


Figure A.2: Wavefronts of traveling waves.

The three dimension and two dimension illustrations of the propagation process is described in Figure A.3 and Figure A.4, where the first two wavefronts can be clearly observed. The Bewley lattice diagram for such a situation is shown in Figure A.5.

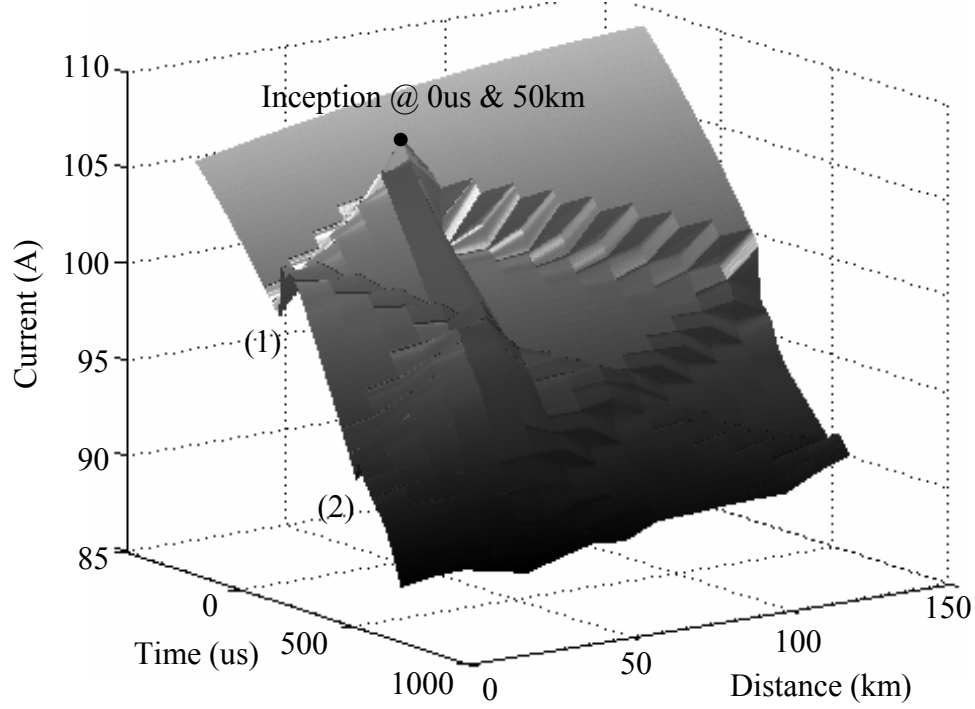


Figure A.3: Illustration of propagation of traveling waves in spatiotemporal domain.

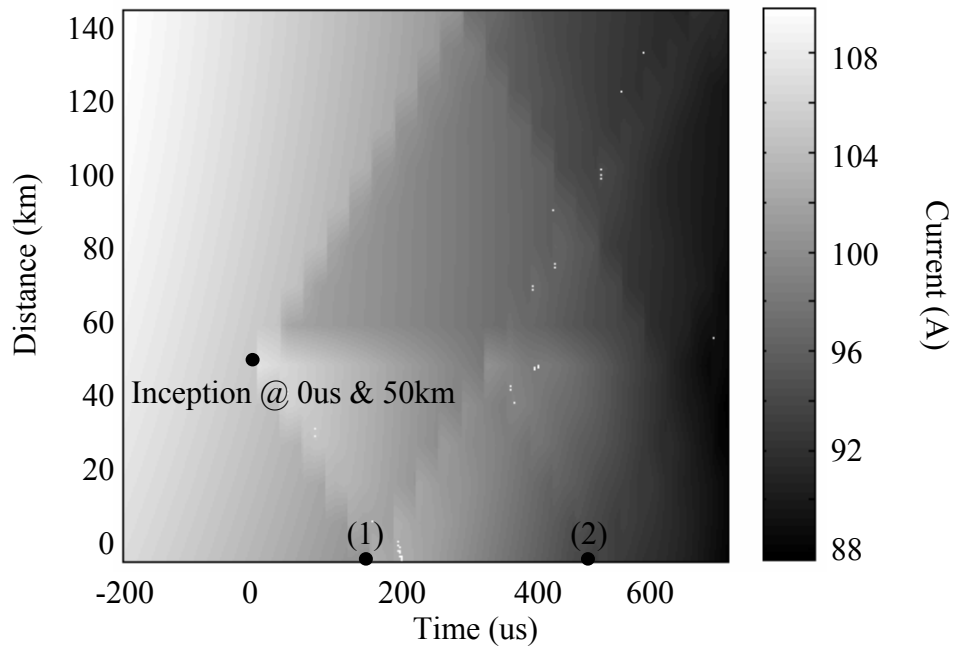


Figure A.4: Two dimension illustration of propagation of traveling wave.

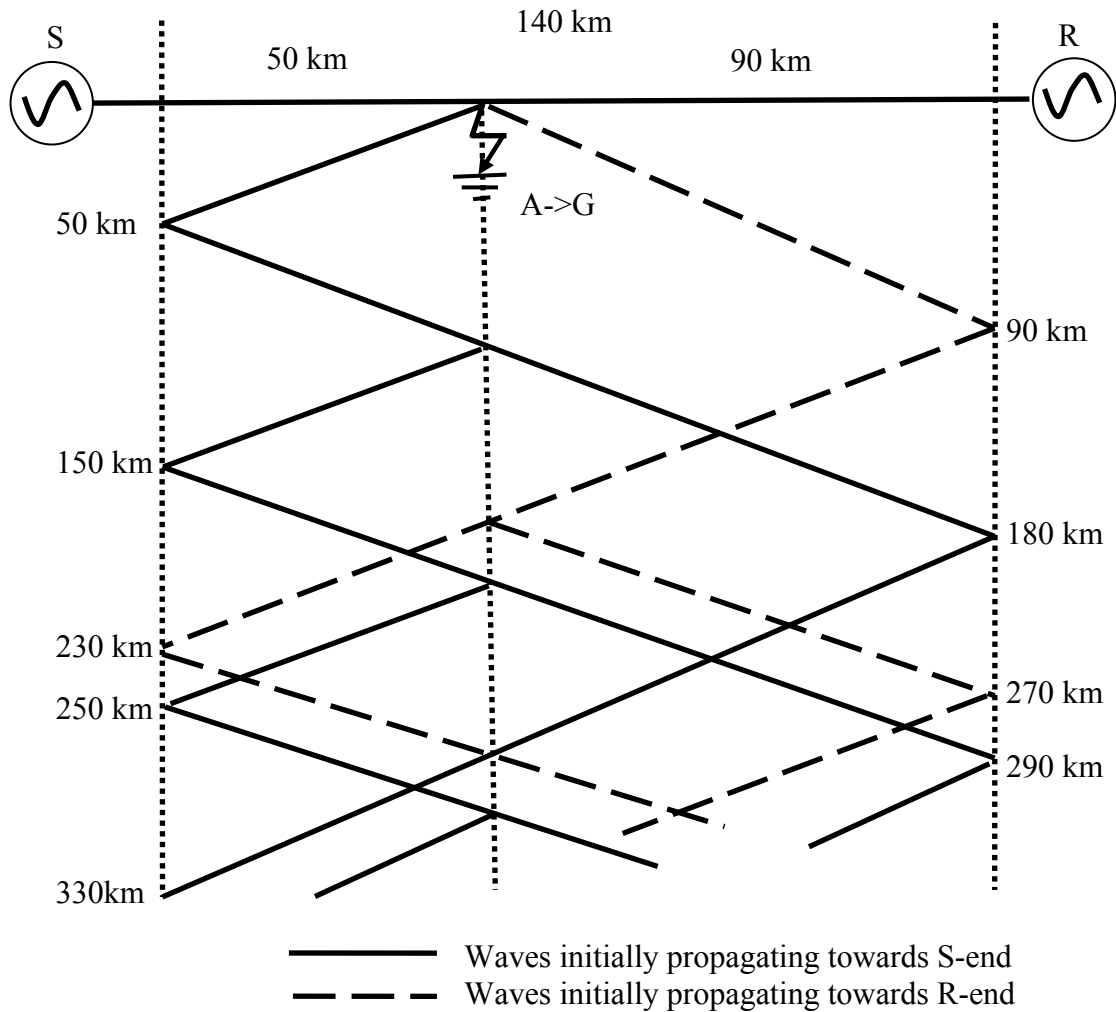


Figure A.5: Bewley lattice diagram.

Appendix B: Example of Kizilcay's Arc Model

An example of Kizilcay's arc model illustrates the behavior and characteristic of the arc voltage, current and resistance. The arc voltage appears like the near square wave with small spikes at the rising and falling edges, as shown in Figure A.6. The arc current looks like any regular fault current in Figure A.7. And the arc resistance is time-varying and nonlinear, changing from 0.01 to 5 ohm in this case shown in Figure A.8.

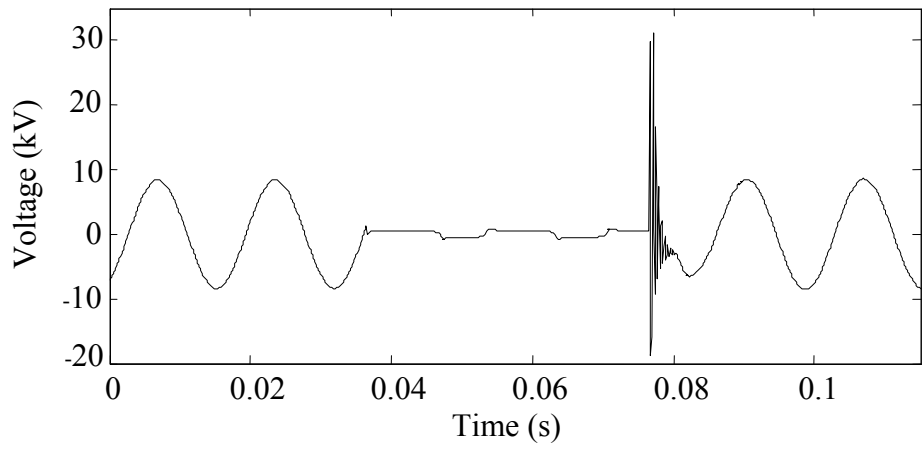


Figure A.6: Arc voltage.

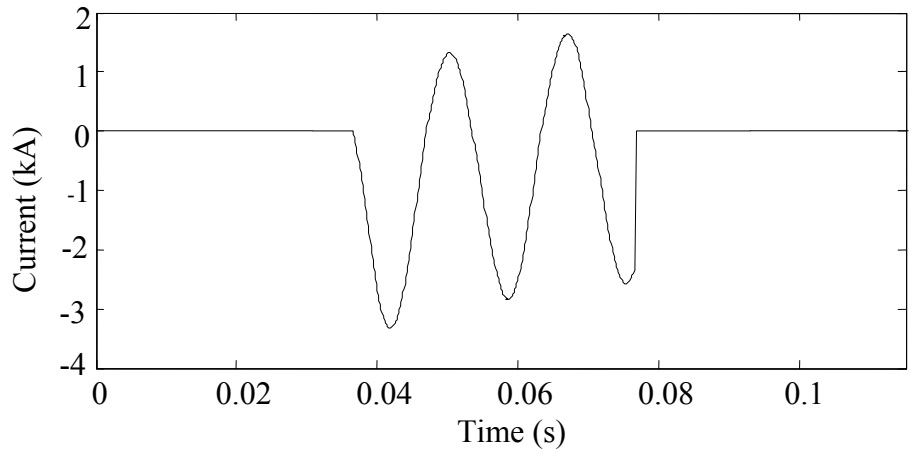


Figure A.7: Arc current.

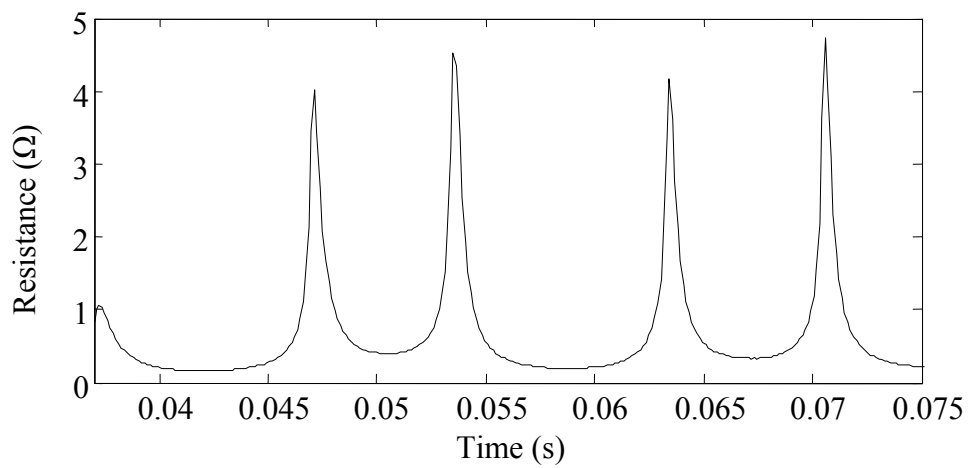


Figure A.8: Arc resistance.

Curriculum Vitae

Name: Zhihan Xu

Post-secondary Education and Degrees: Sichuan University
Chengdu, Sichuan, China
1991-1995 B.E.

Sichuan University
Chengdu, Sichuan, China
1997-2000 M.Sc.

The University of Alberta
Edmonton, Alberta, Canada
2000-2002 M.Sc.

The University of Western Ontario
London, Ontario, Canada
2007-2011 Ph.D.

Honors and Awards: Western Graduate Research Scholarship - Engineering
2007-2011

Related Work Experience Research Assistant and Teaching Assistant
The University of Western Ontario
2007-2011

Publications:

T. S. Sidhu and Z. Xu, "Detection and Classification of Incipient Faults in Underground Cables in Distribution Systems", in Proc. *Canadian Conference on Electrical and Computer Engineering*, pp. 122-126, May 3-6, 2009.

T. S. Sidhu and Z. Xu, "Detection of incipient faults in distribution underground cables," *IEEE Trans. Power Del.*, vol. 25, no. 3, pp. 1363-1371, July 2010.

Z. Xu and T. S. Sidhu, "Fault location method based on single-end measurements for underground cables," *IEEE Trans. Power Del.*, vol. 26, no. 4, pp. 2845-2854, October 2011.

Z. Xu and T. S. Sidhu, "Fault location for cables in distribution networks with the aid of state estimation," to be submitted.